



ICAM

**Institute for Computational
and Applied Mechanics**

IN-34-CR
46092
p-200

INFRARED RADIATIVE ENERGY TRANSFER
IN GASEOUS SYSTEMS
A Progress Report,
(Old Dominion Univ.) 1991

CRCL 200
73/34 UNCLAS
6044002

INFRARED RADIATIVE ENERGY TRANSFER IN GASEOUS SYSTEMS

By

**Surendra N. Thwait, Principal Investigator
and ICAM Director**

**NASA Grant NAG-1-363
NASA Langley Research Center
Hampton, Virginia 23665-5225**

**ODU/ICAM Report 91-102
September 1991**

**Old Dominion University
Norfolk, Virginia 23529-0247**

✓

PREFACE

This research was conducted in cooperation with the NASA Langley Research Center (Fluid Mechanics Division - Theoretical Flow Physics Branch) and the Institute for Computational and Applied Mechanics (ICAM) of Old Dominion University during the period 1984 through 1990. The work on basic formulations and computational procedures was completed by the end of 1985 and was published as a progress report "Radiative Interactions in Transient Energy Transfer in Gaseous Systems," NASA CR-176644, December 1985.

The formulations and procedures developed in this study were applied to solve several realistic problems during 1985-1990. This resulted in various publications in forms of technical reports, technical papers (presented at national and international conferences), and journal articles. Selected articles are included in the appendices of this report to demonstrate the applications of the developed techniques in various fields involving radiative interactions in molecular gases. The procedures developed are being used at present to investigate radiative interactions in other challenging problems.

ABSTRACT

Analyses and numerical procedures are presented to investigate the radiative interactions in various energy transfer processes in gaseous systems. Both gray and nongray radiative formulations for absorption and emission by molecular gases are presented. The gray gas formulations are based on the Planck mean absorption coefficient and the nongray formulations are based on the wide-band model correlations for molecular absorption. Various relations for the radiative flux and divergence of radiative flux are developed. These are useful for different flow conditions and physical problems. Specific plans for obtaining extensive results for different cases are presented. The procedure developed has been applied to several realistic problems. Results of selected studies are presented in the appendices of this report.

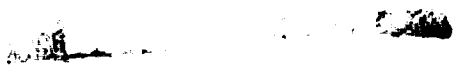


TABLE OF CONTENTS

	<u>Page</u>
PREFACE.	ii
ABSTRACT.	iii
LIST OF SYMBOLS.	v
1. INTRODUCTION	1
2. BAND ABSORPTION AND CORRELATIONS.	2
3. RADIATIVE FLUX EQUATIONS	9
4. BASIC FORMULATION FOR TRANSIENT PROCESSES.	18
5. A SPECIAL CASE OF TRANSIENT INTERACTION.	21
6. METHOD OF SOLUTIONS	25
6.1 Optically Thin Limit	25
6.2 Large Path Length Limit.	27
6.3 Numerical Solutions of Governing Equations	29
7. RADIATIVE INTERACTION IN LAMINAR FLOW	35
8. PLANS FOR SPECIFIC RESULTS.	57
9. CONCLUDING REMARKS.	59
REFERENCE	60
APPENDIX A: EXPONENTIAL INTEGRALS AND EXPRESSIONS FOR RADIATIVE FLUX.	64
APPENDIX B: ALTERNATE FORMS OF RADIATIVE FLUX EQUATIONS.	66
APPENDIX C: DEFINITION AND EVALUATION OF INTEGRAL FUNCTIONS	72
APPENDIX D: INFORMATION FOR NUMERICAL PROCEDURE.	79

TABLE OF CONTENTS - Concluded

	<u>Page</u>
APPENDIX E: EVALUATION OF CONSTANTS FOR STEADY LAMINAR FLOWS	82
APPENDIX F: INTEGRAL FUNCTIONS FOR TRANSIENT LAMINAR FLOWS.	91
APPENDIX G: AIAA PAPER NO. AIAA-87-0323, JANUARY 1987.	
APPENDIX H: AIAA PAPER NO. AIAA-87-1521, JUNE 1987.	
APPENDIX I: AIAA PAPER NO. AIAA-90-0134, JANUARY 1990.	
APPENDIX J: INVESTIGATION OF RADIATIVE INTERACTIONS IN HIGH-SPEED ENTRANCE REGION FLOWS.	

LIST OF FIGURES

<u>Figure</u>	<u>Page</u>
3.1 Plane radiating layer between parallel boundaries.	9a
4.1 Physical model and coordinate system	19a
7.1 Physical model and coordinate system for flow of radiating gases between parallel plates.	35a

LIST OF SYMBOLS

A	band absorptance , cm^{-1}
$A(u,\beta)$	band absorptance of a wide band, cm^{-1}
$A_n(u,\beta)$	band absorptance of a narrow band, cm^{-1}
A_0	band width parameter, cm^{-1}
C_0	correlation parameter, $\text{atm}^{-1} - \text{cm}^{-1}$
e_ω	Planck's function, $(\text{W cm}^{-2})/\text{cm}^{-1}$
$e_{\omega_c}, e_{\omega_0}$	Planck's function evaluated at the wave ω_c, ω_0
$E_n(t)$	exponential integral of order n
H	gas property for the large path length limit
L	distance between plates
M	radiation-conduction interaction parameter for the large path length limit
N	optically thin radiation-conduction interaction parameter
P	pressure, atm
P_i	partial pressure of the ith species
q_r	total radiative flux, W/cm^2
$q_{r\omega}$	spectral radiative flux, $(\text{W}/\text{cm}^2)/\text{cm}^{-1}$
Q	nondimensional radiative heat flux, Eq. (4.4)
S	integrated intensity of a wide band, $\text{atm}^{-1}\text{-cm}^{-2}$
S_j	intensity of the jth spectral line
t	line structure parameter = $B/2 = \pi \gamma_L/d$
T	equilibrium temperature, K
T_1, T_2	wall temperatures, K
u	dimensionless coordinate = SX/A_0 or SPy/A_0
u_0	dimensionless path length = SPL/A_0
X	pressure path length = Py

y	transverse coordinate, cm
β	line structure parameter
γ_j	line half width, cm^{-1}
θ	dimensionless temperature, Eq. (5.4)
K_ω	equilibrium spectral absorption coefficient, cm^{-1}
τ	optical coordinate
τ_0	optical thickness
ξ	dimensionless coordinate = $y/L = u/u_0$
ω	wave number, cm^{-1}
ω_0, ω_c	wave number at the band center, cm^{-1}

1. INTRODUCTION

In the past two decades, a tremendous progress has been made in the field of radiative energy transfer in nonhomogeneous nongray gaseous systems. As a result, several useful books [1-18] and review articles [19-26] have become available for engineering, meteorological, and astrophysical applications. In the sixties and early seventies, radiative transfer analyses were limited to one-dimensional cases. Multidimensional analyses and sophisticated numerical procedures emerged in the mid-to-late seventies. Today, the field of radiative energy transfer in gaseous systems is getting an ever increasing attention because of its applications in the areas of the earth's radiation budget studies and climate modeling, fire and combustion research, entry and reentry phenomena, hypersonic propulsion and defense-oriented research.

In most studies involving combined mass, momentum, and energy transfer, the radiative transfer formulation has been coupled only with the steady processes. The goal of this research is to include the nongray radiative formulation in the general unsteady governing equations and provide the step-by-step analysis and solution procedure for several realistic problems. The specific objective of the present study is to investigate the one-dimensional transient radiative transfer in a nongray gaseous system. In the future work, the present analysis will be extended (in a systematic manner) to the problems of combined transfer processes in chemically reacting flows.

For the present study, the information on band absorption and correlation is summarized in section 2 and fundamental radiative flux equations are presented in section 3. The basic formulation for the transient radiation is given in section 4, and this is applied to a special case in section 5. The

solution procedures are described in section 6, and plans for obtaining specific results are presented in section 7.

2. BAND ABSORPTION AND CORRELATIONS

The study of radiative transmission in nonhomogeneous gaseous systems requires a detailed knowledge of the absorption, emission, and scattering characteristics of the specific species under investigation. In absorbing and emitting mediums, an accurate model for the spectral absorption coefficient is of vital importance in the correct formulation of the radiative flux equations. A systematic representation of the absorption by a gas, in the infrared, requires the identification of the major infrared bands and evaluation of the line parameters (line intensity, line half-width, and spacing between the lines) of these bands. The line parameters depend upon the temperature, pressure and concentration of the absorbing molecules and, in general, these quantities vary continuously along a nonhomogeneous path in the medium. In recent years, considerable efforts have been expended in obtaining the line parameters and absorption coefficients of important atomic and molecular species [27-30].

For an accurate evaluation of the transmittance (or absorptance) of a molecular band, a convenient line model is used to represent the variation of the spectral absorption coefficient. The line models usually employed are Lorentz, Doppler, and Voigt line profiles. A complete formulation (and comparison) of the transmittance and absorptance by these line profiles is given in [22-26]. In a particular band consisting of many lines, the absorption coefficient varies very rapidly with the frequency. Thus, it becomes very difficult and time-consuming task to evaluate the total band absorptance over the actual band contour by employing an appropriate line

profile model. Consequently, several approximate band models (narrow as well as wide) have been proposed which represent absorption from an actual band with reasonable accuracy [22-26, 31-40]. Several continuous correlations for the total band absorption are available in literature [22-26, 36-40]. These have been employed in many nongray radiative transfer analyses with varying degree of success [22-26, 41]. A brief discussion is presented here on the total band absorption, band models, and band absorptance correlations.

The absorption within a narrow spectral interval of a vibration rotation band can quite accurately be represented by the so-called "narrow band models." For a homogeneous path, the total absorptance of a narrow band is given by

$$A_N = \int_{\Delta\omega} [1 - \exp(-k_\omega X)] d\omega \quad (2.1)$$

where k_ω is the volumetric absorption coefficient, ω is the wave number, and $X = py$ is the pressure path length. The limits of integration in Eq. (2.1) are over the narrow band pass considered. The total band absorptance of the so-called "wide band models" is given by

$$A = \int_{-\infty}^{\infty} [1 - \exp(-k_\omega X)] d(\omega - \omega_0) \quad (2.2)$$

where the limits of integration are over the entire band pass and ω_0 is the wave number at the center of the wide band. In actual radiative transfer analyses, the quantity of frequent interest is the derivative of Eqs. (2.1) and (2.2).

Four commonly used narrow band models are Elsasser, Statistical, Random Elsasser, and Quasi-Random. The application of a model to a particular case depends upon the nature of the absorbing emitting molecule. Complete discussion on narrow bands models, and expressions for transmittance and

integrated absorptance are available in the literature [22-26, 31-33]. Detailed discussions on the wide band models are given in [22-26, 34-40]. The relations for total band absorptance of a wide band are obtained from the absorptance formulations of narrow band models by employing the relations for the variation of line intensity as [22-26, 37-40]

$$S_j/d = (S/A_0) \exp\{-b_0 |\omega - \omega_0| / A_0\} \quad (2.3)$$

where S_j is the intensity of the j th spectral line, d is the line spacing, S is the integrated intensity of a wide band, A_0 is the band width parameter, and $b_0 = 2$ for a symmetrical band and $b_0 = 1$ for bands with upper and lower wave number heads at ω_0 . The total absorptance of an exponential wide band, in turn, may be expressed by

$$\bar{A}(u, \beta) \equiv A(u, \beta) / A_0 = \frac{1}{A_0} \int_{\text{wide band}} [A_N(u, \beta)] d(\omega - \omega_0) \quad (2.4)$$

where $u = SX/A_0$ is the nondimensional path length, $\beta = 2\pi\gamma_L/d$ is the line structure parameter, γ_L is the Lorentz line half-width, and $\bar{A}_N(u, \beta)$ represents the mean absorptance of a narrow band.

By employing the Elsasser narrow band absorptance relation and Eq. (2.3) the expression for the exponential wide band absorptance is obtained as [25,16]

$$\bar{A}(u, \beta) = \gamma + (1/\pi) \int_0^\pi [\ln \psi + E_1(\psi)] dz \quad (2.5)$$

where $\psi = u \sinh \beta / (\cosh \beta - \cos z)$, $\gamma = 0.5772156$ is the Euler's constant, and $E_1(\psi)$ is the exponential integral of the first order. Analytic solution of Eq. (2.5) can be obtained in a series form as [25, 26]

$$\bar{A}(u, \beta) = \sum_{n=1}^{\infty} \{-(A)^n [\text{SUM}(mn)] / [n(B+1)^n n!(n-1)!]\} \quad (2.6)$$

where

$$\text{SUM } (mn) = \sum_{m=0}^{\infty} [(n+m-1)!(2m-1)!C^m]/(2^m(m!)^2)$$

$$A = -u \tanh\beta, \quad B = 1/\cosh\beta,$$

$$C = 2/(1+\cosh\beta) = 2B/(B+1).$$

The series in Eq. (2.6) converges rapidly. When the weak line approximation for the Elsasser model is valid (i.e. β is large), then Eq. (2.5) reduces to

$$\bar{A}(u) = \gamma + \ln(u) + E_1(u). \quad (2.7)$$

In the linear limit, Eqs. (2.5) and (2.6) reduce to $\bar{A} = u$, and in the logarithmic limit they reduce to $\bar{A} = \gamma + \ln(u)$. It can be shown that Eq. (2.5) reduces to the correct limiting form in the square-root limit. Results of Eqs. (2.5) and (2.6) are found to be identical for all pressures and pathlengths. For $p > 1$ atm, results of Eqs. (2.5)-(2.7) are in good agreement for all path lengths.

By employing the uniform statistical, general statistical, and random Elsasser narrow band models absorptance relations and Eq. (2.3), three additional expressions for the exponential wide band absorptance were obtained in [25, 26]. The absorptance results of the four wide band models are discussed in detail in [26]. The expression obtained by employing the uniform statistical model also reduces to the relation (2.7) for large β .

Several continuous correlations for the total absorptance of a wide band, which are valid over different values of path length and line structure parameter, are available in the literature. These are discussed, in detail, in [22-26, 37-40] and are presented here in the sequence that they became available in the literature. Most of these correlations are developed to

satisfy at least some of the limiting conditions (nonoverlapping line, linear, weak line, and strong line approximations, and square-root, large pressure, and large path length limits) for the total band absorptance [23-26]. Some of the correlations even have experimental justifications [22,35].

The first correlation for the exponential wide band absorptance (a three piece correlation) was proposed by Edwards et al. [34, 35]. The first continuous correlation was proposed by Tien and Lowder [22], and this is of the form

$$\bar{A}(u, \beta) = \ln(uf(t)(u+2)/[u+2f(t)]+1) \quad (2.8)$$

where

$$f(t) = 2.94[1-\exp(-2.60t)], \quad t = \beta/2.$$

This correlation does not reduce to the correct limiting form in the square-root limit [23,26], and its use should be made for $\beta > 0.1$. Another continuous correlation was proposed by Goody and Belton [39], and in terms of the present nomenclature, this is given by

$$\bar{A}(u, \beta) = 2 \ln(1+u/[4+(\pi u/4t)]^{1/2}), \quad \beta = 2t. \quad (2.9)$$

Use of this correlation is restricted to relatively small β values [23-26]. Tien and Ling [40] have proposed a simple two parameter correlation for $\bar{A}(u, \beta)$ as

$$\bar{A}(u) = \sinh^{-1}(u) \quad (2.10)$$

which is valid only for the limit of large β . A relatively simple continuous correlation was introduced by Cess and Tiwari [23], and this is of the form

$$\bar{A}(u, \beta) = 2 \ln(1+u/\{2+[u(1+1/\bar{\beta})]^{1/2}\}) \quad (2.11)$$

where $\bar{\beta} = 4t/\pi = 2\beta/\pi$. By slightly modifying Eq. (2.11), another form of the wide band absorptance is obtained as [25, 26]

$$\bar{A}(u, \beta) = 2 \ln(1+u/\{2+[u(c+\pi/2\beta)]^{1/2}\}) \quad (2.12)$$

where

$$c = \begin{cases} 0.1, & \beta < 1 \text{ and all } u \text{ values} \\ 0.1, & \beta > 1 \text{ and } u < 1 \\ 0.25, & \beta > 1 \text{ and } u > 1. \end{cases}$$

Equations (2.11) and (2.12) reduce to all the limiting forms [23]. Based on the formulations of slab band absorptance, Edwards and Balakrishnan [37] have proposed the correlation

$$\bar{A}(u) = \ln(u) + E_1(u) + \gamma + \frac{1}{2} - E_3(u) \quad (2.13)$$

which is valid for large β . For present application, this correlation should be modified by using the technique discussed in [25, 26]. Based upon the formulation of the total band absorptance from the general statistical model, Felske and Tien [38] have proposed a continuous correlation for $\bar{A}(u, \beta)$ as

$$\begin{aligned} \bar{A}(u, \beta) = & 2E_1(t\rho_u) + E_1(\rho_u/2) - E_1[(\rho_u/2)(1+2t)] \\ & + \ln[t\rho_u)^2/(1+2t)] + 2\gamma \end{aligned} \quad (2.14)$$

where

$$\rho_u = \{(t/u)[1 + (t/u)]\}^{-1/2}$$

The absorptance relation given by Eq. (2.7) is another simple correlation which is valid for all path lengths and for $t = (\beta/2) > 1$. The relation of Eq. (2.6) can be treated as another correlation applicable to gases whose spectral behavior can be described by the Elsasser model. In [26] Tiwari has shown that the Elsasser as well as random band model formulations for the total band absorptance reduce to Eq. (2.7) for $t > 1$.

Band absorptance results of various correlations are compared and discussed in some detail in [25, 26, 41]. It was found that results of these correlations could be in error by as much as 40% when compared with the exact solutions based on different band models. Felske and Tien's correlation was found to give the least error when compared with the exact solution based on the general statistical model while Tien and Lowder's correlation gave the least error when compared with the exact solution based on the Elsasser model. The results of Cess and Tiwari's correlations followed the trend of general statistical model. Tiwari and Batki's correlation [Eq. 2.6 or 2.7] was found to provide a uniformly better approximation for the total band absorptance at relatively high pressures. The sole motivation in presenting the various correlations here is to see if their use in actual radiative processes made any significant difference in the final results.

In reference 41, use of several continuous correlations for total band absorptance was made to two problems to investigate their influence on the final results of actual radiative processes. For the case of radiative transfer in a gas with internal heat source, it was found that actual center-line temperature results obtained by using the different correlations follow the same general trend as the results of total band absorptance by these correlations. From these results, it may be concluded that use of the Tien and Lowder's correlation should be avoided at lower pressures, but its use is

justified (at moderate and high pressures) to gases whose spectral behavior can be described by the regular Elsassner band model. For all pressures and path length conditions, use of the Cess and Tiwari's correlations could be made to gases with bands of highly overlapping lines. In a more realistic problem involving flow of an absorbing emitting gas, results of different correlations (except the Tien and Lowder's correlation) differ from each other by less than 6% for all pressures and path lengths. Use of Tien and Lowder's correlations is justified for gases like CO at moderate and high pressures. For gases like CO₂, use of any other correlation is recommended. While Felske and Tien's correlation is useful for all pressures and path lengths to gases having random band structure. Tiwari and Batki's simple correlation could be employed to gases with regular or random band structure but for $P > 1.0$ atm.

3. RADIATIVE FLUX EQUATIONS

For many engineering and astrophysical applications, the radiative transfer equations are formulated for one-dimensional planar systems (Fig. 3.1). For diffuse boundaries and in the absence of scattering, expressions for the radiative flux and its derivative are given as [8]

$$q_{R\lambda}(\tau_\lambda) = 2 B_{1\lambda} E_3(\tau_\lambda) - 2 B_{2\lambda} E_3(\tau_{0\lambda} - \tau_\lambda) + 2 \left[\int_0^{\tau_\lambda} e_{b\lambda}(t) E_2(\tau_\lambda - t) dt - \int_{\tau_\lambda}^{\tau_{0\lambda}} e_{b\lambda}(t) E_2(t - \tau_\lambda) dt \right] \quad (3.1)$$

and

$$-\frac{dq_{R\lambda}}{d\tau_\lambda} = 2 B_{1\lambda} E_2(\tau_\lambda) + 2 B_{2\lambda} E_2(\tau_{0\lambda} - \tau_\lambda) + 2 \left[\int_0^{\tau_{0\lambda}} e_{b\lambda}(t) E_1(|\tau_\lambda - t|) dt - 1 \right] e_{b\lambda}(\tau_\lambda) \quad (3.2)$$



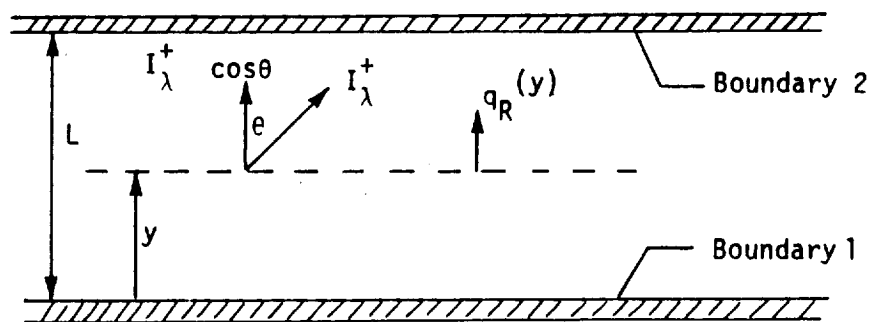


Figure 3.1 Plane radiating layer between parallel boundaries.

where

$$\tau_\lambda = \int_0^y k_\lambda dy, \quad \tau_{0\lambda} = \int_0^L k_\lambda dy \quad (3.3a)$$

$$E_n(t) = \int_0^1 \mu^{n-2} e^{-t/\mu} d\mu \quad (3.3b)$$

In the preceding equations, $E_n(t)$ are the exponential integral functions, and τ_λ and $\tau_{0\lambda}$ represent the optical coordinate and optical path, respectively. The quantities $B_{1\lambda}$ and $B_{2\lambda}$ represent the spectral surface radiosities and for nonreflecting surfaces, $B_{1\lambda} = e_{1\lambda} = \epsilon_{1\lambda} e_{b1\lambda}$ etc. Thus, for non-reflecting boundaries, Eqs. (3.1) and (3.2) are expressed in terms of the wave number as (see Appendix A)

$$q_{R\omega}(\tau_\omega) = e_{1\omega} - e_{2\omega} + 2 \left[\int_0^{\tau_\omega} F_{1\omega}(t) E_2(\tau_\omega - t) dt - \int_{\tau_\omega}^{\tau_{0\omega}} F_{2\omega}(t) E_2(t - \tau_\omega) dt \right] \quad (3.4)$$

and

$$-\frac{dq_{R\omega}}{d\tau_\lambda} = -2 [F_{1\omega}(\tau_\omega) + F_{2\omega}(\tau_\omega)] + 2 \left[\int_0^{\tau_\omega} F_{1\omega}(t) E_1(\tau_\omega - t) dt + \int_{\tau_\omega}^{\tau_{0\omega}} F_{2\omega}(t) E_1(t - \tau_\omega) dt \right] \quad (3.5)$$

where

$$F_{1\omega}(t) = e_\omega(t) - e_{1\omega}; \quad F_{2\omega}(t) = e_\omega(t) - e_{2\omega}$$

Equations (3.4) and (3.5) are the general equations for one-dimensional absorbing-emitting medium with diffuse non-reflecting boundaries. For nongray analyses, it is often convenient to replace the exponential integrals by

appropriate exponential functions [6, 8]. Upon employing the exponential kernel approximation [8]

$$E_2(t) = \frac{3}{4} \exp\left(-\frac{3}{2} t\right); E_1(t) = \frac{9}{8} \exp\left(-\frac{3}{2} t\right)$$

Eqs. (3.4) and (3.5) are expressed in physical coordinates as

$$\begin{aligned} q_{R\omega}(y) &= e_{1\omega} - e_{2\omega} \\ &+ \frac{3}{2} \int_0^y F_{1\omega}(z) k_{\omega} \exp\left[-\frac{3}{2} k_{\omega}(y-z)\right] dz \\ &- \frac{3}{2} \int_y^L F_{2\omega}(z) k_{\omega} \exp\left[-\frac{3}{2} k_{\omega}(z-y)\right] dz \end{aligned} \quad (3.6)$$

$$\begin{aligned} -\frac{dq_{R\omega}}{dy} &= -2 [F_{1\omega}(y) + F_{2\omega}(y)] \\ &+ \frac{9}{4} \int_0^y F_{1\omega}(z) k_{\omega}^2 \exp\left[-\frac{3}{2} k_{\omega}(y-z)\right] dz \\ &+ \frac{9}{4} \int_y^L F_{2\omega}(z) k_{\omega}^2 \exp\left[-\frac{3}{2} k_{\omega}(z-y)\right] dz \end{aligned} \quad (3.7)$$

where z is a dummy variable for y . However, by differentiating Eq. (3.6) directly, there is obtained

$$\begin{aligned} -\frac{dq_{R\omega}}{dy} &= -\frac{3}{2} k_{\omega} [F_{1\omega}(y) + F_{2\omega}(y)] \\ &+ \frac{9}{4} \int_0^y F_{1\omega}(z) k_{\omega}^2 \exp\left[-\frac{3}{2} k_{\omega}(y-z)\right] dz \\ &+ \frac{9}{4} \int_y^L F_{2\omega}(z) k_{\omega}^2 \exp\left[-\frac{3}{2} k_{\omega}(z-y)\right] dz \end{aligned} \quad (3.8)$$

The slight difference in Eqs. (3.7) and (3.8) should be noted. This is a consequence of using the exponential kernel approximation. If one has to make a decision as which equation to use, it is recommended to use Eq. (3.8).

The total band absorptance, as given by Eq. (2.2), can be expressed in a slightly different form as

$$A(y) = \int_0^{\infty} [1 - \exp(-k_{\omega} y)] d\omega \sim \text{cm}^{-1} \quad (3.9a)$$

where both k_{ω} and ω have units of cm^{-1} . Differentiation of Eq. (3.9a) gives

$$A'(y) = \int_0^{\infty} k_{\omega} \exp(-k_{\omega} y) d\omega \sim \text{cm}^{-2} \quad (3.9b)$$

and

$$A''(y) = \int_0^{\infty} -k_{\omega}^2 \exp(-k_{\omega} y) d\omega \sim \text{cm}^{-3} \quad (3.9c)$$

Equations (3.9) are employed to express Eqs. (3.6) and (3.8) in terms of the band absorptance.

The total radiative flux is given by

$$q_R(y) = \int_0^{\infty} q_{R\omega}(y) d\omega \quad (3.10)$$

such that

$$\frac{dq_R(y)}{dy} = \int_0^{\infty} \frac{dq_{R\omega}}{dy} d\omega = \frac{d}{dy} \int_0^{\infty} q_{R\omega} d\omega \quad (3.11)$$

Upon substituting Eq. (3.6) into Eq. (3.10) and Eq. (3.8) into Eq. (3.11) there is obtained for a multiband gaseous system

$$\begin{aligned}
 q_R(y) &= e_1 - e_2 \\
 &+ \frac{3}{2} \sum_{f=1}^n \int_{\Delta\omega_f} \left(\int_0^y F_{1\omega_f}(z) k_{\omega_f} \exp\left[-\frac{3}{2} k_{\omega_f}(y-z)\right] dz \right. \\
 &- \left. \int_y^L F_{2\omega_f}(z) k_{\omega_f} \exp\left[-\frac{3}{2} k_{\omega_f}(z-y)\right] dz \right) d\omega_f \quad (3.12)
 \end{aligned}$$

$$\begin{aligned}
 -\frac{dq_R(y)}{dy} &= -\frac{3}{2} \sum_{f=1}^n \int_{\Delta\omega_f} k_{\omega_f} [F_{1\omega_f}(y) + F_{2\omega_f}(y)] d\omega_f \\
 &+ \frac{9}{4} \sum_{f=1}^n \int_{\Delta\omega_f} \left(\int_0^y F_{1\omega_f}(z) k_{\omega_f}^2 \exp\left[-\frac{3}{2} k_{\omega_f}(y-z)\right] dz \right. \\
 &\quad \left. + \int_y^L F_{2\omega_f}(z) k_{\omega_f}^2 \exp\left[-\frac{3}{2} k_{\omega_f}(z-y)\right] dz \right) d\omega_f \quad (3.13)
 \end{aligned}$$

It should be pointed out that the following relations have been used in obtaining Eqs. (3.12) and (3.13)

$$\int_0^{\infty} e_{1\omega} d\omega = e_1; \quad \int_0^{\infty} e_{2\omega} d\omega = e_2$$

$$\begin{aligned}
 &\int_0^{\infty} \left(\int_0^y F_{1\omega}(z) k_{\omega} \exp\left[-\frac{3}{2} k_{\omega}(y-z)\right] dz \right) d\omega \\
 &= \sum_{f=1}^n \int_{\Delta\omega_f} \left(\int_0^y F_{1\omega_f}(z) k_{\omega_f} \exp\left[-\frac{3}{2} k_{\omega_f}(y-z)\right] dz \right) d\omega_f
 \end{aligned}$$

where n represents the number of bands in a multiband system.

By utilizing the definitions of the band absorptance and its derivatives as given by Eqs. (3.9) and evaluating the value of the Planck function at the center of each band, Eqs. (3.12) and (3.13) are expressed as

$$\begin{aligned}
 q_R(y) = & e_1 - e_2 \\
 & + \frac{3}{2} \sum_{i=1}^n \left\{ \int_0^y F_{1\omega_{0i}}(z) A'_i \left[\frac{3}{2} (y-z) \right] dz \right. \\
 & \quad \left. - \int_y^L F_{2\omega_{0i}}(z) A'_i \left[\frac{3}{2} (z-y) \right] dz \right\} \quad (3.14)
 \end{aligned}$$

$$\begin{aligned}
 \frac{dq_R(y)}{dy} = & \frac{3}{2} \sum_{i=1}^n \left\{ [F_{1\omega_{0i}}(y) + F_{2\omega_{0i}}(y)] \int_{\Delta\omega_i} k_{\omega_i} d\omega_i \right\} \\
 & + \frac{9}{4} \sum_{i=1}^n \left\{ \int_0^y F_{1\omega_{0i}}(z) A''_i \left[\frac{3}{2} (y-z) \right] dz \right. \\
 & \quad \left. + \int_y^L F_{2\omega_{0i}}(z) A''_i \left[\frac{3}{2} (z-y) \right] dz \right\} \quad (3.15)
 \end{aligned}$$

where ω_{0i} represents the center of the i th band.

Equations (3.14) and (3.15) are in proper form for obtaining the nongray solutions of molecular species. However, in order to be able to use the band model correlations, these equations must be transformed in terms of the correlation quantities defined in Eq. (2.4). The following quantities, therefore, are needed for the transformation

$$u = (S/A_0) py; \quad u_0 = (S/A_0) PL; \quad PS = \int_{\Delta\omega} k_{\omega} d\omega \quad (3.16)$$

Now, by using the definition $\bar{A} = A/A_0$, Eq. (3.9b) is written as

$$\bar{A}'(y) = \frac{d}{dy} [\bar{A}(y)] = \frac{1}{A_0} \frac{dA(y)}{dy} = A'(y)/A_0 \sim \text{cm}^{-1}$$

Thus,

$$A'(y) = A_0 \frac{d\bar{A}(y)}{dy} = A_0 \left[\frac{d\bar{A}(u)}{du} \frac{du}{dy} \right] = P S(T) \bar{A}'(u) \quad (3.17a)$$

Similarly

$$A''(y) = [P S(T)]^2 (1/A_0) \bar{A}''(u) \quad (3.17b)$$

The dimensions of both sides in Eqs. (3.17a) and (3.17b) agree with the dimensions given in Eqs. (3.9b) and (3.9c). By employing the definitions of Eqs. (3.16) and (3.17), Eqs. (3.14) and (3.15) are expressed as

$$\begin{aligned} q_R(u) = e_1 - e_2 \\ + \frac{3}{2} \sum_{f=1}^n A_{0f} \left\{ \int_0^{u_f} F_{1\omega_f}(u'_f) \bar{A}'_f \left[\frac{3}{2} (u_f - u'_f) \right] du'_f \right. \\ \left. - \int_{u_f}^{u_{0f}} F_{2\omega_f}(u'_f) \bar{A}'_f \left[\frac{3}{2} (u'_f - u_f) \right] du'_f \right\} \end{aligned} \quad (3.18)$$

$$\begin{aligned} \frac{dq_R(u)}{du} = \frac{3}{2} \sum_{f=1}^n A_{0f} [F_{1\omega_f}(u) + F_{2\omega_f}(u)] \\ + \frac{9}{4} \sum_{f=1}^n A_{0f} \left\{ \int_0^{u_f} F_{1\omega_f}(u') \bar{A}''_f \left[\frac{3}{2} (u_f - u'_f) \right] du'_f \right. \\ \left. + \int_{u_f}^{u_{0f}} F_{2\omega_f}(u') \bar{A}''_f \left[\frac{3}{2} (u'_f - u_f) \right] du'_f \right\} \end{aligned} \quad (3.19)$$

where u' is the dummy variable for u and $\bar{A}'(u) = d\bar{A}/du$. It should be noted that $F_{1\omega_f}$ and $F_{2\omega_f}$ in Eqs. (3.18) and (3.19) represent the values of

$F_{1\omega}$ and $F_{2\omega}$ at the center of the i th band, and $dq_R/dy = (dq_R/du)(du/dy) = [P S(T)/A_0] (dq_R/du)$.

By defining the new independent variables as

$$\xi = u/u_0 = y/L; \xi' = u'/u_0 = z/L \quad (3.20)$$

Eqs. (3.18) and (3.19) can be expressed as

$$\begin{aligned} q_R(\xi) = & e_1 - e_2 \\ & + \frac{3}{2} \sum_{i=1}^n A_{0i} u_{0i} \left(\int_0^{\xi} F_{1\omega_i}(\xi') \bar{A}'_i \left[\frac{3}{2} u_{0i} (\xi - \xi') \right] d\xi' \right. \\ & \left. - \int_{\xi}^1 F_{2\omega_i}(\xi') \bar{A}'_i \left[\frac{3}{2} u_{0i} (\xi' - \xi) \right] d\xi' \right) \end{aligned} \quad (3.21)$$

$$\begin{aligned} \frac{dq_R(\xi)}{d\xi} = & \frac{3}{2} \sum_{i=1}^n \left([F_{1\omega_i}(\xi) + F_{2\omega_i}(\xi)] (A_{0i} u_{0i}) \right) \\ & + \frac{9}{4} \sum_{i=1}^n A_{0i} u_{0i}^2 \left(\int_0^{\xi} F_{1\omega_i}(\xi') \bar{A}''_i \left[\frac{3}{2} u_{0i} (\xi - \xi') \right] d\xi' \right. \\ & \left. + \int_{\xi}^1 F_{2\omega_i}(\xi') \bar{A}''_i \left[\frac{3}{2} u_{0i} (\xi' - \xi) \right] d\xi' \right) \end{aligned} \quad (3.22)$$

where again $\bar{A}'(u)$ denotes the derivative of $A(u)$ with respect to u , and $dq_R/du = (dq_R/d\xi) (d\xi/du) = (1/u_0) (dq_R/d\xi)$.

Equations (3.18) through (3.22) allow us to make use of the band model correlations for the wide-band absorptance because these correlations are expressed in terms of u and β . However, it is often desirable and convenient to express the relations for q_R and $\text{div } q_R$ which only involve $\bar{A}(u)$ and $\bar{A}'(u)$ but not $\bar{A}''(u)$. This is accomplished by integrating the

integrals in the expressions for q_R and $\text{div } q_R$ by parts. This results in simpler integrals. Upon performing the integration by parts on the integrals in Eqs. (3.21) and (3.22), the equations can be expressed in alternate forms as (see Appendix B)

$$\begin{aligned}
 q_R(\xi) = & e_1 - e_2 \\
 & + \sum_{f=1}^n A_{of} \left\{ \int_0^{\xi} [de_{\omega_f}(\xi')/d\xi'] \bar{A}_f \left[\frac{3}{2} u_{of}(\xi-\xi') \right] d\xi' \right. \\
 & \left. + \int_{\xi}^1 [de_{\omega_f}(\xi')/d\xi'] \bar{A}_f \left[\frac{3}{2} u_{of}(\xi'-\xi) \right] d\xi' \right\} \quad (3.23)
 \end{aligned}$$

$$\begin{aligned}
 \frac{dq_R(\xi)}{d\xi} = & \frac{3}{2} \sum_{f=1}^n A_{of} u_{of} \left\{ \int_0^{\xi} [de_{\omega_f}(\xi')/d\xi'] \bar{A}_f \left[\frac{3}{2} u_{of}(\xi-\xi') \right] d\xi' \right. \\
 & \left. - \int_{\xi}^1 [de_{\omega_f}(\xi')/d\xi'] \bar{A}_f \left[\frac{3}{2} u_{of}(\xi'-\xi) \right] d\xi' \right\} \quad (3.24)
 \end{aligned}$$

It should be noted that Eq. (3.24) can be obtained directly by differentiating Eq. (3.23) with respect to ξ using the Leibnitz formula. This is shown in Appendix B.

Equations(3.21), (3.23), and (3.24) are the most convenient equations to use when employing the band-model correlations in radiative transfer analyses.

4. BASIC FORMULATION FOR TRANSIENT PROCESSES

The interaction of radiation in transient transfer processes has received very little attention in the literature. Yet, the transient approach appears to be the logical way of formulating a problem in general sense for elegant numerical and computational solutions. The steady-state solutions can be obtained as limiting solutions for large times.

A few studies available on radiative interactions reveal that the transient behavior of a physical system can be influenced significantly in the presence of radiation [42-45]. Lick investigated the transient energy transfer by radiation and conduction through a semi-finite medium [42]. A kernel substitution technique was used to obtain analytic solutions and display the main features and parameters of the problem. Doornink and Hering studied the transient radiative transfer in a stationary plane layer of a nonconducting medium bounded by black walls [43]. A rectangular Milne-Eddington type relation was used to describe the frequency dependence of the absorption coefficient. It was found that the cooling of the layer initially at a uniform temperature is strongly dependent on the absorption coefficient model employed. Larson and Viskanta investigated the problem of transient combined laminar free convection and radiation in a rectangular enclosure [44]. It was demonstrated that the radiation dominates the heat transfer in the enclosure and alters the convective flow patterns significantly. The transient heat exchange between a radiation^{or} plate and a high-temperature gas flow was investigated by Melnikov and Sukhovich [45]. Only the radiative interaction from the plate was considered; the gas was treated as a non-participating medium. It was proved that the surface temperature is a function of time and of longitudinal coordinate.

The objective of this study is to investigate the interaction of nongray radiation in transient transfer processes in a general sense. Attention, however, will be directed first to a simple problem of the transient radiative exchange between two parallel plates. In subsequent studies, the present analysis and numerical techniques will be extended to include the flow of homogeneous, nonhomogeneous, and chemically reacting species in one- and multi-dimensional systems.

The physical model considered for the present study is the transient energy transfer by radiation in absorbing-emitting gases bounded by two parallel gray plates (Fig. 4.1). In general, T_1 and T_2 can be a function of time and position and there may exist an initial temperature distribution in the gas. It is assumed that the radiative energy transfer in the axial direction is negligible in comparison to that in the normal direction.

For radiation participating medium, the equations expressing conservation of mass and momentum remain unaltered, while the conservation of energy, in general, is expressed as [8]

$$\rho c_p \frac{DT}{Dt} = \text{div} (k \text{ grad } T) + \beta T \frac{DP}{Dt} + \mu \phi - \text{div } q_R \quad (4.1)$$

where β is the coefficient of thermal expansion of the fluid and ϕ is the Rayleigh dissipation function. For a semi-infinite medium capable of transferring energy only by radiation and conduction, Eq. (4.1) reduces to

$$\rho c_p \frac{\partial T}{\partial t} = - \frac{\partial q}{\partial y} \quad (4.2)$$

where q is the sum of the conductive heat flux $q_c = -k (\partial T / \partial y)$ and the radiative flux q_R . For the physical model where radiation is the only mode of energy transfer, the energy equation can be written as

1951

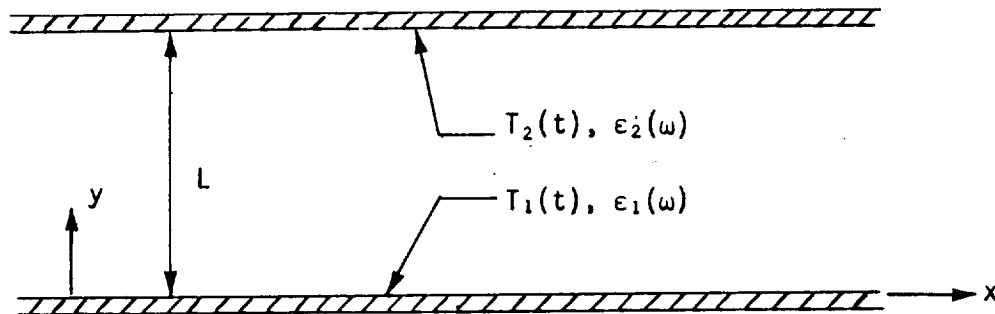


Figure 4.1 Physical model and coordinate system.

$$\rho c_p \frac{\partial T}{\partial t} = - \frac{\partial q_R}{\partial y} \quad (4.3)$$

Use of this simplified equation is made to investigate the transient behavior of a radiation participating medium.

As pointed out in the previous section (Sec. 3), Eqs. (3.21) and (3.23) are convenient equations for the radiative flux. Equations (3.22) and (3.24) are two expressions for the $\text{div } q_R(y)$, but Eq. (3.24) is preferred because it only involves the first derivative of \bar{A} and avoids singularities in the large path length limit.

Upon defining nondimensional radiative heat flux by

$$Q(\xi, t) = q_R(\xi, t) / [e_1(t) - e_2(t)] \quad (4.4)$$

Eq. (3.21) can be written as

$$Q(\xi, t) = 1 + \frac{3}{2} \sum_{i=1}^n A_{oi} u_{oi} \left(\int_0^{\xi} \zeta_{1i}(\xi', t) \bar{A}'_i \left[\frac{3}{2} u_{oi}(\xi - \xi') \right] d\xi' - \int_{\xi}^1 \zeta_{2i}(\xi', t) \bar{A}'_i \left[\frac{3}{2} u_{oi}(\xi' - \xi) \right] d\xi' \right) \quad (4.5)$$

where

$$\zeta_i(\xi, t) = F_{\omega i}(\xi, t) / [e_1(t) - e_2(t)]$$

dimensional $\Rightarrow A_{oi} \zeta_i$ is nondimensional

Note:
 $F_{\omega i} \sim e_{\omega}(T) \sim \text{Watts-cm}^{-2}$
 $A_{oi} \sim \text{cm}^{-1}$
 $e_1, e_2 \sim \text{Watts-cm}^{-2}$

Equation (4.5) provides the general expression for the radiative flux in the nondimensional form. A similar nondimensional form can be obtained also from Eq. (3.23).

By defining $\phi(\xi, t) = T(\xi, t) / T_0$ with T_0 representing some constant reference temperature, Eqs. (4.3) and (3.24) can be combined to yield the energy equation in nondimensional form as

$$\begin{aligned}
 -\partial\phi(\xi, t)/\partial t = & \frac{9}{4} \sum_{i=1}^n \left\{ \int_0^{\xi} \psi_{\omega i}(\xi', t) \bar{A}'_i \left[\frac{3}{2} u_{oi}(\xi - \xi') \right] d\xi' \right. \\
 & \left. - \int_{\xi}^1 \psi_{\omega i}(\xi', t) \bar{A}'_i \left[\frac{3}{2} u_{oi}(\xi' - \xi) \right] d\xi' \right\} \quad (4.6)
 \end{aligned}$$

where

$$\psi_{\omega i}(\xi, t) = \{PS_i(T) [\partial e_{\omega i}(\xi, t)/\partial \xi] / (\rho C_p T_0/t_m)\} \Leftarrow \text{Nondimensional}$$

The time t in Eq. (4.6) is defined as $t^* = t/t_m$ with t_m representing some characteristic time scale of the physical problem; however, for the sake of convenience, the asterisk is left out here as well as in further developments. From the definitions of $\phi(\xi, t)$ and $\psi_{\omega i}(\xi, t)$, it should be noted that Eq. (4.6) is a nonlinear equation in $T(\xi, t)$. Equation (4.6), therefore, represents a general case of the transient energy ^{transfer} by radiation between two semi-infinite parallel plates. A similar expression can be obtained also by combining Eqs. (4.3) and (3.22). ←

5. A SPECIAL CASE OF TRANSIENT INTERACTION

As a special case, it is assumed that the entire system initially is at the fixed (reference) temperature T_0 . For all time, the temperature of the upper plate is maintained at the constant temperature equal to the reference temperature, i.e., $T_2 = T_0$. The temperature of the lower plate is suddenly decreased to a lower but constant temperature, i.e., $T_1 < T_2$. The problem, therefore, is to investigate the transient cooling rate of the gas for a step change in temperature of the lower plate.

Since small temperature differences have been assumed and the absorption coefficient has been taken as independent of temperature one may employ additionally the linearization, employ

$$e_{\omega_i}(T) - e_{\omega_i}(T_w) = (d e_{\omega_i}/dT)_{T_w} (T - T_w) \quad (5.1)$$

where again the subscript i refers to the i th band such that ω_i is the wave number location of the band and T_w represents the temperature of the reference wall which could be either T_1 or T_2 . For the special case considered, since we are interested in investigating the transient behavior of the gas because of a step change in temperature of the lower plate, T_w is taken to be equal to T_1 . Thus,

$$e_{\omega_i}(\xi, t) - e_{\omega_i}(0, t) = (d e_{\omega_i}/dT)_{T_1} (T - T_1) \quad (5.2a)$$

$$e_{\omega_i}(1, t) - e_{\omega_i}(0, t) = (d e_{\omega_i}/dT)_{T_1} (T_2 - T_1) \quad (5.2b)$$

$$e_{\omega_i}(\xi, t) - e_{\omega_i}(1, t) = (d e_{\omega_i}/dT)_{T_1} (T - T_2) \quad (5.2c)$$

Note that Eq. (5.2c) is obtained by subtracting Eq. (5.2b) from Eq. (5.2a). Also, for linearized radiation,

$$T^4 = 4 T_1^3 T - 3 T_1^4 \quad (5.3)$$

Thus, $e_1 = \sigma T_1^4$, $e_2 = \sigma T_2^4 = \sigma (4 T_1^3 T_2 - 3 T_1^4)$ such that $e_1 - e_2 = 4 \sigma T_1^3 (T_1 - T_2)$.

It should be pointed out that for a single-band gas, the linearization is not required because the temperature distribution can be obtained either by combining Eqs. (3.22) and (4.3) or from Eq. (4.6) and the radiative heat flux can be calculated from Eqs. (3.21), (3.23), or (4.5). However, for the case of multiband gases and for systems involving mixtures of gases, it is convenient to employ the linearization procedure in order to use the information on band model correlations. The following definitions are useful

in expressing the governing equations in linearized forms:

$$\theta = (T - T_1) / (T_2 - T_1) \quad (5.4a)$$

$$N_{1f} = (P t_m / \rho c_p) K_{1f}, \quad K_{1f} = S_f(T) (d e_{\omega f} / dT)_{T_1} \quad (5.4b)$$

$$N_1 = (P t_m / \rho c_p) K_1, \quad K_1 = \sum_{f=1}^n K_{1f} \quad (5.4c)$$

$$M_{1f} = (t_m / L \rho c_p) H_{1f}, \quad H_{1f} = A_{of}(T) (d e_{\omega f} / dT)_{T_1} \quad (5.4d)$$

$$M_1 = (t_m / L \rho c_p) H_1, \quad H_1 = \sum_{f=1}^n H_{1f} \quad (5.4e)$$

$$M_{1f} u_{of} = N_{1f}, \quad u_{of} H_{1f} = PL K_{1f} \quad (5.4f)$$

where H_1 , K_1 , N_1 and M_1 represent the values of H , K , N and M evaluated at the temperature T_1 . As explained in Refs. 8 and 23, these quantities represent the properties of the gaseous medium.

By employing the definitions of Eqs. (5.2) - (5.4), relations for the radiative flux, as given by Eqs. (3.21) and (3.23), are expressed as

$$Q(\xi, t) = 1 - (3/8 \sigma T_1^3) \sum_{f=1}^n u_{of} H_{1f} \left\{ \int_0^\xi \theta(\xi', t) \bar{A}_f' \left[\frac{3}{2} u_{of} (\xi - \xi') \right] d\xi' \right. \\ \left. + \int_\xi^1 [1 - \theta(\xi', t)] \bar{A}_f' \left[\frac{3}{2} u_{of} (\xi' - \xi) \right] d\xi' \right\} \leftarrow \text{Nondimensional} \quad (5.5a)$$

Note:
 $\left. \begin{array}{l} H_{1f} / (\sigma T_1^3) \\ \text{is nondimensional} \end{array} \right\}$

and

$$Q(\xi, t) = 1 - (1/4 \sigma T_1^3) \sum_{f=1}^n H_{1f} \left\{ \int_0^\xi \frac{\partial \theta(\xi', t)}{\partial \xi'} \bar{A}_f' \left[\frac{3}{2} u_{of} (\xi - \xi') \right] d\xi' \right. \\ \left. + \int_\xi^1 \frac{\partial \theta(\xi', t)}{\partial \xi'} \bar{A}_f' \left[\frac{3}{2} u_{of} (\xi' - \xi) \right] d\xi' \right\} \leftarrow \text{Nondimensional}$$

$$- \int_{\xi}^1 \frac{\partial \theta(\xi', t)}{\partial \xi'} \bar{A}_f \left[\frac{3}{2} u_{of} (\xi' - \xi) \right] d\xi' \quad (5.5b)$$

Thus, the expressions for the heat flux at the lower wall are given by

$$Q(0, t) = 1 - (3/8 \sigma T_1^3) \sum_{f=1}^n u_{of} H_{1f} \int_0^1 [1 - \theta(\xi', t)] \bar{A}_f \left(\frac{3}{2} u_{of} \xi' \right) d\xi' \quad (5.6a)$$

and

$$Q(0, t) = 1 + (1/4 \sigma T_1^3) \sum_{f=1}^n H_{1f} \int_0^1 \frac{\partial \theta(\xi', t)}{\partial \xi'} \bar{A}_f \left(\frac{3}{2} u_{of} \xi' \right) d\xi' \quad (5.6b)$$

⊆ Note: $H_{1f} / (\sigma T_1^3)$
is nondimensional

It should be pointed out that Eqs. (5.5a) and (5.6a) are convenient forms for the optically thin and general solutions while Eqs. (5.5b) and (5.6b) are useful for solutions in the large path length limit. Once the solutions for $\theta(\xi, t)$ are known from the energy equation, the appropriate relations for the heat flux can be obtained from Eqs. (5.5) and (5.6).

By employing the definitions of Eqs. (5.2) - (5.4), a combination of Eqs. (3.22) and (4.3) provides one form of the energy equation and Eq. (4.6) is transformed to obtain another form; these are expressed as

$$\begin{aligned} \frac{\partial \theta(\xi, t)}{\partial t} + 3 N_1 \theta(\xi, t) - \frac{3}{2} N_1 &= \\ &= - \frac{9}{4} \sum_{f=1}^n M_{1f} u_{of}^2 \left(\int_0^{\xi} \theta(\xi', t) \bar{A}_f' \left[\frac{3}{2} u_{of} (\xi - \xi') \right] d\xi' \right) \\ &+ \int_{\xi}^1 [\theta(\xi', t) - 1] \bar{A}_f' \left[\frac{3}{2} u_{of} (\xi' - \xi) \right] d\xi' \quad \Leftarrow \text{Nondimensional (5.7a)} \end{aligned}$$

Note:
 N_1 is nondimensional
 M_{1f} is nondimensional

and

$$- \frac{\partial \theta(\xi, t)}{\partial t} = \frac{3}{2} \sum_{f=1}^n N_{1f} \left(\int_0^{\xi} \frac{\partial \theta(\xi', t)}{\partial \xi'} \bar{A}_f' \left[\frac{3}{2} u_{of} (\xi - \xi') \right] d\xi' \right)$$

Note:
 N_{1f} is nondimensional

$$- \int_{\xi}^1 \frac{\partial \theta(\xi', t)}{\partial \xi'} \bar{A}'_1 \left[\frac{3}{2} u_{01} (\xi' - \xi) \right] d\xi' \quad \leftarrow \text{Non dimensional} \quad (5.7b)$$

The initial and boundary conditions for Eq. (5.7) are specified as

$$\theta(\xi, 0) = 1 ; \theta(0, t) = 0 ; \theta(1, t) = 1 \quad (5.8)$$

The parameters in Eq. (5.7) are N_1 and u_0 . For a given gas, the parameters are the gas pressure and the temperature of the lower wall. Equation (5.7b) is the convenient form for solutions in the large path length limit.

6. METHOD OF SOLUTIONS

For the general case, the temperature distribution is obtained from the solution of the energy equation, Eqs. (5.7). Once $\theta(\xi, t)$ is known, the radiative heat flux is calculated by using the appropriate form of Eq. (5.6). Before discussing the solution procedure for the general case, however, it is desirable to obtain the limiting forms of Eqs. (5.5) and (5.7) in the optically thin and large path length limits and investigate the solutions of resulting equations.

6.1 Optically Thin Limit

In the optically thin limit [8, 23], $\bar{A}(u) \left. \vphantom{\bar{A}(u)} \right\} = u$, $\bar{A}'(u) = 1$, and $\bar{A}''(u) = 0$. In this limit, therefore, Eq. (5.7a) reduces to \leftarrow

$$\frac{\partial \theta(\xi, t)}{\partial t} + 3 N_1 \theta(\xi, t) - \frac{3}{2} N_1 = 0 \quad (6.1a)$$

From an examination of Eq. (6.1a) along with the definitions given in Eq. (5.4), it is evident that in the optically thin limit the temperature distribution in the medium is independent of the ξ -coordinate. This is a characteristic of the optically thin radiation [8, 23]. Thus, Eq. (6.1a) can

be written as

$$\frac{d\theta(t)}{dt} + 3 N_1(t) \theta(t) - \frac{3}{2} N_1(t) = 0; \theta(\xi, 0) = 1 \quad (6.1b)$$

Since gas properties are evaluated at known reference conditions, N_1 is essentially constant, and solution of Eq. (6.1b) is found to be

$$\theta(t) = \frac{1}{2}[1 + \exp(-3 N_1 t)] \quad (6.2)$$

In the optically thin limit, Eq. (5.7b) reduces to

$$-\frac{\partial\theta(\xi, t)}{\partial t} = \frac{3}{2} \left(\sum_{i=1}^n N_{1i} \right) \left\{ \int_0^{\xi} \frac{\partial\theta(\xi', t)}{\partial \xi'} d\xi' - \int_{\xi}^1 \frac{\partial\theta(\xi', t)}{\partial \xi'} d\xi' \right\} \quad (6.3a)$$

A differentiation of Eq. (6.3a) with respect to ξ (by using the Leibnitz's rule) results in

$$\frac{\partial}{\partial \xi} \left[\frac{\partial\theta(\xi, t)}{\partial t} + 3 N_1 \theta(\xi, t) \right] = 0 \quad (6.3b)$$

or

$$\frac{\partial\theta(\xi, t)}{\partial t} + 3 N_1 \theta(\xi, t) = C(t) \quad (6.3c)$$

The constant of integration $C(t)$ is evaluated through the combination of Eqs. (5.8) and (6.3a) and is found to be $C(t) = \frac{3}{2} N_1$. A substitution of this in Eq. (6.3c) gives Eq. (6.1a) for which the solution is given by Eq. (6.2). Thus, as would be expected, both general forms of the energy equation reduce to the same equation in the optically thin limit.

In the optically thin limit Eqs. (5.5a) and (5.5b) respectively reduce to

$$Q(\xi, t) = 1 - [3/(8\sigma T_1^3)] (PLK_1) \left\{ \int_0^{\xi} \theta(\xi', t) d\xi' + \int_{\xi}^1 [1-\theta(\xi', t)] d\xi' \right\} \quad (6.4a)$$

and

$$Q(\xi, t) = 1 - [3/8\sigma T_1^3] (PLK_1) \left(\int_0^\xi \frac{\partial \theta}{\partial \xi'} (\xi - \xi') d\xi' + \int_\xi^1 \frac{\partial \theta}{\partial \xi'} (\xi' - \xi) d\xi' \right) \quad (6.4b)$$

Through integration by parts, it can be shown that Eq. (6.4b) reproduces Eq. (6.4a). By noting that, in the optically thin limit, $\theta(\xi, t) = \theta(t)$, Eqs. (6.4) can be expressed as

$$Q(\xi, t) = 1 - [3/(8\sigma T_1^3)] (PLK_1) [(1-\xi) + (2\xi-1)\theta(t)] \quad (6.5)$$

Note: $(PLK_1/\sigma T_1^3)$ is nondimensional

It should be pointed out that Eq. (6.5) can be obtained directly from Eq. (6.4b) without performing the integration by parts. The heat transfer from the lower surface in the optically thin limit, therefore, is given by

$$Q(0, t) = 1 - [3/(8\sigma T_1^3)] (PLK_1) [1 - \theta(t)] \quad (6.6)$$

The result of Eq. (6.6) can be obtained directly by letting $\xi = 0$ in either of Eqs. (6.4). The relation for $\theta(t)$ in Eq. (6.6) is obtained from Eq. (6.2). Thus, evaluation of the temperature distribution and radiative heat flux in the optically thin limit does not require numerical solutions.

6.2 Large Path Length Limit

In the large path length limit (i.e., for $u_{0i} \gg 1$ for each band), one has $\bar{A}(u) = \ln(u)$, $\bar{A}'(u) = 1/u$, and $\bar{A}''(u) = -1/u^2$ [8, 23]. Thus, in the large path length limit, Eq. (5.7a) reduces to

$$\begin{aligned} \frac{\partial \theta(\xi, t)}{\partial t} + 3 N_1 \theta(\xi, t) - \frac{3}{2} N_1 \\ = M_1 \left(\int_0^\xi \theta(\xi', t) \frac{d\xi'}{(\xi - \xi')^2} + \int_\xi^1 [\theta(\xi', t) - 1] \frac{d\xi'}{(\xi' - \xi)^2} \right) \end{aligned} \quad (6.7a)$$

Note: M_1 and N_1 are related, see Eq. (5.4f)

It should be noted that for any fixed value T_1 and a given gas, N_1 and M_1 are

$$N_1 = [PL \sum (S_i/A_{0i})] M_1 = [\sum u_{0i}] M_1$$

constants; but, $\theta(\xi, t)$ does depend on ξ . For a given gas and with known values of T_2 and t_m , the solution of Eq. (6.7a) can be obtained by specifying T_1 . Equation (6.7a) involves singular integrals with Cauchy type kernels and, therefore, a closed form solution does not appear to be possible; numerical solutions, however, can be obtained by the variation of parameter technique. Because of the singular nature of integrals, Eq. (6.7a) is not a convenient equation for the large path length limit solutions.

In the large path length limit, Eq. (5.7b) reduces to

$$\frac{\partial \theta(\xi, t)}{\partial t} = -M_1 \int_0^1 \frac{\partial \theta(\xi', t)}{\partial \xi'} \frac{d\xi'}{(\xi - \xi')} \quad (6.7b)$$

Equation (6.7b) is a convenient form for solution in the large path length limit. An analytical solution of Eq. (6.7b) may be possible, but numerical solution can be obtained quite easily.

In the large path length limit, Eqs. (5.5a) and (5.5b) reduce respectively to

$$Q(\xi, t) = 1 - \underbrace{(1/4\sigma T_1^3)}_{\sigma} H_1 \left[\int_0^1 \theta(\xi', t) \frac{d\xi'}{(\xi - \xi')} - \int_{\xi}^1 \frac{d\xi'}{(\xi - \xi')} \right] \quad (6.8a)$$

Note: $H_1 / (\sigma T_1^3)$
is nondimensional

and

$$Q(\xi, t) = 1 - (1/4\sigma T_1^3) \sum_{i=1}^n H_{1i} \left(\int_0^{\xi} \frac{\partial \theta(\xi', t)}{\partial \xi'} \ln \left[\frac{3}{2} u_{0i}(\xi - \xi') \right] d\xi' + \int_{\xi}^1 \frac{\partial \theta(\xi', t)}{\partial \xi'} \ln \left[\frac{3}{2} u_{0i}(\xi' - \xi) \right] d\xi' \right) \quad (6.8b)$$

Note: M_1 and H_1 are
related by Eq. (5.10)

The expressions for dimensionless radiative heat flux from or to the wall are obtained by setting $\xi = 0$ in Eqs. (6.8) as

$$Q(0,t) = 1 - (H_1/4\sigma T_1^3) \int_0^1 [1 - \theta(\xi',t)] \frac{d\xi'}{\xi'} \quad (6.9a)$$

and

Note: $H_1/\sigma T_1^3$
is nondimensional

$$Q(0,t) = 1 - (1/4\sigma T_1^3) \sum_{i=1}^n H_{1i} \int_0^1 \frac{\partial \theta(\xi',t)}{\partial \xi'} \ln\left(\frac{3}{2} u_{oi} \xi'\right) d\xi' \quad (6.9b)$$

Thus, once the temperature distribution is known from solutions of Eq. (6.7), the wall heat flux can be calculated by using the corresponding form of Eqs. (6.9).

6.3 Numerical Solutions of Governing Equations

General solutions of Eqs. (5.7a) and (5.7b) are obtained numerically by employing the method of variation of parameters. For this, a polynomial form for $\theta(\xi,t)$ is assumed in powers of ξ with time dependent coefficients as

$$\theta(\xi,t) = \sum_{m=0}^n c_m(t) \xi^m \quad (6.10)$$

By considering only the quadratic solution in ξ , and satisfying the boundary conditions of Eq. (5.8), one finds

$$\theta(\xi,t) = \xi^2 + g(t) (\xi - \xi^2) \quad (6.11)$$

where $g(t)$ represents the time dependent coefficient. At $t = 0$, a combination of Eqs. (5.8) and (6.11) yields the result

$$g(0) = (1 - \xi^2)/(\xi - \xi^2) \quad (6.12)$$

Also, from Eq. (6.11) there is obtained

$$\frac{\partial \theta(\xi,t)}{\partial t} = (\xi - \xi^2) \frac{dg(t)}{dt} = (\xi - \xi^2) g'(t) \quad (6.13)$$

and

$$\frac{\partial \theta(\xi, t)}{\partial \xi} = 2 \xi + g(t) (1-2\xi) \quad (6.14)$$

Equations (6.11) - (6.14) are employed to obtain specific solutions of Eqs. (5.5) and (5.7).

By substituting Eqs. (6.11) and (6.13) in Eq. (5.7a), there is obtained

$$g'(t) + G_1(\xi) g(t) = G_2(\xi) \quad (6.15)$$

where the integral functions $G_1(\xi)$ and $G_2(\xi)$ are defined in Appendix C. The solution of Eq. (6.15) is given by

$$g(t) = c \exp[-G_1(\xi)t] + G_2(\xi)/G_1(\xi) \quad (6.16a)$$

Since at $t = 0$, $g(t) = g(0)$, then $c = g(0) - G_2(\xi)/G_1(\xi)$. Thus, Eq. (6.16a) becomes

$$g(t) = [g(0) - G_2(\xi)/G_1(\xi)] \exp[-G_1(\xi)t] + G_2(\xi)/G_1(\xi) \quad (6.16b)$$

where $g(0)$ is given by Eq. (6.12). The integrals in functions $G_1(\xi)$ and $G_2(\xi)$ can be evaluated easily by numerical means, after substituting the relation for $\bar{A}''(u)$.

A substitution of Eqs. (6.11), (6.13) and (6.14) into Eq. (5.7b) results in

$$g'(t) + G_3(\xi) g(t) = G_4(\xi) \quad (6.17)$$

where the integral functions $G_3(\xi)$ and $G_4(\xi)$ are defined in Appendix C. The solution of Eq. (6.17) is found to be

$$g(t) = [g(0) - G_4(\xi)/G_3(\xi)] \exp[-G_3(\xi)t] + G_4(\xi)/G_3(\xi) \quad (6.18)$$

where again $g(0)$ is given by Eq. (6.12).

The solutions of Eqs. (5.7a) and (5.7b) can be expressed in a convenient form as

$$\theta(\xi, t) = \xi^2 + \left[\begin{array}{c} g_1(t) \\ g_2(t) \end{array} \right] (\xi - \xi^2) \quad (6.19)$$

In Eq. (6.19), $g_1(t)$ is given by Eq. (6.16b) and is used for the solution of Eq. (5.7a) and $g_2(t)$ is given by Eq. (6.18) and is used in obtaining the solution of Eq. (5.7b). The both approach should result in the same final solution.

For the steady state case, the solution again is given by Eq. (6.19), but functions $g_1(t)$ and $g_2(t)$ are no longer a function of time and are given by

$$g_1 = G_2(\xi)/G_1(\xi); \quad g_2 = G_4(\xi)/G_3(\xi) \quad (6.20)$$

The solutions for the steady case are available in the literature and are useful in comparing the results of this study in the limit of $t \rightarrow \infty$.

The expressions for the nondimensional radiative flux are obtained from a combination of Eqs. (5.5), (6.11) and (6.14) such that

$$Q(\xi, t) = 1 - G_5(\xi) g_1(t) - G_6(\xi) \quad (6.21a)$$

and

$$Q(\xi, t) = 1 - G_7(\xi) g_2(t) - G_8(\xi) \quad (6.21b)$$

where $G_5(\xi)$ through $G_8(\xi)$ are defined in Appendix C, and $q_1(t)$ and $q_2(t)$ are given respectively by Eqs. (6.16b) and 6.18). Consequently, the expressions for the radiative heat flux at the lower wall are obtained as

$$Q(0,t) = 1 + G_9 q_1(t) - G_{10} \quad (6.22a)$$

and

$$Q(0,t) = 1 + G_{11} g_2(t) + G_{12} \quad (6.22b)$$

where G_9 through G_{12} are defined in Appendix C and are not function of ξ . It should be noted that the solutions presented in Eqs. (6.21) and (6.22) require the solution of the energy equation as given by Eqs. (6.19)

6.4 Numerical Solutions of Large Path Length Equations

As mentioned earlier, Eqs. (6.7b), (6.8b) and (6.9b) are the most appropriate equations to use in the large path length limit. However, numerical procedure is presented for both forms of the energy and radiative flux equations. Once again Eqs. (6.11) through (6.14) provide the basis for numerical solutions also in the large path length limit. For this limit, the solution given by Eq. (6.19) is expressed as

$$\theta(\xi,t) = \xi^2 + \begin{bmatrix} g_3(t) \\ g_4(t) \end{bmatrix} (\xi, \xi^2) \quad (6.23)$$

where $g_3(t)$ is used for the solution of Eq. (6.7a) and $g_4(t)$ for Eq. (6.7b).

A substitution of Eq. (6.23) into Eq. (6.7a) results in

$$g_3'(t) + G_{13}(\xi) g_3(t) = G_{14}(\xi) \quad (6.24)$$

where integral functions $G_{13}(\xi)$ and $G_{14}(\xi)$ are defined in Appendix C. The solution of Eq. (6.24) is found to be

$$g_3(t) = [g(0) - G_{14}(\xi)/G_{13}(\xi)] \exp[-G_{13}(\xi)t] + G_{14}(\xi)/G_{13}(\xi) \quad (6.25)$$

where $g(0)$ is defined again by Eq. (6.12). Equation (6.23) along with Eq. (6.25) provides the solution of the energy equation, Eq. (6.7a).

A combination of Eqs. (6.23) and (6.7b) results in

$$g_4'(t) + G_{15}(\xi) g_4(t) = G_{16}(\xi) \quad (6.26)$$

The integral functions $G_{15}(\xi)$ and $G_{16}(\xi)$ appearing in Eq. (6.26) are defined in Appendix C. These, however, can be evaluated easily with the results

$$G_{15}(\xi) = [M_1/(\xi-\xi^2)](2 + (2\xi-1) \ln[(\xi-1)/\xi]) \quad (6.27a)$$

$$G_{16}(\xi) = 2 [M_1/(\xi-\xi^2)](1 + \xi \ln[(\xi-1)/\xi]) \quad (6.27b)$$

The solution of Eq. (6.26) is found to be

$$g_4(t) = [g(0) - G_{16}(\xi)/G_{15}(\xi)] \exp[-G_{15}(\xi)t] + G_{16}(\xi)/G_{15}(\xi) \quad (6.28)$$

where again $g(0)$ is defined by Eq. (6.12). A combination of Eqs. (6.23), (6.27) and (6.28) provides the solution of the energy equation, Eq. (6.7b). The only parameter appearing in the solution of Eq. (6.7b) is M_1 .

The expressions for the nondimensional heat flux in this case is obtained from a combination of Eqs. (6.8) and (6.23) as

$$Q(\xi, t) = 1 - G_{17}(\xi) g_3(t) - G_{18}(\xi) \quad (6.29a)$$

and
$$Q(\xi, t) = 1 - G_{19}(\xi) g_4(t) - G_{20}(\xi) \quad (6.29b)$$

where $G_{17}(\xi)$ through $G_{20}(\xi)$ are defined in Appendix C and can be evaluated in closed forms. The corresponding expressions for the radiative heat flux at the lower wall are found from Eqs. (6.9) and (6.23) as

$$Q(0, t) = 1 - G_{21} g_3(t) - G_{22} \quad (6.30a)$$

and
$$Q(0,t) = 1 - G_{23} g_4(t) - G_{24} \quad (6.30b)$$

where again G_{21} through G_{24} are defined in Appendix C and are not functions of ξ .

7. RADIATIVE INTERACTION IN LAMINAR FLOWS

The physical system considered is the energy transfer in laminar, incompressible, constant properties, fully-developed flow of absorbing-emitting gases between parallel plates (Fig. 7.1). The condition of uniform surface heat flux for each plate is assumed such that the temperature of the plates varies in the axial direction. Fully developed heat transfer is considered, and axial conduction and radiation is assumed to be negligible as compared with the normal components. Consistent with the constant properties flow, the absorption coefficient is taken to be independent of temperature and radiation can be linearized. Extensive treatment of this problem is available in the literature [23, 41]. The primary motivation of studying the problem here is to investigate the extent of radiative interaction for high temperature flow conditions.

7.1 Basic Formulation

For the physical problem considered, the energy equation, Eq. (4.1), can be expressed as [8]

$$\rho C_p \left(\frac{\partial T}{\partial t} + u \frac{\partial T}{\partial x} + v \frac{\partial T}{\partial y} \right) = k \frac{\partial^2 T}{\partial y^2} + \beta T u \frac{dp}{dx} + u \left(\frac{\partial u}{\partial y} \right)^2 - \text{div} q_R \quad (7.1)$$

where u and v denote x and y components of velocity, respectively. In deriving Eq. (7.1) it has been assumed that the net conduction heat transfer in the x direction is negligible compared with the net conduction in the y direction. This represents the physical condition of a large value of the Peclet number. By an analogous reasoning, the radiative heat transfer in the x direction can be neglected in comparison to that transferred in the y direction. If, in addition, it is assumed that the Eckert number of the

[REDACTED] INTENTIONALLY BLANK

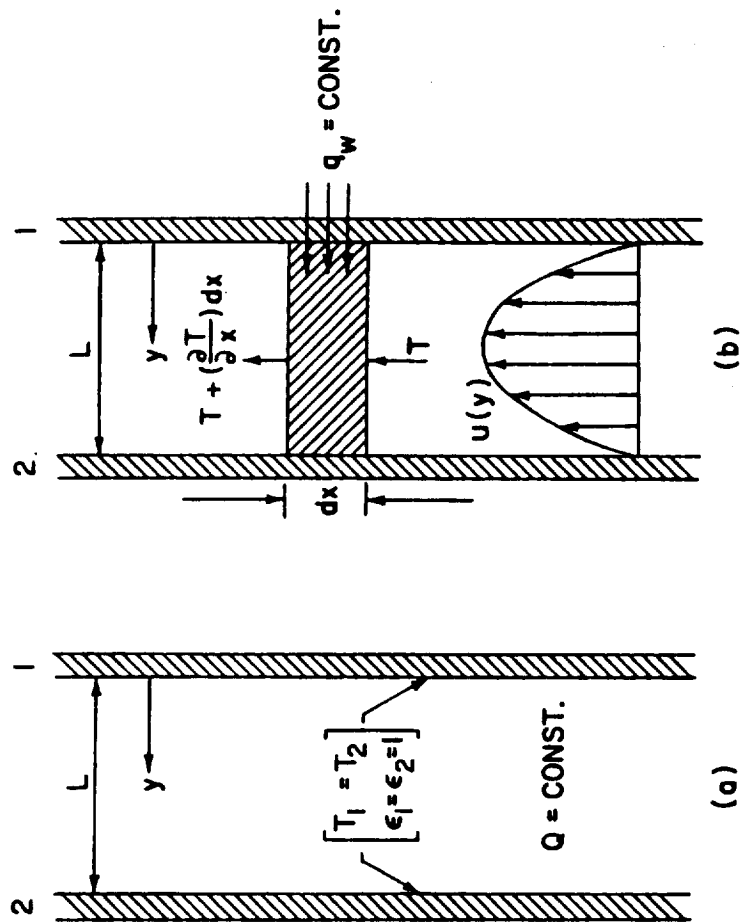


Figure 7.1 Physical model and coordinate systems for flow of radiating gases between parallel plates.

flow is small, then Eq. (7.1) reduces to [8]

$$\frac{\partial T}{\partial t} + u \frac{\partial T}{\partial x} + v \frac{\partial T}{\partial y} = \alpha \frac{\partial^2 T}{\partial y^2} - \frac{1}{\rho C_p} \frac{\partial q_R}{\partial y} \quad (7.2)$$

where $\alpha = (k/\rho C_p)$ represents the thermal diffusivity of the fluid.

For a steady fully-developed flow, $v = 0$, and u is given by the well-known parabolic profile as

$$u = 6 u_m (\xi - \xi^2); \quad \xi = y/L \quad (7.3)$$

where u_m represents the mean fluid velocity. Also, for the flow of a perfect gas with uniform wall heat flux, $\partial T/\partial x$ is constant and is given by

$$\partial T/\partial x = (2\alpha q_w)/(u_m L/k) \quad (7.4)$$

Now, by combining Eqs. (7.2) - (7.4), the energy equation is expressed in nondimensional form as

$$\frac{\partial \theta}{\partial \tau} + 12(\xi - \xi^2) = \frac{\partial^2 \theta}{\partial \xi^2} - \frac{1}{q_w} \frac{\partial q_R}{\partial \xi} \quad (7.5)$$

where

$$\tau = \alpha t/L^2 ; \quad \theta = (T - T_1)/(q_w L/k)$$

The expression for $\partial q_R/\partial \xi$ in Eq. (7.5) is obtained from either Eq. (3.22) or Eq. (3.24).

By assuming that the initial temperature distribution in the gas is

some uniform value $T_0 = T_1$, the initial and boundary conditions for this problem can be expressed as

$$\theta(\xi, 0) = 0 \quad (7.6a)$$

$$\theta(0, \tau) = \theta(1, \tau) = 0 \quad (7.6b)$$

$$\theta_{\xi}(\xi = 1/2) = 0 ; \theta_{\xi}(\xi = 0) = -\theta_{\xi}(\xi = 1) \quad (7.6c)$$

It should be noted that all the boundary conditions given in Eqs. (7.6) are not independent and any two convenient conditions can be used to obtain solutions. Also, the initial temperature distribution can be any specified or calculated value of $\theta(\xi, 0) = f(\xi)$.

For flow problems, the quantity of primary interest is the bulk temperature of the gas, which may be expressed as [41]

$$\theta_b = (T_b - T_1)/(q_w L/k) = 6 \int_0^1 \theta(\xi, \tau) (\xi - \xi^2) d\xi \quad (7.7)$$

The heat transfer q_w is given by the expression, $q_w = h_c (T_1 - T_b)$, where h_c is the convective heat transfer coefficient (W/cm^2-K). In general, the heat transfer results are expressed in terms of the Nusselt number $Nu = h_c D_h/k$. Here, D_h represents the hydraulic diameter, and for the parallel plate geometry it equals twice the plate separation, i.e., $D_h = 2L$. Upon eliminating the convective heat transfer coefficient h_c from the expressions for q_w and Nu , a relation between the Nusselt number and the bulk temperature is obtained as

$$Nu = 2 L q_w / k (T_1 - T_b) = -2/\theta_b \quad (7.8)$$

The heat transfer results, therefore, can be expressed either in terms of Nu or θ_b .

7.1.1 Steady Laminar Flow

For steady-state conditions, $\partial\theta/\partial\tau = 0$ and Eq. (7.5) becomes

$$\theta'' - 12(\xi - \xi^2) = (1/q_w) dq_R/d\xi \quad (7.9)$$

By integrating Eq. (7.9) once and using the conditions that at $\xi = 1/2$, $q_R(\xi)$ and $(d\theta/d\xi)$ are equal to zero, one obtains

$$\theta' - 2(3\xi^2 - 2\xi^3) + 1 = q_R(\xi)/q_w \quad (7.10)$$

The expression for $q_R(\xi)$ in Eq. (7.10) is obtained from either Eq. (3.21) or Eq. (3.23).

For the present physical problem, $e_1 = e_2$ and $F_{1\omega_i} = F_{2\omega_i}$. Thus, for the case of linearized radiation, a combination of Eqs. (3.21), (5.2a), and (7.10) results in

$$\begin{aligned} & \theta' - 2(3\xi^2 - 2\xi^3) + 1 \\ &= \frac{3}{2} (L/k) \sum_{i=1}^n H_{1i} u_{0i} \left\{ \int_0^\xi \theta(\xi') \bar{A}_i' \left[\frac{3}{2} u_{0i} (\xi - \xi') \right] d\xi' \right. \\ & \left. - \int_\xi^1 \theta(\xi') \bar{A}_i' \left[\frac{3}{2} u_{0i} (\xi' - \xi) \right] d\xi' \right\} \end{aligned} \quad (7.11a)$$

A combination of Eqs. (3.23), (5.2a), and (7.10) gives an alternate form of the energy equation for the steady case as

$$\begin{aligned}
\theta' &= 2(3\xi^2 - 2\xi^3) + 1 \\
&= (L/k) \sum_{i=1}^n H_{1i} \left\{ \int_0^\xi (d\theta/d\xi') \bar{A}_i \left[\frac{3}{2} u_{0i}(\xi - \xi') \right] d\xi' \right. \\
&\quad \left. + \int_\xi^1 (d\theta/d\xi') \bar{A}_i \left[\frac{3}{2} u_{0i}(\xi' - \xi) \right] d\xi' \right\} \quad (7.11b)
\end{aligned}$$

Note that this equation can be obtained directly by integrating the left-hand side of Eq. (7.11a) by parts. Equations (7.11) provide two forms of the energy equation for the steady-state conditions.

For the case of negligible radiation, Eqs. (7.11) reduce to

$$\theta' = 2(3\xi^2 - 2\xi^3) - 1 \quad (7.12)$$

The solution of Eqs. (7.12) is found to be

$$\theta(\xi) = \xi(2\xi^2 - \xi^3 - 1) \quad (7.13)$$

Thus, a combination of Eqs. (7.7) and (7.13) gives the result for the bulk temperature for the steady case with no radiation as

$$-\theta_b = 17/70 \quad (7.14)$$

This result is useful in determining the extent of radiative contributions.

7.1.2 Transient Radiative Interactions

For the transient case, a combination of Eqs. (3.22), (5.2a), and (7.5) gives the energy equation for the linearized radiation as

$$\begin{aligned}
\theta_{\xi\xi} - \theta_{\tau} - 3N\theta - 12(\xi - \xi^2) \\
= \frac{9}{4} (L/k) \sum_{i=1}^n H_{1i} u_{0i}^2 \left\{ \int_0^{\xi} \theta(\xi', \tau) \bar{A}_i'' \left[\frac{3}{2} u_{0i}(\xi - \xi') \right] d\xi' \right. \\
\left. + \int_{\xi}^1 \theta(\xi', \tau) \bar{A}_i'' \left[\frac{3}{2} u_{0i}(\xi' - \xi) \right] d\xi' \right\} \quad (7.15a)
\end{aligned}$$

where

$$N = (PL^2/k) K_1 = (PL^2/k) \sum_{i=1}^n S_i(T) (de_{\omega_i}/dT)_{T_1}$$

Note that this definition of N is slightly different than the definition of N_1 in Eq. (5.4c). The dimensionless gas property N characterizes the relative importance of radiation versus conduction within the gas under optically thin conditions [23, 41]. Also, by combining Eqs. (3.24), (5.2a), and (7.5) another form of the transient energy equation is obtained as

$$\begin{aligned}
\theta_{\xi\xi} - \theta_{\tau} - 12(\xi - \xi^2) \\
= \frac{3}{2} (L/k) \sum_{i=1}^n H_{1i} u_{0i} \left\{ \int_0^{\xi} (\partial\theta/\partial\xi') \bar{A}_i' \left[\frac{3}{2} u_{0i}(\xi - \xi') \right] d\xi' \right. \\
\left. - \int_{\xi}^1 (\partial\theta/\partial\xi') \bar{A}_i' \left[\frac{3}{2} u_{0i}(\xi' - \xi) \right] d\xi' \right\} \quad (7.15b)
\end{aligned}$$

Note again that Eq. (7.15b) can be obtained directly by integrating the left-hand side of Eq. (7.15a) by parts. Quite often, Eq. (7.15b) is the convenient form to use in radiative transfer analyses.

For the case of negligible radiation, $N = 0$ and both forms of Eq. (7.15) reduce to

$$\theta_{\xi\xi} - \theta_{\tau} = 12 (\xi - \xi^2) \quad (7.16)$$

By employing the product solution procedure, the solution of Eq. (7.16) can be obtained and the result can be expressed in terms of the bulk temperature through use of Eq. (7.7).

The solution of Eq. (7.16) is assumed to be of the form

$$\theta(\xi, \tau) = g(\xi) + h(\xi, \tau) \quad (7.17)$$

From Eqs. (7.16) and (7.17), there is obtained two separate equations as

$$g'' = 12(\xi - \xi^2) \quad (7.18)$$

$$h_{\xi\xi} - h_{\tau} = 0 \quad (7.19)$$

The solution of Eq. (7.18) is obtained by direct integration as

$$g(\xi) = \xi(2\xi^2 - \xi^3 - 1) \quad (7.20)$$

This is the same result as given by Eq. (7.13) for the steady case if $g(\xi)$ is replaced by $\theta(\xi)$. The solution of Eq. (7.19) is found to be (see Sec. 7.2)

$$h(\xi, \tau) = \sum_{n=1}^{\infty} C_n \sin(n\pi\xi) \exp[-(n\pi)^2\tau] \quad (7.21a)$$

where

$$C_n = -2 \int_0^1 g(\xi) \sin(n\pi\xi) d\xi, \quad n = 1, 2, \dots \quad (7.21b)$$

Thus, the complete solution of Eq. (7.16) is given by

$$\theta(\xi, \tau) = \xi (2\xi^2 - \xi^3 - 1) + \sum_{n=1}^{\infty} C_n \sin(a\xi) \exp(-a^2\tau); \quad a = n\pi \quad (7.22)$$

The expression for C_n is obtained from Eqs. (7.20) and (7.21b) as

$$C_n = (4/a^5) [12 - 12a^2 + a^4] \cos(a) - 24], \quad n = 1, 2, \dots \quad (7.23)$$

where a is defined in Eq. (7.22). By combining Eqs. (7.7) and (7.22), the expression for the bulk temperature is obtained as

$$\theta_b = -17/70 + 6 \sum_{n=1}^{\infty} C_n [(1/a) + (4/a^3)] \exp(-a^2\tau) \quad (7.24)$$

where C_n is given by Eq. (7.23).

7.2 Optically Thin Limit

In the optically thin limit, the steady-state energy equations, Eqs. (7.11a) and (7.11b), reduce to

$$\theta' - 2(3\xi^2 - 2\xi^3) + 1 = \frac{3}{2} N \left[\int_0^\xi \theta(\xi') d\xi' - \int_0^1 \theta(\xi') d\xi' \right] \quad (7.25a)$$

$$\theta' - 2(3\xi^2 - 2\xi^3) + 1 = \frac{3}{2} N \int_0^\xi (\xi - \xi') (d\theta/d\xi') d\xi'$$

$$+ \int_{\xi}^1 (\xi' - \xi) (d\theta/d\xi') d\xi' \quad (7.25b)$$

The differentiation of Eqs. (7.25a) and (7.25b) yields the same energy equation for the optically thin limit as

$$\theta'' - 3N\theta = 12 (\xi - \xi^2) \quad (7.26)$$

The solution of Eq. (7.26) satisfying the boundary conditions $\theta(0, \tau) = 0$ and $\theta(1, \tau) = 0$ is found to be

$$\begin{aligned} \theta(\xi) = & (16/3N^2) [\sinh(-\sqrt{3N}/2)/\sinh(\sqrt{3N})] \cosh[\sqrt{3N}(\xi - 1/2)] \\ & + (4/N)(\xi^2 - \xi + 2/3N) \end{aligned} \quad (7.27a)$$

Alternately, the solution of Eq. (7.26) is written as

$$\begin{aligned} \theta(\xi) = & C_1 \exp(\sqrt{m} \xi) + C_2 \exp(-\sqrt{m} \xi) \\ & + (1/m^2) (24 - 12 m \xi + 12 m \xi^2) ; m = 3N \end{aligned}$$

The constants C_1 and C_2 are obtained by using the boundary conditions $\theta(0) = 0$ and $\theta'(1/2) = 0$, and the solution for $\theta(\xi)$ is found to be

$$\begin{aligned} \theta(\xi) = & (1/m^2) \{-24/(1+e^{-\sqrt{m}})\} (e^{-\sqrt{m}} e^{\sqrt{m} \xi} + e^{-\sqrt{m} \xi}) \\ & + 24 - 12 m \xi + 12 m \xi^2 \end{aligned} \quad (7.27b)$$

Equations (7.27a) and (7.27b) should produce identical results. The expression for the bulk temperature, in this case, is obtained by combining

Eqs. (7.7) and (7.27b) as

$$\theta_b = \frac{576}{m^{7/2}} \left[\frac{(1-e^{-\sqrt{m}})}{(1+e^{-\sqrt{m}})} \right] - \frac{288}{m^3} + \frac{24}{m^2} - \frac{12}{5m} \quad (7.28a)$$

or

$$\theta_b = [1/(3N)^3] \{ 576(3N)^{-1/2} (\text{NEXP}) - 21.6N^2 + 72N - 288 \} \quad (7.28b)$$

where

$$\text{NEXP} = \{ 1 - \exp[-(3N)^{1/2}] \} / \{ 1 + \exp[-(3N)^{1/2}] \}$$

In the optically thin limit, the transient energy equations, Eqs. (7.15a) and (7.15b), reduce to

$$\theta_{\xi\xi} - \theta_{\tau} - 3N\theta = 12(\xi - \xi^2) \quad (7.29a)$$

$$\begin{aligned} \theta_{\xi\xi} - \theta_{\tau} - 12(\xi - \xi^2) \\ = \frac{3}{2} N \left[\int_0^{\xi} (\partial\theta/\partial\xi') d\xi' - \int_{\xi}^1 (\partial\theta/\partial\xi') d\xi' \right] \end{aligned} \quad (7.29b)$$

Note that Eq. (7.29b) is identical to Eq. (7.29a).

The solution of Eq. (7.29) is assumed to be of the form

$$\theta(\xi, \tau) = g(\xi) + h(\xi, \tau) \quad (7.30)$$

Thus, Eq. (7.29) can be written as

$$h_{\xi\xi} - h_{\tau} - 3Nh = -g_{\xi\xi} + 3Ng + 12(\xi - \xi^2) \quad (7.31)$$

Consequently,

$$g'' - 3Ng = 12(\xi - \xi^2) \quad (7.32)$$

and

$$h_{\xi\xi} - h_{\tau} - 3Nh = 0. \quad (7.33)$$

The conditions for Eqs. (7.32) and (7.33) are obtained from Eq. (7.6) as

$$\theta(0,\tau) = h(0,\tau) + g(0) = 0; \quad h(0,\tau) = 0, \quad g(0) = 0 \quad (7.34a)$$

$$\theta(1,\tau) = h(1,\tau) + g(1) = 0; \quad h(1,\tau) = 0, \quad g(1) = 0 \quad (7.34b)$$

$$\theta(\xi,0) = h(\xi,0) + g(\xi) = 0; \quad h(\xi,0) = -g(\xi) \quad (7.34c)$$

The solution of Eq. (7.32) satisfying the boundary conditions given by Eqs. (7.34a) and (7.34b) is identical to the solution of Eq. (7.26) as given by Eq. (7.27) if $\theta(\xi)$ is replaced by $g(\xi)$, i.e.,

$$g(\xi) = (16/3N^2) [\sinh(-\sqrt{3N}/2) / \sinh(\sqrt{3N})] \cosh[\sqrt{3N}(\xi-1/2)] \\ + (4/N)(\xi^2 - \xi + 2/3N) \quad (7.35)$$

The solution of Eq. (7.33) is obtained by using the product solution procedure and implying the conditions $h(0,\tau) = h(1,\tau) = 0$ and $h(\xi,0) = -g(\xi)$. For the product solution, it is assumed that

$$h(\xi,\tau) = F(\xi) G(\tau) \quad (7.36)$$

By using Eq. (7.36), Eq. (7.33) is separated into two ordinary differential equations which are expressed along with appropriate conditions as

$$F'' + \lambda^2 F = 0; \quad F(0) = 0, \quad F(1) = 0 \quad (7.37)$$

$$\dot{G} + (3N + \lambda^2) G = 0 ; h(\xi, 0) = G(0) = g(\xi) \quad (7.38)$$

The solution of Eq. (7.37) is given by

$$F_n(\xi) = \sin(n\pi\xi), \quad n = 1, 2, \dots$$

and the solution of Eq. (7.38) is found to be

$$G_n(\tau) = C_n \exp\{-[3N + (n\pi)^2]\tau\}$$

Thus, the complete solution of Eq. (7.33) is

$$h(\xi, \tau) = \sum_{n=1}^{\infty} C_n \sin(n\pi\xi) \exp\{-[3N + (n\pi)^2]\tau\} \quad (7.39)$$

where

$$C_n = -2 \int_0^1 g(\xi) \sin(n\pi\xi) d\xi, \quad n = 1, 2, \dots \quad (7.40)$$

Now, the solution of Eq. (7.29), as expressed by Eq. (7.30), is written as

$$\begin{aligned} \theta(\xi, \tau) = & (16/3N^2) [\sinh(-\sqrt{3N}/2) / \sinh(\sqrt{3N})] \cosh[\sqrt{3N}(\xi - 1/2)] \\ & + (4/N)(\xi^2 - \xi + 2/3N) \\ & + \sum_{n=1}^{\infty} C_n \sin(n\pi\xi) \exp\{-[3N + (n\pi)^2]\tau\} \end{aligned} \quad (7.41)$$

From Eqs. (7.35) and (7.40), it follows that

$$C_n = 0, \text{ for } n \text{ even} \quad (7.42a)$$

$$= 32[3N+(n\pi)^2]/[3N^2(n\pi)^3] + 2(n\pi)/\{3N^2[3N+(n\pi)^2]\}, \text{ for } n \text{ odd} \quad (7.42b)$$

By combining Eqs. (7.7) and (7.41), the expression for the bulk temperature is obtained as

$$\begin{aligned} \theta_b = & 6 \left\{ (16/3N^2) [\sinh(-\sqrt{3N}/2)/\sinh(\sqrt{3N})] [(1/3N) \cosh(\sqrt{3N}/2)] \right. \\ & - (4 + \sqrt{3N}) (3N)^{-3/2} \sinh(\sqrt{3N}/2) \left. \right\} + (4/N) [-1/30 + 1/(9N)] \\ & + \sum_{n=1}^{\infty} C_n [1/(n\pi) + 4/(n\pi)^3] \exp[-(3N + n^2\pi^2)\tau] \end{aligned} \quad (7.43)$$

where C_n is given by Eq. (7.42).

7.3 Large Path Length Limit

In the large path length limit, the steady-state energy equations, Eqs. (7.11a) and (7.11b), reduce to

$$\theta' - 2(3\xi^2 - 2\xi^3) + 1 = M \int_0^1 \theta(\xi') d\xi' / (\xi - \xi') \quad (7.44a)$$

$$\begin{aligned} \theta' - 2(3\xi^2 - 2\xi^3) + 1 &= (L/k) \sum_{i=1}^n H_{1i} \left\{ \int_0^\xi (d\theta/d\xi') \ln \left[\frac{3}{2} u_{0i}(\xi - \xi') \right] d\xi' \right. \\ & \left. + \int_\xi^1 (d\theta/d\xi') \ln \left[\frac{3}{2} u_{0i}(\xi' - \xi) \right] d\xi' \right\} \end{aligned} \quad (7.44b)$$

where

$$M = H_1 L/k = (L/k) \sum_{i=1}^n A_{0i} (de_{wi}/dT)_{T_1} \quad (7.44c)$$

Through integration by parts, it can be shown that Eq. (7.44b) reduces to Eq. (7.44a). The parameter M in Eq. (7.44c) is defined differently than M_1

in Eq. (5.4e). The nondimensional parameter M constitutes the radiation-conduction interaction parameter for the large path length limit [23, 41]. Equation (7.44a) does not appear to possess a closed form solution; a numerical solution, however, can be obtained easily.

In the large path length limit, the transient energy equations, Eqs. (7.15a) and (7.15b), reduce to

$$\begin{aligned} \theta_{\xi\xi} - \theta_{\tau} - 3N\theta - 12(\xi - \xi^2) \\ = - (H_1 L/k) \left[\int_0^{\xi} \theta(\xi', \tau) d\xi' / (\xi - \xi')^2 + \int_{\xi}^1 \theta(\xi', \tau) d\xi' / (\xi' - \xi)^2 \right] \end{aligned} \quad (7.45a)$$

$$\theta_{\xi\xi} - \theta_{\tau} - 12(\xi - \xi^2) = (H_1 L/k) \int_0^1 (\partial\theta/\partial\xi') d\xi' / (\xi - \xi') \quad (7.45b)$$

Since $|(\xi - \xi')^2| = |(\xi' - \xi)^2|$, Eq. (7.45a) can be written as

$$\begin{aligned} \theta_{\xi\xi} - \theta_{\tau} - 3N\theta - 12(\xi - \xi^2) \\ = - (H_1 L/k) \int_0^1 \theta(\xi', \tau) d\xi' / (\xi - \xi')^2 \end{aligned} \quad (7.45c)$$

Through integration by parts, Eq. (7.45c) can be expressed as

$$\theta_{\xi\xi} - \theta_{\tau} - 3N\theta - 12(\xi - \xi^2) = (H_1 L/k) \int_0^1 (\partial\theta/\partial\xi') d\xi' / (\xi - \xi') \quad (7.45d)$$

Equations (7.45a) - (7.45d) represent different forms of the governing equations in the large path length limit. With the exception of the term $(-3N\theta)$ on the left-hand side, Eq. (7.45d) is identical to Eq. (7.45b). Since N represents the radiation-conduction interaction parameter only in the optically thin limit [23], it should not appear in the governing equation

for the large path length limit. Thus, Eq. (7.45b) is the correct equation to use for solution in the large path length limit; the solution of this equation is obtained by numerical techniques.

7.4 Method of Solution

The solution procedures for both steady and unsteady cases are presented in this section. In principle, the same numerical procedure applies to both the general and large path length limit cases.

7.4.1 Steady-State Solutions

The general solution of Eq. (7.11a) or Eq. (7.11b) is obtained numerically by employing the method of variation of parameters. For this, a polynomial form for $\theta(\xi)$ is assumed in powers of ξ as

$$\theta(\xi) = \sum_{m=0}^n a_m \xi^m \quad (7.46)$$

By considering a five term series solution (a quartic solution in ξ) and satisfying the boundary conditions $\theta(0) = \theta'(1/2) = 0$ and $\theta'(0) = -\theta'(1)$, one obtains

$$\theta(\xi) = a_1(\xi - 2\xi^3 + \xi^4) + a_2(\xi^2 - 2\xi^3 + \xi^4) \quad (7.47)$$

Thus,

$$\theta'(\xi) = a_1(1 - 6\xi^2 + 4\xi^3) + a_2(2\xi - 6\xi^2 + 4\xi^3) \quad (7.48)$$

A substitution of Eq. (7.48) in Eq. (7.11a) results in

$$a_1(1 - 6\xi^2 + 4\xi^3) + a_2(2\xi - 6\xi^2 + 4\xi^3) - 2(3\xi^2 - 2\xi^3) + 1$$

$$\begin{aligned}
&= \frac{3}{2} (L/k) \sum_{i=1}^n H_{1i} u_{0i} \left\{ \int_0^\xi \theta(\xi') \bar{A}_i' \left[\frac{3}{2} u_{0i} (\xi - \xi') \right] d\xi' \right. \\
&\quad \left. - \int_\xi^1 \theta(\xi') \bar{A}_i' \left[\frac{3}{2} u_{0i} (\xi' - \xi) \right] d\xi' \right\} \quad (7.49)
\end{aligned}$$

where expressions for $\theta(\xi')$ are obtained from Eq. (7.47).

The two unknown constants a_1 and a_2 in Eq. (7.49) are evaluated by satisfying the integral equation at two convenient locations ($\xi=0$ and $\xi = 1/4$ in the present case). The entire procedure for obtaining a_1 and a_2 is described in Appendix E from which it follows that

$$a_1 = (11a_2 - 16\alpha_4)/\text{DEN} \quad (7.50a)$$

$$a_2 = (16\alpha_3 - 11a_1)/\text{DEN} \quad (7.50b)$$

where

$$\text{DEN} = 16 (\alpha_1\alpha_4 - \alpha_2\alpha_3) \quad (7.50c)$$

and coefficients α_1 through α_4 are defined in Appendix E.

Now, with known values of a_1 and a_2 , Eq. (7.47) provides the general solution for $\theta(\xi)$. The expression for the bulk temperature is obtained by combining Eqs. (7.7) and (7.47) as

$$\theta_b = (1/70) (17a_1 + 3a_2) \quad (7.51)$$

Note that for the case of no radiative interaction α_2 , α_3 , and α_4 are equal to zero and $\alpha_1 = 1$. Thus, $a_2 = 0$ and $a_1 = -1$, and Eq. (7.51) gives the result of Eq. (7.14).

The governing equation for the large path length limit is Eq. (7.44a).

For this equation also the solution is given by Eq. (7.47) but the values of α 's are completely different in this case. There are two approaches to obtain solutions in the large path length limit. One approach is to make use of Eq. (7.44a) and go through the entire numerical procedure described in Appendix E for the general solution. Another approach is to work with the general solution but evaluate all R_i and S_i integrals of Appendix E in the large path limit. In the large path length limit, the integrals can be evaluated in closed forms. Both procedures are described briefly in Appendix E. In order to distinguish the large path length limit solution from the general solution, constants a_1 and a_2 are replaced by b_1 and b_2 , and coefficients α_1 through α_4 are replaced by β_1 through β_4 . The solution for the large path length limit, therefore, is given by

$$\theta(\xi) = b_1(\xi - 2\xi^3 + \xi^4) + b_2(\xi^2 - 2\xi^3 + \xi^4) \quad (7.52a)$$

where

$$b_1 = (11\beta_2 - 16\beta_4)/\text{BOTTOM} \quad (7.52b)$$

$$b_2 = (16\beta_3 - 11\beta_1)/\text{BOTTOM} \quad (7.52c)$$

$$\text{BOTTOM} = 16(\beta_1\beta_4 - \beta_2\beta_3) \quad (7.52d)$$

and coefficients β_1 through β_4 are defined in Appendix E. For this case, the bulk temperature is given by

$$\theta_b = (1/70)(17b_1 + 3b_2) \quad (7.53)$$

Note that in this case the value of coefficients β_1 through β_4 are obtained in closed form.

7.4.2 Transient Solutions

The governing energy equations for the transient case are Eqs. (7.15a) and (7.15b). As in Sec. 6.3, general solutions of these equations are obtained numerically by employing the method of variation of parameters. For the present problem, a polynomial form for $\theta(\xi, \tau)$ is assumed as

$$\theta(\xi, \tau) = \sum_{m=0}^n a_m(\tau) \xi^m \quad (7.54)$$

For a quadratic temperature distribution in ξ (with time dependent coefficients), Eq. (7.54) is written as

$$\theta(\xi, \tau) = a_0(\tau) + a_1(\tau) \xi + a_2(\tau) \xi^2 \quad (7.55a)$$

By using the boundary conditions $\theta(0, \tau) = 0$ and $\theta_{\xi}(\xi=1/2) = 0$, this reduces to

$$\theta(\xi, \tau) = g(\tau) (\xi - \xi^2) \quad (7.55b)$$

where $g(\tau)$ represents the time dependent coefficient. Consequently,

$$\theta_{\xi}(\xi, \tau) = g(\tau) (1 - 2\xi); \theta_{\xi\xi}(\xi, \tau) = -2g(\tau); \theta_{\tau}(\xi, \tau) = (\xi - \xi^2)g'(\tau) \quad (7.56)$$

Also, a combination of Eq. (7.6a) and (7.55b) yields the initial condition

$$\theta(\xi, 0) = g(0) = 0 \quad (7.57)$$

Note that essential boundary conditions are used already in obtaining the

solution represented by Eq. (7.55b).

By employing Eqs. (7.55b) and (7.56), Eqs. (7.15a) and (7.15b) are transformed in alternate forms which are expressed in a compact form as

$$g'(\tau) + \begin{bmatrix} J_1(\xi) \\ J_2(\xi) \end{bmatrix} g(\tau) + 12 = 0 \quad (7.58)$$

where $J_1(\xi)$ and $J_2(\xi)$ are defined in Appendix F. The function $J_1(\xi)$ is used for solution of Eq. (7.15a) and $J_2(\xi)$ is used for solution of Eq. (7.15b). The solution of Eq. (7.58) satisfying the initial conditions of Eq. (7.57) is given by

$$g(\tau) = \frac{12}{J(\xi)} \{ \exp [-J(\xi)\tau] - 1 \} \quad (7.59)$$

The temperature distribution given by Eq. (7.56b) can be expressed now as

$$\theta(\xi, \tau) = \frac{12}{J(\xi)} \{ \exp [-J(\xi)\tau] - 1 \} (\xi - \xi^2) \quad (7.60)$$

The expression for the bulk temperature is obtained through use of Eq. (7.7) as

$$\theta_b = 72 \int_0^1 [(\xi - \xi^2)^2 / J(\xi)] \{ \exp [-J(\xi)\tau] - 1 \} \quad (7.61)$$

Note that in Eqs. (7.59)-(7.61), $J(\xi)$ becomes $J_1(\xi)$ for solution of Eq. (15a) and $J_2(\xi)$ for solution of Eq. (15b).

For a quartic solution in ξ , Eq. (7.54) gives the result identical to

Eq. (7.47) which for the transient case is expressed as

$$\theta(\xi, \tau) = g(\tau)(\xi - 2\xi^3 + \xi^4) + h(\tau)(\xi^2 - 2\xi^3 + \xi^4) \quad (7.62)$$

Thus,

$$\theta_{\xi}(\xi, \tau) = (1 - 6\xi^2 + 4\xi^3)g(\tau) + 2(\xi - 3\xi^2 + 2\xi^3)h(\tau) \quad (7.63a)$$

$$\theta_{\xi\xi}(\xi, \tau) = 12(-\xi + \xi^2)g(\tau) + 2(1 - 6\xi + 6\xi^2)h(\tau) \quad (7.63b)$$

$$\theta_{\tau}(\xi, \tau) = (\xi - 2\xi^3 + \xi^4)g'(\tau) + (\xi^2 - 2\xi^3 + \xi^4)h'(\tau) \quad (7.63c)$$

By substituting Eqs. (7.62) and (7.63) into Eq. (7.15a), one obtains

$$x g'(\tau) + J_3(\xi) g(\tau) + y h'(\tau) + J_4(\xi) h(\tau) = -z \quad (7.64)$$

where

$$x = (\xi - 2\xi^3 + \xi^4); y = (\xi^2 - 2\xi^3 + \xi^4); z = 12(\xi - \xi^2)$$

and functions $J_3(\xi)$ and $J_4(\xi)$ are defined in Appendix F. Equation (7.64) constitutes one equation in two unknowns, namely $g(\tau)$ and $h(\tau)$. However, since the equation is linear in τ , the principle of superposition can be used to split the solution into two solutions as

$$x g'(\tau) + J_3(\xi) g(\tau) = -z/2 \quad (7.65)$$

$$y h'(\tau) + J_4(\xi) h(\tau) = -z/2 \quad (7.66)$$

The initial condition for this case can be written as

$$\theta(\xi, 0) = g(0)(\xi - 2\xi + \xi^3) + h(0)(\xi^2 - 2\xi^3 + \xi^4) = 0 \quad (7.67a)$$

Consequently,

$$g(0) = 0; h(0) = 0 \quad (7.67b)$$

The solution of Eqs. (7.65) and (7.66) satisfying the appropriate initial condition of Eq. (7.67b) is given respectively as

$$g(\tau) = [z(\xi)/2J_3(\xi)] \{ \exp[-J_3(\xi)\tau/x(\xi)] - 1 \} \quad (7.68)$$

$$h(\tau) = [z(\xi)/2J_4(\xi)] \{ \exp[-J_4(\xi)\tau/y(\xi)] - 1 \} \quad (7.69)$$

By substituting Eqs. (7.68) and (7.69) into Eq. (7.62), the expression for the temperature distribution is obtained as

$$\begin{aligned} \theta(\xi, \tau) = & [6(\xi - \xi^2)(\xi - 2\xi^3 + \xi^4)/J_3(\xi)] \{ \exp[-J_3(\xi)\tau/x(\xi)] - 1 \} \\ & + [6(\xi - \xi^2)(\xi^2 - 2\xi^3 + \xi^4)/J_4(\xi)] \{ \exp[-J_4(\xi)\tau/y(\xi)] - 1 \} \end{aligned} \quad (7.70)$$

The bulk temperature in this case is given by

$$\begin{aligned} \theta_b = & 36 \int_0^1 [(\xi - \xi^2)(\xi - 2\xi^3 + \xi^4)/J_3(\xi)] \{ \exp[-J_3(\xi)\tau/x(\xi)] - 1 \} d\xi \\ & + 36 \int_0^1 [(\xi - \xi^2)(\xi^2 - 2\xi^3 + \xi^4)/J_4(\xi)] \{ \exp[-J_4(\xi)\tau/y(\xi)] - 1 \} d\xi \end{aligned} \quad (7.71)$$

where x and y are defined in Eq. (7.64).

By substituting Eqs. (7.62) and (7.63) into Eq. (7.15b), there is obtained

$$xg' + J_5(\xi) g(\tau) + yh' + J_6(\xi) h(\tau) = -z \quad (7.72)$$

where again x, y, z are defined in Eq. (7.64) and functions $J_5(\xi)$ and $J_6(\xi)$ are defined in Appendix F. The solution procedure for this equation is

identical to that for Eq. (7.64) and the results for temperature distribution and bulk temperature are given respectively by Eqs. (7.70) and (7.71) with J_3 replaced by J_5 and J_4 by J_6 .

In the large path length limit, the two applicable governing equations are Eqs. (7.45b) and (7.45d). The solutions of these equations can be obtained from the general solutions by evaluating the integrals in J function in the large path length limit.

Alternately, for a quadratic temperature distribution, Eqs. (7.45d) and (7.45b) are transformed respectively to

$$g'(\tau) + \left[\begin{array}{c} J_7(\xi) \\ J_8(\xi) \end{array} \right] g(\tau) + 12 = 0 \quad (7.73)$$

where $J_7(\xi)$ and $J_8(\xi)$ are defined in Appendix F. The solution of Eq. (7.73) is given by Eq. (7.59) and expressions for $\theta(\xi, \tau)$ and θ_b can be obtained from Eqs. (7.60) and (7.61) respectively. Of course, proper care should be taken to use the correct relation for J functions for different equations. The large path length limit solutions for a quartic temperature distribution can be obtained in a similar manner.

8. PLANS FOR SPECIFIC RESULTS

Some specific results have been obtained and these are being analyzed. The present plans are to obtain extensive results for the following cases with varying physical and flow conditions:

A. Physical Geometries

1. Parallel Plates: One-Dimensional Radiation
2. Parallel Plates: Two-Dimensional Radiation
3. Diffusing Channel Flow: One- and Two-Dimensional Radiation
4. Channel Flow: Top Plate Flat, Bottom Plate with a 5-15° ramp
5. Scramjet Inlet Configurations

B. Radiative Interaction Cases

1. Transient Radiative Transfer in Homogeneous Gases
2. Transient Energy Transfer By Radiation and Conduction in Homogeneous Gaseous Systems
3. Transient Energy Transfer By Radiation, Conduction, and Convection in Homogeneous Gaseous Systems
4. Applications to Flow of Homogeneous Gaseous Mixture
5. Applications to Flow of Chemically Reacting Gaseous Mixtures
6. Applications to the Scramjet Inlet Configurations.

C. Boundary Conditions

1. Isothermal Black Boundaries
2. Isothermal Gray Boundaries
3. Nonisothermal Boundaries
4. Boundaries with Uniform Heat Flux
5. Actual Scramjet Inlet Configurations

D. Flow Conditions

1. Incompressible - Various Cases
2. Compressible - $M_\infty = 0.5, 1, 2, 3, 4, \text{ and } 5$
3. Temperature Range - 300, 500, 1000, 2000, and 5000 K
4. Pressure Range - 0.1, 1, 2, 5, and 10 atm.
5. Realistic Conditions for Scramjet Inlet Flows

E. Participating Medium

1. CO - One Fundamental Band
2. CO₂ - Three Important Bands
3. H₂O - Five Important Bands
4. OH - One Fundamental Band
5. CO₂ + H₂O (Different Concentrations)
6. OH + H₂O (Different Concentrations)
7. OH + H₂ + O₂ + H₂O (Different Concentrations)
8. A Realistic Combustion Model for the Hydrogen Air System

F. Specific Results

1. Nongray Solutions Based on Band-Model Correlations
2. Optically Thin Solutions
3. Large Path Length Limit Solutions
4. Gray Solutions
5. Nongray Solutions for Scramjet Inlet Flows

The procedure developed in this study has been applied to several realistic problems. This has resulted in various publications in forms of technical reports, technical papers (presented at national and international conferences) and journal articles. Results of selected studies are presented in appendices G through J.

9. CONCLUDING REMARKS

A brief review is presented on various band models and band model correlations that are useful in nongray radiative transfer analyses. Different formulations for one-dimensional radiative flux are provided. These are used to develop the basic governing equations for transient energy transfer in gaseous systems. Limiting forms of these equations are obtained in the optically thin and large path length limits. Numerical procedures are described to solve the governing equations for different physical and flow conditions. The plans for obtaining extensive results for different cases are provided. The formulation and numerical procedure presented in this study can be extended easily to multi-dimensional analyses. In the near future, the influence of radiative interactions will be investigated for the realistic flow of hydrogen-air mixture in the scramjet inlet configuration.

REFERENCES

1. Chandrasekhar, S., Radiative Transfer, Dover Publications, Inc., New York, 1960.
2. Kourganoff, V., Basic Methods in Transfer Problems, Dover Publications, Inc., New York, 1963.
3. Sobolev, V. V., A Treatise on Radiative Transfer, D. Van Nostrand Company, Inc., Princeton, New Jersey, 1963.
4. Goody, R.M., Atmospheric Radiation I: Theoretical Basis, Oxford University Press, London and New York, 1965.
5. Preisendorfer, R. W., Radiative Transfer on Discrete Spaces, Pergamon Press, London and New York, 1965.
6. Vincenti, W. G. and Kruger, C. H., Introduction to Physical Gas Dynamics, John Wiley & sons, Inc., New York, 1965. Printed and Published by Robert E. Krieger Publishing Co., Inc., Huntington, N.Y.
7. Pai, Shih-I., Radiation Gas Dynamics, Springer-Verlag New York Inc., New York, 1966.
8. Sparrow, E. M. and Cess, R. D., Radiation Heat Transfer, Brooks/Cole, Belmont, Calif., 1966 and 1970. New Augmented Edition, Hemisphere Publishing Corp., Washington, D.C., 1978.
9. Hottel, H.C. and Sarofim, A. F., Radiative Transfer, McGraw-Hill Book Co., New York, 1967.
10. Love, T. J., Radiative Heat Transfer, Charles E. Merrill Publishing Co., Columbus, Ohio, 1968.
11. Penner, S. S. and Olfe, D. B., Radiation and Reentry, Academic Press, New York, 1968.
12. Kondratyev, K. Ya., Radiation in Atmosphere, Academic Press, New York, 1969.
13. Siegel, R. and Howell, J. R., Thermal Radiation Heat Transfer, McGraw-Hill Book Co., New York, 1971; Second Edition, 1981.
14. Ozisik, M. N., Radiative Transfer and Interactions with Conduction and Convection, John Wiley & Sons, Inc., 1973.
15. Pomraning, G. C., Radiation Hydrodynamics, Pergamon Press, London and New York, 1973.
16. Paltridge, G. and Platt, C., Radiation Process in Meteorology and Climatology, American Elsevier Publishing Co., Inc., New York, 1976.
17. Rybicki, G. B. and Lightman, A. P., Radiative Processes in Astrophysics, John Wiley and Sons, New York, 1979.

18. Liou, K. N., An Introduction to Atmospheric Radiation, Academic Press, 1980.
19. Cess, R. D., "The Interaction of Thermal Radiation with Conduction and Convection Heat Transfer," Advances in Heat Transfer, Vol. 1, Academic Press, New York, 1964.
20. Sparrow, E. M., "Radiation Heat Transfer between Surfaces," Advances in Heat Transfer, Vol. 2, Academic Press, New York, 1965.
21. Viskanta, R., "Radiative Transfer and Interaction of Convection with Radiation Heat Transfer," Advances in Heat Transfer, Vol. 3, Academic Press, New York, 1966.
22. Tien, C. L., "Thermal Radiation Properties of Gases," Advances in Heat Transfer, Vol. 5, Academic Press, New York, 1968.
23. Cess, R. D. and Tiwari, S. N., "Infrared Radiative Energy Transfer in Gases," Advances in Heat Transfer, Vol. 8, Academic Press, New York, 1972.
24. Edwards, D. K., "Molecular Gas Band Radiation," Advances in Heat Transfer, Vol. 12, Academic Press, New York, 1976;
25. Tiwari, S. N., "Band Models and Correlations for Infrared Radiation," Radiative Transfer and Thermal Control (Progress in Astronautics and Aeronautics), Vol. 49, American Institute of Aeronautics and Astronautics, New York, 1976.
26. Tiwari, S. N., "Models for ^{Infrared} Atmospheric Radiation," Advances in Geophysics, Vol. 20, Academic Press, New York, 1978.
27. McClatchey, R. A., Benedict, W. S., Clough, S. A., Burch, D. E., Calfee, R. F., Fox, K., Rothman, L. S., and Garing, J. S., "AFCRL Atmospheric Line Parameters Compilation," Air Force Cambridge Research Laboratories, Bedford, Mass., AFCRL-TR-73-0096, January 1973 (also, NTIS AD A762904).
28. Ludwig, C. B., Malkmus, W., Reardon, J. E., and Thomson, J. A. L., Handbook of Infrared Radiation from Combustion Gases, R. Goulard and J. A. L. Thomson (Editors), NASA SP-3080, 1973.
29. Ludwig, C.B. (Editor), Atmospheric Effects on Radiative Transfer, Proceedings of the Society of Photo-Optical Instrumentation Engineers, Vol. 195, August 1979.
30. Rothman, L. S., Gamache, R. R., Barbe, A., Goldman, A., Gillis, J. R., Brown, L. R., Toth, R. A., Flaud, J. M., and Camy-Peyret, C., "AFGL Atmospheric Absorption Line Parameters Compilation: 1982 Edition," Applied Optics, Vol. 22, No. 15, August 1983, pp. 2247-2256.
31. Plass, G. N., "Models for Spectral Band Absorption," Journal of the Optical Society of America, Vol. 8, No. 10, October 1958, pp. 690-703.

also, Radiation Heat Transfer Notes,
Hemisphere Publishing Corporation,
Washington, D.C., 1981.

32. Plass, G. N., "Useful Representation for Measurements of Spectral Band Absorption," Journal of the Optical Society of America, Vol. 50, No. 9 September 1960, pp. 868-875.
33. Wyatt, P. J., Stull, V. R., and Plass, G. N., "Quasi-Random Model of Band Absorption," Journal of the Optical Society of America, Vol. 52, No. 11, November 1962, pp. 1209-1217.
34. Edwards, D. K. and Menard, W. A., "Comparison of Methods for Correlation of Total Band Absorption," Applied Optics, Vol. 3, No. 5, May 1964, pp. 621-625.
35. Edwards, D. K., Glassen, L. K., Hauser, W. C., and Tucher, J.S., "Radiation Heat Transfer in Nonisothermal Nongray Gases," Journal of Heat Transfer, Vol. 89C, No. 3, 1967, pp. 219-229.
36. Edwards, D. K. and Balakrishnan, A., "Slab Band Absorptance for Molecular Gas Radiation," Journal of the Quantitative Spectroscopy and Radiative Transfer, Vol. 12, 1972, pp. 1379-1387.
37. Edwards, D. K. and Balakrishnan, A., "Thermal Radiation by Combustion Gases," International Journal of Heat and Mass Transfer, Vol. 16, No. 1, January 1973, pp. 25-40.
38. Felske, J. D. and Tien, C. L., "A Theoretical Closed Form Expression for the Total Band Absorptance of Infrared Radiating Gases," International Journal of Heat and Mass Transfer, Vol. 17, No. 1, January 1974, pp. 155-158.
39. Goody, R. M. and Belton, M. J. S., "Radiative Relaxation Times for Mars (A Discussion of Martian Atmospheric Dynamics)," Planetary and Space Science, Vol. 1r, No. 2, 1967, pp. 247-256.
40. Tien, C. L. and Ling, G. R., "On a Simple Correlation for Total Band Absorptance of Radiating Gases," International Journal of Heat and Mass Transfer, Vol. 12, No. 9, September 1969, pp. 1179-1181.
41. Tiwari, S. N., "Applications of Infrared Band Model Correlations to Nongray Radiation," International Journal of Heat and Mass Transfer, Vol. 20, No. 7, July 1977, pp. 741-751.
42. Lick, W., "Transient Energy Transfer by Radiation and Conduction," International Journal of Heat and Mass Transfer, Vol. 8, 1965, pp. 119-127.
43. Doornink, D. G. and Hering, R. G., "Transient Radiative Heat Transfer in a Nongray Medium," Journal of the Quantitative Spectroscopy and Radiative Transfer, Vol. 12, 1972, pp. 1161-1174.
44. Larson, D. W. and Viskanta, R., "Transient Combined Laminar Free Convection and Radiation in a Rectangular Enclosure," Journal of Fluid Mechanics, Vol. 78, Part 1, 1976, pp. 65-85.
45. Melnikov, V. I. and Sukhovich, E. P., "Transient Heat Exchange Between a Radiating Plate and a High-Temperature Gas Flow," Heat Transfer-Soviet Research, Vol. 10, No. 3, May-June 1978, pp. 11-20 (Translation).

APPENDICES

APPENDIX A

EXPONENTIAL INTEGRALS AND EXPRESSIONS FOR RADIATIVE FLUX

Some important relations for the exponential integrals are given in Appendix B of Ref. 8; and it is noted that

$$\int E_n(t) dt = -E_{n+1}(t); \quad E_n(0) = 1/(n-1) \quad . \quad (\text{A.1})$$

Now, consider the first integral in Eq. (3.1) as

$$I(1) = \int_0^{\tau_\lambda} E_2(\tau_\lambda - t) dt \quad (\text{A.2})$$

By defining $x = \tau_\lambda - t$, $dt = -dx$, and Eq. (A.2) becomes

$$\begin{aligned} I(1) &= \int_{\tau_\lambda}^0 E_2(x)(-dx) = \int_0^{\tau_\lambda} E_2(x) dx \\ &= -[E_3(x)]_0^{\tau_\lambda} = E_3(0) - E_3(\tau_\lambda) \quad . \end{aligned}$$

Thus,

$$E_3(\tau_\lambda) = E_3(0) - I(1) = \frac{1}{2} - \int_0^{\tau_\lambda} E_2(\tau_\lambda - t) dt \quad (\text{A.3})$$

The second integral in Eq. (3.2) is written as

$$I(2) = \int_{\tau_\lambda}^{\tau_{0\lambda}} E_2(t - \tau_2) dt \quad . \quad (\text{A.4})$$

By defining $x = t - \tau_\lambda$, Eq. (A.4) is expressed as

$$\begin{aligned} I(2) &= \int_0^{\tau_{0\lambda} - \tau_\lambda} E_2(x) dx = [E_3(x)]_0^{\tau_{0\lambda} - \tau_\lambda} \\ &= - [E_3(\tau_{0\lambda} - t_\lambda) - E_3(0)] \end{aligned}$$

or

$$E_3(\tau_{0\lambda} - \tau_\lambda) = E_3(0) - I(2) = \frac{1}{2} - \int_{\tau_\lambda}^{\tau_{0\lambda}} E_2(t - \tau_\lambda) dt \quad . \quad (A.5)$$

A substitution of Eqs. (A.3) and (A.5) into Eq. (3.1) results in (for the case $B_{1\lambda} = e_{1\lambda}$ and $B_{2\lambda} = e_{2\lambda}$)

$$\begin{aligned} q_{R\lambda} &= e_{1\lambda} - e_{2\lambda} \\ &+ 2 \left\{ \int_0^{\tau_\lambda} [e_{b\lambda}(t) - e_{1\lambda}] E_2(\tau_\lambda - t) dt \right\} \\ &- 2 \left\{ \int_{\tau_\lambda}^{\tau_{0\lambda}} [e_{b\lambda}(t) - e_{2\lambda}] E_2(t - \tau_\lambda) dt \right\} \quad . \quad (A.6) \end{aligned}$$

This equation when expressed in terms of the wave number ω is exactly the same as Eq. (3.4). Following a similar procedure, Eq. (3.5) is obtained from Eq. (3.2).

APPENDIX B

ALTERNATE FORMS OF RADIATIVE FLUX EQUATIONS

In radiative formulations, it is desirable to express the relations for q_r and $\text{div } q_r$ in terms of \bar{A} and \bar{A}' , and avoid the use of \bar{A}'' . This is accomplished by expressing the integrals containing \bar{A}' and \bar{A}'' in alternate forms through the procedure of integration by parts. This is performed by using the relation

$$\int_a^b m \, dn = (mn)_a^b - \int_a^b n \, dm \quad . \quad (\text{B.1})$$

Consider now the first integral in Eq. (3.21) and express as

$$\text{BI}(1) = \int_0^\xi F_{1\omega}(\xi') \bar{A}' \left[\frac{3}{2} u_{0i}(\xi - \xi') \right] d\xi' \quad (\text{B.2})$$

For integration by parts, let

$$m = F_{1\omega}; \quad dn = \bar{A}' \left[\frac{3}{2} u_0(\xi - \xi') \right] d\xi' .$$

Then,

$$dm = (dF_{1\omega}/d\xi') d\xi' = (de/d\xi') d\xi' .$$

In order to get n , let

$$u = \frac{3}{2} u_0(\xi - \xi'), \quad du/d\xi' = -3 u_0/2$$

and

$$\begin{aligned} dn &= [d\bar{A}(u)/du] d\xi' = [d\bar{A}(u)/d\xi' \times d\xi'/du] d\xi' \\ &= - (2/3u_0) [d\bar{A}(u)/d\xi'] d\xi' = (-2/3u_0) d\bar{A}(u) . \end{aligned}$$

Thus,

$$n = -(2/3u_0) \bar{A}(u) = -(2/3u_0) \bar{A} \left[\frac{3}{2} u_0 (\xi - \xi') \right] .$$

Consequently Eq. (B.2) can be written as

$$\begin{aligned} BI(1) = & F_{1\omega}(\xi) \left[-\frac{2}{3u_0} \bar{A}(0) \right] - F_{1\omega}(0) \left[-\frac{2}{3u_0} \bar{A} \left(\frac{3}{2} u_0 \xi \right) \right] \\ & + \frac{2}{3u_0} \int_0^\xi [de_\omega(\xi')/d\xi'] \bar{A} \left[\frac{3}{2} u_0 (\xi - \xi') \right] d\xi' \end{aligned} \quad (B.3)$$

Note that by the definitions given in Eqs. (2.2) and (2.8), $\bar{A}(0) = 0$. In the present case, only the definition given in Eq. (2.8) is acceptable for $\bar{A}(0) = 0$. Also by definition, $F_{1\omega}(0) = 0$. Thus, Eq. (B.3) reduces to

$$BI(1) = (2/3u_0) \int_0^\xi [de_\omega(\xi')/d\xi'] \bar{A} \left[\frac{3}{2} u_0 (\xi - \xi') \right] d\xi' \quad (B.4)$$

The second integral in Eq. (3.21) is written as

$$BI(2) = (2/3u_0) \int_0^\xi [de_\omega(\xi') \bar{A} \left[\frac{3}{2} u_0 (\xi' - \xi) \right] d\xi' \quad (B.5)$$

Let,

$$m = F_{2\omega}; \quad dn = \bar{A}' \left[\frac{3}{2} u_0 (\xi' - \xi) \right] d\xi'$$

Then,

$$dm = (dF_{2\omega}/d\xi')d\xi' = (de_{\omega}/d\xi')d\xi'$$

Now, to get n , let

$$u = \frac{3}{2} u_0 (\xi' - \xi), \quad du/d\xi' = 3u_0/2$$

and

$$\begin{aligned} dn &= [d\bar{A}(u)/du]d\xi' = [d\bar{A}(u)/d\xi' \times d\xi'/du]d\xi' \\ &= (2/3u_0)[d\bar{A}(u)/d\xi'] d\xi' = (2/3u_0) d\bar{A}(u) \end{aligned}$$

Thus,

$$n = (2/3u_0)\bar{A}(u) = (2/3u_0)\bar{A}\left[\frac{3}{2} u_0 (\xi' - \xi)\right]$$

Consequently, Eq. (B.5) is expressed as

$$\begin{aligned} BI(2) &= F_{2\omega}(1) \left\{ (2/3u_0) \bar{A} \left[\frac{3}{2} u_0 (1 - \xi) \right] \right\} - \left\{ F_{2\omega}(\xi) \left[(2/3u_0) \bar{A}(0) \right] \right\} \\ &\quad - (2/3u_0) \int_{\xi}^1 [de_{\omega}(\xi')/d\xi'] \bar{A} \left[\frac{3}{2} u_0 (\xi' - \xi) \right] d\xi' \end{aligned} \quad (B.6)$$

Since, by definition, $F_{2\omega}(1) = 0$ and $A(0) = 0$, Eq. (B.6) reduces to

$$BI(2) = - (2/3u_0) \int_{\xi}^1 [de_{\omega}(\xi')/d\xi'] \bar{A} \left[\frac{3}{2} u_0 (\xi' - \xi) \right] d\xi' \quad (B.7)$$

By use of Eqs. (B.4) and (B.7), the integrals in Eq. (3.21) can be expressed in alternate forms and this results in Eq. (3.23).

Consider now the integrals in Eq. (3.22); the first integral is written as

$$BI(3) = \int_0^{\xi} F_{1\omega}(\xi') \bar{A}'' \left[\frac{3}{2} u_0 (\xi - \xi') \right] d\xi' \quad (B.8)$$

For integration by parts, let

$$m = F_{1\omega}(\xi'); \quad dn = \bar{A}'' \left[\frac{3}{2} u_0 (\xi - \xi') \right] d\xi'$$

Then

$$dm = (dF_{1\omega}/d\xi') d\xi' = (de_{\omega}/d\xi') d\xi'$$

As before, to obtain n, let

$$u = \frac{3}{2} u_0 (\xi - \xi'), \quad du/d\xi' = -3u_0/2$$

and, therefore,

$$\begin{aligned}
dn &= \frac{d}{du} [d\bar{A}(u)/du] d\xi' \\
&= \left\{ \frac{d}{d\xi'} \frac{d\xi'}{du} [d\bar{A}(u)/du] \right\} d\xi' \\
&= d\{(-2/3 u_0)[d\bar{A}(u)/du]\}
\end{aligned}$$

Thus,

$$n = (-2/3u_0) \bar{A}'(u) = (-2/3 u_0) \bar{A} \left[\frac{3}{2} u_0 (\xi - \xi') \right]$$

and Eq. (B.8) can be written as

$$\begin{aligned}
BI(3) &= \{F_{1\omega} (-2/3 u_0) \bar{A}' \left[\frac{3}{2} u_0 (\xi - \xi') \right]\}_0^\xi \\
&\quad - \int_0^\xi \{(-2/3 u_0) \bar{A}' \left[\frac{3}{2} u_0 (\xi - \xi') \right]\} [dF_{1\omega}(\xi')/d\xi'] d\xi' \quad (B.9)
\end{aligned}$$

Since $F_{1\omega}(0) = 0$ and $\bar{A}'(0) = 1$, Eq.(B.9) reduces to

$$BI(3) = (2/3u_0) \{-F_{1\omega}(\xi) + \int_0^\xi [de_\omega(\xi')/d\xi'] \bar{A}' \left[\frac{3}{2} u_0 (\xi - \xi') \right] d\xi'\} \quad (B.10)$$

Similarly, for the second integral in Eq. (3.22), one can find

$$\begin{aligned}
BI(4) &= \int_\xi^1 F_{2\omega}(\xi') \bar{A}'' \left[\frac{3}{2} u_0 (\xi' - \xi) \right] d\xi' \\
&= (-2/3u_0) \{F_2(\xi) + \int_\xi^1 [de_\omega(\xi')/d\xi'] \bar{A}' \left[\frac{3}{2} u_0 (\xi' - \xi) \right] d\xi'\} \quad (B.11)
\end{aligned}$$

A substitution of Eqs. (B.10) and (B.11) in Eq. (3.22) results in Eq. (3.24). Also, a differentiation of Eq. (3.23) with respect to ξ , by using the Leibnitz formula, gives

$$\begin{aligned}
 \frac{dq_r(\xi)}{d\xi} &= \sum_{i=1}^n A_{oi} \left\{ \frac{de_{\omega i}(\xi)}{d\xi} \bar{A}(0) - 0 \right. \\
 &+ \frac{3u_{oi}}{2} \int_0^{\xi} \left\{ \frac{de_{\omega i}(\xi')}{d\xi'} \bar{A}_i' \left[\frac{3}{2} u_{oi} (\xi - \xi') \right] d\xi' \right. \\
 &+ 0 - \frac{de_{\omega i}(\xi)}{d\xi} \bar{A}_i(0) \\
 &\left. \left. - \frac{3u_{oi}}{2} \int_{\xi}^1 \frac{de_{\omega i}(\xi')}{d\xi'} \bar{A}_i' \left[\frac{3}{2} u_{oi} (\xi') \right] d\xi' \right\} \right. \quad (B.12)
 \end{aligned}$$

Since $\bar{A}(0) = 0$, Eq. (B.12) reduces to Eq. (3.24).

APPENDIX C

DEFINITION AND EVALUATION OF INTEGRAL FUNCTIONS

For the convenience and use in the computational procedure, the following definitions are employed in expressing the relations for the integral functions:

$$\begin{aligned} b_i &= 3u_{0i}/2 \\ c_i &= 1/b_i = 2/3u_{0i} \\ C(\xi) &= 1/(\xi - \xi^2) \\ \Gamma &= 1/(\sigma T_1^3) \end{aligned}$$

Various integrals are defined and simplified as follows:

$$\begin{aligned} G_1(\xi) &= C(\xi) (3N_1 (\xi - \xi^2) + \\ &+ \frac{9}{4} \sum_{i=1}^n M_{1i} u_{0i}^2 \{ \int_0^\xi (\xi' - \xi'^2) \bar{A}_i'' [b_i (\xi - \xi')] d\xi' \\ &+ \int_\xi^1 (\xi' - \xi'^2) \bar{A}_i'' [b_i (\xi' - \xi)] d\xi' \}) \end{aligned} \quad (C.1a)$$

$$\begin{aligned} &= C(\xi) (3N_1 (\xi - \xi^2) + \\ &+ \frac{3}{2} \sum_{i=1}^n M_{1i} u_{0i} \{ \int_0^{b_i \xi} [\xi - c_i u - \xi^2 + 2\xi c_i u - (c_i u)^2] \bar{A}_i''(u) du \\ &+ \int_0^{b_i(1-\xi)} [\xi + c_i u - \xi^2 - 2\xi c_i u - (c_i u)^2] \bar{A}_i''(u) du \}) \end{aligned} \quad (C.1b)$$

$$\begin{aligned}
G_2(\xi) &= C(\xi) \left(3N_1 \left(\frac{1}{2} - \xi^2 \right) \right. \\
&\quad - \frac{9}{4} \sum_{i=1}^n (M_{1i} u_{0i}^2 \{ \int_0^\xi \xi'^2 A_i'' [b_i(\xi - \xi')] d\xi' \\
&\quad \left. + \int_\xi^1 (\xi'^2 - 1) \bar{A}_i'' [b_i(\xi' - \xi)] d\xi' \}) \right) \quad (C.2a)
\end{aligned}$$

$$\begin{aligned}
&= C(\xi) \left(3N_1 \left(\frac{1}{2} - \xi^2 \right) \right. \\
&\quad - \frac{3}{2} \sum_{i=1}^n M_{1i} u_{0i} \left\{ \int_0^{b_i \xi} [\xi^2 - 2\xi c_i u + (c_i u)^2] \bar{A}_i''(u) du \right. \\
&\quad \left. + \int_0^{b_i(1-\xi)} [\xi^2 + 2\xi c_i u + (c_i u)^2 - 1] \bar{A}_i''(u) du \right\} \right) \quad (C.2b)
\end{aligned}$$

$$\begin{aligned}
G_3(\xi) &= C(\xi) \left(\frac{3}{2} \sum_{i=1}^n N_{1i} \left\{ \int_0^\xi (1 - 2\xi') \bar{A}_i' [b_i(\xi - \xi')] d\xi' \right. \right. \\
&\quad \left. \left. - \int_\xi^1 (1 - 2\xi') \bar{A}_i' [b_i(\xi' - \xi)] d\xi' \right\} \right) \quad (C.3a)
\end{aligned}$$

$$\begin{aligned}
&= C(\xi) \left(\sum_{i=1}^n M_{1i} \left\{ \int_0^{b_i \xi} [1 - 2\xi + 2 c_i u] \bar{A}_i'(u) du \right. \right. \\
&\quad \left. \left. - \int_0^{b_i(1-\xi)} [1 - 2\xi - c_i u] \bar{A}_i'(u) du \right\} \right) \quad (C.3b)
\end{aligned}$$

$$\begin{aligned}
G_4(\xi) &= C(\xi) \left(-3 \sum_{i=1}^n N_{1i} \left\{ \int_0^\xi \xi' \bar{A}_i' [b_i(\xi - \xi')] d\xi' \right. \right. \\
&\quad \left. \left. - \int_\xi^1 \xi' \bar{A}_i' [b_i(\xi' - \xi)] d\xi' \right\} \right) \quad (C.4a)
\end{aligned}$$

$$\begin{aligned}
&= C(\xi) \left(-2 \sum_{i=1}^n M_{1i} \left\{ \int_0^{b_i \xi} [\xi - c_i u] \bar{A}_i'(u) du \right. \right. \\
&\quad \left. \left. + \int_{\xi}^{b_i(1-\xi)} [\xi + c_i u] \bar{A}_i'(u) du \right\} \right) \quad (C4.b)
\end{aligned}$$

$$\begin{aligned}
G_5(\xi) &= (3\Gamma/8) \sum_{i=1}^n u_{0i} H_{1i} \left\{ \int_0^{\xi} (\xi' - \xi'^2) \bar{A}_i' [b_i(\xi - \xi')] d\xi' \right. \\
&\quad \left. - \int_{\xi}^1 (\xi' - \xi'^2) \bar{A}_i' [b_i(\xi - \xi')] d\xi' \right\} \quad (C.5a)
\end{aligned}$$

$$\begin{aligned}
&= (\Gamma/4) \sum_{i=1}^n H_{1i} \left\{ \int_0^{b_i \xi} [\xi - c_i u - \xi^2 + 2\xi c_i u - (c_i u)^2] \bar{A}_i'(u) du \right. \\
&\quad \left. - \int_0^{b_i(1-\xi)} [\xi + c_i u - \xi^2 - 2\xi c_i u - (c_i u)^2] \bar{A}_i'(u) du \right\} \quad (C.5b)
\end{aligned}$$

$$\begin{aligned}
G_6(\xi) &= (3\Gamma/8) \sum_{i=1}^n u_{0i} H_{1i} \left\{ \int_0^{\xi} \xi'^2 \bar{A}_i' [b_i(\xi - \xi')] d\xi' \right. \\
&\quad \left. + \int_{\xi}^1 (1 - \xi'^2) \bar{A}_i' [b_i(\xi' - \xi)] d\xi' \right\} \quad (C.6a)
\end{aligned}$$

$$\begin{aligned}
&= (\Gamma/4) \sum_{i=1}^n H_{1i} \left\{ \int_0^{b_i \xi} [\xi^2 - 2\xi c_i u + (c_i u)^2] \bar{A}_i'(u) du \right. \\
&\quad \left. + \int_0^{b_i(1-\xi)} [1 - \xi^2 - 2\xi c_i u - (c_i u)^2] \bar{A}_i'(u) du \right\} \quad (C.6b)
\end{aligned}$$

$$G_7(\xi) = (\Gamma/4) \sum_{i=1}^n H_{1i} \left\{ \int_0^\xi (1-2\xi') \bar{A}_i [b_i(\xi-\xi')] d\xi' \right. \\ \left. - \int_\xi^1 (1-2\xi') \bar{A}_i [b_i(\xi'-\xi)] d\xi' \right\} \quad (C.7a)$$

$$= (\Gamma/6) \sum_{i=1}^n (H_{1i}/u_{0i}) \left\{ \int_0^{b_i \xi} (1-2\xi + 2c_i u) \bar{A}_i(u) du \right. \\ \left. - \int_0^{b_i(1-\xi)} (1-2\xi - 2c_i u) \bar{A}_i(u) du \right\} \quad (C.7b)$$

$$G_8(\xi) = (\Gamma/4) \sum_{i=1}^n H_{1i} \left\{ \int_0^\xi (2\xi') \bar{A}_i [b_i(\xi-\xi')] d\xi' \right. \\ \left. - \int_\xi^1 (2\xi') \bar{A}_i [b_i(\xi'-\xi)] d\xi' \right\} \quad (C.8a)$$

$$= (\Gamma/6) \sum_{i=1}^n (H_{1i}/u_{0i}) \left\{ \int_0^{b_i \xi} (2\xi - 2c_i u) \bar{A}_i(u) du \right. \\ \left. - \int_0^{b_i(1-\xi)} (2\xi + 2c_i u) \bar{A}_i(u) du \right\} \quad (C.8b)$$

$$G_9 = (3\Gamma/8) \sum_{i=1}^n u_{0i} H_{1i} \left\{ \int_0^1 (\xi' - \xi'^2) \bar{A}_i (b_i \xi') d\xi' \right\} \quad (C.9a)$$

$$= (\Gamma/4) \sum_{i=1}^n H_{1i} \left\{ \int_0^{b_i} [c_i u - (c_i u)^2] \bar{A}_i(u) du \right\} \quad (C.9b)$$

$$G_{10} = (3\Gamma/8) \sum_{i=1}^n u_{0i} H_{1i} \left\{ \int_0^1 (1-\xi') \bar{A}_i (b_i \xi') d\xi' \right\} \quad (C.10a)$$

$$= (\Gamma/4) \sum_{i=1}^n H_{1i} \left\{ \int_0^{b_i} (1-c_i u) \bar{A}_i (u) du \right\} \quad (C.10b)$$

$$G_{11} = (\Gamma/4) \sum_{i=1}^n H_{1i} \left\{ \int_0^1 (1-2\xi') \bar{A}_i (b_i \xi') d\xi' \right\} \quad (C.11a)$$

$$= (\Gamma/6) \sum_{i=1}^n (H_{1i}) \left\{ \int_0^{b_i} (1-2c_i u) \bar{A}_i (u) du \right\} \quad (C.11b)$$

$$G_{12} = (\Gamma/4) \sum_{i=1}^n (H_{1i}/u_{0i}) \left\{ \int_0^1 (2\xi') \bar{A}_i (b_i \xi') d\xi' \right\} \quad (C.12a)$$

$$= (\Gamma/6) \sum_{i=1}^n (H_{1i}/u_{0i}) \left\{ \int_0^{b_i} (2c_i u) \bar{A}_i (u) du \right\} \quad (C.12b)$$

$$G_{13}(\xi) = C(\xi) \left\{ 3N_1 (\xi - \xi^2) - M_1 \left[\int_0^\xi (\xi' - \xi'^2) \frac{d\xi'}{(\xi - \xi')^2} \right. \right. \\ \left. \left. + \int_\xi^1 (\xi' - \xi'^2) \frac{d\xi'}{(\xi' - \xi)^2} \right] \right\} \quad (\text{improper}) \quad (C.13)$$

$$G_{14}(\xi) = C(\xi) \left\{ 3N_1 \left(\frac{1}{2} - \xi^2 \right) + M_1 \left[\int_0^\xi \xi'^2 \frac{d\xi'}{(\xi - \xi')^2} \right. \right. \\ \left. \left. + \int_\xi^1 (\xi'^2 - 1) \frac{d\xi'}{(\xi' - \xi)^2} \right] \right\} \quad (\text{improper}) \quad (C.14)$$

$$G_{15}(\xi) = M_1 C(\xi) \int_0^1 (1-2\xi') \frac{d\xi'}{(\xi-\xi')} \quad (C.15a)$$

$$= M_1 C(\xi) \{2 + (2\xi-1) \ln [(\xi-1)/\xi]\} \quad (C.15b)$$

$$G_{16}(\xi) = -2M_1 C(\xi) \int_0^1 \xi' \frac{d\xi'}{(\xi-\xi')} \quad (C.16a)$$

$$= 2 M_1 C(\xi) \{1 + \xi \ln [(\xi-1)/\xi]\} \quad (C.16b)$$

$$G_{17}(\xi) = (\Gamma H_1/4) \int_0^1 (\xi' - \xi'^2) \frac{d\xi'}{(\xi-\xi')} \quad (C.17a)$$

$$= (\Gamma H_1/4) \left\{ -\frac{1}{2} + \xi - (\xi - \xi^2) \ln [(\xi-1)/\xi] \right\} \quad (C.17b)$$

$$G_{18}(\xi) = (\Gamma H_1/4) \left[\int_0^1 \xi'^2 \frac{d\xi'}{(\xi-\xi')} - \int_{\xi}^1 \frac{d\xi'}{(\xi-\xi')} \right] \text{ (improper)} \quad (C.18)$$

$$G_{19}(\xi) = (\Gamma/4) \sum_{i=1}^n H_{1i} \left\{ \int_0^{\xi} (1-2\xi') \ln [b_i(\xi-\xi')] d\xi' \right.$$

$$\left. + \int_{\xi}^1 (1-2\xi') \ln [b_i(\xi'-\xi)] d\xi' \right\} \quad (C.19a)$$

$$= (\Gamma H_1/4) \left\{ -\frac{1}{2} + \xi + (\xi^2 - \xi) \ln [(1-\xi)/\xi] \right\} \quad (C.19b)$$

$$G_{20}(\xi) = (\Gamma/4) \sum_{i=1}^n H_{1i} \left\{ \int_0^{\xi} 2\xi' \ln [b_i(\xi-\xi')] d\xi' \right.$$

$$+ \int_{\xi}^1 2\xi' \ln [b_i (\xi' - \xi)] d\xi' \quad (\text{C.20a})$$

$$= (\Gamma/4) (H_1 \{ \xi^2 \ln [\xi/(1-\xi)] - \xi - \frac{1}{2} \}$$

$$+ \sum_{i=1}^n H_{1i} \ln [b_i (1-\xi)]) \quad (\text{C.20b})$$

$$G_{21} = (\Gamma H_1 / 4) \int_0^1 (\xi' - \xi'^2) d\xi' / \xi' = (\Gamma H_1 / 8) \quad (\text{C.21})$$

$$G_{22} = (\Gamma H_1 / 4) \int_0^1 (1 - \xi'^2) d\xi' / \xi' \quad (\text{C.22a})$$

$$= - (\Gamma H_1 / 4) \left[\frac{1}{2} + \ln(0) \right] \quad (\text{improper}) \quad (\text{C.22b})$$

$$G_{23} = (\Gamma/4) \sum_{i=1}^n H_{1i} \int_0^1 (1 - 2\xi') \ln (b_i \xi') d\xi' \quad (\text{C.23a})$$

$$= - (\Gamma H_1 / 8) = - H_1 / (8\sigma T_1^3) \quad (\text{C.23b})$$

$$G_{24} = (\Gamma/4) \sum_{i=1}^n H_{1i} \int_0^1 2\xi' \ln (b_i \xi') d\xi' \quad (\text{C.24a})$$

$$= (\Gamma/4) \left[- (H_1 / 2) + \sum_{i=1}^n H_{1i} \ln (b_i) \right] \quad (\text{C.24b})$$

APPENDIX D

INFORMATION FOR NUMERICAL PROCEDURE

1. Data:

$T = 300, 500, 1000, 2000, 5000, \text{ etc. } \sim K$

$P = 0.1, 1, 2, 5, 10, \text{ etc. } \sim \text{atm}$

$L = 1, 2, 5, 10, 20, \text{ etc. } \sim \text{cm}$

$\xi \rightarrow x = 0.0 \rightarrow 1.0; x = U(I)$

2. Thermal conductivity of the gas:

$$K_f = K_f(T, P) \quad (D.1)$$

3. The Planck function and its derivative:

$$e_{b\omega}(T) = \frac{C_1}{\exp(C_2/T) - 1} \equiv \text{PF} \quad (D.2)$$

$$\frac{de_{b\omega}}{dT} = \frac{C_1 C_2 \exp(C_2/T)}{T^2 [\exp(C_2/T) - 1]^2} \equiv \text{PFD} \quad (D.3)$$

where

$$C_1 = (2\pi hc^2)\omega^3$$

$$C_2 = (hc/k)\omega$$

$$C_1 C_2 = (2\pi h^2 c^3/k)\omega^4$$

and $\omega = \omega_c = \omega_0 = \text{wave number center of the } i\text{th band.}$

By defining

$$\text{TEXP} = \exp(C_2/T)$$

Eq. (D.3) is expressed as

$$\text{PFD} = (C_1 C_2)(\text{TEXP}) / [(T^2)(\text{TEXP} - 1)^2] \quad (\text{D.4})$$

All values in Eqs. (D.2) - (D.4) should be evaluated for each band.

4. Information or relation for A_0 for each band, $A_0 = f(T)$.
5. Information on C_0^2 for each band, $C_0^2 = f(T)$.
6. Information on u_0 for each band, $u_0 = C_0^2 PL$ (nondimensional).
7. Information on $B^2(T)$ for each band (nondimensional).
8. Equivalent or effective pressure relation for each band.

$$P_{ei} = [(P/P_0) + (P_i/P_0)(b_i - 1)]^n \quad (\text{nondimensional}) \quad (\text{D.5})$$

In Eq. (D.5), $P_0 = 1$ atm and, therefore, P_i and P must be in the units of atm. Note that P_i is the partial pressure of the i th species in a gases mixture and P is the total pressure; b_i (the self broadening coefficient) and n are different for different bands. For a single component system, Eq. (D.5) is usually expressed as

$$P_e = (b P/P_0)^n \quad (\text{nondimensional}) \quad (\text{D.6})$$

9. Line structure parameter for each band:

$$\beta = B^2 P_e \equiv \text{BETA} \quad (\text{D.7})$$

10. Correlation for each band (for Tien and Lowder's correlation):

$$f(\beta) = 2.94 [1 - \exp(-2.60\beta)] \equiv F \quad (\text{D.8})$$

11. Band absorptance correlation for each band (Tien and Lowder's correlation):

$$\bar{A}(u, \beta) = \epsilon n \left[uF \left(\frac{u + 2}{u + 2F} \right) + 1 \right] \equiv AU \quad (\text{D.9})$$

12. The derivative of the band absorptance correlation for each band (Tien and Lowder's correlation)

$$\bar{A}'(u, \beta) = [F(u^2 + 4uF + 4F)] / \text{DEN} \equiv \text{AUD} \quad (\text{D.10})$$

where

$$\text{DEN} = [F(u^2 + 2u + 2) + u](u + 2F)$$

These basic relations are used in the governing equations of Section 6 to obtain numerical solutions for specific gaseous systems. The spectroscopic and correlation quantities needed for these calculations are available in [22,24].

APPENDIX E

EVALUATION OF CONSTANTS FOR STEADY LAMINAR FLOWS

To determine the constants in Eq. (7.47), Eq. (7.49) is evaluated at $\xi = 0$ and $\xi = 1/4$. To avoid excessive writing, the following notations are used (some of which are also used in Appendix C)

$$\begin{aligned}\xi' &= n, \quad d\xi' = dn \\ b_i &= 3u_{0i}/2; \quad c_i = 1/b_i = 2/3u_{0i}\end{aligned}$$

For $\xi = 0$, Eq. (7.49) reduces to

$$\begin{aligned}a_1 + 1 + \frac{3}{2} (L/k) \sum_{i=1}^n H_{1i} u_{0i} \left\{ \int_0^1 [a_1 (n^2 - 2n^3 + n^4) \right. \\ \left. + a_2 (n^2 - 2n^3 + n^4)] \bar{A}_i'(b_i n) dn \right\} = 0\end{aligned}\quad (E.1)$$

By defining $u = b_i n$, Eq. (E.1) is expressed in an alternate form as

$$\begin{aligned}a_1 \left\{ 1 + (L/k) \sum_{i=1}^n H_{1i} \int_0^{b_i} [c_i u - 2(c_i u)^3 + (c_i u)^4] \bar{A}_i'(u) du \right\} \\ + a_2 \left\{ (L/k) \sum_{i=1}^n H_{1i} \int_0^{b_i} [(c_i u)^2 - 2(c_i u)^3 + (c_i u)^4] \bar{A}_i'(u) du \right\} = -1\end{aligned}\quad (E.2)$$

Now, by defining the following integral functions,

$$R_{1i} = \int_0^{b_i} u_i \bar{A}_i'(u_i) du_i \quad (\text{E.3a})$$

$$R_{2i} = \int_0^{b_i} u_i^2 \bar{A}_i'(u_i) du_i \quad (\text{E.3b})$$

$$R_{3i} = \int_0^{b_i} u_i^3 \bar{A}_i'(u_i) du_i \quad (\text{E.3c})$$

$$R_{4i} = \int_0^{b_i} u_i^4 \bar{A}_i'(u_i) du_i \quad (\text{E.3d})$$

Eq. (E.2) is expressed as

$$a_1 \alpha_1 + a_2 \alpha_2 = -1 \quad (\text{E.4a})$$

where

$$\alpha_1 = 1 + (L/k) \sum_{i=1}^n H_{1i} (c_i R_{1i} - 2 c_i^3 R_{3i} + c_i^4 R_{4i}) \quad (\text{E.4b})$$

$$\alpha_2 = (L/k) \sum_{i=1}^n H_{1i} (c_i^2 R_{2i} - 2 c_i^3 R_{3i} + c_i^4 R_{4i}) \quad (\text{E.4c})$$

For $\xi = 1/4$, Eq. (7.49) reduces to

$$\begin{aligned} & \frac{11}{16} a_1 + \frac{3}{16} a_2 + \frac{11}{16} \\ & = \frac{3}{2} (L/k) \sum_{i=1}^n H_{1i} u_{0i} \left\{ \int_0^{1/4} \theta(n) \bar{A}_i' \left[b_i \left(\frac{1}{4} - n \right) \right] dn \right. \\ & \quad \left. - \int_{1/4}^1 \theta(n) \bar{A}_i' \left[b_i \left(n - \frac{1}{4} \right) \right] dn \right\} \quad (\text{E.5}) \end{aligned}$$

By defining $u = b_i \left(\frac{1}{4} - n\right)$ for the first integral and $u = b_i \left(n - \frac{1}{4}\right)$ for the second integral, Eq. (E.5) is written as

$$\begin{aligned} \frac{11}{16} + \frac{11}{16} a_1 + \frac{3}{16} a_2 = (L/k) \sum_{i=1}^n H_{1i} \left[\int_0^{b_i/4} \theta \left(\frac{1}{4} - c_i u \right) \bar{A}_i'(u) du \right. \\ \left. - \int_0^{3b_i/4} \theta \left(\frac{1}{4} + c_i u \right) \bar{A}_i'(u) du \right] \end{aligned} \quad (E.6)$$

By denoting $d = c_i u$, the following relations are obtained from Eq. (7.47):

$$\begin{aligned} \theta \left(\frac{1}{4} - d \right) = a_1 \left(\frac{57}{256} - \frac{11}{16} d - \frac{9}{8} d^2 + d^3 + d^4 \right) \\ + a_2 \left(\frac{9}{256} - \frac{13}{16} d - \frac{1}{8} d^2 - d^3 + d^4 \right) \end{aligned} \quad (E.7a)$$

and

$$\begin{aligned} \theta \left(\frac{1}{4} + d \right) = a_1 \left(\frac{57}{256} + \frac{11}{16} d - \frac{9}{8} d^2 - d^3 + d^4 \right) \\ + a_2 \left(\frac{9}{256} + \frac{3}{16} d - \frac{1}{8} d^2 - d^3 + d^4 \right) \end{aligned} \quad (E.7b)$$

A combination of Eqs. (E.6) and (E.7) results in

$$\begin{aligned} a_1 \left(\frac{L}{K} \sum_{i=1}^n H_{1i} \left[\frac{57}{256} \int_0^{b_i/4} \bar{A}_i'(u) du - \int_0^{3b_i/4} \bar{A}_i'(u) du \right] \right. \\ \left. - \frac{11}{16} c_i \left[\int_0^{b_i/4} u \bar{A}_i'(u) du + \int_0^{3b_i/4} u \bar{A}_i'(u) du \right] \right) \end{aligned}$$

$$\begin{aligned}
& - \frac{9}{8} c_i^2 \left[\int_0^{b_i/4} u^2 \bar{A}'_i(u) du - \int_0^{3b_i/4} u^2 \bar{A}'_i(u) du \right] \\
& + c_i^3 \left[\int_0^{b_i/4} u^3 \bar{A}'_i(u) du + \int_0^{3b_i/4} u^3 \bar{A}'_i(u) du \right] \\
& + c_i^4 \left[\int_0^{b_i/4} u^4 \bar{A}'_i(u) du - \int_0^{3b_i/4} u^4 \bar{A}'_i(u) du \right] - \frac{11}{16} \\
& + a_2 \left(\frac{L}{K} \sum_{i=1}^n H_{1i} \left\{ \frac{9}{256} \left[\int_0^{b_i/4} \bar{A}'_i(u) du - \int_0^{3b_i/4} \bar{A}'_i(u) du \right] \right. \right. \\
& \quad - \frac{3}{16} c_i \left[\int_0^{b_i/4} u \bar{A}'_i(u) du + \int_0^{3b_i/4} u \bar{A}'_i(u) du \right] \\
& \quad - \frac{1}{8} c_i^2 \left[\int_0^{b_i/4} u^2 \bar{A}'_i(u) du - \int_0^{3b_i/4} u^2 \bar{A}'_i(u) du \right] \\
& \quad + c_i^3 \left[\int_0^{b_i/4} u^3 \bar{A}'_i(u) du + \int_0^{3b_i/4} u^3 \bar{A}'_i(u) du \right] \\
& \quad \left. \left. + c_i^4 \left[\int_0^{b_i/4} u^4 \bar{A}'_i(u) du - \int_0^{3b_i/4} u^4 \bar{A}'_i(u) du \right] - \frac{3}{16} \right\} \right) \\
& = 11/16
\end{aligned}$$

(E.8)

By noting that for any continuous function $F(x)$

$$\int_0^{3/4} F(x) dx = \int_0^{1/4} F(x) dx + \int_{1/4}^{3/4} F(x) dx$$

and defining

$$S_{1i} = \int_{b_i/4}^{3b_i/4} \bar{A}'_i(u_i) du_i \quad (\text{E.9a})$$

$$S_{2i} = \int_0^{b_i/4} u_i \bar{\pi}'_i(u_i) du_i \quad (\text{E.9b})$$

$$S_{3i} = \int_0^{3b_i/4} u_i \bar{\pi}'_i(u_i) du_i \quad (\text{E.9c})$$

$$S_{4i} = \int_{b_i/4}^{3b_i/4} u_i^2 \bar{\pi}'_i(u_i) du_i \quad (\text{E.9d})$$

$$S_{5i} = \int_0^{b_i/4} u_i^3 \bar{\pi}'_i(u_i) du_i \quad (\text{E.9e})$$

$$S_{6i} = \int_0^{3b_i/4} u_i^3 \bar{\pi}'_i(u_i) du_i \quad (\text{E.9f})$$

$$S_{7i} = \int_{b_i/4}^{3b_i/4} u_i^4 \bar{\pi}'_i(u_i) du_i \quad (\text{E.9g})$$

Eq. (E.8) can be written as

$$a_1 \alpha_3 + a_2 \alpha_4 = -11/16 \quad (\text{E.10a})$$

where

$$\alpha_3 = (L/k) \sum_{i=1}^n H_{1i} \left[(57/256) S_{1i} + (11/16) c_i (S_{2i} + S_{3i}) \right. \\ \left. - (9/8) c_i^2 S_{4i} - c_i^3 (S_{5i} + S_{6i}) + c_i^4 S_{7i} \right] + 11/16 \quad (\text{E.10b})$$

$$\alpha_4 = (L/k) \sum_{i=1}^n H_{1i} \left[(9/256) S_{1i} + (3/16) c_i (S_{2i} + S_{3i}) \right. \\ \left. - (1/8) c_i^2 S_{4i} - c_i^3 (S_{5i} + S_{6i}) + c_i^4 S_{7i} \right] + 3/16 \quad (\text{E.10c})$$

By solving Eqs. (E.4a) and (E.10a) simultaneously, there is obtained the results for constants a_1 and a_2 as

$$a_1 = (11 \alpha_2 - 16 \alpha_4) / \text{DEN} \quad (\text{E.11a})$$

$$a_2 = (16 \alpha_3 - 11 \alpha_1) / \text{DEN} \quad (\text{E.11b})$$

where

$$\text{DEN} = 16 (\alpha_1 \alpha_4 - \alpha_2 \alpha_3) \quad (\text{E.11c})$$

The governing equation for the large path length limit is Eq. (7.44a) for which the solution is also given by Eq. (7.47). For the large path length limit, Eq. (7.47) is expressed in the form of Eq. (7.52) which is represented here as

$$\theta(\xi) = b_1 (\xi - 2\xi^3 + \xi^4) + b_2 (\xi^2 - 2\xi^3 + \xi^4) \quad (\text{E.12})$$

Thus,

$$\theta'(\xi) = b_1 (1 - 6\xi^2 + 4\xi^3) + b_2 (2\xi - 6\xi^2 + 4\xi^3) \quad (\text{E.13})$$

A substitution of Eqs. (E.12) and (E.13) in Eq. (7.44a) gives

$$\begin{aligned} b_1 (1 - \epsilon \epsilon^2 + 4\epsilon^3) + b_2 (2\epsilon - 6\epsilon^2 + 4\epsilon^3) - 2 (3\epsilon^2 - 2\epsilon^3) + 1 \\ = M \int_0^1 \theta(\epsilon') d\epsilon' / (\epsilon - \epsilon') \end{aligned} \quad (\text{E.14})$$

For $\epsilon = 0$, Eq. (E.14) reduces to

$$b_1 + 1 = -M \int_0^1 [\theta(\epsilon') / \epsilon'] d\epsilon' \quad (\text{E.15})$$

Upon substituting for $\theta(\epsilon')$ from Eq. (E.12) into Eq. (E.15), the integrals can be evaluated in closed form and there is obtained

$$b_1 \beta_1 + b_2 \beta_2 = -1 \quad (\text{E.16a})$$

where

$$\beta_1 = 1 + (7/12) M; \quad \beta_2 = (1/12) M \quad (\text{E.16b})$$

For $\epsilon = 1/4$, Eq. (E.14) reduces to

$$\frac{11}{16} b_1 + \frac{3}{16} b_2 + \frac{11}{16} = M \int_0^1 \theta(\epsilon') d\epsilon' / \left(\frac{1}{4} - \epsilon'\right) \quad (\text{E.17})$$

By substituting for $\theta(\epsilon')$ in this equation, another relation between b_1 and b_2 can be obtained in terms of β_3 and β_4 . But, this appears to involve the evaluation of a few improper integrals. Thus, this approach is abandoned in

favor of an alternate procedure discussed below.

The solution in the large path length limit can be obtained from the general solution by evaluating the integrals R_i and S_i in the limit of large path length. Since in this limit $\bar{A}'(u) = 1/u$, the integrals in Eqs. (E.3) and (E.9) are evaluated to obtain

$$R_{1i} = b_i; R_{2i} = b_i^2/2; R_{3i} = b_i^3/3; R_{4i} = b_i^4/4 \quad (\text{E.18a})$$

$$S_{1i} = \ln(3); S_{2i} = b_i/4; S_{3i} = 3b_i/4; S_{4i} = b_i^2/4; \\ S_{5i} = b_i^3/192; S_{6i} = 9b_i^3/64; S_{7i} = 5b_i^4/64 \quad (\text{E.18b})$$

From Eqs. (E.4) and (E.18a), there is obtained for the large path length limit

$$b_1 \beta_1 + b_2 \beta_2 = -1 \quad (\text{E.19a})$$

$$\beta_1 = 1 + (7/12) M; \beta_2 = (1/12) M \quad (\text{E.19b})$$

which is the same result as given by Eq. (E.16). From Eqs. (E.10) and (E.18b), one obtains in the large path length limit

$$b_1 \beta_3 + b_2 \beta_4 = -11/16 \quad (\text{E.20a})$$

where

$$\beta_3 = 11/16 + M [(57/256) \ln(3) + 65/192] \\ = 11/16 + 0.583154559 M \quad (\text{E.20b})$$

$$\begin{aligned}\beta_4 &= 3/16 + M [(9/256) \ln(3) + 17/192] \\ &= 3/16 + 0.127164755 M\end{aligned}\tag{E.20c}$$

The solution of Eqs. (E.19a) and (E.20a) yields

$$b_1 = (11\beta_2 - 16\beta_4)/\text{BOTTOM}\tag{E.21a}$$

$$b_2 = (16\beta_3 - 11\beta_1)/\text{BOTTOM}\tag{E.21b}$$

where

$$\text{BOTTOM} = 16(\beta_1\beta_4 - \beta_2\beta_3)\tag{E.21c}$$

With b_1 and b_2 known, the solution for the temperature distribution is obtained from Eq. (E.12).

APPENDIX F

INTEGRAL FUNCTIONS FOR TRANSIENT LAMINAR FLOWS

For convenience and use in the computational procedure, the following definitions are employed in expressing the relations for the integral functions:

$$b_i = 3 u_{0i}/2; c_i = 1/b_i; C(\xi) = 1/(\xi - \xi^2)$$

$$x = \xi - 2\xi^3 + \xi^4; y = \xi^2 - 2\xi^3 + \xi^4; z = 12 (\xi - \xi^2)$$

$$a(\xi) = 1 - 6\xi^2 + 4\xi^3; b(\xi) = 2\xi - 6\xi^2 + 4\xi^3$$

Various integrals are defined as follows:

$$J_1(\xi) = 3N + C(\xi) \left(2 + \frac{9}{4} (L/k) \sum_{i=1}^n H_{1i} u_{0i}^2 \left\{ \int_0^\xi (\xi' - \xi'^2) \bar{A}_i'' [b_i(\xi - \xi')] d\xi' \right. \right. \\ \left. \left. + \int_\xi^1 (\xi' - \xi'^2) \bar{A}_i'' [b_i(\xi' - \xi)] d\xi' \right\} \right) \quad (F.1)$$

$$J_2(\xi) = C(\xi) \left(2 + \frac{3}{2} (L/k) \sum_{i=1}^n H_{1i} u_{0i}^2 \left\{ \int_0^\xi (1 - 2\xi') \bar{A}_i'' [b_i(\xi - \xi')] d\xi' \right. \right. \\ \left. \left. - \int_\xi^1 (1 - 2\xi') \bar{A}_i'' [b_i(\xi' - \xi)] d\xi' \right\} \right) \quad (F.2)$$

$$J_3(\xi) = z + 3Nx + \frac{9}{4} (L/k) \sum_{i=1}^n H_{1i} u_{0i}^2 \left\{ \int_0^\xi x(\xi') \bar{A}_i'' [b_i(\xi - \xi')] d\xi' \right.$$

$$+ \int_{\xi}^1 x(\xi') \bar{A}_i^n [b_i(\xi' - \xi)] d\xi' \quad (F.3)$$

$$J_4(\xi) = (z-2) + 3Ny + \frac{9}{4} (L/k) \sum_{i=1}^n H_{1i} u_{0i}^2 \left\{ \int_0^{\xi} y(\xi') \bar{A}_i^n [b_i(\xi - \xi')] d\xi' \right. \\ \left. + \int_{\xi}^1 y(\xi') \bar{A}_i^n [b_i(\xi - \xi')] d\xi' \right\} \quad (F.4)$$

$$J_5(\xi) = z + \frac{3}{2} (L/k) \sum_{i=1}^n H_{1i} u_{0i} \left\{ \int_0^{\xi} a(\xi') \bar{A}_i^n [b_i(\xi - \xi')] d\xi' \right. \\ \left. - \int_{\xi}^1 a(\xi') \bar{A}_i^n [b_i(\xi' - \xi)] d\xi' \right\} \quad (F.5)$$

$$J_6(\xi) = (z - 2) + \frac{3}{2} (L/k) \sum_{i=1}^n H_{1i} u_{0i} \left\{ \int_0^{\xi} b(\xi') \bar{A}_i^n [b_i(\xi - \xi')] d\xi' \right. \\ \left. - \int_{\xi}^1 b(\xi') \bar{A}_i^n [b_i(\xi' - \xi)] d\xi' \right\} \quad (F.6)$$

$$J_7(\xi) = 3N + C(\xi) \left[2 + M \int_0^1 (1 - 2\xi') d\xi' / (\xi - \xi') \right] \\ = 3N + C(\xi) \left\{ 2 + M \left[2 + (2\xi - 1) \ln \left(\frac{\xi - 1}{\xi} \right) \right] \right\} \quad (F.7)$$

$$J_8(\xi) = J_7(\xi) - 3N \quad (F.8)$$

AIAA'87

12/1/87
12/1/87

AIAA-87-0323

**TRANSIENT RADIATIVE ENERGY
TRANSFER IN NONGRAY GASES**

**S.N. Tiwari & D.J. Singh,
Old Dominion University, Norfolk, VA.**

**A. Kumar,
NASA Langley Research Center,
Hampton, VA**

AIAA 25th Aerospace Sciences Meeting
January 12-15, 1987/Reno, Nevada

PAGE _____ INTERNATIONAL BANKING

TRANSIENT RADIATIVE ENERGY TRANSFER IN NONGRAY GASES

S. N. Tiwari* and D. J. Singh†
 Old Dominion University, Norfolk, VA 23508
 and
 A. Kumar††

NASA Langley Research Center, Hampton, VA 23665

Abstract

A general formulation is presented to investigate the transient radiative interaction in nongray absorbing-emitting species between two parallel plates. Depending on the desired sophistication and accuracy, any nongray absorption model from the line-by-line models to the wide-band model correlations can be employed in the formulation to investigate the radiative interaction. Special attention is directed to investigate the radiative interaction in a system initially at a uniform reference temperature and suddenly the temperature of the bottom plate is reduced to a lower but constant temperature. The interaction is considered for the case of radiative equilibrium as well as for combined radiation and conduction. General as well as limiting forms of the governing equations are presented and solutions are obtained numerically by employing the method of variation of parameters. Specific results are obtained for CO, CO₂, H₂O, and OH. The information on species H₂O and OH is of special interest for the proposed scramjet engine application. The results demonstrate the relative ability of different species for radiative interactions.

Nomenclature

A band absorptance = $A(u, \beta)$, cm⁻¹
 A₀ band width parameter, cm⁻¹
 C₀ correlation parameter, atm⁻¹ - cm⁻¹
 C_p specific heat at constant pressure, kJ/kg-K = erg/gm-K
 e_ω Planck's function, (W-cm⁻²)/cm⁻¹
 e_{ω₀} Planck's function evaluated at wave number ω₀
 e_{1, e₂} emissive power of surfaces with temperatures T₁ and T₂, W-cm⁻²
 H_{1f, H₁} gas property for the large path length limit
 k thermal conductivity, erg/cm-sec-K
 K_{1f, K₁} gas property for the optically thin limit
 L distance between plates

M_{1f, M₁} large path length parameter, nondimensional
 N_{1f, N₁} optically thin parameter, nondimensional
 N optically thin radiation-conduction parameter = N₁/R, nondimensional
 P pressure, atm
 q conduction plus radiation heat flux = q_c + q_R, w/cm²
 q_R total radiative heat flux, w/cm²
 q_c conduction heat flux, w/cm²
 q_{Rω} spectral radiation heat flux, (w-cm⁻²)/cm⁻¹
 Q nondimensional radiative heat flux
 Q̄ nondimensional conduction plus radiation heat flux
 R nondimensional transient conduction parameter
 S integrated intensity of a wide band, atm⁻¹-cm⁻²
 t time, sec (also used as t*)
 t_m characteristic time, sec
 t* nondimensional time = t/t_m
 T temperature, K
 T_{1, T₂} wall temperature, K; T₁ = T_w
 u nondimensional coordinate = SPy/A₀
 u₀ nondimensional path length = SPL/A₀
 y transverse coordinate, cm
 θ nondimensional temperature
 κ_ω spectral absorption coefficient, cm⁻¹
 ε nondimensional coordinate = y/L = u/u₀
 ρ density, kg/m³
 σ Stefan-Boltzmann constant, erg/(sec-cm²-K⁴)
 ω wave number, cm⁻¹
 ω₀ wave number at the band center, cm⁻¹

Introduction

The field of radiative energy transfer in gaseous systems is getting an ever increasing attention recently because of its applications in the areas of the earth's radiation budget studies and climate modeling, fire and combustion research, entry and reentry phenomena, hypersonic propulsion and defense-oriented research. In most studies involving combined mass, momentum, and energy transfer, however, the radiative transfer formulation has been coupled mainly with the steady processes¹⁻¹¹ and the interaction of radiation in transient processes has received very little attention. Yet, the transient approach appears to be the logical way of formulating a problem in a general sense for elegant numerical and computational solutions. The steady-state solutions can be obtained as limiting solutions for large times.

A few studies available on radiative interactions reveal that the transient behavior of

*Eminent Professor, Department of Mechanical Engineering and Mechanics. AIAA Associate Fellow.

†Graduate Research Assistant, Department of Mechanical Engineering and Mechanics. AIAA Student Member.

††Senior Research Scientist, Computational Methods Branch, High-Speed Aerodynamics Division. AIAA Associate Fellow.

a physical system can be influenced significantly in the presence of radiation¹²⁻¹⁷. Lick investigated the transient energy transfer by radiation and conduction through a semi-finite medium¹². A kernal substitution technique was used to obtain analytic solutions and display the main features and parameters of the problem. Steady and transient heat transfer in conducting and radiating planar and cylindrical mediums were analyzed in Refs. 13 and 14 according to the differential formulation. The analyses based essentially on the gray formulation provide some qualitative insight into the effect of absorption and emission on the transient temperature distribution in the gas. Doornink and Hering¹⁵ studied the transient radiative transfer in a stationary plane layer of a nonconducting medium bounded by black walls. A rectangular Milne-Eddington type relation was used to describe the frequency dependence of the absorption coefficient. It was found that the cooling of the layer initially at a uniform temperature is strongly dependent on the absorption coefficient model employed. Larson and Viskanta¹⁶ investigated the problem of transient combined laminar free convection and radiation in a rectangular enclosure. It was demonstrated that the radiation dominates the heat transfer in the enclosure and alters the convective flow patterns significantly. The transient heat exchange between a radiating plate and a high-temperature gas flow was investigated by Melnikov and Sukhovich¹⁷. Only the radiative interaction from the plate was considered; the gas was treated as a non-participating medium. It was proved that the surface temperature is a function of time and of longitudinal coordinate. Some other works on transient radiation and related areas are available in Refs. 18-22.

The goal of this research is to include the nongray radiative formulation in the general unsteady governing equations and provide the step-by-step analysis and solution procedure for several realistic problems. The specific objective of the present study is to investigate the interaction of nongray radiation in transient transfer processes in a general sense. Attention, however, will be directed first to a simple problem of the transient radiative exchange between two parallel plates. In subsequent studies, the present analysis and numerical techniques will be extended to include the flow of homogeneous, nonhomogeneous, and chemically reacting species in one- and multi-dimensional systems.

Basic Theoretical Formulation

The physical model considered for the present study is the transient energy transfer by radiation in absorbing-emitting gases bounded by two parallel gray plates (Fig. 1). In general, T_1 and T_2 can be a function of time and position and there may exist an initial temperature distribution in the gas. It is assumed that the radiative energy transfer in the axial direction is negligible in comparison to that in the normal direction.

For radiation participating medium, the equations expressing conservation of mass and

momentum remain unaltered, while the conservation of energy, in general, is expressed as¹

$$\rho c_p \frac{DT}{Dt} = \text{div} (k \text{ grad } T) + \beta T \frac{DP}{Dt} + \mu \phi - \text{div } q_R \quad (1)$$

where μ is dynamic viscosity, β is the coefficient of thermal expansion of the fluid and ϕ is the Rayleigh dissipation function. For a semi-infinite medium capable of transferring energy only by radiation and conduction, Eq. (1) reduces to

$$\rho c_p \frac{\partial T}{\partial t} = - \frac{\partial q}{\partial y} \quad (2)$$

where q is the sum of the conductive heat flux $q_c = -k (\partial T / \partial y)$ and the radiative flux q_R . For the physical model where radiation is the only mode of energy transfer, the energy equation can be written as

$$\rho c_p \frac{\partial T}{\partial t} = - \frac{\partial q_R}{\partial y} \quad (3)$$

Use of this simplified equation is made to investigate the transient behavior of a radiation participating medium.

For many engineering and astrophysical applications, the radiative transfer equations are formulated for one-dimensional planar systems. For diffuse nonreflecting boundaries and in the absence of scattering, the expression for the total radiative flux is given, for a n-band gaseous system, by^{1,8,23}

$$q_R(y) = e_1 - e_2 + \frac{3}{2} \sum_{i=1}^n \int_{\Delta\omega_i} \left(\int_0^y F_{1\omega_i}(z) \kappa_{\omega_i} \exp\left[-\frac{3}{2} \kappa_{\omega_i}(y-z)\right] dz - \int_y^L F_{2\omega_i}(z) \kappa_{\omega_i} \exp\left[-\frac{3}{2} \kappa_{\omega_i}(z-y)\right] dz \right) d\omega_i \quad (4)$$

where

$$F_{1\omega_i}(z) = e_{\omega_i}(z) - e_{1\omega_i}; \quad F_{2\omega_i}(z) = e_{\omega_i}(z) - e_{2\omega_i}$$

Equation (4) is in proper form for obtaining the nongray solutions of molecular species. In fact, this is an ideal equation for the line-by-line and narrow-band model formulations. However, in order to be able to use the wide band models and correlations, Eq. (4) is transformed in terms of the correlation quantities as^{1,7-11,23}

$$q_R(\xi) = e_1 - e_2$$

$$+ \frac{3}{2} \sum_{i=1}^n A_{0i} u_{0i} \left\{ \int_0^{\xi} F_{1\omega_i}(\xi') \bar{A}'_i \left[\frac{3}{2} u_{0i}(\xi - \xi') \right] d\xi' \right. \\ \left. - \int_{\xi}^1 F_{2\omega_i}(\xi') \bar{A}'_i \left[\frac{3}{2} u_{0i}(\xi' - \xi) \right] d\xi' \right\} \quad (5)$$

where

$$\xi = u/u_0 = y/L; \xi' = u'/u_0 = z/L; \bar{A} = A/A_0;$$

$$u = (S/A_0) Py; u_0 = (S/A_0) PL; PS = \int_{\Delta\omega} \kappa_{\omega} d\omega$$

It should be noted that $F_{1\omega_i}$ and $F_{2\omega_i}$ in Eq. (5) represent the values at the center of the i th band and $\bar{A}'(u)$ denotes the derivative of $\bar{A}(u)$ with respect to u . Upon performing the integration by parts, Eq. (5) can be expressed in an alternate form as²³

$$q_R(\xi) = e_1 - e_2 \\ + \sum_{i=1}^n A_{0i} \left\{ \int_0^{\xi} [de_{\omega_i}(\xi')/d\xi'] \bar{A}'_i \left[\frac{3}{2} u_{0i}(\xi - \xi') \right] d\xi' \right. \\ \left. + \int_{\xi}^1 [de_{\omega_i}(\xi')/d\xi'] \bar{A}'_i \left[\frac{3}{2} u_{0i}(\xi' - \xi) \right] d\xi' \right\} \quad (6)$$

A direct differentiation of Eq. (6) provides the expression for the divergence of radiative flux as

$$\frac{dq_R(\xi)}{d\xi} = \frac{3}{2} \sum_{i=1}^n A_{0i} u_{0i} \left\{ \int_0^{\xi} [de_{\omega_i}(\xi')/d\xi'] \times \right.$$

$$\bar{A}'_i \left[\frac{3}{2} u_{0i}(\xi - \xi') \right] d\xi' - \int_{\xi}^1 [de_{\omega_i}(\xi')/d\xi'] \times$$

$$\bar{A}'_i \left[\frac{3}{2} u_{0i}(\xi' - \xi) \right] d\xi' \quad (7)$$

Equations (5) through (7) are the most convenient equations to use when employing the band-model correlations in radiative transfer analyses.

Upon defining nondimensional radiative heat flux by

$$Q(\xi, t) = q_R(\xi, t) / [e_1(t) - e_2(t)] \quad (8)$$

Eq. (5) can be written as

$$Q(\xi, t) = 1 + \frac{3}{2} \sum_{i=1}^n u_{0i} \left\{ \int_0^{\xi} c_{1i}(\xi', t) \times \right. \\ \left. \bar{A}'_i \left[\frac{3}{2} u_{0i}(\xi - \xi') \right] d\xi' - \int_{\xi}^1 c_{2i}(\xi', t) \times \right. \\ \left. \bar{A}'_i \left[\frac{3}{2} u_{0i}(\xi' - \xi) \right] d\xi' \right\} \quad (9)$$

where

$$c_i(\xi, t) = F_{\omega_i}(\xi, t) / [e_1(t) - e_2(t)] A_{0i}$$

Equation (9) provides the general expression for the radiative flux in the nondimensional form.

Radiative Interaction

Specific consideration is given first to the case where radiation is the sole mode of energy transfer.

By defining $\phi(\xi, t) = T(\xi, t)/T_0$ with T_0 representing some constant reference temperature, Eqs. (3) and (7) can be combined to yield the energy equation in nondimensional form as

$$-\partial\phi(\xi, t)/\partial t = \frac{3}{2} \sum_{i=1}^n \left\{ \int_0^{\xi} \phi_{\omega_i}(\xi', t) \times \right.$$

$$\bar{A}'_i \left[\frac{3}{2} u_{0i}(\xi - \xi') \right] d\xi' - \int_{\xi}^1 \phi_{\omega_i}(\xi', t) \times$$

$$\bar{A}'_i \left[\frac{3}{2} u_{0i}(\xi' - \xi) \right] d\xi' \quad (10)$$

where

$$\phi_{\omega_i}(\xi, t) = (PS_i(T) [\partial e_{\omega_i}(\xi, t) / \partial \xi]) / (\rho C_p T_0 / t_m)$$

The time t in Eq. (10) is defined as $t^* = t/t_m$ with t_m representing some characteristic time scale of the physical problem; however, for the sake of convenience, the asterisk is left out here as well as in further developments. From the definitions of $\phi(\xi, t)$ and $\phi_{\omega_i}(\xi, t)$, it should be noted that Eq. (10) is a nonlinear equation in $T(\xi, t)$. Equation (10), therefore, represents a general case of the transient energy transfer by radiation between two semi-infinite parallel plates.

As a special case, it is assumed that the entire system initially is at the fixed (reference) temperature T_0 . For all time, the temperature of the upper plate is maintained at the constant temperature equal to the reference

temperature, i.e., $T_2 = T_0$. The temperature of the lower plate is suddenly decreased to a lower but constant value, i.e., $T_1 < T_2$. The problem, therefore, is to investigate the transient cooling rate of the gas for a step change in temperature of the lower plate.

In many radiative transfer analyses, it is often convenient (although not essential) to employ the relation for the linearized radiation as

$$e_{\omega_i}(T) - e_{\omega_i}(T_w) = (d e_{\omega_i}/dT)_{T_w} (T - T_w) \quad (11)$$

where again the subscript i refers to the i th band such that ω_i is the wave number location of the band and T_w represents the temperature of the reference wall which could be either T_1 or T_2 . For the special case considered, since we are interested in investigating the transient behavior of the gas because of a step change in temperature of the lower plate, T_w is taken to be equal to T_1 . It should be pointed out that for a single-band gas, the linearization is not required because the temperature distribution can be obtained from Eq. (10) and the radiative heat flux can be calculated from Eqs. (5), (6), or (9). However, for the case of multiband gases and for systems involving mixtures of gases, it is convenient to employ the linearization procedure in order to use the information on band model correlations. The following definitions are useful in expressing the governing equations in linearized forms:

$$\theta = (T - T_1)/(T_2 - T_1) \quad (12a)$$

$$N_{1i} = (P t_m / \rho c_p) K_{1i} \cdot K_{1i} = S_i(T) (d e_{\omega_i}/dT)_{T_1} \quad (12b)$$

$$N_1 = (P t_m / \rho c_p) K_1 \cdot K_1 = \sum_{i=1}^n K_{1i} \quad (12c)$$

$$M_{1i} = (t_m / L \rho c_p) H_{1i} \cdot H_{1i} = A_{0i}(T) (d e_{\omega_i}/dT)_{T_1} \quad (12d)$$

$$M_1 = (t_m / L \rho c_p) H_1 \cdot H_1 = \sum_{i=1}^n H_{1i} \quad (12e)$$

$$M_{1i} u_{0i} = N_{1i} \cdot u_{0i} H_{1i} = PL K_{1i} \quad (12f)$$

where H_i , K_i , N_i and M_i represent the values of H , K , N and M evaluated at the temperature T_1 . As explained in Refs. 1 and 8, these quantities represent the properties of the gaseous medium.

By employing the definitions of Eqs. (11) and (12), Eq. (10) is transformed to obtain a convenient form of the energy equation as²³

$$-\frac{\partial \theta(\xi, t)}{\partial t} = \frac{3}{2} \sum_{i=1}^n N_{1i} \left(\int_0^\xi \frac{\partial \theta(\xi', t)}{\partial \xi'} x \bar{A}_i' \left[\frac{3}{2} u_{0i} (\xi - \xi') \right] d\xi' - \int_\xi^1 \frac{\partial \theta(\xi', t)}{\partial \xi'} x \bar{A}_i' \left[\frac{3}{2} u_{0i} (\xi' - \xi) \right] d\xi' \right) \quad (13)$$

The parameters in Eq. (13) are N_1 and u_0 . For a given gas, the parameters are the gas pressure and the temperature of the lower wall.

The initial and boundary conditions for the physical problem considered are

$$\theta(\xi, 0) = 1 ; \theta(0, t) = 0 ; \theta(1, t) = 1 \quad (14)$$

It is important to note that the boundary conditions given in Eq. (14) are not applicable to Eq. (13) because this equation does not require a boundary condition. Thus, in this case, the temperature of the medium adjacent to a surface differs from the surface temperature. This is because the temperature of the medium adjacent to a surface is affected not only by the surface but also by all other volume elements and surfaces. The radiation slip method is a means of accounting for such temperature jumps and this is discussed in Ref. 1.

By employing the definitions of Eqs. (8), (11), and (12), relations for the radiative flux, as given by Eqs. (5) and (6), are expressed as

$$Q(\xi, t) = 1 - (3/8 \sigma T_1^3) \sum_{i=1}^n u_{0i} H_{1i} \left(\int_0^\xi \theta(\xi', t) x \bar{A}_i' \left[\frac{3}{2} u_{0i} (\xi - \xi') \right] d\xi' + \int_\xi^1 [1 - \theta(\xi', t)] x \bar{A}_i' \left[\frac{3}{2} u_{0i} (\xi' - \xi) \right] d\xi' \right) \quad (15a)$$

and

$$Q(\xi, t) = 1 - (1/4 \sigma T_1^3) \sum_{i=1}^n H_{1i} \left(\int_0^\xi \frac{\partial \theta(\xi', t)}{\partial \xi'} x \bar{A}_i' \left[\frac{3}{2} u_{0i} (\xi - \xi') \right] d\xi' - \int_\xi^1 \frac{\partial \theta(\xi', t)}{\partial \xi'} x \bar{A}_i' \left[\frac{3}{2} u_{0i} (\xi' - \xi) \right] d\xi' \right) \quad (15b)$$

It should be pointed out that Eq. (15a) is a convenient form for the optically thin and general solutions while Eq. (15b) is useful for solutions in the large path length limit. Once the solutions for $\theta(\xi, t)$ are known from the energy equation, the appropriate relations for the heat flux can be obtained from Eqs. (15). It should be noted that the quantity $H_1/(\sigma T_1^3)$ in Eqs. (15) is nondimensional.

Radiation and Conduction

For this case where conduction heat transfer takes place simultaneously with radiative transfer, the energy equation is given by Eq. (2). Thus, a combination of Eqs. (2), (11) and (12) results in

$$\frac{\partial \theta}{\partial \xi} = R \frac{\partial^2 \theta}{\partial \xi^2} - \frac{3}{2} \sum_{i=1}^n N_{1i} \left(\int_0^{\xi} \frac{\partial \theta(\xi', t)}{\partial \xi'} x \right)$$

$$\bar{A}_1 \times \frac{3}{2} u_{01}(\xi - \xi') d\xi' - \int_{\xi}^1 \frac{\partial \theta(\xi', t)}{\partial \xi'} x$$

$$\bar{A}_1 \left[\frac{3}{2} u_{01}(\xi' - \xi) d\xi' \right] \quad (16)$$

where

$$R = k t_m / (\rho C_p L^2)$$

The nondimensional parameter R in Eq. (16) is analogous to the Fourier number. For $R = 0$, Eq. (16) reduces to Eq. (13). Since the presence of conduction implies continuity of temperatures at the boundaries, the boundary conditions for Eq. (16) are those given in Eq. (14). The quantity N_1/R can be expressed as $N = N_1/R = (PL^2/k)K_1$. The nondimensional parameter N denotes the relative importance of radiation versus conduction in the gas. For particular values of P and L , it is actually the dimensional gas property $N_1/(RPL^2) = K_1/k$ that represents the relative importance of radiation versus conduction.

For the case of no radiation, Eq. (16) becomes

$$\frac{\partial \theta}{\partial \xi} = R \frac{\partial^2 \theta}{\partial \xi^2} \quad (17)$$

The separation of variables results in a general solution of Eq. (17) as

$$\theta = \exp(-\lambda^2 Rt) (B_1 \sin \lambda \xi + B_2 \cos \lambda \xi) \quad (18)$$

where λ^2 is the separation parameter. The particular solution of Eq. (18) can be obtained by satisfying the boundary conditions. Alternately, by defining a similarity variable $\eta = \xi/\sqrt{4Rt}$, Eq. (17) can be written as

$$\frac{d^2 \theta}{d\eta^2} + 2\eta \frac{d\theta}{d\eta} = 0 \quad (19)$$

The solution of Eq. (19), with initial and boundary conditions given by Eq. (14), is found to be

$$\theta(\xi, t) = (2/\sqrt{\pi}) \operatorname{erf} \eta \quad (20)$$

This solution is applicable for relatively large separations between the plates.

In the case of simultaneous conduction and radiation heat transfer, the nondimensional heat flux is defined as

$$\bar{Q} = [q_c(\xi, t) + q_R(\xi, t)]/[e_1(t) - e_2(t)] \quad (21)$$

Expressions similar to Eqs. (15a) and (15b) can be obtained easily in this case also (Ref. 24).

Method of Solutions

The solution procedures for the radiative equilibrium and radiation with conduction cases are available in Ref. 24. For the sake of brevity, only the solution procedure for the radiative equilibrium case is given here.

For the general case of radiative equilibrium, the temperature distribution is obtained from the solution of the energy equation, Eq. (13). Once $\theta(\xi, t)$ is known, the radiative heat flux is calculated by using the appropriate form of Eq. (15). Before discussing the solution procedure for the general case, however, it is desirable to obtain the limiting forms of Eqs. (13) and (15) in the optically thin and large path length limits and investigate the solutions of resulting equations.

Optically Thin Limit

In the optically thin limit $\bar{A}(u) = u$ and $\bar{A}'(u) = 1$, and therefore, Eq. (13) reduces to 1,8,23

$$\frac{\partial \theta(\xi, t)}{\partial \xi} + 3 N_1 \theta(\xi, t) - \frac{3}{2} N_1 = 0 \quad (22a)$$

From an examination of Eq. (22a) along with the definitions given in Eq. (12), it is evident that in the optically thin limit the temperature distribution in the medium is independent of the ξ -coordinate for the case of pure radiative exchange. This is a characteristic of the optically thin radiation in the absence of other modes of energy transfer. Thus, Eq. (22a) can be written as

$$\frac{d\theta(t)}{dt} + 3 N_1 \theta(t) - \frac{3}{2} N_1 = 0; \theta(\xi, 0) = 1 \quad (22b)$$

Since gas properties are evaluated at known reference conditions, N_1 is essentially constant, and solution of Eq. (22b) is found to be

$$\theta(t) = \frac{1}{2}[1 + \exp(-3 M_1 t)] \quad (23)$$

In the optically thin limit both forms of Eq. (15) yield the same final relation for the radiative flux as²³

$$Q(\xi, t) = 1 - [3/(8\sigma T_1^3)] (PLK_1) [(1-\xi) + (2\xi - 1)\theta(t)] \quad (24)$$

It should be pointed out that in Eq. (24) the quantity $(PLK_1/\sigma T_1^3)$ is nondimensional. The relation for $\theta(t)$ in Eq. (24) is obtained from Eq. (23). Thus, evaluation of the temperature distribution and radiative heat flux in the optically thin limit does not require numerical solutions.

Large Path Length Limit

In the large path length limit (i.e., for $u_{01} \gg 1$ for each band), one has $\bar{A}(u) = \ln(u)$, $\bar{A}'(u) = 1/u$, and $\bar{A}''(u) = -1/u^2$. Thus, in this limit, Eq. (13) reduces to^{1,8,23}

$$\frac{\partial \theta(\xi, t)}{\partial t} = -M_1 \int_0^1 \frac{\partial \theta(\xi', t)}{\partial \xi'} \frac{d\xi'}{(\xi - \xi')} \quad (25)$$

An analytical solution of Eq. (25) may be possible, but numerical solution can be obtained quite easily.

In the large path length limit, Eqs. (15a) and (15b) reduce respectively to

$$Q(\xi, t) = 1 - (1/4\sigma T_1^3) H_1 \left[\int_0^1 \theta(\xi', t) \frac{d\xi'}{(\xi - \xi')} - \int_{\xi}^1 \frac{d\xi'}{(\xi - \xi')} \right] \quad (26a)$$

and

$$Q(\xi, t) = 1 - (1/4\sigma T_1^3) \sum_{i=1}^n H_{1i} \left\{ \int_0^{\xi} \frac{\partial \theta(\xi', t)}{\partial \xi'} x \ln\left[\frac{3}{2} u_{01}(\xi - \xi')\right] d\xi' + \int_{\xi}^1 \frac{\partial \theta(\xi', t)}{\partial \xi'} x \ln\left[\frac{3}{2} u_{01}(\xi' - \xi)\right] d\xi' \right\} \quad (26b)$$

The expressions for dimensionless radiative heat flux from or to the wall are obtained by setting $\xi = 0$ in Eqs. (26).

Numerical Solutions of Governing Equations

The general solutions of Eqs. (13) and (25) are obtained numerically by employing the method

of variation of parameters. For this, a polynomial form for $\theta(\xi, t)$ is assumed in powers of ξ with time dependent coefficients as

$$\theta(\xi, t) = \sum_{m=0}^n c_m(t) \xi^m \quad (27)$$

By considering only the quadratic solution in ξ , and satisfying the boundary conditions of Eq. (14), one finds

$$\theta(\xi, t) = \xi^2 + g(t) (\xi - \xi^2) \quad (28)$$

where $g(t)$ represents the time dependent coefficient. At $t = 0$, a combination of Eqs. (14) and (28) yields the result

$$g(0) = (1 - \xi^2)/(\xi - \xi^2) \quad (29)$$

Equations (28) and (29) are used to obtain specific solutions of Eqs. (13) and (25). Once the temperature distribution is known, the expressions for heat flux are obtained by numerically integrating the corresponding equations. The entire numerical procedure is described in detail in Refs. 23 and 24. The numerical procedure is similar for higher order solutions in ξ of Eq. (27), but computational resources required are considerably higher.

Physical Conditions and Data Source

For the physical problem considered (Fig. 1) four specific absorbing-emitting species were selected for an extensive study; these are CO, CO₂, OH and H₂O. The species CO was selected because it contains only one fundamental vibration-rotation (VR) band and all spectral information are easily available in the literature. It is a very convenient gas to test the numerical procedure without requiring excessive computational resources. Species OH and H₂O are the primary radiation participating species for the pressure and temperature range anticipated in the combustor of the scramjet engine. Species CO₂, and combinations of CO₂ and H₂O are important absorbing-emitting species in many other combustion processes.

In radiative transfer analyses, it is essential to employ a suitable model to represent the absorption-emission characteristics of specific species under investigation. Several line-by-line, narrow-band, and wide-band models are available to model the absorption of a VR band (Refs. 7-11). However, it is often desirable to use a simple correlation to represent the total absorption of a wide band. Several such correlations are available in the literature (Refs. 7-11). The relative merits of these correlations are discussed in Ref. 11. In this study, the correlation proposed by Tien and Lowder⁷ is employed and this is given by

$$\bar{A}(u) = \ln(u f(\beta) \left[\frac{u + 2}{u + 2f(\beta)} \right] + 1) \quad (30)$$

where

$$f(\beta) = 2.94[1 - \exp(-2.60 \beta)]$$

and β represents the line structure parameter.

The spectral information and correlation quantities needed for CO, CO₂ and H₂O were obtained from Refs. 7-9. The spectral data for OH were obtained from Ref. 25 and correlation quantities were developed in Ref. 24. The specific VR bands considered for each species are: CO (4.7 μ fundamental), OH (2.8 μ fundamental), CO₂ (15 μ , 4.3 μ and 2.7 μ), and H₂O (20 μ , 6.3 μ , 2.7 μ , 1.87 μ , and 1.38 μ).

For the specific problem considered, the dependent variables are θ , Q , and \bar{Q} , and independent variables are ξ and t . The parameters for general solutions are T_1 , T_2/T_1 , u_0 , and t_m . For the radiative equilibrium case, θ and Q depend only on t and N_1 in the optically thin limit and on ξ , t , and M_1 in the large path length limit. For the case of combined radiation and conduction, θ and Q depend on ξ , t , and M_1/R in the large path length limit. The parameters for specific solutions for different species are T_1 , T_2/T_1 , P , L , and t_m . Extensive results, therefore, can be obtained by varying these parameters. For parametric studies, however, only certain values of pressure, temperature, and plate spacing were selected and results were obtained for the general as well as limiting cases. Unless stated otherwise, specific results were obtained for $T_2 = 2 T_1$.

Results and Discussion

Results have been obtained for different radiation participating species for both cases, the radiative equilibrium and radiation with conduction. Selected results are presented here and extensive results are provided in Ref. 24. It should be realized at the outset that, according to the physics of the problem, the gas initially is at a high temperature $T_1 = T_2$. At $t = 0$, the temperature T_1 is lowered to a constant value. The energy exchange then occurs and the gas cools down in time until a steady-state condition is reached. At this time, a certain temperature profile is established and a fixed amount of energy exchange occurs irrespective of the time. The rate of cooling of the gas layer, therefore, is dependent on the nature of the participating species and on the physical parameters of the problem.

Some limiting solutions that are independent of any participating species are presented first in Fig. 2 for the radiative equilibrium case. The temperature distribution in the channel is plotted as a function of the optically thin parameter N_1 for different times. These results show an exponential decay with time reaching the steady-state value of $\theta=1/2$ for $t \rightarrow \infty$. The temperature distribution for the large path length limit is shown in Fig. 2 (with broken lines) as a function of the large path length parameter M_1 and for different times. Although

the numerical values are entirely different, these results also show the exponential decay with time and reach the limiting value of $\theta = 1/2$ for $t \rightarrow \infty$. It should be noted that while the optically thin solutions are independent of the ξ -coordinate, the large path length solutions do depend on ξ and they have been obtained for $\xi = 0.5$. In the case of simultaneous radiation and conduction, both optically thin and large path length solutions for temperature distribution depend on ξ . These results, however, can be expressed in terms of the radiation-conduction parameter $N=N_1/R$ in the optically thin limit and $M = M_1/R$ in the large path length limit.

The radiative equilibrium temperature distribution for CO are shown in Fig. 3 for three different characteristic times and for $P = 1$ atm, $L = 10$ cm, and $T_w = 500$ K. For small t_m , $t^* = t/t_m$ becomes large and, therefore, θ varies slowly with t^* ; the reverse is true for large t_m values. This trend is evident clearly from the simplest case of the optically thin solution given by Eq. (23). Similar trends in results were observed also for other species for different values of P , T_w and L . Thus, to demonstrate typical transient trends, other results presented in this study were obtained for an intermediate value of the characteristic time $t_m = 0.00001$ sec.

The centerline temperature variations with time are illustrated in Fig. 4a for CO and in Fig. 4b for OH. General and limiting solutions are shown for pure conduction, radiation, and radiation with conduction for $P = 1$ atm, $T_w = 500$ K, and $L = 10$ cm. It is noted that for both gases the optically thin solutions approach the steady-state conditions faster than the large path length and general solutions. For the physical conditions considered, the energy is transferred faster by conduction than by radiation, and the steady-state conditions are reached earlier by the combined radiation and conduction process. Although OH is a relatively better heat conducting gas, CO is seen to be more effective in the radiative transfer. For the same physical conditions as in Figs. 4, the radiation and radiation with conduction results are compared for CO, OH, H₂O, and CO₂ in Fig. 5. It is seen that H₂O is most effective and OH is least effective in transferring the radiative energy. The ability of a gas to transfer radiative energy depends on the molecular structure of the gas, band intensities and physical conditions of the problem. Thus, H₂O with five strong VR bands is a highly radiation participating species and the steady-state conditions are reached quickly for H₂O than for other species. However, CO with one fundamental band is seen to be a better radiating gas than CO₂ with three VR bands. This is because for the given physical conditions, the optical thickness of CO₂ is sufficiently large and in the large path length limit CO₂ is relatively less effective in transferring the radiative energy (Ref. 8). Further results for CO and OH are illustrated in Figs. 6 for different wall temperatures. It is seen that while radiation is

less effective than conduction at $T_w = 500$ K, it is highly effective at $T_w = 1,000$ K. This, however, would be expected because radiation becomes considerably important at higher temperatures. The steady-state condition is reached quicker for $T_w = 1,000$ K than for $T_w = 500$ K. In fact for the characteristic time considered ($t_m = 0.00001$ sec.), the steady-state condition is reached quickly for all species for temperatures higher than $T_w = 1,000$ K. Results for the pure radiation case are illustrated in Figs. 7 for CO and OH for $L = 1$ cm and 10 cm. It is seen that while the general and large path length solutions depend on the plate spacing the optically thin solutions are independent of the spacing. This fact was pointed out earlier in the method of solution. In the presence of other modes of energy transfer, the optically thin solutions also depend on the plate spacings. As would be expected, for the same physical conditions, the steady-state condition is reached quicker for the lower plate spacing.

The temperature variations within the plates are shown in Figs. 8-11 for different species and for $P = 1$ atm and $L = 5$ cm. In the absence of molecular conduction, temperature jumps (radiation slips) occur at the boundaries and, therefore, the general solutions for the case of radiative equilibrium are not presented. However, general as well as limiting solutions are presented for the case of radiation with conduction. It is noted, in general, that for the case of radiation with conduction, the steady-state conditions are reached for all species at $t \geq 0.1$ and for $T_w \geq 500$ K. For the case of pure radiation, the steady-state conditions are reached at relatively longer times. The optically thin results are seen to be independent of the ξ -coordinate for the case of radiative equilibrium and are seen to vary slowly in the central portion of the plates for the case of radiation with conduction. This is because, in this limit, the gas interacts directly with the boundaries and conduction is predominant near the walls. Specific results for CO are illustrated in Figs. 8 for $T_w = 1,000$ K. For the case of radiation with conduction, general and limiting solutions are compared in Fig. 8a; and for both cases, the radiative equilibrium and radiation with conduction, limiting solutions are compared in Fig. 8b. The steady-state results for pure conduction are also shown in Fig. 8b for comparative purposes. The results demonstrate the typical trends for limiting and general solutions, i.e., a lower temperature gradient implies a higher rate of energy transfer. Specific results for OH are illustrated in Figs. 9 for $T_w = 500$ K. General and limiting solutions are shown in Fig. 9a; and limiting solutions are compared in Figs. 9b and 9c. For the case of radiation with conduction, the limiting and general solutions are seen to be in good agreement for all times (Fig. 9a). This is because for the conditions of the illustrated results, conduction dominates the energy transfer process in OH. The typical trends in results for the optically thin and large path length limits are shown in Figs. 9b and 9c, respectively. Figure 9b clearly shows that for all times the radiative equilibrium results are independent of the ξ -coordinate in the optically thin limit.

Figure 9 shows that at earlier times the rate of energy transfer is higher in the presence of conduction. Specific results for H_2O are illustrated in Figs. 10 for the case of radiation with conduction. It is seen clearly that the rate of cooling is significantly higher in the large path length limit (Fig. 10a), and the steady-state conditions are reached at relatively longer times for lower T_w values (Fig. 10b). For the case of combined radiation and conduction, a comparison of results for different species is shown in Fig. 11 for $t = 0.01$ and 0.1. The results for $t = 0.1$ essentially correspond to the steady-state conditions. For $t = 0.01$, the variation in temperature is seen to be relatively small between $\xi=0.2$ and 0.9. The centerline temperature is found to be the lowest for H_2O , and this is followed by OH, CO, and CO_2 . However, it is noted that OH is very effective in transferring the net energy in comparison to the other species. As discussed earlier, this is mainly due to relatively higher conductive ability of OH at $T_w = 500$ K.

The centerline temperature distributions are shown in Figs. 12-15 for different gases as a function of the spacing between the plates. In most figures, results are presented for both cases, the radiative equilibrium and radiation with conduction. In selected figures, results for the case of pure conduction are included also for comparative purposes. For a particular gas, specific results are presented for various times to demonstrate the radiative nature of the gas under different pressure and temperature conditions.

The results for CO are presented in Figs. 12 for different cases. For $P = 1$ and $T_w = 500$ K, the results illustrated in Fig. 12a show that the time required to reach the steady-state condition increases with increasing plate spacings. For a particular plate spacing, the centerline temperature is lower for the case of radiation with conduction than for pure radiation for all times. For $P = 1$ atm and $T_w = 1,000$ K, results presented in Fig. 12b show that the large path length solutions are closer to the general solutions for $L > 20$ cm; and the results for pure radiation and radiation with conduction are identical for $t \geq 0.5$. The centerline temperature variations are shown in Fig. 12c for $t = 0.5$, $T_w = 500$ K, and different pressures. It is noted that while the heat transfer by conduction is insensitive to the change in pressure, the radiative heat transfer is strongly dependent on it. The rate of radiative interaction increases with increasing pressure until the large path length limit is reached for sufficiently large values of L . For the case of pure radiation, the results for $P = 0.1$ atm differ considerably from other results. This is due to use of the Tien and Lowder's correlation which is suitable only at relatively higher pressures (Ref. 11). The centerline temperature variations are shown in Fig. 12d for $t = 0.5$, $P = 1$ atm, and different values of T_w . As would be expected, both conductive and radiative interactions increase with increasing temperatures, although the increase in radiative transfer is comparatively higher. It should be noted that for $T_w = 300$ K, $T_2 = 2 T_w = 600$ K, for $T_w = 500$ K, $T_2 = 1,000$ K, and so on. Thus, for a

higher value of $T_w = T_1$, the energy interactions occur at a sufficiently large temperature difference between the upper and lower plates. At these temperatures, if the plate spacing is small, the energy is transferred quickly and the steady-state condition is reached at relatively shorter times. This fact was pointed out also in the discussion of results of Figs. 7.

The centerline temperature variations for OH are illustrated in Figs. 13 for different conditions. The results presented in Fig. 13a for $P = 1$ atm and $T_w = 500$ K show the similar trend as CO in Fig. 12a, although the extent of energy transfer by simultaneous radiation and conduction is relatively higher. This is because at $T_w = 500$ the energy transfer in OH is dominated by the conduction heat transfer. General and limiting solutions for radiative equilibrium are shown in Fig. 13b and for radiation with conduction in Fig. 13c. These results clearly demonstrate the typical radiative interaction trends for different times. The results show that the optically thin solutions are independent of the plate spacing in the case of pure radiation but depend on the spacing when molecular conduction is included. The large path length results are seen to be valid only for large values of L for the case of pure radiation (Fig. 13b), but they appear to be valid in the entire range for the case of radiation with conduction (Fig. 13c). The results for pure conduction, pure radiation, and conduction with radiation are illustrated in Fig. 13d for $P = 1$ atm and $T_w = 1,000$ K. For this temperature, the results for pure radiation and radiation with conduction are found to be identical. This indicates that at higher temperatures, OH becomes a highly radiation participating gas. The results for variation of the centerline temperature for OH with pressure and temperature are given in Ref. 24 and they show the same general trend as the results for CO shown in Figs. 12c and 12d.

Extensive results of $\theta(\xi = 0.5)$ versus L have been obtained for H_2O and CO_2 for different conditions and these are discussed in Ref. 24. In general, these results show similar trends as exhibited by the results for CO and OH but the extent of radiative interactions is entirely different. For example, a comparison of results presented in Fig. 14a for H_2O with the results of Fig. 12a for CO and Fig. 13a for OH for identical conditions reveals that H_2O is a highly radiation participating gas even for shorter times. For H_2O , results presented in Fig. 14b demonstrate that the large path length solutions are closer to the general solutions for both cases, the radiative equilibrium and radiation with conduction.

The centerline temperature variations are compared for different gases in Fig. 15 for $P = 1$ atm, $T_w = 500$ K, and $t = 0.05$. For the case of radiative equilibrium, it is noted that OH is the least effective and H_2O is the most effective gas in transferring the radiative energy for plate spacings greater than two centimeters. When molecular conduction is included, OH becomes more effective because of its relatively higher conductive ability. These points were noted also in earlier discussions. The story, however, can be entirely different for other physical

conditions because of the radiative/conductive nature of participating species (Refs. 8 and 24). This fact is partially evident from the steady-state results, for the case of combined radiation and conduction, presented in Fig. 16 for two different temperatures, $T_w = 300$ K and 500 K. For example, for $T_w = 300$ K and $L = 10$ cm, the temperature values for CO and CO_2 are about the same, for H_2O it is lower, and for OH it is the lowest; however, for plate spacing greater than $L = 20$ cm, the trend is entirely different. Also, it should be noted that the steady-state ($t = 0.5$) results for $T_w = 500$ K in Fig. 16 show different trend than the results for the same temperature in Fig. 15 for $t = 0.05$. Thus, in order to predict the relative ability of a gas for radiative interactions, it is very important to consider the exact physical conditions for all species. These predictions may not be applicable if physical conditions of the problem are changed.

Extensive results for the variation in heat transfer can be presented analogous to the variation of temperature for different conditions. However, this should not be necessary because the heat transfer variation follows the trend of the temperature variation in a reverse manner. If the temperature differences are higher, the rate of heat transfer will be higher and the steady-state conditions will be reached at earlier times. The results for heat transfer variations have been obtained for selected conditions and these are available in Ref. 24. Only a few results are presented here to show the trend in cooling rates for different wall temperatures and plate spacings.

For $P = 1$ atm, the results for Q and \bar{Q} are illustrated, as a function of t^* , in Figs. 17 for H_2O and in Fig. 18 for CO_2 . The results for $t^* = 0.0 - 1.0$ are shown in Fig. 17a for H_2O . However, it is found that for the t_m value selected in this study, the steady-state conditions are reached in most cases at about $t^* = 0.2$. Consequently, the results in Figs. 17b, 17c, and 18 are presented only in the range of $t^* = 0.0 - 0.2$ to demonstrate the rate of cooling at different temperatures. As would be expected, the results show that for a given plate spacing the gas layer reaches the steady-state condition faster at higher values of T_w because of stronger radiative interactions. It should be noted that the rate of energy transfer increases with time for a gas layer closer to the upper wall ($\xi = 0.75$) and decreases with time for a gas layer closer to the lower wall ($\xi = 0.25$) until the steady-state conditions are reached. The rate of cooling is entirely different if the plate spacing is changed (Fig. 17c). From a comparison of results of Figs. 17 and 18, it is noted that the trend and rate of energy transfer are different for different species. This, however, would be expected because of the relative ability of different species to participate in the radiation-conduction interaction process.

Conclusions

The problem of transient radiative interaction in nongray absorbing-emitting species has been formulated in a general sense such that sophisticated absorption models can be used to

obtain accurate results if desired. Results have been obtained for the special case of radiative interactions in a plane gas layer bounded by two parallel plates when the temperature of the bottom plate is suddenly reduced to a lower but constant temperature. The energy transfer by pure radiation, and by simultaneous radiation and conduction were considered and specific results have been obtained for CO, CO₂, H₂O, and OH by employing the Tien and Lowder's correlation for band absorption. It is noted that the extent of radiative interaction is dependent on the nature of the participating species and parameters T_1 , T_2/T_1 , P , L , and t_m . The steady-state conditions are reached at relatively longer times for radiative equilibrium than for radiation with conduction. For a particular value of P and T_1 , the time required to reach the steady-state condition increases with increasing plate spacing. For a fixed plate spacing, the energy is transferred quickly for higher T_1 values because of large temperature differences between the plates. The rate of radiative interaction increases with increasing pressure until the large path length limit is reached. The radiative equilibrium solutions are found to be independent of the plate spacing in the optically thin limit. In the case of simultaneous radiation and conduction, both optically thin and large path length solutions depend on the y -location between the plates. At moderate temperatures, OH is a poor radiating but better heat conducting gas. For most conditions, H₂O is found to be highly radiation participating species, and the steady-state conditions are reached quickly for H₂O than for other species. The information on radiative interactions for OH and H₂O is useful in the analysis of the flow field in the scramjet engine.

Acknowledgement

This work was supported in part by the NASA Langley Research Center through the ICAM Project Grant NAG-1-363.

References

1. Sparrow, E. M. and Cess, R. D., Radiation Heat Transfer, Brooks/Cole, Belmont, Calif., 1966 and 1970. New Augmented Edition, Hemisphere Publishing Corp., Washington, D.C., 1978.
2. Hottel, H. C. and Sarofim, A. F., Radiative Transfer, McGraw-Hill Book Co., New York, 1967.
3. Siegel, R. and Howell, J. R., Thermal Radiation Heat Transfer, McGraw-Hill Book Co., New York, 1971; Second Edition, 1981.
4. Cess, R. D., "The Interaction of Thermal Radiation with Conduction and Convection Heat Transfer," Advances in Heat Transfer, Vol. 3, Academic Press, New York, 1966.
5. Sparrow, E. M., "Radiation Heat Transfer between Surfaces," Advances in Heat Transfer, Vol. 2, Academic Press, New York, 1965.
6. Viskanta, R., "Radiation Transfer and Interaction of Convection with Radiative Heat Transfer," Advances in Heat Transfer, Vol. 3, Academic Press, New York, 1966.
7. Tien, C. L., "Thermal Radiation Properties of Gases," Advances in Heat Transfer, Vol. 5, Academic Press, New York, 1968.
8. Cess, R. D. and Tiwari, S. N., "Infrared Radiative Energy Transfer in Gases," Advances in Heat Transfer, Vol. 8, Academic Press, New York, 1972.
9. Edwards, D. K., "Molecular Gas Band Radiation," Advances in Heat Transfer, Vol. 12, Academic Press, New York, 1976.
10. Tiwari, S. N. "Band Models and Correlations for Infrared Radiation," Radiative Transfer and Thermal Control (Progress in Astronautics and Aeronautics), Vol. 49, American Institute of Aeronautics and Astronautics, New York, 1976.
11. Tiwari, S. N., "Models for Infrared Atmospheric Radiation," Advances in Geophysics, Vol. 20, Academic Press, New York, 1978.
12. Lick, W., "Transient Energy Transfer by Radiation and Conduction," International Journal of Heat and Mass Transfer, Vol. 8, 1965, pp. 119-127.
13. Chang, Y. P. and Kang, C. S., "Transient and Steady Heat Transfer in a Conducting and Radiating Medium," AIAA Journal, Vol. 8, No. 4, April 1970, pp. 609-614.
14. Chang, Y. P. and Smith, R. C., Jr., "Steady and Transient Heat Transfer by Radiative and Conduction in a Medium Bounded by Two Coaxial Cylindrical Surfaces," International Journal of Heat and Mass Transfer, Vol. 13, 1970, pp. 69-80.
15. Doornink, D. G. and Hering, R. G., "Transient Radiative Heat Transfer in a Nongray Medium," Journal of the Quantitative Spectroscopy and Radiative Transfer, Vol. 12, 1972, pp. 1161-1174.
16. Larson, D. W. and Viskanta, R., "Transient Combined Laminar Free Convection and Radiation in a Rectangular Enclosure," Journal of Fluid Mechanics, Vol. 78, Part 1, 1976, pp. 65-85.
17. Melnikov, V. I. and Sukhovich, E. P., "Transient Heat Exchange Between a Radiating Plate and a High-Temperature Gas Flow," Heat Transfer-Soviet Research, Vol. 10, No. 3, May-June 1978, pp. 11-20 (Translation).
18. Heinsch, R. P. and Viskanta, R., "Transient Combined Conduction-Radiation in an Optically Thick Semi-Infinite Medium," AIAA Journal, Vol. 6, 1968, pp. 1409-1411.

19. Hazzah, A. S. and Beck, J. V., "Unsteady Combined Conduction-Radiation Energy Transfer Using a Rigorous Differential Method," International Journal of Heat and Mass Transfer, Vol. 13, March 1970, pp. 517-522.
20. Lii, C. C. and Özisik, M. N., "Transient Radiation and Conduction in an Absorbing, Emitting and Scattering Slab with Reflecting Boundaries," International Journal of Heat and Mass Transfer, Vol. 15, May 1972, pp. 1175-1179.
21. Weston, K. C. and Hauth, J. L., "Unsteady, Combined Radiation and Conduction in an Absorbing, Scattering and Emitting Medium," Journal of Heat Transfer, Vol. 95, August 1973, pp. 357-364.
22. Sutton, W. H., "A Short Time Solution for Coupled Conduction and Radiation in a Participating Slab Geometry," ASME Paper No. 84-HT-34, 1984.
23. Tiwari, S. N., "Radiative Interactions in Transient Energy Transfer in Gaseous Systems," Progress Report NAG-1-423, Dept. of Mechanical Engineering and Mechanics, Old Dominion University, Norfolk, VA, December 1985.
24. Tiwari, S. N. and Singh, D. J., "Interaction of Transient Radiation in Nongray Gaseous Systems," Progress Report NAG-1-423, Dept. of Mechanical Engineering and Mechanics, Old Dominion University, Norfolk, VA, January 1987.
25. Goulard, R. and Thomson, J. A. L. (Editors), Handbook of Infrared Radiation from Combustion Gases, NASA SP-3090, 1973.

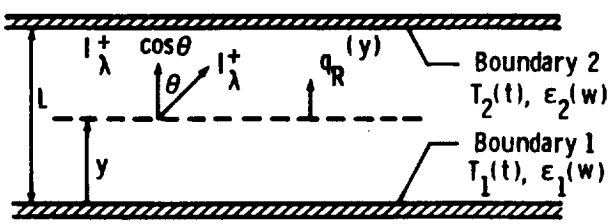


Fig. 1 Physical model and coordinate system.

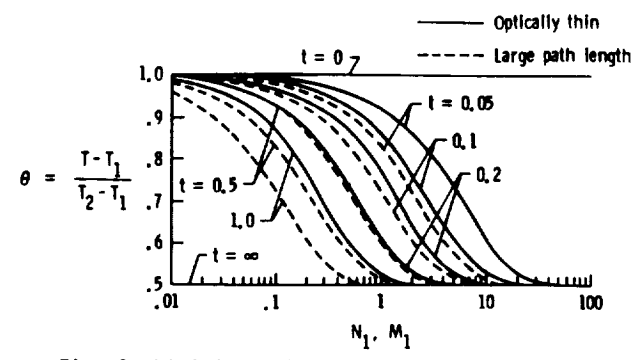


Fig. 2 Limiting solutions for the radiative equilibrium case.

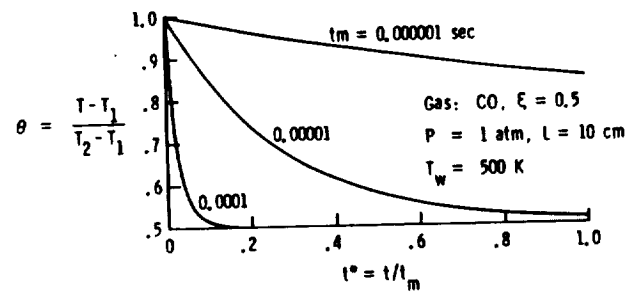


Fig. 3 Temperature variation for transient radiation for different characteristic times (CO, P=1 atm, Tw=500 K, L=10 cm, and xi=0.5).

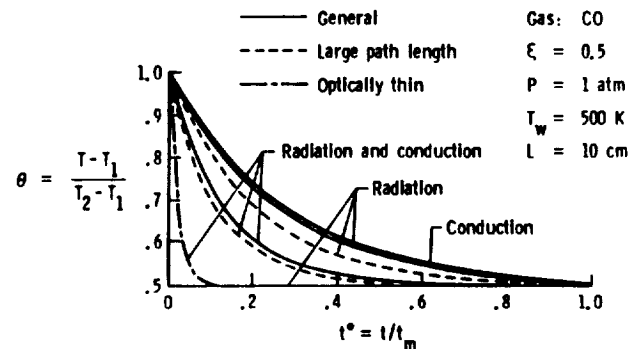


Fig. 4a Centerline temperature variation with time for CO with P=1 atm, Tw=500 K, and L=10 cm.

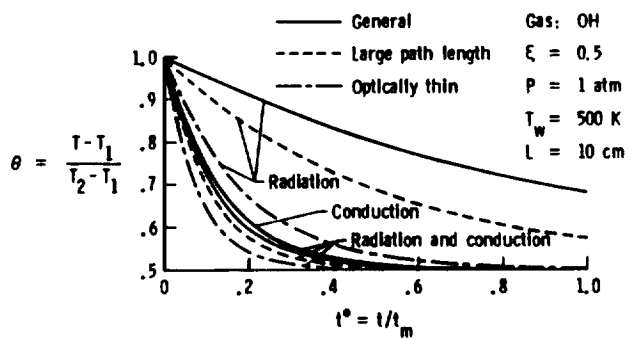


Fig. 4b Centerline temperature variation with time for OH with P=1 atm, Tw=500 K, and L=10 cm.

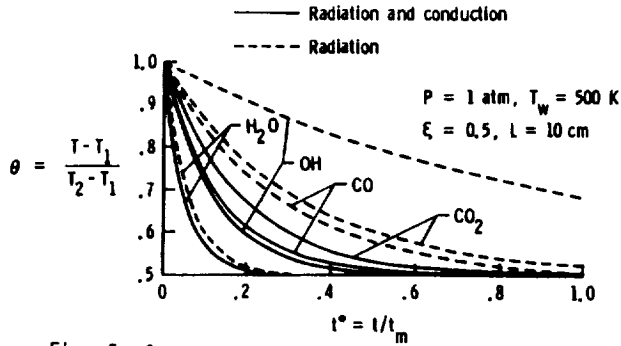


Fig. 5 Comparison of centerline temperature variation with time for $P = 1 \text{ atm}$, $T_w = 500 \text{ K}$, and $L = 10 \text{ cm}$.

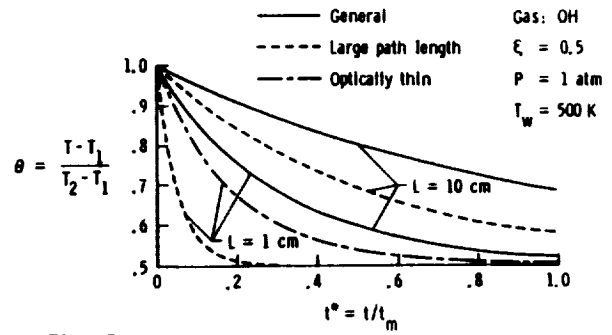


Fig. 7b Centerline temperature results for pure radiation (OH, $P = 1 \text{ atm}$, and $T_w = 500 \text{ K}$).

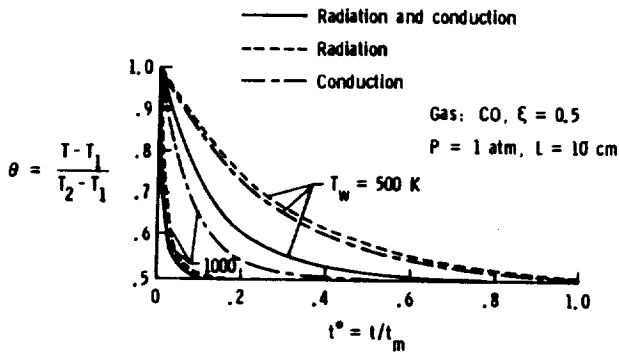


Fig. 6a Centerline temperature variation with time for CO with $P = 1 \text{ atm}$ and $L = 10 \text{ cm}$.

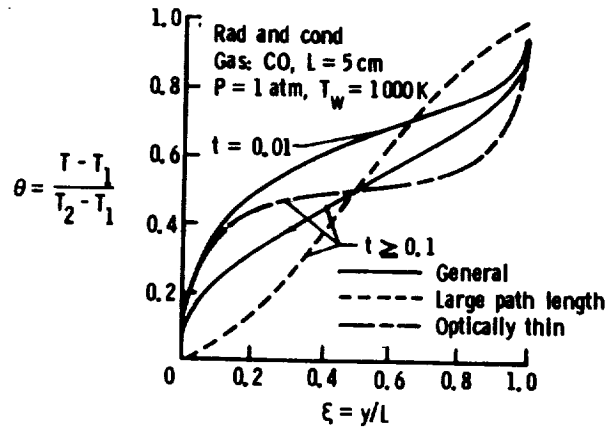


Fig. 8a Temperature variation for combined radiation and conduction for CO with $P = 1 \text{ atm}$, $T_w = 1,000 \text{ K}$, and $L = 5 \text{ cm}$.

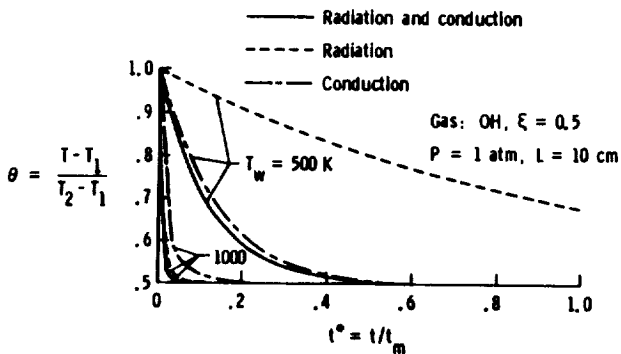


Fig. 6b Centerline temperature variation with time for OH with $P = 1 \text{ atm}$ and $L = 10 \text{ cm}$.

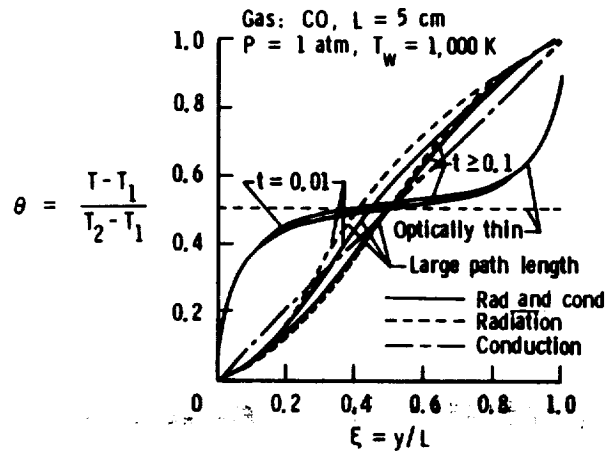


Fig. 8b Temperature variation for CO with $P = 1 \text{ atm}$, $T_w = 1,000 \text{ K}$, and $L = 5 \text{ cm}$.

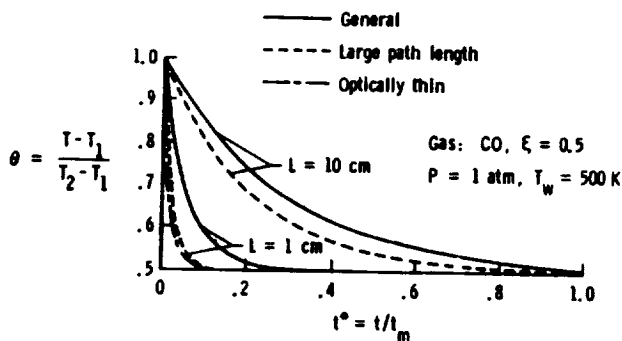


Fig. 7a Centerline temperature results for pure radiation (CO, $P = 1 \text{ atm}$, and $T_w = 500 \text{ K}$).

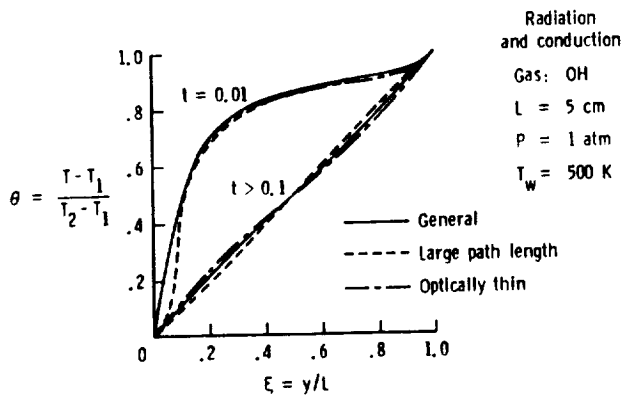


Fig. 9a Temperature variation for combined radiation and conduction for OH with $P=1$ atm, $T_w=500$ K, and $L=5$ cm.

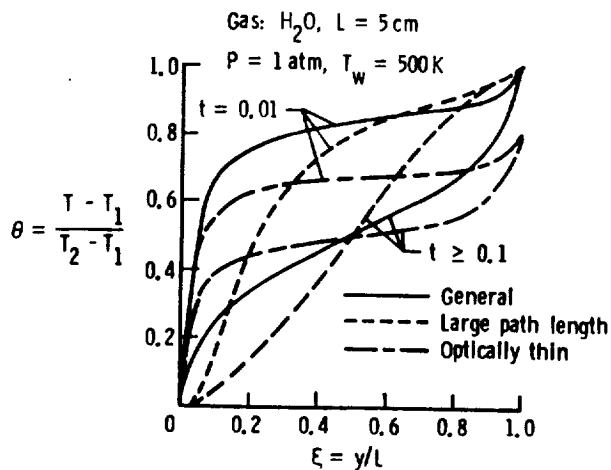


Fig. 10a Temperature variation for combined radiation and conduction for H_2O with $P=1$ atm, $T_w=500$ K, and $L=5$ cm.

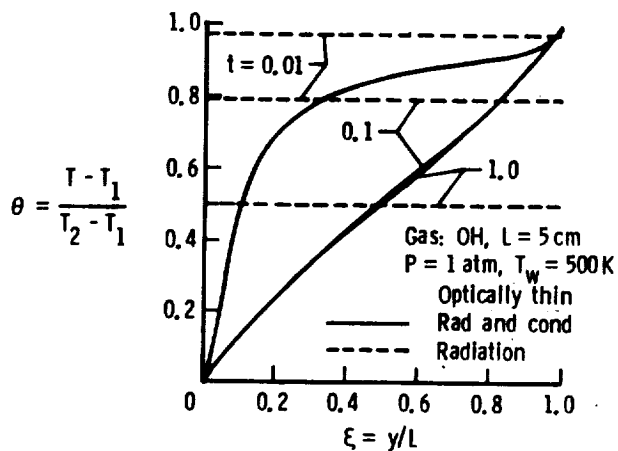


Fig. 9b Temperature variation in optically thin limit for OH with $P=1$ atm, $T_w=500$ K, and $L=5$ cm.

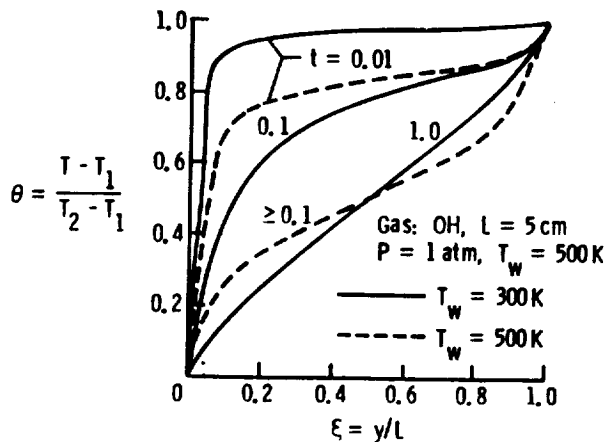


Fig. 10b Temperature variation for combined radiation and conduction for H_2O with $P=1$ atm, and $L=5$ cm.

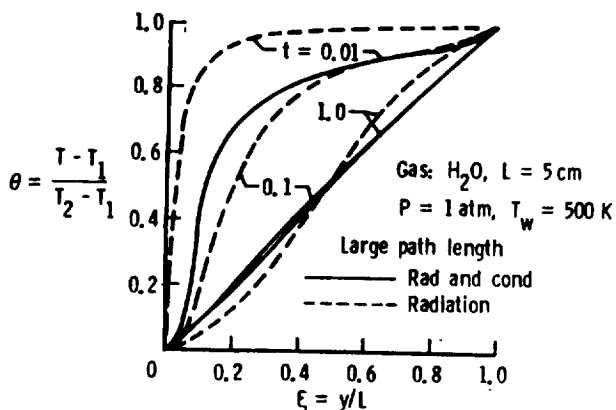


Fig. 9c Temperature variation in large path length limit for OH with $P=1$ atm, $T_w=500$ K, and $L=5$ cm.

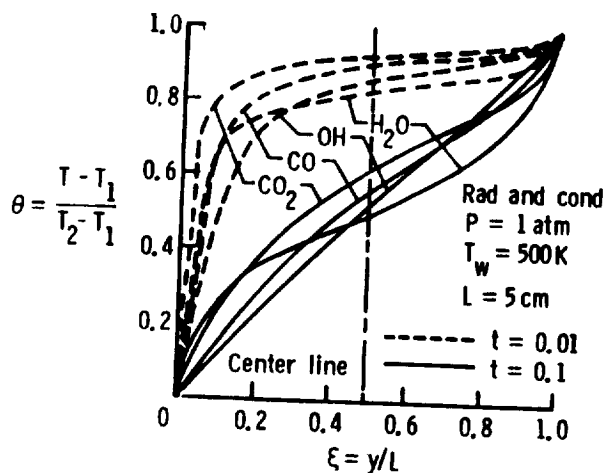


Fig. 11 Comparison of temperature variation for combined radiation and conduction for $P=1$ atm, $T_w=500$ K, and $L=5$ cm.

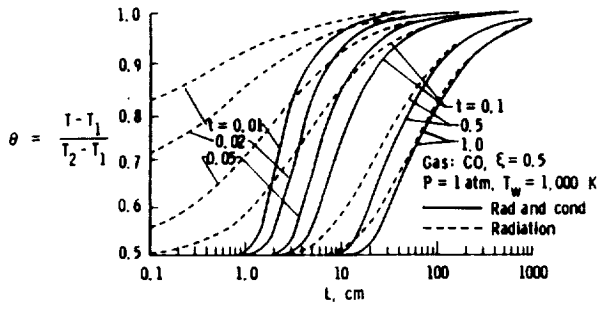


Fig. 12a Centerline temperature variation with L for CO ($P=1$ atm and $T_w=500$ K).

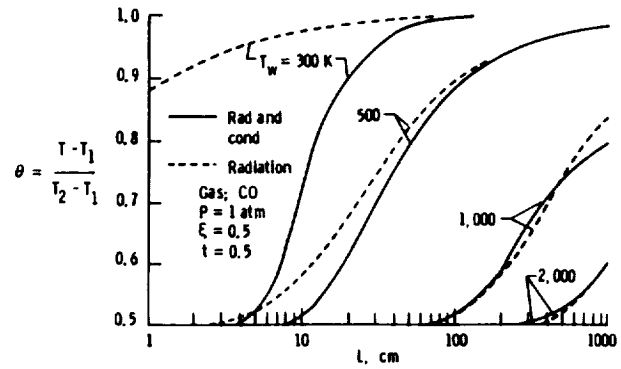


Fig. 12d Centerline temperature variation with L for CO ($P=1$ atm and $t=0.5$).

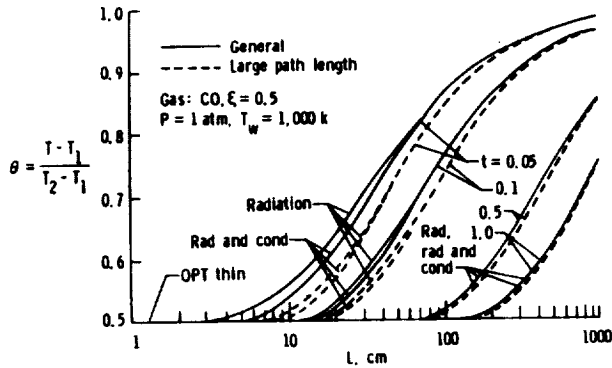


Fig. 12b Centerline temperature variation with L for CO ($P=1$ atm and $T_w=1,000$ K).

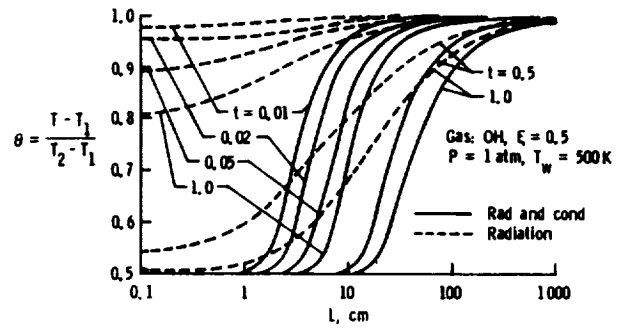


Fig. 13a Centerline temperature variation with L for OH ($P=1$ atm and $T_w=500$ K).

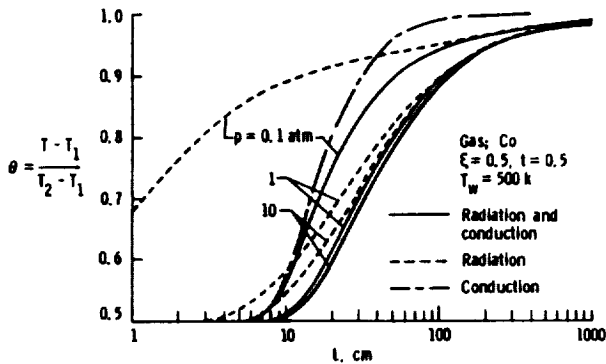


Fig. 12c Centerline temperature variation with L for CO ($T_w=500$ K and $t=0.5$).

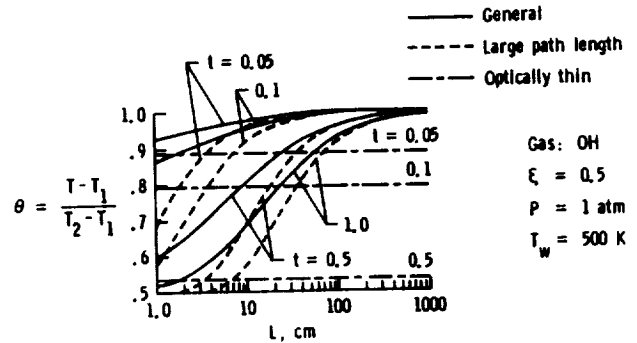


Fig. 13b Centerline temperature variation with L for pure radiation (OH, $P=1$ atm, and $T_w=500$ K).

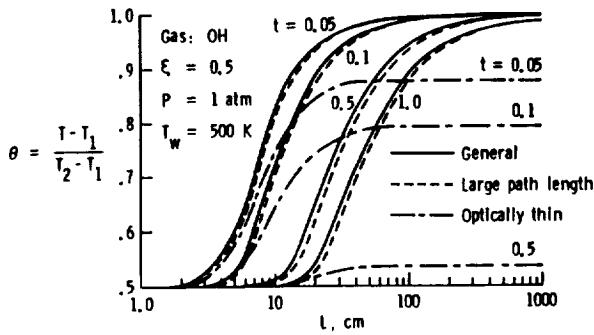


Fig. 13c Centerline temperature variation with L for combined radiation and conduction (OH, P=1 atm, and $T_w=500$ K).

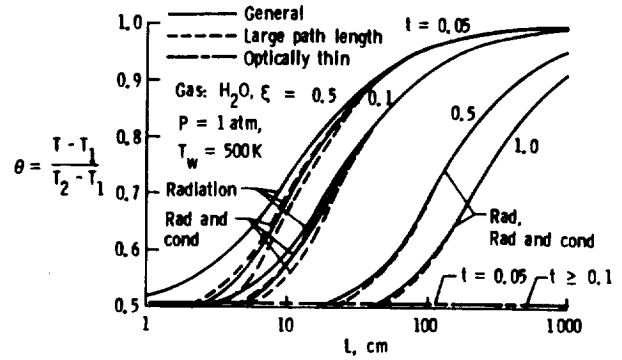


Fig. 14b Centerline temperature variation with L for H_2O (general and limiting solutions, P=1 atm and $T_w=500$ K).

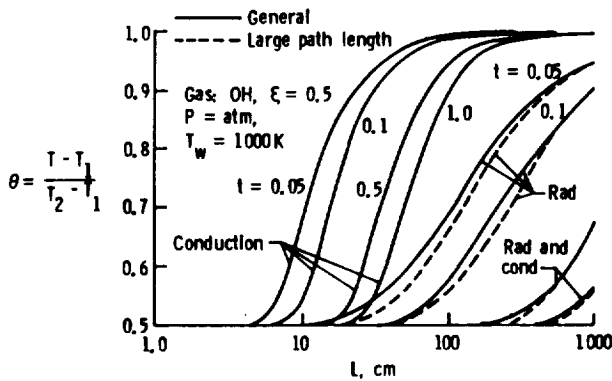


Fig. 13d Centerline temperature variation with L for OH (P=1 atm and $T_w=1,000$ K).

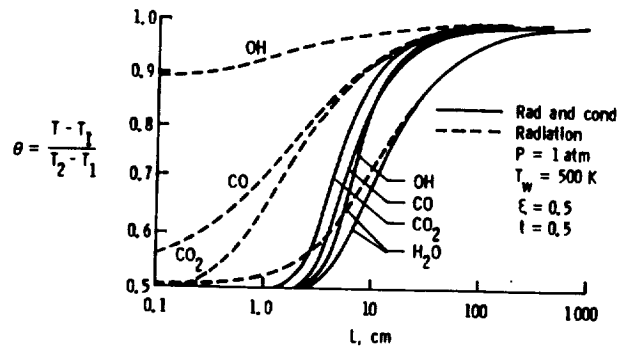


Fig. 15 Comparison of centerline temperature variation with L for P=1 atm, $T_w=500$ K, and $t=0.05$.

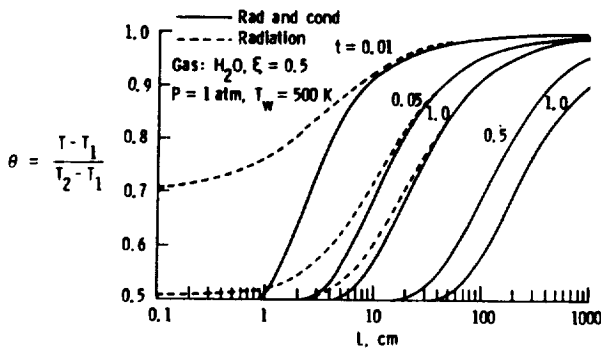


Fig. 14a Centerline temperature variation with L for H_2O (P=1 atm and $T_w=500$ K).

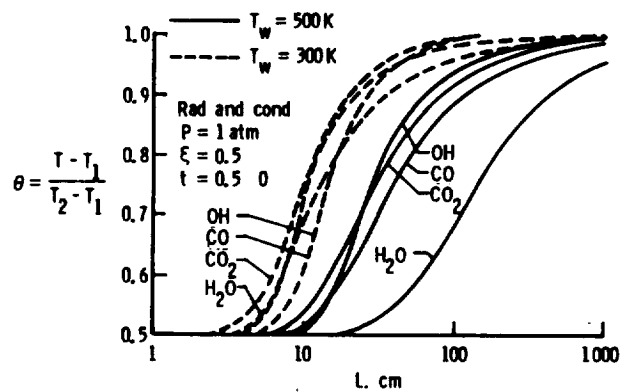


Fig. 16 Comparison of centerline temperature variation with L for combined radiation and conduction (P=1 atm and $t=0.5$).

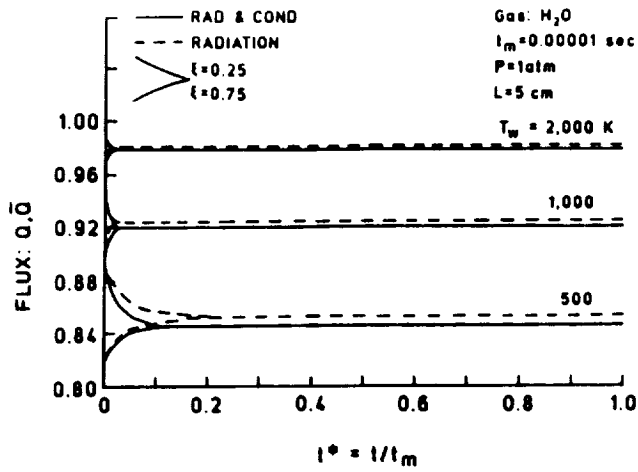


Fig. 17a Variation in heat flux with time for H_2O ($P=1$ atm, $L=5$ cm, and $t^*=0.0-1.0$)

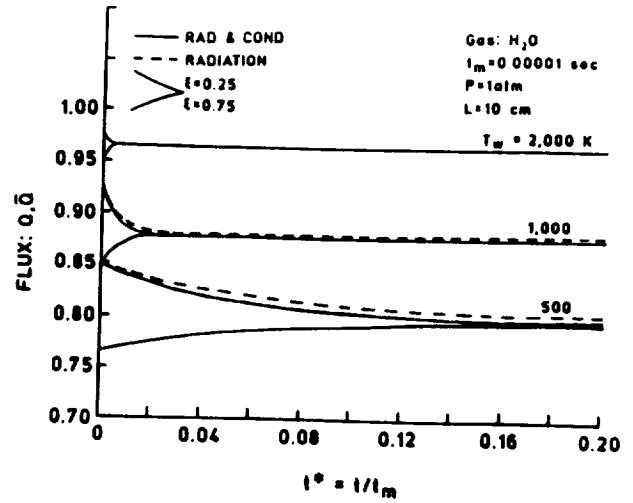


Fig. 17c Variation in heat flux with time for H_2O ($P=1$ atm, $L=10$ cm, and $t^*=0.0-0.2$).

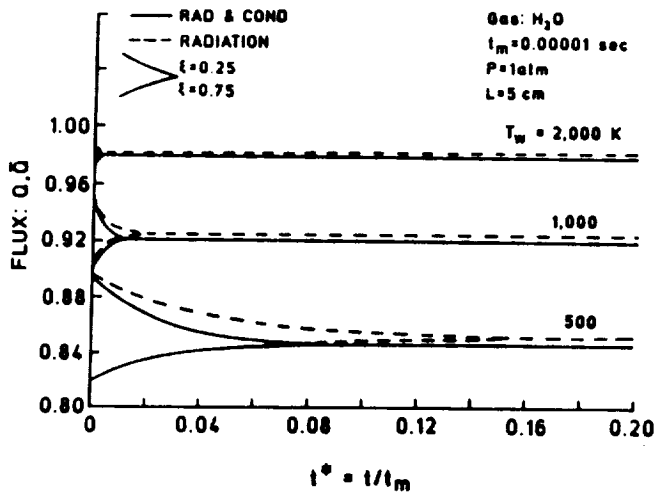


Fig. 17b Variation in heat flux with time for H_2O ($P=1$ atm, $L=5$ cm, and $t^*=0.0-0.2$).

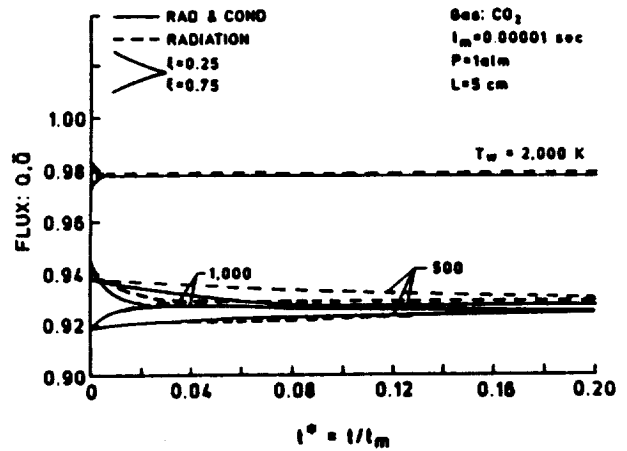


Fig. 18 Variation in heat flux with time for CO_2 ($P=1$ atm, $L=5$ cm, and $t^*=0.0-0.2$).

AIAA'87

4-2945

AIAA - 87 - 1521

**INTERACTION OF
TRANSIENT RADIATION
IN FULLY DEVELOPED
LAMINAR FLOWS**

S.N. Tiwari and D.J. Singh

Old Dominion University, Norfolk, Va

AIAA 22nd Thermophysics Conference

June 8-10, 1987/Honolulu, Hawaii

PAGE _____ INTENTIONALLY BLANK

INTERACTION OF TRANSIENT RADIATION IN FULLY DEVELOPED LAMINAR FLOWS

S. N. Tiwari¹ and D. J. Singh²
 Old Dominion University, Norfolk, Virginia 23508

Abstract

Analysis and numerical procedures are presented to investigate the transient radiative interactions of nongray absorbing-emitting species in laminar fully-developed flows between two parallel plates. The particular species considered are OH, CO, CO₂, and H₂O and different mixtures of these species. Transient and steady-state results are obtained for the temperature distribution and bulk temperature for different plate spacings, wall temperatures, and pressures. Results, in general, indicate that the rate of radiative heating can be quite high during earlier times. This information is useful in designing thermal protection systems for transient operations.

Nomenclature

<p>A band absorptance = $A(u, \beta)$, cm^{-1}</p> <p>A_0 band width parameter, cm^{-1}</p> <p>C_0 correlation parameter, $\text{atm}^{-1} - \text{cm}^{-1}$</p> <p>$C_p$ specific heat at constant pressure, $\text{kJ/kg-k} = \text{erg/gm-k}$</p> <p>$e_\omega$ Planck's function, $(\text{W-cm}^{-2})/\text{cm}^{-1}$</p> <p>$e_{\omega_0}$ Planck's function evaluated at wave number ω_0</p> <p>e_1, e_2 emissive power of surfaces with temperatures T_1 and T_2, W-cm^{-2}</p> <p>H_1, H_1 gas property for the large path length limit</p> <p>k thermal conductivity, erg/cm-sec-K</p> <p>K_1 gas property for the optically thin limit distance between plates</p> <p>M large path length parameter, nondimensional</p> <p>N optically thin parameter, nondimensional</p> <p>P pressure, atm</p> <p>q_R total radiative heat flux, w/cm^2</p>	<p>$q_{R\omega}$ spectral radiation heat flux, $(\text{w-cm}^{-2})/\text{cm}^{-1}$</p> <p>$q_\omega$ wall heat flux, w/cm^2</p> <p>S integrated intensity of a wide band, $\text{atm}^{-1}\text{-cm}^{-2}$</p> <p>$t$ time, sec</p> <p>T temperature, K</p> <p>T_1 wall temperature, K; $T_1 = T_w$</p> <p>T_b bulk temperature, K</p> <p>u nondimensional coordinate = SPy/A_0</p> <p>u_0 nondimensional path length = SPL/A_0</p> <p>y transverse coordinate, cm</p> <p>β line structures parameter</p> <p>θ nondimensional temperature</p> <p>θ_b dimensionless bulk temperature</p> <p>κ_ω spectral absorptin coefficient, cm^{-1}</p> <p>ξ nondimensional coordinate = $y/L = u/u_0$</p> <p>ρ density, kg/m^3</p> <p>τ nondimensional time</p> <p>ω wave number, cm^{-1}</p> <p>ω_0 wave number at the band center, cm^{-1}</p>
--	---

Introduction

The radiative energy transfer in participating medium has received special attention in recent years because of its applications in the areas of the remote sensing, earth's radiation budget studies and climate modeling, fire and combustion research, entry and reentry phenomena, hypersonic propulsion and defense-oriented research. In most studies involving combined mass, momentum, and energy transfer, however, the radiative transfer formulation has been coupled mainly with the steady processes [1-13] and the interaction of radiation in transient processes has received very little attention. However, the transient approach appears to be the logical way of formulating a problem in general sense for elegant numerical and computational solutions. The steady-state solutions can be obtained as limiting solutions for large times.

The limited number of studies available on the transient radiative transfer in gaseous

¹Eminent Professor, Dept. of Mechanical Engineering and Mechanics. AIAA Associate Fellow.

²Graduate Research Assistant, Dept. of Mechanical Engineering and Mechanics. AIAA Student Member.

systems [14-24] are reviewed critically in [25-27]. The literature survey reveals that the transient behavior of a physical system can be influenced significantly in the presence of radiation.

The goal of this research is to include the nongray radiative formulation in the general governing equations and provide the step-by-step analysis and solution procedure for several realistic problems. The basic formulations are presented in [25] and the specific case of transient radiative exchange in nongray gases between two parallel plates is investigated in [26, 27]. The objective of this study is to investigate the interaction of transient radiation in fully-developed laminar flows between two parallel plates. Thus, special attention is directed to include the nonsteady phenomenon only in the energy equation. Homogeneous as well as nonhomogeneous mixtures of absorbing-emitting species are considered. In subsequent studies, the present analysis and numerical techniques will be used to investigate the unsteady flow of compressible and chemically reacting species in one- and multi-dimensional systems.

Basic Formulation

The physical system considered is the energy transfer in laminar, incompressible, constant properties, fully-developed flow of absorbing-emitting gases between parallel plates (Fig. 1). The condition of uniform surface heat flux for each plate is assumed such that the temperature of the plates varies in the axial direction. Extensive treatment of this problem is available in the literature under steady state conditions [8, 11]. The primary motivation of this study is to investigate the extent of transient radiative interaction for high temperature flow conditions.

For the physical problem considered, the energy equation can be expressed as [1]

$$\rho C_p \left(\frac{\partial T}{\partial t} + u \frac{\partial T}{\partial x} + v \frac{\partial T}{\partial y} \right) = k \frac{\partial^2 T}{\partial y^2} + \beta T u \frac{dp}{dx} + \mu \left(\frac{\partial u}{\partial y} \right)^2 - \text{div} q_R \quad (1)$$

where u and v denote x and y components of velocity, respectively. In deriving Eq. (1) it has been assumed that the net conduction heat transfer in the x direction is negligible compared with the net conduction in the y direction. This represents the physical condition of a large value of the Peclet number. By an analogous reasoning, the radiative heat transfer in the x direction can be neglected in comparison to that transferred in the y direction. If, in addition, it is assumed that the Eckert number of the flow is small, then Eq. (1) reduces to

$$\frac{\partial T}{\partial t} + u \frac{\partial T}{\partial x} + v \frac{\partial T}{\partial y} = \alpha \frac{\partial^2 T}{\partial y^2} - \frac{1}{\rho C_p} \frac{\partial q_R}{\partial y} \quad (2)$$

where $\alpha = (k/\rho C_p)$ represents the thermal diffusivity of the fluid.

For a steady fully-developed flow, $v = 0$,

and u is given by the well-known parabolic profile as

$$u = 6 u_m (\xi - \xi^2); \quad \xi = y/L \quad (3)$$

where u_m represents the mean fluid velocity. Also, for the flow of a perfect gas with uniform heat flux, $\partial T/\partial x$ is constant and is given by

$$\partial T/\partial x = (2\alpha q_w)/(u_m L/k) \quad (4)$$

Now, by combining Eqs. (2) - (4), the energy equation is expressed in nondimensional form as

$$\frac{\partial \theta}{\partial \tau} + 12 (\xi - \xi^2) = \frac{\partial^2 \theta}{\partial \xi^2} - \frac{1}{q_w} \frac{\partial q_R}{\partial \xi} \quad (5)$$

where

$$\tau = \alpha t/L^2; \quad \theta = (T - T_1)/(q_w L/k)$$

By assuming that the initial temperature distribution in the gas is some uniform value $T_0 = T_1$, the initial and boundary conditions for this problem can be expressed as

$$\theta(\xi, 0) = 0 \quad (6a)$$

$$\theta(0, \tau) = \theta(1, \tau) = 0 \quad (6b)$$

$$\theta_{\xi}(\xi = 1/2) = 0; \quad \theta_{\xi}(\xi = 0) = -\theta_{\xi}(\xi = 1) \quad (6c)$$

It should be noted that all the boundary conditions given in Eqs. (6) are not independent and any two convenient conditions can be used to obtain solutions. Also, the initial temperature distribution can be any specified or calculated value of $\theta(\xi, 0) = f(\xi)$.

As discussed in Refs. 25-27, the radiative transfer equations are formulated for one-dimensional planar systems for many engineering and astrophysical applications. For diffuse nonreflecting boundaries and in the absence of scattering, the expression for the total radiative flux is given, for an n -band gaseous system, by [1, 8, 25]

$$q_R(y) = e_1 - e_2$$

$$+ \frac{3}{2} \sum_{i=1}^n \int_{\Delta \omega_i} \left(\int_0^y F_{1\omega_i}(z) \kappa_{\omega_i} \exp[-\frac{3}{2} \kappa_{\omega_i}(y-z)] dz \right. \\ \left. - \int_y^L F_{2\omega_i}(z) \kappa_{\omega_i} \exp[-\frac{3}{2} \kappa_{\omega_i}(z-y)] dz \right) d\omega_i \quad (7)$$

where

$$F_{1\omega_i}(z) = e_{\omega_i}(z) - e_{1\omega_i}; F_{2\omega_i}(z) = e_{\omega_i}(z) - e_{2\omega_i}$$

Equation (7) is in proper form for obtaining the nongray solutions of molecular species. In fact, this is an ideal equation for the line-by-line and narrow-band model formulations. However, in order to be able to use the wide band models and correlations, Eq. (7) is transformed in terms of the correlation quantities as [1, 7-13, 25]

$$\begin{aligned} q_R(\xi) &= e_1 - e_2 \\ &+ \frac{3}{2} \sum_{i=1}^n A_{0i} u_{0i} \left(\int_0^\xi F_{1\omega_i}(\xi') \bar{A}'_i \left[\frac{3}{2} u_{0i}(\xi - \xi') \right] d\xi' \right. \\ &\left. - \int_\xi^1 F_{2\omega_i}(\xi') \bar{A}'_i \left[\frac{3}{2} u_{0i}(\xi' - \xi) \right] d\xi' \right) \end{aligned} \quad (8)$$

where

$$\begin{aligned} \xi &= u/u_0 = y/L; \xi' = u'/u_0 = z/L; \bar{A} = A/A_0; \\ u &= (S/A_0) py; u_0 = (S/A_0) PL; PS = \int_{\Delta\omega} \kappa_\omega d\omega \end{aligned}$$

It should be noted that $F_{1\omega_i}$ and $F_{2\omega_i}$ in Eq. (8) represent the values at the center of the i th band and $\bar{A}'(u)$ denotes the derivative of $\bar{A}(u)$ with respect to u . Upon performing the integration by parts, Eq. (8) can be expressed in an alternate form as [25]

$$\begin{aligned} q_R(\xi) &= e_1 - e_2 \\ &+ \sum_{i=1}^n A_{0i} \left(\int_0^\xi [de_{\omega_i}(\xi')/d\xi'] \bar{A}'_i \left[\frac{3}{2} u_{0i}(\xi - \xi') \right] d\xi' \right. \\ &\left. + \int_\xi^1 [de_{\omega_i}(\xi')/d\xi'] \bar{A}'_i \left[\frac{3}{2} u_{0i}(\xi' - \xi) \right] d\xi' \right) \end{aligned} \quad (9)$$

A direct differentiation of Eq. (9) provides the expression for the divergence of radiative flux as

$$\begin{aligned} \frac{dq_R(\xi)}{d\xi} &= \frac{3}{2} \sum_{i=1}^n A_{0i} u_{0i} \left(\int_0^\xi [de_{\omega_i}(\xi')/d\xi'] \times \right. \\ &\bar{A}'_i \left[\frac{3}{2} u_{0i}(\xi - \xi') \right] d\xi' - \int_\xi^1 [de_{\omega_i}(\xi')/d\xi'] \times \\ &\left. \bar{A}'_i \left[\frac{3}{2} u_{0i}(\xi' - \xi) \right] d\xi' \right) \end{aligned} \quad (10)$$

Equations (8) through (10) are the most convenient equations to use when employing the band-model correlations in radiative transfer analyses.

For the present physical problem, $e_1 = e_2$ and $F_{1\omega_i} = F_{2\omega_i}$. Thus, for the case of linearized radiation, a combination of Eqs. (5) and (8) results in [8, 18]

$$\begin{aligned} \theta_{\xi\xi} - \theta_\tau - 3N\theta - 12(\xi - \xi^2) \\ = \frac{9}{4} (L/k) \sum_{i=1}^n H_{1i} u_{0i}^2 \left(\int_0^\xi \theta(\xi', \tau) \times \right. \\ \bar{A}'_i \left[\frac{3}{2} u_{0i}(\xi - \xi') \right] d\xi' + \int_\xi^1 \theta(\xi', \tau) \times \\ \left. \bar{A}'_i \left[\frac{3}{2} u_{0i}(\xi' - \xi) \right] d\xi' \right) \end{aligned} \quad (11a)$$

where

$$\begin{aligned} N &= (PL^2/k) K_1 = (PL^2/k) \sum_{i=1}^n S_i(T) (de_{\omega_i}/dT)_{T_1} \\ H_{1i} &= A_{0i}(T) (de_{\omega_i}/dT)_{T_1}, H_i = \sum_{i=1}^n H_{1i} \end{aligned}$$

The dimensionless gas property N characterizes the relative importance of radiation versus conduction within the gas under optically thin conditions. Also, by combining Eqs. (5) and (10) another form of the transient energy equation is obtained as

$$\begin{aligned} \theta_{\xi\xi} - \theta_\tau - 12(\xi - \xi^2) \\ = \frac{3}{2} (L/k) \sum_{i=1}^n H_{1i} u_{0i} \left(\int_0^\xi (\partial\theta/\partial\xi') \times \right. \\ \bar{A}'_i \left[\frac{3}{2} u_{0i}(\xi - \xi') \right] d\xi' - \int_\xi^1 (\partial\theta/\partial\xi') \times \\ \left. \bar{A}'_i \left[\frac{3}{2} u_{0i}(\xi' - \xi) \right] d\xi' \right) \end{aligned} \quad (11b)$$

Note again that Eq. (11b) can be obtained directly by integrating the right-hand side of Eq. (11a) by parts. Quite often, Eq. (11b) is the convenient form to use in radiative transfer analyses.

For flow problems, the quantity of primary interest is the bulk temperature of the gas, which may be expressed as [11]

$$\theta_b = (T_b - T_1) / (q_w L / k) = 6 \int_0^1 \theta(\xi, \tau) (\xi - \xi^2) d\xi \quad (12)$$

The heat transfer q_w is given by the expression, $q_w = h_c (T_1 - T_b)$, where h_c is the convective heat transfer coefficient (W/cm^2-K). In general, the heat transfer results are expressed in terms of the Nusselt number $Nu = h_c D_h / k$. Here, D_h represents the hydraulic diameter, and for the parallel plate geometry it equals twice the plate separation, i.e., $D_h = 2L$. Upon eliminating the convective heat transfer coefficient h_c from the expressions for q_w and Nu , a relation between the Nusselt number and the bulk temperature is obtained as

$$Nu = 2 L q_w / k (T_1 - T_b) = -2 / \theta_b \quad (13)$$

The heat transfer results, therefore, can be expressed either in terms of Nu or θ_b .

Limiting Cases and Solutions

Before discussing the method of solution for the general case, it is advisable to explore the various limiting cases. Quite often, closed form solutions can be obtained for some of these cases. Specifically four limiting cases are considered here and these are the steady laminar flows, the case of negligible radiation, the optically thin limit, and the large path length limit.

Steady Laminar Flow

For steady-state conditions $\partial\theta/\partial\tau = 0$ and Eqs. (11) provide two forms of the energy equation for this case. Another convenient form is obtained by letting $\partial\theta/\partial\tau = 0$ in Eq. (5) such that

$$\theta'' - 12(\xi - \xi^2) = (1/q_w) dq_R/d\xi \quad (14)$$

By integrating Eq. (14) once and using the conditions that at $\xi = 1/2$, $q_R(\xi)$ and $(d\theta/d\xi)$ are equal to zero, one obtains

$$\theta' - 2(3\xi^2 - 2\xi^3) + 1 = q_R(\xi)/q_w \quad (15)$$

A combination of Eqs. (8) and (15) results in

$$\begin{aligned} \theta' - 2(3\xi^2 - 2\xi^3) + 1 \\ = \frac{3}{2} (L/k) \sum_{l=1}^{\infty} H_{1l} u_{0l} \left\{ \int_0^{\xi} \theta(\xi') x \right. \end{aligned}$$

$$\left. \bar{A}_l' \left[\frac{3}{2} u_{0l} (\xi - \xi') \right] d\xi' - \int_{\xi}^1 \theta(\xi') x \right.$$

$$\left. \bar{A}_l' \left[\frac{3}{2} u_{0l} (\xi' - \xi) \right] d\xi' \right\} \quad (16)$$

It should be pointed out that by combining Eqs. (9) and (15) another useful form of the energy equation can be obtained for the steady case.

For the case of negligible radiation, Eq. (16) reduces to a very simple form and utilizing the boundary condition $\theta(0) = 0$, the solution of the resulting equation is found to be

$$\theta(\xi) = \xi(2\xi^2 - \xi^3 - 1) \quad (17a)$$

The result for the bulk temperature is found by combining Eqs. (12) and (17a) as

$$-\theta_b = 17/70 \quad (17b)$$

The results provided by Eqs. (17) are useful in determining the extent of radiative contributions.

Negligible Radiation

For the case of negligible radiation, $M = 0$ and both forms of Eq. (11) reduce to

$$\theta_{\xi\xi} - \theta_{\tau} = 12(\xi - \xi^2) \quad (18)$$

By employing the product solution procedure, the solution of Eq. (18) can be obtained and the result can be expressed in terms of the bulk temperature through use of Eq. (12). Alternately, the solution of Eq. (18) is assumed to be of the form

$$\theta(\xi, \tau) = g(\xi) + h(\xi, \tau) \quad (19)$$

From Eqs. (18) and (19), there is obtained two separate equations as

$$g'' = 12(\xi - \xi^2) \quad (20)$$

$$h_{\xi\xi} - h_{\tau} = 0 \quad (21)$$

Solutions of Eqs. (20) and (21) are found separately from which the complete solution for the temperature distribution is obtained as [25]

$$\begin{aligned} \theta(\xi, \tau) = \xi(2\xi^2 - \xi^3 - 1) \\ + \sum_{n=1}^{\infty} C_n \sin(a\xi) \exp(-a^2\tau); a = n\pi \end{aligned} \quad (22a)$$

where

$$C_n = (4/a^5) [(12 - 12a^2 + a^4) \cos(a)]$$

- 24], $n = 1, 2, \dots$

Finally, the expression for the bulk temperature is found by using Eq. (12) as

$$\theta_b = -17/70 + 6 \sum_{n=1}^{\infty} C_n \left[\left(\frac{1}{a} + \frac{4}{a^3} \right) \exp(-a^2 \tau) \right] \quad (22b)$$

Equations (22) are useful in determining the extent of radiative contributions for the transient case.

Optically Thin Limit

In the optically thin limit, the expression for the bulk temperature for the steady case is found to be [11, 25]

$$\theta_b = \left[\frac{1}{(3N)^3} \right] \{ 576(3N)^{-1/2} (\text{NEXP}) - 21.6N^2 + 72N - 288 \} \quad (23)$$

where

$$\text{NEXP} = \{ 1 - \exp[-(3N)^{1/2}] \} / \{ 1 + \exp[-(3N)^{1/2}] \}$$

Both forms of the transient energy equation, Eqs. (11a) and (11b), reduce to a simplified form in the optically thin limit as [25]

$$\theta_{\xi\xi} - \theta_{\tau} - 3N\theta = 12(\xi - \xi^2) \quad (24)$$

Assuming a solution of the form given by Eq. (19), Eq. (24) is written as

$$h_{\xi\xi} - h_{\tau} - 3Nh = -g_{\xi\xi} + 3Ng + 12(\xi - \xi^2) \quad (25)$$

Consequently,

$$g'' - 3Ng = 12(\xi - \xi^2) \quad (26)$$

$$\text{and} \quad h_{\xi\xi} - h_{\tau} - 3Nh = 0 \quad (27)$$

From the solution of Eqs. (26) and (27), the solution for Eq. (24) is obtained as

$$\theta(\xi, \tau) = \left(\frac{16}{3N^2} \right) \left[\frac{\sinh(-\sqrt{3N}/2)}{\sinh(\sqrt{3N})} \right] \cosh[\sqrt{3N}(\xi - 1/2)] + \frac{4}{N}(\xi^2 - \xi + 2/3N) + \sum_{n=1}^{\infty} C_n \sin(a\xi) \exp[-(3N + a^2)\tau]; \quad a = n\pi \quad (28a)$$

where

$$C_n = 0, \quad \text{for } n \text{ even} \quad (28b)$$

$$= 32(3N + a^2)/(3N^2 a^3) + 2a/[3N^2(3N + a^2)], \quad \text{for } n \text{ odd} \quad (28c)$$

By combining Eqs. (12) and (28), the expression for the bulk temperature is obtained as

$$\theta_b = 6 \left[\frac{16}{3N^2} \right] \left[\frac{\sinh(-\sqrt{3N}/2)}{\sinh(\sqrt{3N})} \right] \times \left[\left(\frac{1}{3N} \right) \cosh(\sqrt{3N}/2) - (4 + \sqrt{3N})(3N)^{-3/2} \times \sinh(\sqrt{3N}/2) \right] + \frac{4}{N} \left[-\frac{1}{30} + \frac{1}{(9N)} \right] + \sum_{n=1}^{\infty} C_n \left(\frac{1}{a} + \frac{4}{a^3} \right) \exp[-(3N + a^2)\tau] \quad (29)$$

Large Path Length Limit

In this limit, the steady-state energy equation, Eq. (16), reduces to [8, 11, 25]

$$\theta' - 2(3\xi^2 - 2\xi^3) + 1 = M \int_0^1 \theta(\xi') d\xi' / (\xi - \xi') \quad (30)$$

where

$$M = H_1 L/k = (L/k) \sum_{i=1}^n A_{oi} (de_{\omega i}/dT)_{T_1}$$

The nondimensional parameter M constitutes the radiation-conduction interaction parameter for the large path length limit. Equation (30) does not appear to possess a closed form solution; a numerical solution, however, can be obtained easily.

In the large path length limit, the transient energy equations, Eqs. (11a) and (11b), reduce to

$$\theta_{\xi\xi} - \theta_{\tau} - 3N\theta = 12(\xi - \xi^2) = -M \left[\int_0^{\xi} \theta(\xi', \tau) d\xi' / (\xi - \xi')^2 + \int_{\xi}^1 \theta(\xi', \tau) d\xi' / (\xi' - \xi)^2 \right] \quad (31a)$$

$$\theta_{\xi\xi} - \theta_{\tau} - 12(\xi - \xi^2)$$

$$= M \int_0^1 (\partial\theta/\partial\xi') d\xi' / (\xi - \xi') \quad (31b)$$

Since $|(\xi - \xi')^2| = |(\xi' - \xi)^2|$, Eq. (31a) can be written as

$$\begin{aligned} \theta_{\xi\xi} - \theta_{\tau} - 3N\theta - 12(\xi - \xi')^2 \\ = -M \int_0^1 \theta(\xi', \tau) d\xi' / (\xi - \xi')^2 \end{aligned} \quad (31c)$$

Through integration by parts, Eq. (31c) can be expressed as

$$\begin{aligned} \theta_{\xi\xi} - \theta_{\tau} - 3N\theta - 12(\xi - \xi')^2 \\ = M \int_0^1 (\partial\theta/\partial\xi') d\xi' / (\xi - \xi') \end{aligned} \quad (31d)$$

Equations (31a) - (31d) represent different forms of the governing equations in the large path length limit. With the exception of the term $(-3N\theta)$ on the left-hand side, Eq. (31d) is identical to Eq. (31b). Since N represents the radiation-conduction interaction parameter only in the optically thin limit [8], it should not appear in the governing equation for the large path length limit. Thus, Eq. (31b) is the correct equation to use for solution in the large path length limit; the solution of this equation is obtained by numerical techniques.

Method of Solution

The solution procedures for both steady and unsteady cases are presented in this section. In principle, the same numerical procedure applies to both the general and large path length limit cases.

Steady-State Solutions

The general solution of Eq. (16) is obtained numerically by employing the method of variation of parameters. For this, a polynomial form for $\theta(\xi)$ is assumed in powers of ξ as

$$\theta(\xi) = \sum_{m=0}^n a_m \xi^m \quad (32)$$

By considering a five term series solution (a quartic solution in ξ) and satisfying the boundary conditions $\theta(0) = \theta'(1/2) = 0$ and $\theta'(0) = -\theta'(1)$, one obtains

$$\theta(\xi) = a_1(\xi - 2\xi^3 + \xi^4) + a_2(\xi^2 - 2\xi^3 + \xi^4) \quad (33)$$

$$\theta'(\xi) = a_1(1 - 6\xi^2 + 4\xi^3) + a_2(2\xi - 6\xi^2 + 4\xi^3) \quad (34)$$

A substitution of Eq. (34) in Eq. (16) results in

$$a_1(1 - 6\xi^2 + 4\xi^3) + a_2(2\xi - 6\xi^2 + 4\xi^3)$$

$$- 2(3\xi^2 - 2\xi^3) + 1 = \frac{3}{2} (L/k) \sum_{n=1}^n H_{11} u_{01} \times$$

$$\left(\int_0^{\xi} \theta(\xi') \bar{A}_1' \left[\frac{3}{2} u_{01} (\xi - \xi') \right] d\xi' \right.$$

$$\left. - \int_{\xi}^1 \theta(\xi') \bar{A}_1' \left[\frac{3}{2} u_{01} (\xi' - \xi) \right] d\xi' \right) \quad (35)$$

where expressions for $\theta(\xi')$ are obtained from Eq. (33).

The two unknown constants a_1 and a_2 in Eq. (35) are evaluated by satisfying the integral equation at two convenient locations ($\xi=0$ and $\xi=1/4$ in the present case). The entire procedure for obtaining a_1 and a_2 is described in [25]. With known values of a_1 and a_2 , Eq. (33) provides the general solution for $\theta(\xi)$. The expression for the bulk temperature is obtained by combining Eqs. (12) and (33) as

$$\theta_b = (1/70) (17a_1 + 3a_2) \quad (36)$$

It should be noted that for the case of no radiative interaction $a_2 = 0$ and $a_1 = -1$, and Eq. (36) gives the result of Eq. (17).

The governing equation for the large path length limit is Eq. (30). For this equation also the solution is given by Eqs. (33) and (36) but the values of a 's are completely different in this case [25].

Transient Solutions

The governing energy equations for the transient case are Eqs. (11a) and (11b). General solutions of these equations are obtained also numerically by employing the method of variation of parameters. For the present problem, a polynomial form for $\theta(\xi, \tau)$ is assumed as

$$\theta(\xi, \tau) = \sum_{m=0}^n a_m(\tau) \xi^m \quad (37)$$

For a quadratic temperature distribution in ξ (with time dependent coefficients), Eq. (37) is written as

$$\theta(\xi, \tau) = a_0(\tau) + a_1(\tau) \xi + a_2(\tau) \xi^2 \quad (38a)$$

By using the boundary conditions $\theta(0, \tau) = 0$ and $\theta_{\xi}(\xi=1/2) = 0$, this reduces to

$$\theta(\xi, \tau) = g(\tau) (\xi - \xi^2) \quad (38b)$$

where $g(\tau)$ represents the time dependent coefficient. Consequently,

$$\begin{aligned} \theta_{\xi}(\xi, \tau) &= g(\tau) (1-2\xi); \theta_{\xi\xi}(\xi, \tau) \\ &= -2g(\tau); \theta_{\tau}(\xi, \tau) = (\xi - \xi^2) g'(\tau) \end{aligned} \quad (39)$$

Also, a combination of Eq. (6a) and (38b) yields the initial condition

$$\theta(\xi, 0) = g(0) = 0 \quad (40)$$

Note that essential boundary conditions are used already in obtaining the solution represented by Eq. (38b).

By employing Eqs. (38b) and (39), Eqs. (11a) and (11b) are transformed in alternate forms which are expressed in a compact form as

$$g'(\tau) + \begin{bmatrix} J_1(\xi) \\ J_2(\xi) \end{bmatrix} g(\tau) + 12 = 0 \quad (41)$$

where $J_1(\xi)$ and $J_2(\xi)$ are defined in [25]. The function $J_1(\xi)$ is used for solution of Eq. (11a) and $J_2(\xi)$ is used for solution of Eq. (11b). The solution of Eq. (41) satisfying the initial conditions of Eq. (40) is given by

$$g(\tau) = \frac{12}{J(\xi)} (\exp[-J(\xi)\tau] - 1) \quad (42)$$

The temperature distribution given by Eq. (38b) can be expressed now as

$$\theta(\xi, \tau) = \frac{12}{J(\xi)} (\exp[-J(\xi)\tau] - 1)(\xi - \xi^2) \quad (43)$$

The expression for the bulk temperature is obtained through use of Eq. (12) as

$$\theta_D = 72 \int_0^1 [(\xi - \xi^2)^2 / J(\xi)] (\exp[-J(\xi)\tau] - 1) \quad (44)$$

Note that in Eqs. (42)-(44), $J(\xi)$ becomes $J_1(\xi)$ for solution of Eq. (11a) and $J_2(\xi)$ for solution of Eq. (11b).

For a quartic solution in ξ , Eq. (37) gives the result similar to Eq. (33) which for the transient case is expressed as

$$\begin{aligned} \theta(\xi, \tau) &= g(\tau) (\xi - 2\xi^3 + \xi^4) \\ &+ h(\tau) (\xi^2 - 2\xi^3 + \xi^4) \end{aligned} \quad (45)$$

By substituting Eq. (45) into Eq. (11a), one

obtains

$$x g'(\tau) + J_3(\xi) g(\tau) + y h'(\tau) + J_4(\xi) h(\tau) = -z \quad (46)$$

where

$$\begin{aligned} x &= (\xi - 2\xi^3 + \xi^4); y = (\xi^2 - 2\xi^3 + \xi^4); \\ z &= 12(\xi - \xi^2) \end{aligned}$$

and functions $J_3(\xi)$ and $J_4(\xi)$ are defined in [25]. Equation (46) constitutes one equation in two unknowns, namely $g(\tau)$ and $h(\tau)$. However, since the equation is linear in τ , the principle of superposition can be used to split the solution into two equations as

$$x g'(\tau) + J_3(\xi) g(\tau) = -z/2 \quad (47)$$

$$y h'(\tau) + J_4(\xi) h(\tau) = -z/2 \quad (48)$$

The initial condition for this case can be written as

$$\begin{aligned} \theta(\xi, 0) &= g(0) (\xi - 2\xi + \xi^3) \\ &+ h(0) (\xi^2 - 2\xi^3 + \xi^4) = 0 \end{aligned} \quad (49a)$$

Consequently,

$$g(0) = 0; h(0) = 0 \quad (49b)$$

The solution of Eqs. (47) and (48) satisfying the appropriate initial condition of Eq. (49b) is given respectively as

$$g(\tau) = [z(\xi)/2J_3(\xi)] (\exp[-J_3(\xi)\tau/x(\xi)] - 1) \quad (50)$$

$$h(\tau) = [z(\xi)/2J_4(\xi)] (\exp[-J_4(\xi)\tau/y(\xi)] - 1) \quad (51)$$

By substituting Eqs. (50) and (51) into Eq. (45), the expression for the temperature distribution is obtained as

$$\begin{aligned} \theta(\xi, \tau) &= [6(\xi - \xi^2)(\xi - 2\xi^3 + \xi^4)/J_3(\xi)] x \\ &(\exp[-J_3(\xi)\tau/x(\xi)] - 1) + [6(\xi - \xi^2) x \\ &(\xi^2 - 2\xi^3 + \xi^4)/J_4(\xi)] (\exp[-J_4(\xi)\tau/y(\xi)] - 1) \end{aligned} \quad (52)$$

The bulk temperature in this case is given by

$$\theta_b = 36 \int_0^1 [(\xi - \xi^2)(\xi - 2\xi^3 + \xi^4)/J_3(\xi)] \times \\ (\exp[-J_3(\xi)\tau/x(\xi)] - 1) d\xi + 36 \int_0^1 [(\xi - \xi^2) \times \\ (\xi^2 - 2\xi^3 + \xi^4)/J_4(\xi)] (\exp[-J_4(\xi)\tau/y(\xi)] - 1) d\xi. \quad (53)$$

where x and y are defined in Eq. (46).

By substituting Eq. (45) into Eq. (11b), there is obtained

$$xg' + J_5(\xi) g(\tau) + yh + J_6(\xi) h(\tau) = -z \quad (54)$$

where again x, y, z are defined in Eq. (46) and functions $J_5(\xi)$ and $J_6(\xi)$ are defined in [25]. The solution procedure for this equation is identical to that for Eq. (46) and the results for temperature distribution and bulk temperature are given respectively by Eqs. (52) and (53) with J_3 replaced by J_5 and J_4 by J_6 .

In the large path length limit, the two applicable governing equations are Eqs. (31b) and (31d). The solutions of these equations can be obtained from the general solutions by evaluating the integrals in J function in the large path length limit [25].

Physical Conditions and Data Source

As discussed in [25-27], four specific absorbing emitting species were selected for an extensive study; these are CO, CO₂, OH and H₂O. The species CO was selected because it contains only one fundamental vibration-rotation (VR) band and all spectral information are easily available in the literature. It is a very convenient gas to test the numerical procedure without requiring excessive computational resources. Species OH and H₂O are the primary radiation participating species for the pressure and temperature range anticipated in the combustor of the scramjet engine. Species CO₂, and combinations of CO₂ and H₂O are important absorbing-emitting species in many other combustion processes. Different mixtures of various species (such as CO₂ + H₂O, OH + H₂O, and CO₂ + H₂O + OH) were selected for parametric studies. Thermophysical properties of these species are given in [26] for different temperatures.

In radiative transfer analyses, it is essential to employ a suitable model to represent the absorption-emission characteristics of specific species under investigation. Several line-by-line (LBL), narrow-band, and wide-band models are available to model the absorption of a VR band [7-12]. However, it is often desirable to use a simple correlation to represent the total absorption of a wide band. Several such correlations are available in the literature [7-12]. The relative merits of these correlations are discussed in [12]. In this study, the correlation proposed by Tien and Lowder [7] is

employed and this is given by

$$\bar{A}(u) = \ln \{uf(\beta) \left[\frac{u+2}{u+2f(\beta)} + 1 \right] \} \quad (55)$$

where

$$f(\beta) = 2.94[1 - \exp(-2.60\beta)]$$

and β represents the line structure parameter.

The spectral information and correlation quantities needed for different species were obtained from Refs. 7-9, 26 and 28. The specific VR bands considered for each species are: CO (4.7 μ fundamental), OH (2.8 μ fundamental), CO₂ (15 μ , 4.3 μ and 2.7 μ), and H₂O (20 μ , 6.3 μ , 2.7 μ , 1.87 μ , and 1.38 μ).

In a mixture of several species, spectral lines and bands overlap in certain spectral regions. The total absorptance in such regions cannot be calculated simply by adding the contributions of different bands and corrections should be made to account for the partial overlapping. If line-by-line or narrow band models are employed in the general formulation of the physical problem, then there is no need for such corrections [12, 29, 30]. The solution of LBL formulation, however, requires considerably large computational resources. Use of narrow band models offers some computational relief but certain spectral information needed are not available for many species for temperatures higher than about 600 K. A relatively easier procedure (called the block method) is suggested by Edwards [13] and is useful in calculating the total emissivity of a mixture of several species. Another method suggested by Penner and Varanasi [31] is probably the most convenient method to use in the frame work of the radiative flux formulation expressed in terms of the wide-band model absorptance and correlations.

For a homogeneous path, the total absorptance of a band is given by

$$A(y) = \int_0^{\infty} [1 - \exp(-\kappa_{\omega} y)] d\omega \quad (56)$$

where both κ_{ω} and ω have units of cm⁻¹. If in a spectral range $\Delta\omega_1$, there are contributions from bands of different species, then for a homogeneous path the transmittance is given by

$$\tau_{\Delta\omega_1} = \exp\left(-\sum_{j=1}^N \kappa_{\omega_j} y\right)$$

where N represents the number of participating species in the gaseous mixture. Consequently, Eq. (56) can be expressed as

$$A_1 = \int_{\Delta\omega_1} [1 - \exp\left(-\sum_{j=1}^N \kappa_{\omega_j} y\right)] d\omega \quad (58)$$

If two bands of different (or same) species are

occupying approximately the same spectral range $\Delta\omega_i$, then Eq. (58) reduces to

$$A_i = \int_{\Delta\omega_i} \{1 - \exp(\kappa_{\omega_{i1}} + \kappa_{\omega_{i2}})y\} d\omega \quad (59)$$

By employing the relations for the exponentials, Eqs. (59) can be expressed as [31]

$$A_i = \int_{\Delta\omega_i} [1 - \exp(-\kappa_{\omega_{i1}}y)] d\omega + \int_{\Delta\omega_i} [1 - \exp(-\kappa_{\omega_{i2}})] d\omega - \Delta A \quad (60a)$$

or

$$A = A_1 + A_2 - \Delta A \quad (60b)$$

where

$$\Delta A = \int_{\Delta\omega_i} \{[1 - \exp(-\kappa_{\omega_{i1}}y)] \times [1 - \exp(-\kappa_{\omega_{i2}}y)]\} d\omega \quad (60c)$$

Use of Eqs. (60) has been made by Felske and Tien [32] to calculate absorptances of homogeneous and nonhomogeneous mixtures of CO_2 and H_2O in the 2.7 μ region for different pressure and temperature conditions. A similar procedure is used in this study to account for the overlapping effects of different species [28].

For the physical problem considered, the dependent variables are θ and θ_b (or Nu) and independent variables are τ and ξ . The parameters, in general, are T_w , P , and L . The large path length and optically thin limits are characterized respectively by parameters M and N . Radiative and thermophysical properties of participating species are evaluated at different specified pressures and temperatures.

Results and Discussions

Extensive results have been obtained for variation of θ and θ_b for different conditions. Selected results are presented here to compare solutions of quadratic and quartic formulations and demonstrate the variation of θ with τ and ξ and of θ_b with L for single component systems and homogeneous mixtures. Some other results are available in [28]. For all results presented here, a lower value of θ (or θ_b) in the figures indicates a higher value of temperature in the medium; this, in turn, implies a relatively higher ability of the gas to transfer radiative energy.

Results of quadratic and quartic formulations are compared in Figs. 2-5 for different species. The centerline temperature variations with nondimensional time are compared in Fig. 2 for $P = 1$ atm, $T_w = 500$ K, and $L = 5$ cm. The

results show that the steady-state conditions are reached at an earlier time for H_2O ; and this is followed respectively by CO_2 , CO , and OH . Significant differences are noted between the quadratic and quartic solutions for larger times. For the conditions of results presented in the figure, the difference are found to be greatest for OH and lowest for H_2O . The results for θ versus ξ are compared for $P = 1$ atm, $L = 10$ cm, and $T_w = 500$ K in Fig. 3 and $T_w = 1,000$ K in Fig. 4. The results demonstrate that considerable differences in solutions can occur at different locations in the channel and that the differences are larger for the lower wall temperature. Results for θ_b versus L presented in Fig. 5 show that the differences in two solutions are relatively larger at lower plate spacings and that quartic solutions approach the correct limiting solution for the case of no radiative interaction ($\theta_b = -0.243$). From the results presented in Figs. 2-5 and in Refs. 26 and 27 it is concluded that while quadratic and quartic solutions are identical for radiative equilibrium and radiation with conduction cases, they differ significantly for the case of combined conduction, convection and radiation. As such, all other results for this study were obtained by using the quartic formulation.

The results for temperature variations with nondimensional time are presented in Figs. 6-9 for various species and for different physical conditions. The centerline temperature distribution for general and limiting cases are illustrated in Fig. 6 for $T_w = 500$ K, $P = 1$ atm, and $L = 5$ cm. The results show that the steady-state conditions are reached at about $\tau = 0.5$ for all species. As noted earlier, these results also demonstrate that H_2O is a highly radiation participating gas as compared to CO_2 , CO , and OH . In comparison to other species considered, OH takes relatively longer times to reach the steady state and is least effective in transferring the radiative energy. For the specified physical conditions, the large path length solutions are closer to the general solutions and optically thin solutions provide higher rate of energy transfer. For all species, optically thin solutions reach the steady state faster than other solutions. Also, in the optically thin limit, CO_2 is more effective in the radiative transfer process than other species. The reasons for such trends are given in [8, 26, 27]. The results for $T_w = 500$ K and 1,000 K are compared in Fig. 7, and they simply indicate that the rate of energy transfer is higher at the higher temperature. The results for $\xi = 0.25$ and 0.5 are compared in Fig. 8 for $T_w = 1,000$ K, $P = 1$ atm, and $L = 5$ cm. It is noted that the rate of energy transfer is higher at earlier times and at locations closer to the wall. The centerline temperature variations for $L = 5$ cm and 10 cm are illustrated in Fig. 9 for $T_w = 1,000$ K and $P = 1$ atm. As would be expected, the rate of energy transfer is seen to increase with the increasing path length.

The results for temperature variations within the plates are presented in Figs. 10-14 for different conditions. Since the temperature profiles are symmetric, most of these results are illustrated only for $\xi = 0$ to $\xi = 0.5$. The steady-state solutions for various species are

compared in Fig. 10 for $P = 1$ atm, $L = 10$ cm, and different wall temperatures. Results again demonstrate the relative importance of different species for energy transfer. It is noted that the results for CO_2 at $T_w = 500$ K are exactly the same as for OH at $T_w = 1,000$ K, and the results for CO and H_2O are about the same at $T_w = 1,000$ K and $2,000$ K. This obviously is a coincidence for the physical case considered. The general and limiting solutions for OH, CO, CO_2 , and H_2O are presented, respectively, in Figs. 11 through 14a for $T_w = 500$ K, $P = 1$ atm, and $L = 10$ cm. These results also show that the steady-state conditions reach earlier for H_2O and CO_2 than for CO and OH. In general, the differences between limiting and general solutions are found to be small at earlier times; the maximum difference occurs at the steady-state conditions. In each case, the large path length solutions are closer to the general solutions, but the optically thin solutions are found to deviate considerably. This is because for $P = 1$ atm and $L = 10$ cm, the pressure path length is sufficiently high and the optically thin limit is not the correct limit for the physical case considered. It should be noted that for CO, CO_2 , and H_2O , the optically thin solutions are identical for $\tau > 0.05$. Additional results given in [28] reveal that the differences between general and large path length solutions are insignificant at higher temperatures for all species. The general solutions for the temperature variation across the entire duct are illustrated in Fig. 14b for H_2O for the physical conditions of $T_w = 1,000$ K, $P = 1$ atm, and $L = 5$ cm. The parabolic nature of the transient profiles is clearly evident and, in this case, the steady-state is reached at $\tau > 0.5$.

The bulk temperature results as a function of the distance between the plates are presented in Figs. 15-19 for different times. General as well as limiting solutions are illustrated in these figures. As mentioned earlier, the limiting value of $\theta_b = -0.243$ corresponds to negligible radiation. For all species, the results presented in the figures are for a pressure of one atmosphere. However, for any particular L , the large path length results essentially represent the limiting solutions for high pressures. The results, in general, demonstrate that the rate of energy transfer is higher at earlier times, the effect of radiation increases with increasing plate spacing, and the radiative transfer is more pronounced at the higher wall temperature.

General as well as limiting solutions for the bulk temperature are illustrated in Figs. 15-18 for individual species. It is seen that for all species the general solutions for $\tau = 0.5$ and 1.0 are essentially the same for all plate spacings, and the large path length results are valid for spacings greater than $L = 10$ cm for all times. The results for OH are presented in Figs. 15a and 15b for $T_w = 500$ K and $1,000$ K, respectively. It is noted that optically thin results provide the correct limiting solutions for plate spacings up to $L = 3$ cm for all times. The results for $T_w = 500$ K show only slight difference between general and large path length solutions for $\tau = 0.5$, and no significant difference was noted at earlier times (Fig. 15a). This, however, is not the case for the results

presented in Fig. 15b at $T_w = 1,000$ K. This trend in results for OH was noted also in [26, 27]. The results for CO are illustrated in Fig. 16 for $T_w = 500$ K and $P = 1$ atm. In this case, the optically thin solutions are seen to be valid only up to $L = 1.5$ cm. For $T_w = 1,000$ K and $P = 1$ atm, the results presented in Fig. 17 for CO_2 and in Fig. 18 for H_2O show the same general trend but the extent of radiative interaction is entirely different. For CO_2 , there is a considerable difference in general and optically thin solutions for all times. For H_2O , however, the optically thin results are closer to the general solutions for spacings up to $L = 2.5$ cm. The results presented in Figs. 15-18 clearly reveal that for a fixed spacing between the plates the rate of radiative heating will be considerably higher at earlier times than at the steady state. Thus, in a particular physical system, the extent of radiative heating can be very intense during the initial stages of operation. It is also important to note that both the optically thin and large path length results overestimate the influence of radiation. Since these solutions can be obtained with less numerical complications, they can be utilized to assess whether or not, for a given gas, the interaction of radiation is going to be important.

A comparison of the general band absorptance results for the four gases is shown in Fig. 19 for a pressure of one atmosphere and a wall temperature of $1,000$ K. The results clearly demonstrate the relative ability of the four species for radiative transfer at different path lengths. For a plate spacing of greater than $L = 3.0$ cm, the results show the same trend as noted in Figs. 2-10. For lower plate spacings and relatively higher temperatures, however, CO_2 shows a significantly higher ability for radiative transfer than other species. This is a typical distinguishing feature of the CO_2 under optically thin conditions [8, 26, 27].

For steady-state conditions, bulk temperature results were obtained for mixtures of different absorbing-emitting species under various conditions and some of these are presented in Figs. 20-27. The relative amount of each species in the mixture and the relative ability of the species for radiative transfer in a given physical condition determine the extent of radiative interaction.

As mentioned before, in many combustion processes involving fossil fuels, the predominant products of combustion are carbon dioxide and water vapor. Extensive studies have been conducted in the literature to determine the total emissivity of CO_2 and H_2O for homogeneous and nonhomogeneous conditions. However, only limited studies are available involving mixtures of CO_2 and H_2O for realistic and important physical conditions. The bulk temperature results for three different mixtures of $\text{CO}_2 + \text{H}_2\text{O}$ are presented in Figs. 20-23 for different temperatures and pressures. As would be expected, the results, in general, show that the extent of radiative interaction increases with increasing temperature, pressure, and path length. It is seen that the radiative interaction is stronger for higher amount of H_2O in the

mixture. However, for the optically thin conditions, the radiative contribution is seen to increase with increasing amount of CO_2 at relatively higher temperatures.

The bulk temperatures results for mixtures of OH and H_2O are illustrated in Figs. 24-26 and for mixtures of CO_2 , H_2O , and OH in Fig. 27 for different pressures and temperatures. All these results clearly demonstrate that the radiative ability of a gaseous mixture essentially depends on the amount of highly radiation participating species in the mixture. For example, a comparison of results presented in Figs. 24 and 27 for $P = 1$ atm indicates that the rate of radiative transfer is significantly higher with the inclusion of 20% CO_2 in the mixture of OH and H_2O . It is further noted that OH becomes a highly radiation participating species at higher temperatures and pressures.

Concluding Remarks

Analytical formulations and numerical procedures have been developed to investigate the transient radiative interaction of absorbing-emitting species in laminar fully-developed flows. Extensive results have been obtained for OH, CO , CO_2 and H_2O for different physical conditions. Illustrative results for the temperature distribution and bulk temperature are presented for different pressures and wall temperatures. In these results, a lower value of temperature implies a relatively higher ability of the gas to transfer radiative energy.

Comparative results of quadratic and quartic formulations confirm the need to use the quartic formulation in the numerical procedures for the case of combined conduction, convection, and radiation. The results, in general, demonstrate that the steady-state conditions are reached at about $\tau = 0.5$ for all species, H_2O is a highly radiation participating species (as compared to CO_2 , CO , and OH), the rate of energy transfer is higher at earlier times and at locations closer to the wall, differences between the limiting and general solutions are small at earlier times, the effect of radiation increases with increasing plate spacing, and the radiative transfer is more pronounced at higher wall temperature and pressure. Similar conclusions can be drawn from the results presented for various mixtures. The results clearly show that for a given physical condition the radiative ability of a gaseous mixture depends essentially on the amount of highly radiating species in the mixture. From the results presented in this study, the extent of total heating can be determined for different times. This information is essential in designing thermal protection systems for operations during the initial stages of intense heating.

Acknowledgements

This work was supported, in part, by the NASA Langley Research Center through Grant NAG-1-423. Some of the limiting formulations were suggested by R. R. Batki.

References

1. Sparrow, E. M. and Cess, R. D., Radiation Heat Transfer, Brooks/Cole, Belmont, Calif., 1966 and 1970. New Augmented Edition, Hemisphere Publishing Corp., Washington, D.C., 1978.
2. Hottel, H. C. and Sarofim, A. F., Radiative Transfer, McGraw-Hill Book Co., New York, 1967.
3. Siegel, R. and Howell, J. R., Thermal Radiation Heat Transfer, McGraw-Hill Book Co., New York, 1971; Second Edition, 1981.
4. Cess, R. D., "The Interaction of Thermal Radiation with Conduction and Convection Heat Transfer," Advances in Heat Transfer, Vol. 3, Academic Press, New York, 1966.
5. Sparrow, E. M., "Radiation Heat Transfer between Surfaces," Advances in Heat Transfer, Vol. 2, Academic Press, New York, 1965.
6. Viskanta, R., "Radiation Transfer and Interaction of Convection with Radiation Heat Transfer," Advances in Heat Transfer, Vol. 3, Academic Press, New York, 1966.
7. Tien, C. L., "Thermal Radiation Properties of Gases," Advances in Heat Transfer, Vol. 5, Academic Press, New York, 1968.
8. Cess, R. D. and Tiwari, S. N., "Infrared Radiative Energy Transfer in Gases," Advances in Heat Transfer, Vol. 8, Academic Press, New York, 1972.
9. Edwards, D. K., "Molecular Gas Band Radiation," Advances in Heat Transfer, Vol. 12, Academic Press, New York, 1976.
10. Tiwari, S. N. "Band Models and Correlations for Infrared Radiation," Radiative Transfer and Thermal Control (Progress in Astronautics and Aeronautics), Vol. 49, American Institute of Aeronautics and Astronautics, New York, 1976.
11. Tiwari, S. N., "Applications of Infrared Band Model Correlations to Nongray Radiation," International Journal of Heat and Mass Transfer, Vol. 20, No. 7, July 1977, pp. 741-751.
12. Tiwari, S. N., "Models for Atmospheric Radiation," Advances in Geophysics, Vol. 20, Academic Press, New York, 1978.
13. Edwards, D. K., Radiation Heat Transfer Notes, Hemisphere Publishing Corporation, Washington, D.C., 1981.
14. Lick, W., "Transient Energy Transfer by Radiation and Conduction," International Journal of Heat and Mass Transfer, Vol. 8, 1965, pp. 119-127.

15. Chang, Y. P. and Kang, C. S., "Transient and Steady Heat Transfer in a Conducting and Radiating Medium," AIAA Journal, Vol. 8, No. 4, April 1970, pp. 609-614.
16. Chang, Y. P. and Smith, R. C., Jr., "Steady and Transient Heat Transfer by Radiative and Conduction in a Medium Bounded by Two Coaxial Cylindrical Surfaces," International Journal of Heat and Mass Transfer, Vol. 13, 1970, pp. 69-80.
17. Doornink, D. G. and Hering, R. G., "Transient Radiative Heat Transfer in a Nongray Medium," Journal of the Quantitative Spectroscopy and Radiative Transfer, Vol. 12, 1972, pp. 1161-1174.
18. Larson, D. W. and Vikanta, R., "Transient Combined Laminar Free Convection and Radiation in a Rectangular Enclosure," Journal of Fluid Mechanics, Vol. 78, Part 1, 1976, pp. 65-85.
19. Melnikov, V. I. and Sukhovich, E. P., "Transient Heat Exchange Between a Radiating Plate and a High-Temperature Gas Flow," Heat Transfer-Soviet Research, Vol. 10, No. 3, May-June 1978, pp. 11-20 (Translation).
20. Heinisch, R. P. and Viskanta, R., "Transient Combined Conduction-Radiation in an Optically Thick Semi-Infinite Medium," AIAA Journal, Vol. 6, 1968, pp. 1409-1411.
21. Hazzah, A. S. and Beck, J. V., "Unsteady Combined Conduction-Radiation Energy Transfer Using a Rigorous Differential Method," International Journal of Heat and Mass Transfer, Vol. 13, March 1970, pp. 517-522.
22. Lii, C. C. and Özisik, M. N., "Transient Radiation and Conduction in an Absorbing, Emitting and Scattering Slab with Reflecting Boundaries," International Journal of Heat and Mass Transfer, Vol. 15, May 1972, pp. 1175-1179.
23. Weston, K. C. and Hauth, J. L., "Unsteady, Combined Radiation and Conduction in an Absorbing, Scattering and Emitting Medium," Journal of Heat Transfer, Vol. 95, August 1973, pp. 357-364.
24. Sutton, W. H., "A Short Time Solution for Coupled Conduction and Radiation in a Participating Slab Geometry," ASME Paper No. 84-HT-34, 1984.
25. Tiwari, S. N., "Radiative Interactions in Transient Energy Transfer in Gaseous Systems," Progress Report NAG-1-423, Dept. of Mechanical Engineering and Mechanics, College Engineering and Technology, Old Dominion University, Norfolk, VA, December 1985.
26. Tiwari, S. N. and Singh, D. J., "Interaction of Transient Radiation in Nongray Gaseous Systems," Progress Report NAG-1-423, Dept. of Mechanical Engineering and Mechanics, College of Engineering and Technology, Old Dominion University, Norfolk, VA, January 1987.
27. Tiwari, S. N., Singh, D. J. and Kumar, A., "Transient Radiative Energy Transfer in Nongray Gases," AIAA Paper 87-0323, January 1987.
28. Tiwari, S. N. Singh, D. J., "Transient Radiative Energy Transfer in Incompressible Laminar Flows," Progress Report NAG-1-423, Dept. of Mechanical Engineering and Mechanics, College of Engineering and Technology, Old Dominion University, Norfolk, VA, June 1987.
29. Soufiani, A., Hartmann, J. M., and Taine, J., "Validity of Band-Model Calculations for CO₂ and H₂O Applied to Radiative Properties and Conductive-Radiative Transfer," Journal of Quantitative Spectroscopy and Radiative Transfer, Vol. 33, No. 3, March 1985, pp. 243-257.
30. Soufiani, A. and Taine, J., "Application of Statistical Narrow-Band Model to Coupled Radiation and Convection at High Temperature," International Journal of Heat and Mass Transfer, Vol. 30, No. 3, March 1987, pp. 437-447.
31. Penner, S. S. and Varanasi, P., "Effect of (Partial) Overlapping of Spectral Lines on the Total Emissivity of H₂O-CO₂ Mixtures (T > 800 K)," Journal of Quantitative Spectroscopy and Radiative Transfer, Vol. 6, No. 2, March/April 1966, pp. 181-192.
32. Felske, J. D. and Tien, C. L., "Wide Band Characterization of the Total Band Absorptance of Overlapping Infrared Gas Bands," Combustion Science and Technology, Vol. 11, 1975, pp. 111-117.

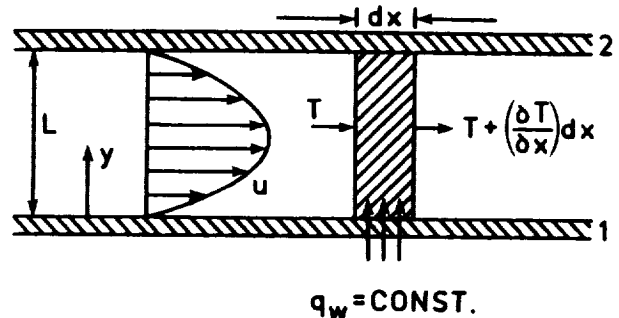


Fig. 1 Physical model and coordinate systems for flow of radiating gases between parallel plates.

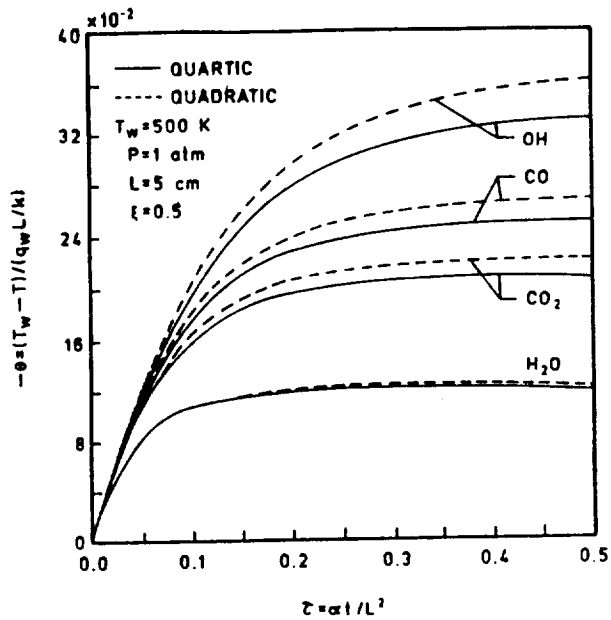


Fig. 2 Comparison of quadratic and quartic results for the centerline temperature variations with time; $T_w=500$ K, $P=1$ atm, and $L=5$ cm.

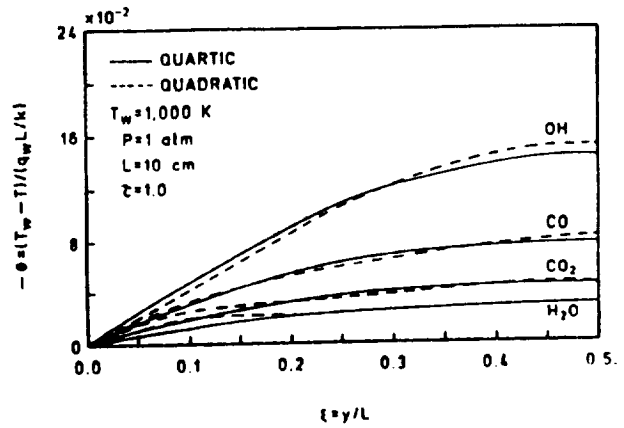


Fig. 4 Comparison of quadratic and quartic results for temperature variations across the duct; $P=1$ atm, $L=10$ cm, and $T_w=1,000$ K.

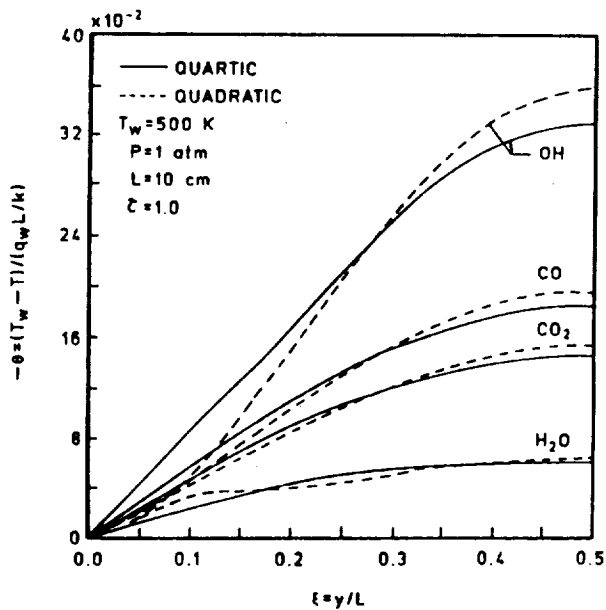


Fig. 3 Comparison of quadratic and quartic results for temperature variations across the duct; $P=1$ atm, $L=10$ cm, and $T_w=500$ K.

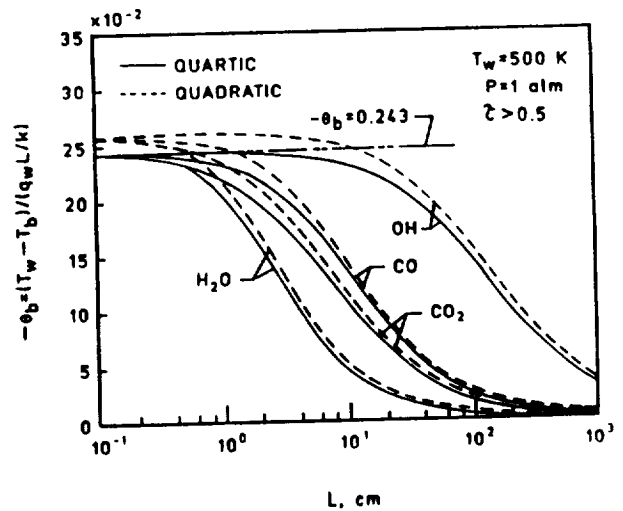


Fig. 5 Comparison of quadratic and quartic results for the bulk temperature; $P=1$ atm and $T_w=500$ K.

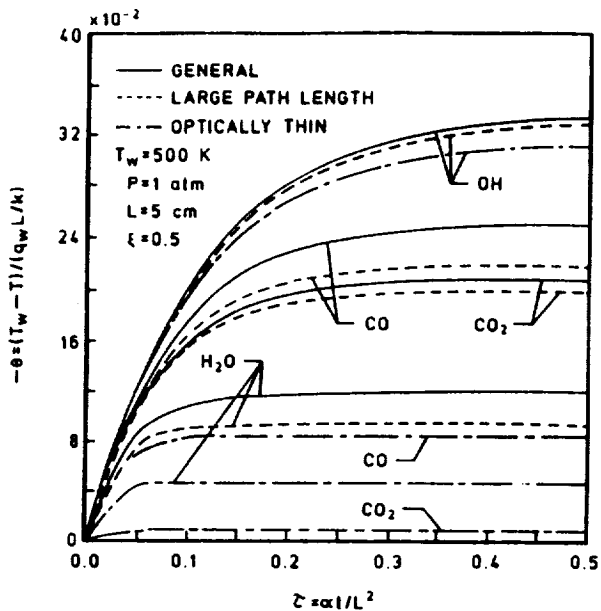


Fig. 6 Comparison of general and limiting results for the centerline temperature variations with time; $T_w=500$ K, $P=1$ atm, and $L=5$ cm.

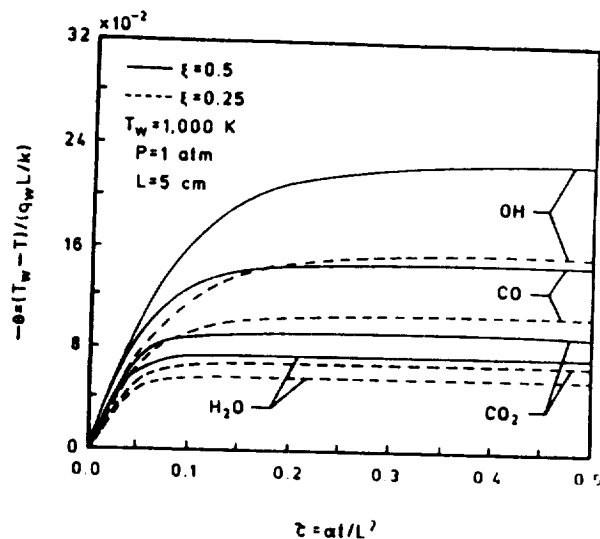


Fig. 8 Comparison of temperature variations with time for $\xi=0.25$ and 0.5 ; $T_w=1,000$ K, $P=1$ atm, and $L=5$ cm.

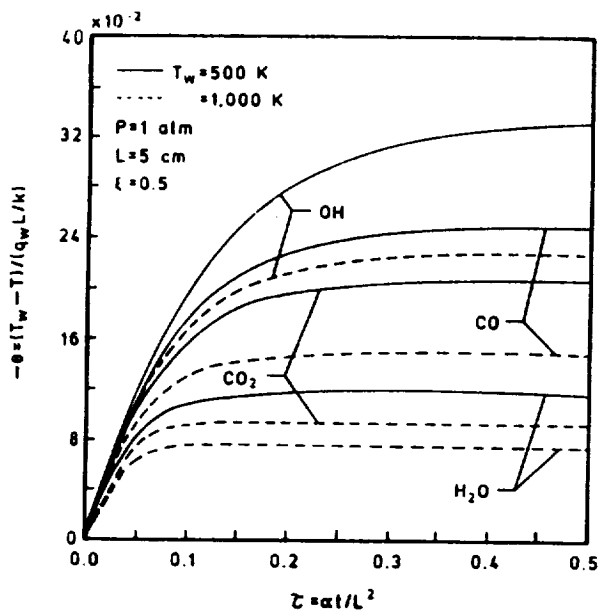


Fig. 7 Comparison of centerline temperature variations with time for $T_w=500$ K and $1,000$ K; $P=1$ atm and $L=5$ cm.

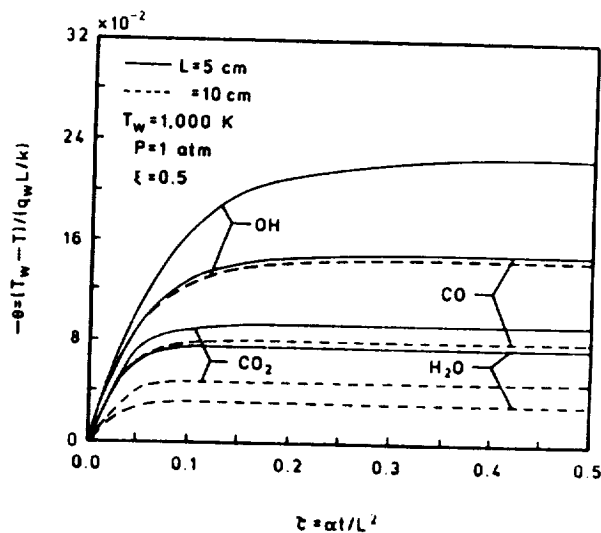


Fig. 9 Comparison of centerline temperature variations with time for $L=5$ cm and 10 cm; $T_w=1,000$ K and $P=1$ atm.

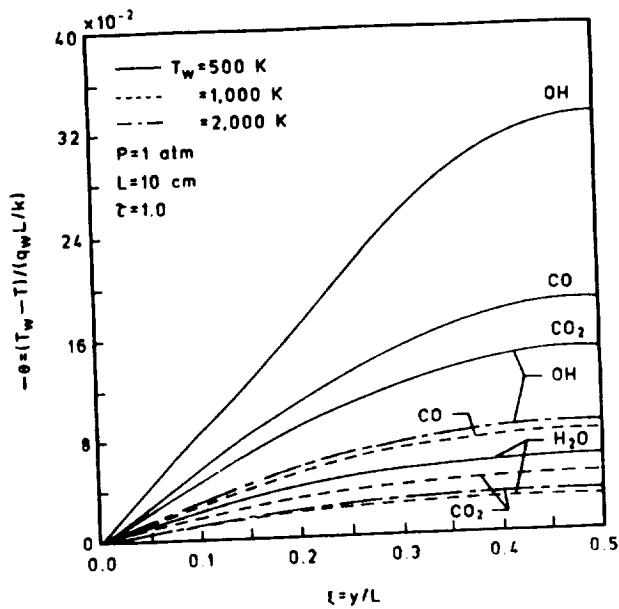


Fig. 10 Comparison of temperature variations across the duct for $T_w=500$ K, 1,000 K, and 2,000 K; $P=1$ atm and $L=10$ cm.

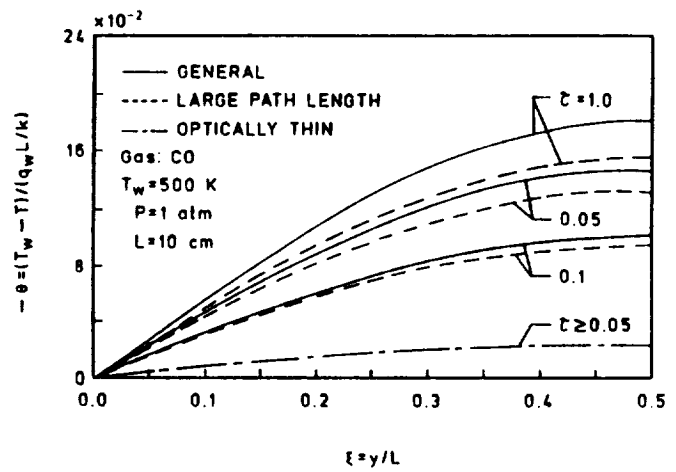


Fig. 12 Comparison temperature variations across the duct for CO; $T_w=500$ K, $P=1$ atm, and $L=10$ cm.

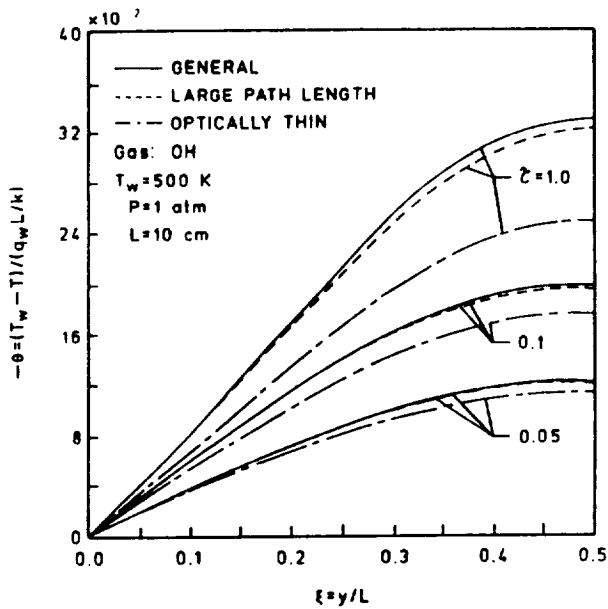


Fig. 11 Comparison of temperature variations across the duct for OH; $T_w=500$ K, $P=1$ atm, and $L=10$ cm.

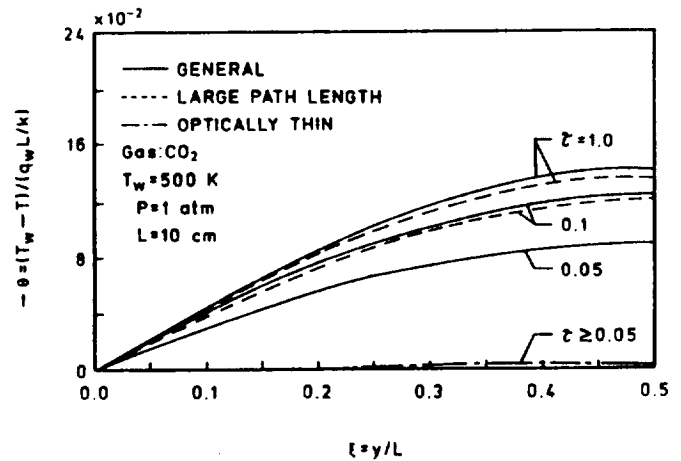


Fig. 13 Comparison of temperature variations across the duct for CO_2 ; $T_w=500$ K, $P=1$ atm, and $L=10$ cm.

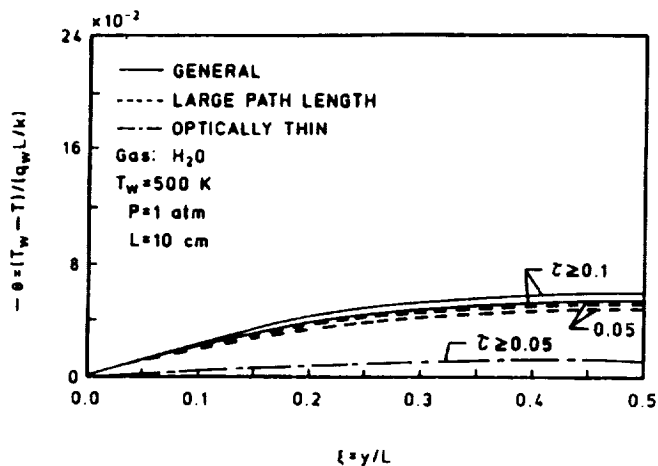


Fig. 14a Comparison of temperature variations across the duct for H_2O ; $T_w=500$ K, $P=1$ atm, and $L=10$ cm.

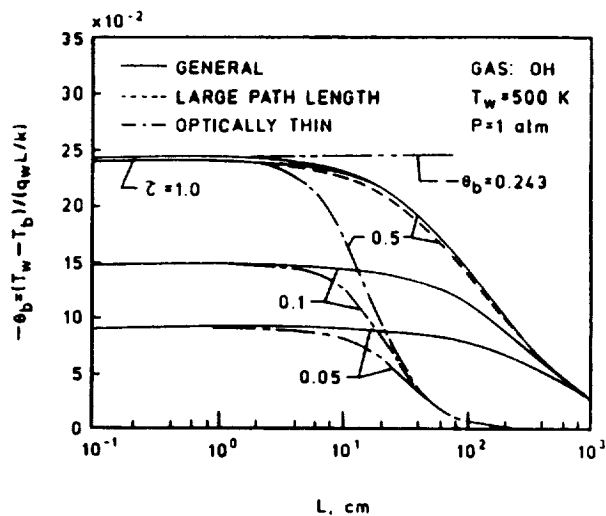


Fig. 15a Variation of bulk temperature with plate spacing for OH ; $T_w=500$ K and $P=1$ atm.

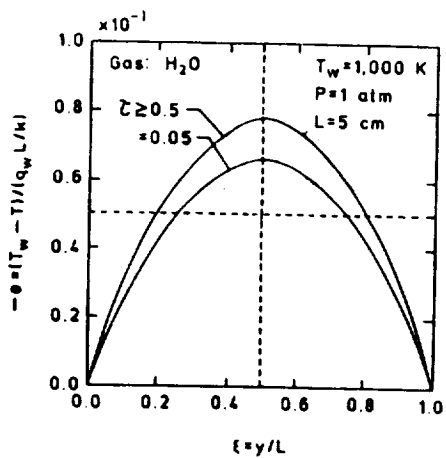


Fig. 14b Comparison of temperature variations across the duct for H_2O ; $T_w=1,000$ K, $P=1$ atm, and $L=5$ cm.

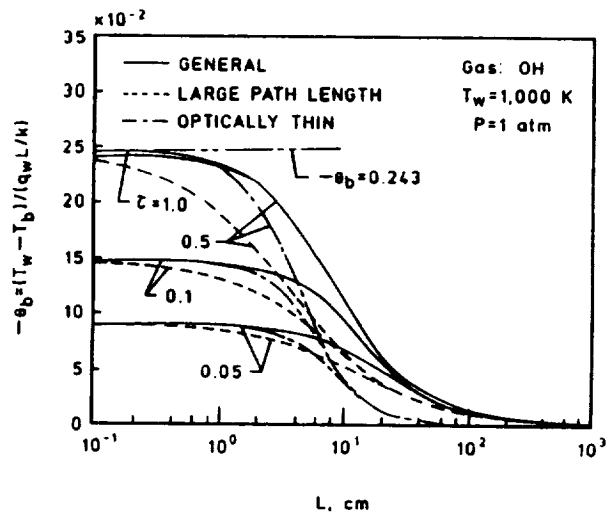


Fig. 15b Variation of bulk temperature with plate spacing for OH ; $T_w=1,000$ K and $P=1$ atm.

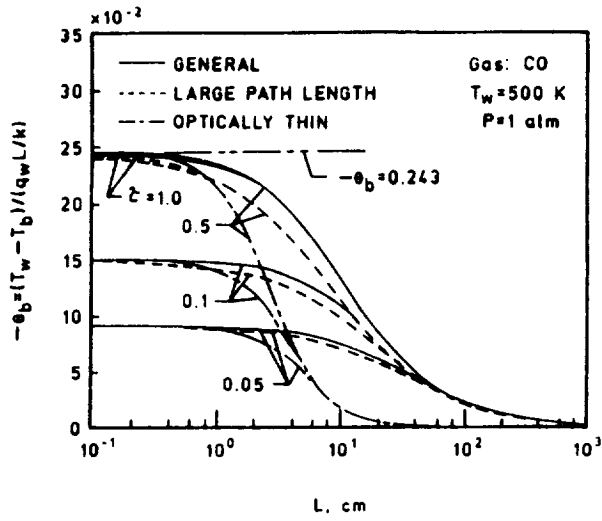


Fig. 16 Variation of bulk temperature with plate spacing for CO; $T_w = 500 \text{ K}$ and $P = 1 \text{ atm}$.

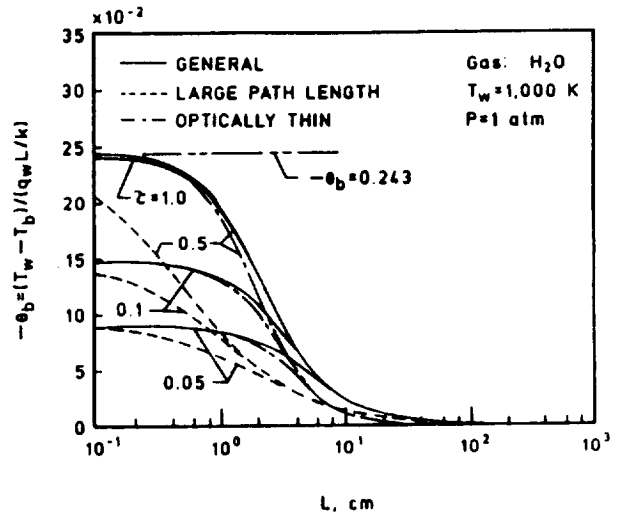


Fig. 18 Variation of bulk temperature with plate spacing for H₂O; $T_w = 1,000 \text{ K}$ and $P = 1 \text{ atm}$.

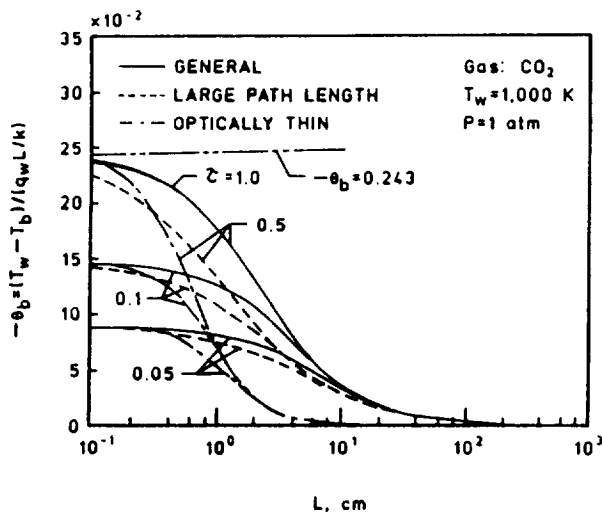


Fig. 17 Variation of bulk temperature with plate spacing for CO₂; $T_w = 1,000 \text{ K}$ and $P = 1 \text{ atm}$.

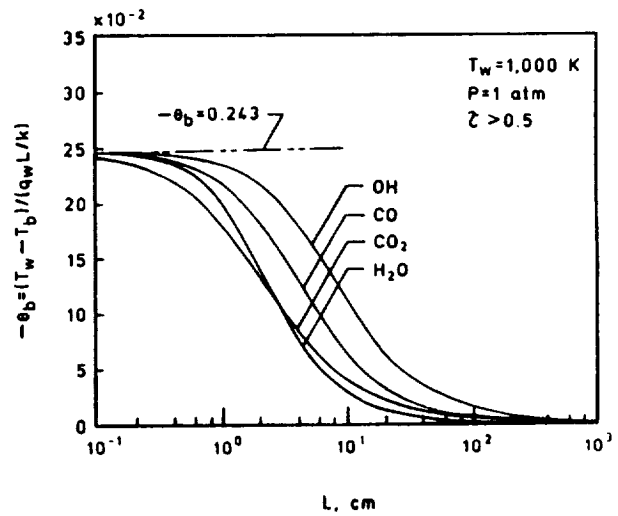


Fig. 19 Comparison of bulk temperature results for $T_w = 1,000 \text{ K}$ and $P = 1 \text{ atm}$.

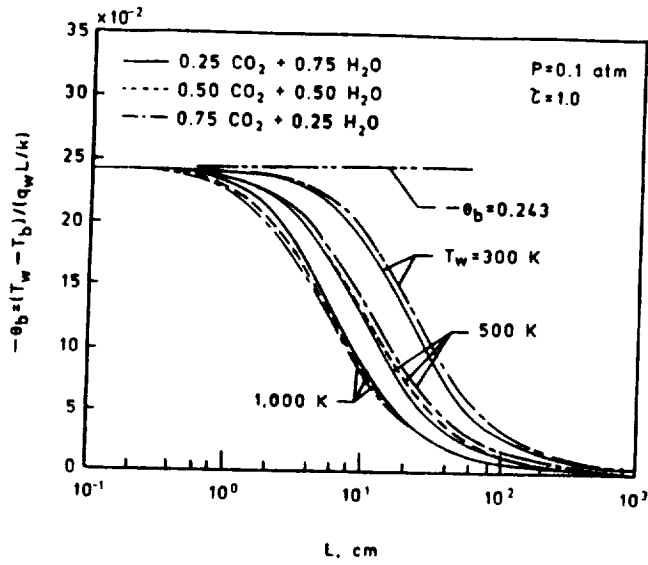


Fig. 20 Bulk temperature results for $\text{CO}_2 + \text{H}_2\text{O}$ for $P=0.1$ atm.

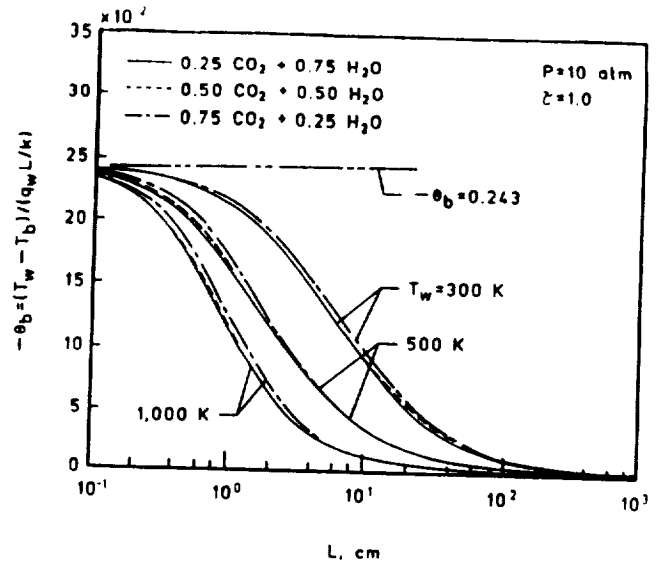


Fig. 22 Bulk temperature results for $\text{CO}_2 + \text{H}_2\text{O}$ for $P=10$ atm.

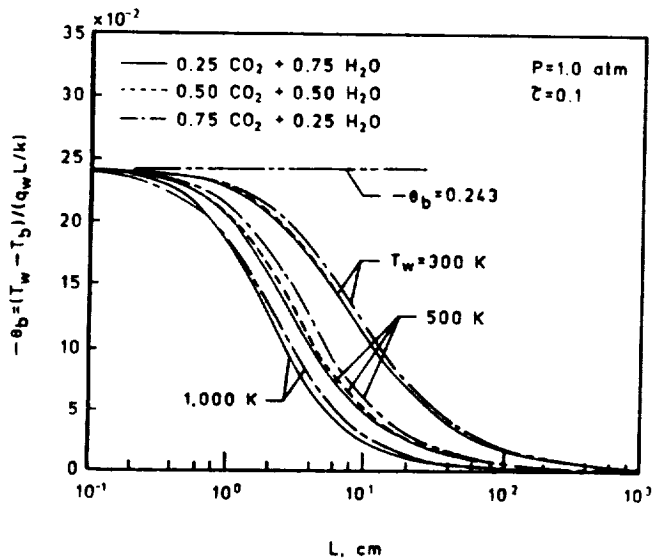


Fig. 21 Bulk temperature results for $\text{CO}_2 + \text{H}_2\text{O}$ for $P=1$ atm.

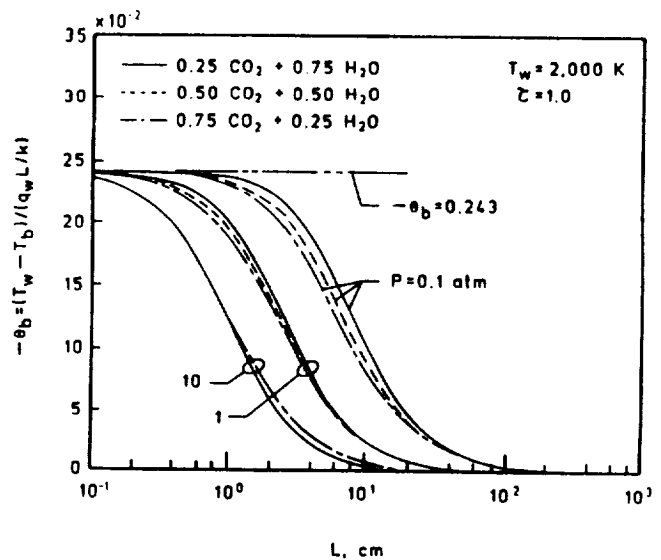


Fig. 23 Bulk temperature results for $\text{CO}_2 + \text{H}_2\text{O}$ for $T_w=2,000$ K.

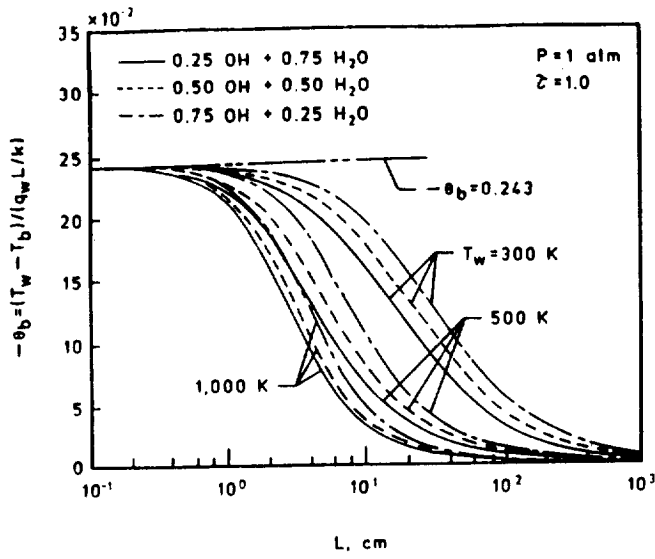


Fig. 24 Bulk temperature results for OH and H₂O for P=1 atm.

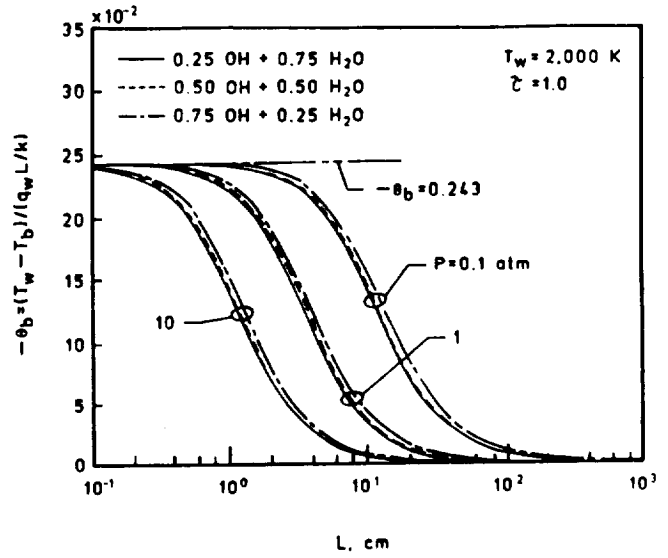


Fig. 26 Bulk temperature results for OH and H₂O for T_w=2,000 K.

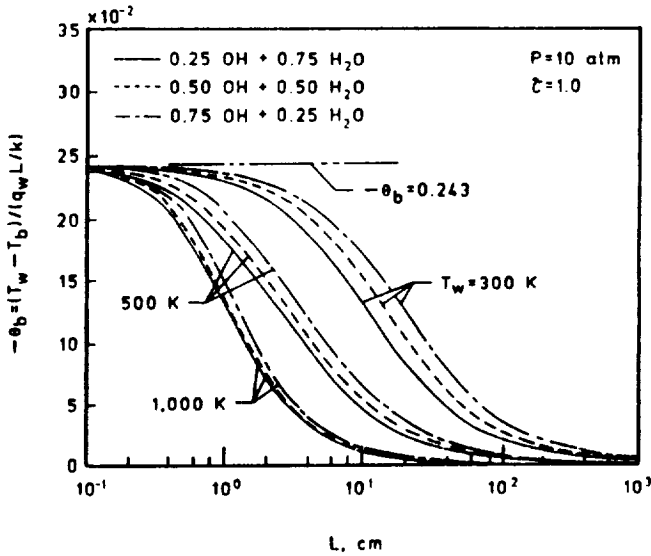


Fig. 25 Bulk temperature results for OH and H₂O for P=10 atm.

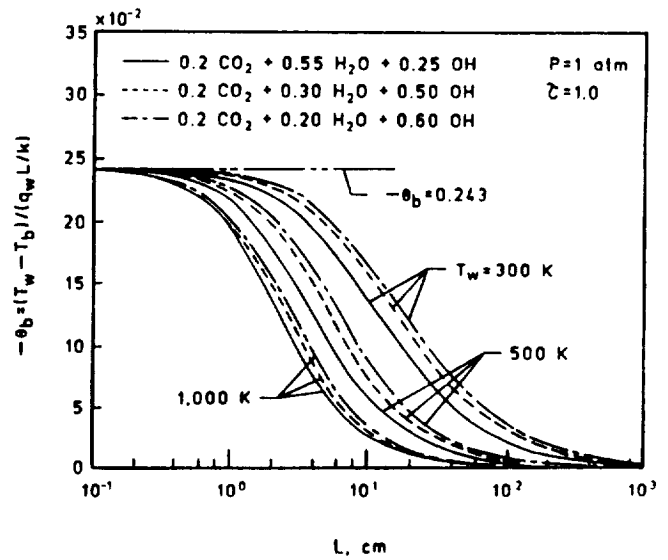


Fig. 27 Bulk temperature results for CO₂ + H₂O + OH for P=1 atm.

RACE _____ **INTENTIONALLY BLANK**



APPENDIX I

AIAA-90-0134

**RADIATIVE INTERACTIONS IN
LAMINAR INCOMPRESSIBLE AND
COMPRESSIBLE INTERNAL FLOWS**

S. N. Tiwari, D. J. Singh, and P. A. Trivedi
Department of Mechanical Engineering and Mechanics,
Old Dominion University
Norfolk, Virginia 23529-0247

28th Aerospace Sciences Meeting

January 8-11, 1990/Reno, Nevada

PAGE _____ INTENTIONALLY BLANK

RADIATIVE INTERACTIONS IN LAMINAR INCOMPRESSIBLE AND COMPRESSIBLE INTERNAL FLOWS

S. N. Tiwari¹, D. J. Singh² and P. A. Trivedi³
Old Dominion University, Norfolk, Virginia 23529-0247

Abstract

Analyses and numerical procedures are presented to investigate the radiative interactions of gray and nongray absorbing-emitting species between two parallel plates and in a circular tube. Laminar fully developed incompressible as well as entrance region subsonic flows are considered. The participating species considered are OH, CO, CO₂, CH₄, and H₂O. Results obtained for different flow conditions indicate that the radiative interactions can be quite significant in fully developed incompressible flows. For subsonic flows, however, the flowfield is not changed significantly due to radiative interaction.

Nomenclature

A	band absorptance = $A(u, \beta)$, cm^{-1}
A_o	band width parameter, cm^{-1}
C_o	correlation parameter, $\text{atm}^{-1} - \text{cm}^{-1}$
C_p	specific heat at constant pressure $\text{kJ/kg-K} = \text{erg/gm-K}$
e_ω	Planck's function, $(\text{W-cm}^{-2})/\text{cm}^{-1}$
e_{ω_o}	Planck's function evaluated at wave number ω_o
e_1, e_2	emissive power of surfaces with temperature T_1 and T_2 , W-cm^{-2}
k	thermal conductivity, erg/cm-sec-K
L	distance between the plates
P	pressure
P_i	partial pressure
P_t	stagnation pressure
Pr	Prandtl number
QR	total radiative heat flux, $\text{J/m}^2\text{-s}$
q_c	conduction heat flux, $\text{J/m}^2\text{-s}$
QR_ω	spectral radiation heat flux, $(\text{w-cm}^{-2})/\text{cm}^{-1}$
r	physical coordinate for circular tube
r_o (X1)	radius of the tube

¹ Eminent Professor, Dept. of Mechanical Engineering and Mechanics. AIAA Associate Fellow

² Graduate Research Assistant, Dept. of Mechanical Engineering and Mechanics. Present affiliation: Analytical Systems and Materials Inc., Hampton, Virginia.

³ Graduate Research Assistant, Dept. of Mechanical Engineering and Mechanics.

S	integrated intensity of a wide band, $\text{atm}^{-1}\text{-cm}^{-2}$
T	temperature, K
T_1, T_2	wall temperature, K; $T_1 = T_w$
T_b	bulk temperature, K
u	nondimensional coordinate = $S\text{Py}/A_o$
u_o	nondimensional path length = $S\text{PL}/A_o$
θ	flow angle
κ_ω	spectral absorption coefficient, cm^{-1}
κ_p	Planck mean absorption coefficient, cm^{-1}
ξ, η	computational coordinate
ρ	density, kg/m
σ	Stefan-Boltzmann constant, $\text{erg}/(\text{sec-cm-K}^4)$
ω	wave number, cm^{-1}
ω_o, ω_i	wave number at the band center, cm^{-1}

I. Introduction

There is a renewed interest in investigating various aspects of radiative energy transfer in participating mediums. Radiative interactions become important in many engineering problems involving high temperature gases. Recent interest lies in the areas of design of high pressure combustion chambers and high enthalpy nozzles, entry and reentry phenomena, hypersonic propulsion, and defense oriented research.

Basic formulations on radiative energy transfer in participating mediums are available in standard references [1–8]. The review articles presented in [9–15] are useful in understanding the radiative properties of participating species and the nature of nongray radiation. The validity of radiative transfer analyses depends upon the accuracy with which absorption-emission and scattering characteristics of participating species are modeled. There are several models available to represent the absorption-emission characteristics of molecular species and these are reviewed in [12, 13].

The purpose of this study is to present analyses and solution procedures for infrared radiative energy transfer in molecular gases when other modes of energy transfer simultaneously occur. Attention is directed to investigate radiative interactions in laminar incompressible and compressible internal flows between two parallel plates and in a circular tube. Radiative interactions in incompressible duct flows have been investigated extensively in the literature with certain inherent simplifying assumptions [16–35]. The main thrust of this research is to develop procedures for investigating radiative interactions in subsonic compressible entrance region flows and provide a parametric study for different participating species. However, basic formulations, numerical procedures, and certain results of incompressible fully-developed duct flows are also presented for comparative purposes.

II. Basic Formulation

Basic governing equations and boundary conditions are provided here for the two physical problems considered in this study. These are fully developed laminar incompressible flow between two parallel plates and within a circular tube, and developing laminar compressible flow in ducts.

A. Fully-Developed Incompressible Flow

The physical problem considered is the energy transfer in laminar, incompressible, constant properties, fully developed flow of absorbing-emitting gases between two parallel plates (Fig. 1a) and within a circular tube (Fig. 1b). The condition of uniform surface heat flux is assumed such that the surface temperature varies in the axial direction. Extensive treatment of this problem for the parallel plate geometry is available in the literature. However, only limited attentions have been directed in obtaining nongray solutions for the circular tube geometry [19, 20, 23, 26]. One of the objective of this study is to obtain extensive nongray solutions for the circular tube geometry for different flow and physical conditions.

For the parallel plate geometry (Fig. 1a), the energy equation can be expressed as [1]

$$u \frac{\partial T}{\partial x} + v \frac{\partial T}{\partial y} = \alpha \frac{\partial^2 T}{\partial y^2} - \frac{1}{\rho C_p} \frac{\partial q_R}{\partial y} \quad (1)$$

where $\alpha = (k/\rho C_p)$, represents the thermal diffusivity of the fluid. In deriving Eq. (1), it has been assumed that conduction as well as radiation heat transfer in the x direction are negligible compared to that transferred in the y direction. In addition, it has been assumed that the Eckert number of the flow is small. These assumptions are consistent with the formulations presented in [4, 6, 8, 10, 11].

The justification for a fully developed flow in the presence of radiative interaction is provided in [4, 8] and in cited references. For a fully developed flow, $v = 0$, and u is given by the well-known parabolic profile $u = 6 u_m (\xi - \xi^2)$, where $\xi = y/L$ and u_m represents the mean fluid velocity. Also, for the flow of a perfect gas with uniform heat flux, $\partial T/\partial x$ is constant and is given by

$$\partial T/\partial x = (2\alpha q_w)/(u_m L k) \quad (2)$$

A combination of Eqs. (1) and (2), therefore, results in

$$\frac{d^2 \theta}{d\xi^2} - 12(\xi - \xi^2) = \frac{1}{q_w} \frac{dq_R}{d\xi} \quad (3)$$

where

$$\theta = (T - T_1)/(q_w L/k); \quad T_1 = T_w$$

Equation (3) is the governing energy equation in nondimensional form for the parallel plate geometry. The boundary conditions for this problem can be expressed as

$$\theta = (0) = \theta(1) = 0; \theta_\xi(\xi = 1/2) = 0; \theta_\xi(\xi = 0) = -\theta_\xi(\xi = 1) \quad (4)$$

It should be noted that all boundary conditions given in Eq. (4) are not independent; any two convenient conditions can be used to obtain specific solutions. By integrating Eq. (3) once and using the conditions that at $\xi = 1/2$, $q_R(\xi)$ and $(d\theta/d\xi)$ are equal to zero, one obtains

$$d\theta/d\xi - 2(3\xi^2 - 2\xi^3) + 1 = q_R(\xi)/q_w \quad (5)$$

Either Eq. (3) or Eq. (5) can be used to investigate the effect of radiative interaction.

For the circular tube geometry (Fig. 1b), the energy equation, as given by Eq. (1), can be expressed as

$$u \frac{\partial T}{\partial x} = \frac{\alpha}{r} \frac{\partial}{\partial r} \left(r \frac{\partial T}{\partial r} \right) - \frac{1}{\rho C_p} \frac{1}{r} \frac{\partial}{\partial r} (r q_R) \quad (6)$$

where u is given by the relation $u = u_m [1 - (r_o)^2]$. For a uniform wall heat flux and fully developed heat transfer, in this case, $\partial T/\partial x$ is given by

$$\partial T/\partial x = (2\alpha q_w)/(u_m r_o/k) \quad (7)$$

Consequently, Eq. (6) may be expressed as

$$\frac{d}{d\xi} \left(\xi \frac{d\theta}{d\xi} \right) - 4(\xi - \xi^3) = \frac{1}{q_w} \frac{d}{d\xi} (\xi q_R) \quad (8)$$

where

$$\theta = (T - T_w)/(q_w r_o/k), \xi = r/r_o$$

It is important to note the difference in the definitions of θ given in Eqs. (3) and (8). Upon integrating Eq. (8) and noting that $d\theta/d\xi = 0$ and $q_R = 0$ at $\xi = 0$, there is obtained

$$d\theta/d\xi + \xi^3 - 2\xi = q_R/q_w \quad (9)$$

The boundary condition for this equation is given as $\theta(1) = 0$.

For incompressible flow problems, the quantity of primary interest is the bulk temperature of the gas. For a fully-developed flow between parallel plates, this is expressed as

$$\theta_b = (T_b - T_1)/(q_w L/k) = 6 \int_0^1 \theta(\xi)(\xi - \xi^2) d\xi \quad (10)$$

where $q_w = \bar{h} (T_1 - T_b)$, and \bar{h} represents the equivalent (or effective) heat transfer coefficient ($W/cm^2 - K$).

For the fully-developed flow in a circular tube, the expression for the bulk temperature is given by

$$\theta_b (T_b - T_w)/(q_w r_o/k) = 4 \int_0^1 \theta(\xi)(\xi - \xi^3) d\xi \quad (11)$$

where $q_w = \bar{h} (T_w - T_b)$.

In general, the heat transfer results are expressed in terms of the Nusselt number $N_u = \bar{h} D_h/k$. Here, D_h represents the hydraulic diameter. For the parallel plate geometry, D_h equals twice the plate separation, i.e., $D_h = 2L$. For the circular tube geometry, D_h represents the actual diameter of the tube, i.e., $D_h = 2r_o$. Upon eliminating the heat transfer coefficient \bar{h} from the expressions for q_w and N_u , a relation between the Nusselt number and the bulk temperature is obtained for both geometries as $N_u = -2/\theta_b$. The heat transfer results, therefore, can be expressed either in terms of N_u or θ_b .

B. Laminar Compressible Flow

The physical problem considered for basic understanding of radiative interaction in compressible flows is two-dimensional variable property laminar flow between two parallel plates. For this model, two-dimensional Navier-Stokes equations in fully conservative form are used to describe the flow field. These equations, in physical domain, can be written as (Fig. 1c)

$$\frac{\partial U}{\partial t} + \frac{\partial F}{\partial x} + \frac{\partial G}{\partial y} = 0 \quad (12)$$

where vectors U, F and G are expressed as

$$U = \begin{bmatrix} \rho \\ \rho u \\ \rho v \\ \rho H - P \end{bmatrix}, \quad F = \begin{bmatrix} \rho \\ \rho u^2 + P - \tau_{xx} \\ \rho uv - \tau_{xy} \\ (E + P)u - u\tau_{xx} - v\tau_{xy} + q_{Cx} + q_{Rx} \end{bmatrix},$$

$$G = \begin{bmatrix} \rho \\ \rho uv - \tau_{xy} \\ \rho v^2 + P - \tau_{yy} \\ (E + P)v - u\tau_{xy} - v\tau_{yy} + q_{Cy} + q_{Ry} \end{bmatrix}, \quad P = \rho RT$$

The viscous stress terms appearing in the definitions of F and G are given in [36]. The relations for conduction heat transfer in x and y directions are given by

$$q_{Cx} = -k \frac{\partial T}{\partial x}; \quad q_{Cy} = -k \frac{\partial T}{\partial y} \quad (13)$$

The terms q_{Rx} and q_{Ry} represent radiative fluxes in x and y directions, respectively; expressions for these are provided in the next section. The total energy flux in a given direction is given by the corresponding last term in the definition of F or G. Consequently, this formulation involves all kinds of energy interaction including frictional (aerodynamic) heating. The coefficient of viscosity is evaluated by using the Sutherland's formula and the coefficient of thermal conductivity is calculated by using a constant value of the Prandtl number.

Equation (12) can be used to obtain solutions for all kinds of compressible flows. However, boundary conditions and numerical procedures for different flows are quite different. For subsonic flows the treatment of the inflow conditions is guided by the theory of characteristic. A locally one-dimensional flow has four characteristic equations with slopes u, u+c, u and u-c. If the flow is subsonic at the inflow, then the u-c characteristic has a negative slope and it propagates informations from the interior upstream to the inflow boundary. In this case, only three quantities can be specified at the inflow and the fourth quantity must be allowed to vary as the solution progresses.

In this study, the stagnation pressure, stagnation temperature and flow angle are specified at the inflow. These quantities are related to the state pressure and state temperature by the following equations

$$\begin{aligned} \frac{P_t}{P} &= \left(1 + \frac{\gamma - 1}{2} M^2\right)^{\gamma/(\gamma-1)}; \\ \frac{T_t}{T} &= \left(1 + \frac{\gamma - 1}{2} M^2\right); \frac{v}{u} = \tan(\theta_{IF}) \end{aligned} \quad (14)$$

Equations (14) is a system of three equations in four unknowns, P, T, u and v. To complete the system of equations, a zero order extrapolation is used for the pressure at the inflow. The outflow boundary is also calculated based on the theory of characteristic. For subsonic flow at the outflow, the u-c characteristic propagates information upstream from the boundary to the interior, i.e., only one quantity can be specified at the outflow. The state pressure is specified at the outflow while u, v and T are calculated using a zeroth-order extrapolation. Along the surfaces, following boundary conditions were applied

$$u = 0, v = 0, \partial P / \partial y = 0, T = T_w \quad (15)$$

The density is obtained from the equation of state using the computed surface pressure and prescribed surface temperature.

III. Radiative Transfer Models

Evaluation of the energy equation presented in Eqs. (3), (5), (8), (9) and (12) requires an appropriate expression for the net radiative flux. A suitable radiative transport model is needed to represent the true nature of participating species and transfer processes. In this section, a brief discussion of various absorption models is given and essential equations for the radiative flux are presented.

A. Absorption Models

Several models are available in the literature to represent the absorption-emission characteristics of molecular species. The total band absorptance of a vibration-rotation band is given by

$$A = \int_{-\infty}^{\infty} [1 - \exp(-\kappa_{\omega} X)] d(\omega - \omega_0) \quad (16)$$

where κ_{ω} is the volumetric absorption coefficient, ω is the wave number, ω_0 is the wave number at the band center, $X = Py$ is the pressure path length, and the limits of integration are over the entire band pass. Various models are used to obtain the relation for A in Eq. (16).

The gray gas model is probably the simplest model to employ in radiative transfer analyses. In this model, the absorption coefficients is assumed to be independent of frequency, i. e., κ_{ω}

is not a function of ω . A convenient model to represent the average absorption coefficient of a gray gas is the Planck mean absorption coefficient κ_p which is defined as [1]

$$\kappa_p = \int_0^{\infty} \kappa_{\omega} e_{b\omega}(T) d\omega / e_b(T) \quad (17a)$$

For a multiband gaseous system, this is expressed as

$$\kappa_p = [P_j / (\sigma T^4)] \sum_i^n e_{\omega_i}(T) S_i(T) \quad (17b)$$

where P_j is the partial pressure of j th species in a gaseous mixture, $e_{\omega_i}(T)$ is the Planck function evaluated at the i th band center, and $S_i(T)$ is the integrated band intensity of the i th band.

Several other models for the mean absorption coefficient are available in the literature [1, 37]. Since these models account for detailed spectral information of molecular bands, this approach of radiative formulation is referred to as the "pseudo-gray formulation." The gray gas formulation for radiative transport is very useful in parametric studies.

There are several nongray models available in the literature to represent the absorption-emission characteristics of vibration-rotation bands. These are classified generally in four classes, (1) line-by-line (LBL) models, (2) narrow band models, (3) wide band models, and (4) band model correlations. A complete discussion on usefulness and application of these models is provided in [12, 13]. For many engineering applications, wide band model correlations provide quite accurate results. The most commonly used wide band model correlations are due to Edwards [11, 16] and Tien and Lowder [9]. The Tien and Lowder correlation for the total band absorptance is a continuous correlation and is given by the relation

$$\bar{A}(u, \beta) = A(u, \beta) / A_o = \ln \{ u f(t) [(u + 2) / (u + 2f(t))] + 1 \} \quad (18)$$

where

$$f(t) = 2.94[1 - \exp(-2.60t)], t = \beta/2$$

and $u = SX/A_o$ is the nondimensional path length, $\beta = 2\pi\gamma/d$ is the line structure parameter, γ is the line half width, S is the integrated band intensity, and A_o is the band width parameter. Equation (18) provides accurate results for pressures higher than 0.5 atmosphere [12, 13].

Spectral properties and correlation quantities for various radiation participating species are available in [5, 9, 11]. These are useful in gray as well as nongray radiative formulations.

B. Radiative Flux Equations

For many engineering and astrophysical applications, the radiative transfer equations are formulated assuming one-dimensional planar systems. For diffuse nonreflecting boundaries and in absence of scattering, the expression for the spectral radiative flux is given by [1, 38]

$$q_{R\omega}(y) = e_{1\omega} - e_{2\omega} + \frac{3}{2} \int_0^y F_{1\omega}(z) \kappa_\omega \exp\left[-\frac{3}{2} \kappa_\omega(z-y)\right] dz - \frac{3}{2} \int_y^L F_{2\omega}(z) \kappa_\omega \exp\left[-\frac{3}{2} \kappa_\omega(z-y)\right] dz \quad (19)$$

where

$$F_\omega(z) = e_\omega(z) - e_{1\omega}; F_{2\omega}(z) = e_\omega(z) - e_{2\omega}$$

It should be pointed out that the exponential kernel approximation has been used in obtaining Eq. (19). The total radiative flux in a given direction is expressed as

$$q_R = \int_0^\infty q_{R\omega} d\omega \quad (20)$$

A combination of Eqs. (19) and (20) provides a proper form of total radiative flux equation for obtaining nongray solutions of molecular species. Any convenient absorption model can be used to obtain nongray results.

For a gray medium, Eq. (20) reduces to a simpler form and upon differentiating the resulting equation twice, the integrals are eliminated and there is obtained a nonhomogeneous ordinary differential equation as [1, 39]

$$\frac{1}{\kappa^2} \frac{d^2 q_R(y)}{dy^2} - \frac{9}{4} q_R(y) = \frac{3}{\kappa} \frac{de(y)}{dy} \quad (21)$$

where $\kappa = \kappa_p$. Equation (21) is a second order differential equation and, therefore, requires two boundary conditions. For nonblack diffuse surfaces, these are given as

$$\left(\frac{1}{\varepsilon_1} - \frac{1}{2}\right) [q_R(y)]_{y=0} - \frac{1}{3\kappa} \left[\frac{dq_R}{dy}\right]_{y=0} = 0 \quad (22a)$$

$$\left(\frac{1}{\varepsilon_2} - \frac{1}{2}\right) [q_R(y)]_{y=L} - \frac{1}{3\kappa} \left[\frac{dq_R}{dy}\right]_{y=L} = 0 \quad (22b)$$

Equation (21) along with boundary conditions can be used to obtain the energy equation for gray gas radiative interaction. In this formulation, there is no need to linearize the radiative interaction. For linearized radiation, however, $T^4 - T_1^4 = 4T_1^3(T - T_1)$ and Eq. (21) can be written as

$$d^2 q_R/d\xi^2 - \frac{9}{4} \tau_o^2 q_R = \gamma_1 q_\omega d\theta/d\xi \quad (23)$$

where

$$\gamma_1 = 3\tau_o^2/\bar{N}; \bar{N} = k \kappa_p/(4\sigma T_1^3); \tau_o = \kappa_p L$$

For black walls and $T_1 = T_2$, the boundary conditions for Eq. (21) become

$$q_{R(1/2)} = 0; \frac{3}{2}q_{R(0)} = \frac{1}{\tau_o}(dq_{R}/d\xi)_{\xi=0} \quad (24)$$

Equation (23) is useful in obtaining closed form solutions of simplified problems such as fully-developed flows. The parameters for this equation are \bar{N} and τ_o ; \bar{N} characterizes the relative importance of radiation versus conduction for a gray gas.

For a black circular tube, the spectral radiative heat flux is given by the expression [23]

$$q_{R\omega}(r) = \frac{4}{\pi} \int_0^{\pi/2} \left\{ \int_{r \sin \gamma}^r F_{\omega}(r') \kappa_{\omega} a \exp \left[-\frac{b\kappa_{\omega}}{\cos \gamma} (r - r') \right] dr' \right. \\ \left. - \int_r^{r_o} F_{\omega}(r') \kappa_{\omega} a \exp \left[-\frac{b\kappa_{\omega}}{\cos \gamma} (r' - r) \right] dr' \right. \\ \left. + \int_{r \sin \gamma}^{r_o} F_{\omega}(r') \kappa_{\omega} a \exp \left[-\frac{b\kappa_{\omega}}{\cos \gamma} (r + r' - 2r \sin \gamma) dr' \right] \right\} d\gamma \quad (25)$$

where $F_{\omega}(r') = e_{\omega}(r') - e_{\omega}(T_w)$, and constants a and b have values of unity and $5/4$, respectively. A combination of Eqs. (20) and (25) provides a convenient form of the total radiative flux for nongray analyses.

For a gray medium, the expression for the total radiative flux can be obtained from differential approximation as [1, 23]

$$\frac{d}{dr} \left[\frac{1}{r} \frac{d}{dr} (r q_{R}) \right] - \frac{9}{4} \kappa^2 q_{R} = 3\sigma \kappa \frac{dT^4}{dr} \quad (26)$$

For linearized radiation, $dT^4/dr = 4 T_w^3 (dT/dr)$ and Eq. (26) is expressed as

$$\frac{d}{d\xi} \left[\frac{1}{\xi} \frac{d}{d\xi} (\xi q_{R}) \right] - \frac{9}{4} \bar{\tau}_o^2 q_{R} = \gamma_2 q_w \frac{d\theta}{d\xi} \quad (27)$$

where

$$\gamma_2 = 3 \bar{\tau}_o^2 / \bar{N}; \bar{N} = k \kappa_p / (4\sigma T_w^3); \bar{\tau}_o = \kappa_p r_o; \xi = r/r_o$$

The difference in definition for τ_o for parallel plate case and $\bar{\tau}_o$ for the circular tube case should be noted. For a black tube, the boundary conditions for Eqs. (26) and (27) are found to be

$$\frac{3}{2}q_{R(1)} = -\frac{1}{\bar{\tau}_o} \left[\frac{1}{\xi} \frac{d}{d\xi} (\xi q_{R}) \right]_{\xi=1}; q_{R(0)} = 0 \quad (28)$$

Equation (26) is used for general one-dimensional gray gas formulation and Eq. (27) for the case of linearized radiation.

IV. Transformed Equations and Limiting Forms

Depending upon the physical problem considered, a convenient form of the total radiative flux should be used in the governing energy equations. For nongray formulations, in order to be able to use the band model correlations, the equations for radiative flux must be expressed in terms of the correlation quantities. These equations are provided in this section.

For a nongray gas consisting of n-molecular bands, a combination of Eqs. (5), (19) and (20) provides the governing equation for black parallel plate geometry as [17, 35, 40]

$$\begin{aligned}
 & d\theta/d\xi - 2(3\xi^2 - 3\xi^3) + 1 \\
 &= \frac{3L}{2k} \sum_{i=1}^n H_i u_{oi} \left\{ \int_0^\xi \theta(\xi') \bar{A}'_i \left[\frac{3}{2} u_{oi} (\xi - \xi') \right] d\xi' \right. \\
 & \quad \left. - \int_\xi^1 \theta(\xi') \bar{A}'_i \left[\frac{3}{2} u_{oi} (\xi' - \xi) \right] d\xi' \right\}
 \end{aligned} \tag{29}$$

where

$$\begin{aligned}
 \xi &= u/u_o = y/L; \xi' = u'/u_o = z/L; \bar{A} = A/A_o; \\
 u &= (S/A_o)Py; u_o = (S/A_o)PL; PS = \int_{\Delta\omega} \kappa_\omega d\omega; \\
 H_i &= A_{oi}(T)(de_{\omega_i}/dT)_{T_w}
 \end{aligned}$$

and $\bar{A}'(u)$ denotes the derivative of $\bar{A}(u)$ with respect to u . Equation (29) is the most convenient equation to use when employing the band model correlations in nongray radiative transfer analyses. The limiting forms and their solutions, in the optically thin and large path length limits, are provided in [35, 40].

A combination of Eqs. (9), (20) and (25) provides the nongray form of the energy equation for the circular tube geometry as [23]

$$\begin{aligned}
 & \frac{d\theta}{d\xi} + \xi^3 - 2\xi \\
 &= \frac{4r_o}{\pi k} \sum_{i=1}^n H_i u_{oi} \int_0^{\pi/2} \left\{ \int_{\xi \sin \gamma}^\xi \theta(\xi') \bar{A}'_i \left[\frac{b u_{oi}}{\cos \gamma} (\xi - \xi') \right] d\xi' \right. \\
 & \quad - \int_\xi^1 \theta(\xi') \bar{A}'_i \left[\frac{b u_{oi}}{\cos \gamma} (\xi' - \xi) \right] d\xi' \\
 & \quad \left. + \int_{\xi \sin \gamma}^1 \theta(\xi') \bar{A}'_i \left[\frac{b u_{oi}}{\cos \gamma} (\xi + \xi' - 2\xi \sin \gamma) \right] d\xi' \right\} d\gamma
 \end{aligned} \tag{30}$$

where

$$\xi = u/u_o = r/r_o; u = (S/A_o)Pr, u_o = (S/A_o)Pr_o$$

The limiting forms of Eq. (30) are available in [23]. The large path length limit (large u_{oi} limit) constitutes a very useful limit for analyzing the radiative transfer capability of gases like CO₂ at room temperature and at one atmospheric pressure. For gases such as CO and C₄, the results

obtained in this limit constitute an upper bound in radiative transfer capability. In the large path length limit, Eq. (30) reduces to

$$\begin{aligned} & \frac{d\theta}{d\xi} + \xi^3 - 2\xi \\ &= \frac{4r_o}{\pi bk} \sum_{i=1}^n H_i \int_0^{\pi/2} \left\{ \cos \gamma \int_{\xi \sin \gamma}^1 \theta(\xi') \left[\frac{d\xi'}{\xi - \xi'} + \frac{d\xi'}{\xi + \xi' - 2\xi \sin \gamma} \right] \right\} d\gamma \end{aligned} \quad (31)$$

Equations (30) and (31) are useful in determining the extent of radiative interaction of participating species in a circular tube.

For linearized gray gas radiation, a combination of Eqs. (5) and (23) provides the equation for the radiative flux for the parallel plate geometry as

$$d^2 q_R / d\xi^2 - \left(\gamma_1 + \frac{9}{4} \tau_o^2 \right) q_R = \gamma_1 q_w (6\xi^2 - 4\xi^3 - 1) \quad (32)$$

The solution of Eq. (32) is obtained first, then the solution for θ is obtained from Eq. (5), and finally the relation for the bulk temperature is obtained from Eq. (10) as [17]

$$\begin{aligned} \theta_b = C_1 & \left[24 - 12M_1 + M_1^3 + (M_1^3 - 12M_1 - 24)e^{-M_1} \right] \\ & - \frac{12}{5} \frac{\gamma_1}{M_1^4} + \frac{17}{70} \frac{\gamma_1}{M_1^2} - \frac{17}{70} \end{aligned} \quad (33)$$

where

$$\begin{aligned} C_1 &= \frac{\gamma_1}{M_1^8} \left[\frac{48 - 3\tau_o M_1^2 + 36\tau_o}{3\tau_o(1 - e^{-M_1}) + 2M_1(1 + e^{-M_1})} \right] \\ M_1^2 &= 3\tau_o^2 \left(\frac{3}{4} + \frac{1}{N} \right) \end{aligned}$$

Limiting forms (optically thin and optically thick) of Eqs. (33) are available in [17].

From a combination of Eqs. (9) and (27) the relation for linearized gray gas radiative flux for the circular tube is obtained as

$$\xi^2 \frac{d^2 q_R}{d\xi^2} + \xi \frac{dq_R}{d\xi} - (1 + M_2^2 \xi^2) q_R = \gamma_2 q_w (2\xi^3 - \xi^5) \quad (34)$$

where

$$M_2^2 = \frac{9}{4} \bar{\tau}_o^2 + \gamma_2$$

Equation (34) is solved first for q_R , then the solution for θ is obtained from Eq. (9), and finally the bulk temperature result is obtained from Eq. (11) as [23]

$$\begin{aligned} \theta_b = C_2 & \left[M_2(8 - M_2^2) I_0(M_2) - 16 I_1(M_2) \right] \\ & + \frac{11}{24} \frac{\gamma_2}{M_2^2} - \frac{8}{3} \frac{\gamma_2}{M_2^4} - \frac{11}{24} \end{aligned} \quad (35)$$

where

$$C_2 = \frac{\gamma_2}{M_2^8} \left[\frac{3\bar{\tau}_o M_2^2 - 24\bar{\tau}_o - 32}{2M_2 I_o(M_2) + 3\bar{\tau}_o I_1(M_2)} \right]$$

Limiting forms of Eq. (35) are available in the cited reference.

No attempt is made to simplify the radiative flux equation for use in Eq. (12). In this study, however, the nonlinear form of Eq. (21) is used to obtain solutions for laminar compressible flow between two parallel black plates.

V. Method of Solution

The solution procedure for the fully-developed incompressible flow is completely different than the solution procedure for the laminar compressible flow. These procedures are discussed here briefly.

A. Fully Developed Incompressible Flow

For both the parallel plate and circular tube geometries, the general nongray solutions are obtained numerically by employing the method of variation of parameters. For both geometries, it was essential to assume quartic formulations for $\theta(\xi)$ to obtain converged solution. In principle, the same numerical procedure applies to both the general and large path length limit cases. The entire solution procedure for the parallel plate geometry is provided in [38, 40] and for the circular tube in [41].

B. Laminar Compressible Flow

The governing equations, Eqs. (12) and (13), are transformed from the physical plane (x, y, t) to computational domain (ξ, η, t) to facilitate the treatment of general geometry. Equation (12) is expressed in the computational domain as

$$\frac{\partial \hat{U}}{\partial t} + \frac{\partial \hat{F}}{\partial \xi} + \frac{\partial \hat{G}}{\partial \eta} = 0 \quad (36)$$

where

$$\begin{aligned} \hat{U} &= UJ; & \hat{G} &= Gx_\xi - Fy_\xi; \\ \hat{F} &= Fy_\eta - Gx_\eta; & J &= x_\xi y_\eta - y_\xi x_\eta \end{aligned}$$

Equation (36) is solved by a time-asymptotic two step, explicit MacCormack method [42]. This method is second order accurate in space. If a solution to Eq. (36) is known at some time $t = n\Delta t$, then the solution at next time step $t = (n+1)\Delta t$ can be calculated from

$$\hat{U}_{i,j}^{n+1} = L(\Delta t)\hat{U}_{i,j}^n$$

for each grid point (i, j). The operator L consists of predictor and corrector steps. For this study, the code developed by Kumar [43] was modified to include the radiation model. The details of the solution procedure are available in [44].

The radiative flux equations, Eq. (21), is discretized using the central differencing scheme as [39, 44]

$$\begin{aligned} \frac{2}{\Delta y_j^2(1 + \beta_j)} q_{j-1} - \left[\frac{2}{\Delta y_j(1 + \beta_j)} \left(\frac{1}{\beta_j \Delta y_j} + \frac{1}{\Delta y_j} \right) + \frac{9}{4} \kappa_j^2 \right] q_j \\ + \frac{2}{\Delta y_j^2(1 + \beta_j) \beta_j} q_{j+1} = 1.5 \kappa_j \left[\frac{e_{j+1} - e_j}{\beta_j \Delta y_j} + \frac{e_j - e_{j-1}}{\Delta y_j} \right] \end{aligned} \quad (37)$$

where

$$\Delta y_j = y_j - y_{j-1}; \quad \beta_j = \frac{y_{j+1} - y_j}{y_j - y_{j-1}}$$

Equation (37) along with Eq. (22) forms a tridiagonal system of equation which can be solved efficiently by the Thomas algorithm.

In the nongray gas formulation, the divergence of the radiative flux is evaluated using a central differencing scheme and is treated as radiative source term in the energy equation. Since the nongray formulation involves an integro-differential equation, the radiative flux term is uncoupled and treated separately [39].

VI. Results and Discussion

Extensive results have been obtained from fully developed incompressible laminar flows between two parallel plates and within a circular tube for participating species OH, CO, CH₄, CO₂ and H₂O. For the case of compressible flow between two parallel plates, however, results have been obtained only for pure H₂O as participating species and different mixtures of H₂O and air. Selected results for both cases are presented and discussed in this section.

A. Fully-Developed Laminar Flows

A complete discussion (and physical interpretations) of the various parameters entering into the present problem is given in [1, 10, 17, 23]. Numerical solutions were obtained in terms of nondimensional temperature and bulk temperature. Specific results were obtained for OH (2.8 μ fundamental), 4.7 μ fundamental + 1st overtone bands), CO₂ (15 μ , 4.3 μ and 2.7 μ bands), H₂O (rotational, 6.3 μ , 2.7 μ , 1.87 μ and 1.38 μ bands), and CH₄ (7.6 μ and 3.3 μ bands) for which spectral information were obtained from [5, 9, 11, 16].

For CO, CO₂, H₂O, and CH₄, the results obtained by employing the Tien and Lowder's correlation for band absorptance are illustrated in Figs. 2–6 for the parallel plate geometry. The limiting value of $\theta_b = -0.243$ corresponds to negligible radiation, and the effect of radiation increases with increasing plate spacing. As would be expected, radiative transfer is more pronounced for higher pressures and wall temperatures. Also shown in Figs. 2–5 are the limiting solutions for large u_0 (LLU). It is seen that, for a given wall temperature, the large u_0 limit can be obtained either by going to large values of L or to high pressures. These results also indicate that, for a particular wall temperature, the large u_0 limit for CO₂ is achieved at a relatively lower pressure than for other gases. As a matter of fact, for most practical purposes involving CO₂ at room temperature, the results for the four gases is shown in Fig. 6 for a pressure of one

atmosphere and a wall temperature of 1,000 °K. As discussed in [1, 10, 17], the relative order of the four curves, for small values L is characteristic of the interaction parameter for optically thin radiation, and for large L is characteristic of the interaction parameter for the large u_0 limit.

For the circular tube geometry, preliminary results have been obtained for different gases under varying conditions and selected results are presented in Figs. 7–12. The results for temperature variations within the tube are presented in Figs. 7 and 8 for different conditions. Since the temperature profiles are symmetric, the results are illustrated only for $\xi = 0$ to $\xi = 0.5$. The general band absorptance and large u_0 solutions for OH are illustrated in Fig. 7 for $T_w = 500\text{K}$ and 1000K . It seems that the LLU limit is achieved for OH at $T_w = 500\text{K}$ and $P = 1$ atm. General results for different species are compared in Fig. 8 for $T_2 = 300\text{K}$, $P = 1$ atm, and $r_0 = 5$ cm. These results demonstrate the relative importance of radiative interactions in a circular tube. This is analogous to the case of parallel plate results presented in [40].

The bulk temperature results for the circular tube geometry are presented in Figs. 9–12 for different gases. The results are expressed in normalized form as $\theta_b/\theta_b(\text{NR})$, where θ_b (NR) represents the case with no radiative interaction. The results, in general, exhibit the same trend as presented in Figs. 2–6 for the parallel plate geometry. However, the extent of radiative interactions is entirely different. This is because the circular geometry provides additional degrees of freedom for radiative interactions [23]. This is the first effort where general nongray band absorptance results have been obtained for the circular tube geometry.

B. Laminar Compressible Flow

A computer code was developed to solve the two-dimensional Navier-Stokes equations for radiating subsonic laminar flows between two parallel black plates. The dimensions of the duct were taken as 3cm x 15cm. The radiative interaction was considered only in the normal direction. Extensive results have been obtained for pure H_2O as participating species and different mixtures of H_2O and air flowing laminarily between the plates. These are available in [39, 44] and selected results are presented in this section.

The results for subsonic flows were obtained for two specific Mach numbers, $M_\infty = 0.3$ and $M_\infty = 0.8$. Most results presented here are for $M_\infty = 0.3$; however, certain results for $M_\infty = 0.8$ are also presented for comparative purposes. For $M_\infty = 0.3$, the free stream (inflow) conditions considered are, $P_t = 1.064 P_\infty$, $T_t = 1.018 T_\infty$, $P_\infty = 1$ atm, $T_\infty = 500$ K, $f_{\text{H}_2\text{O}} = 0.5$, and $f_{\text{air}} = 0.5$. The freestream conditions corresponding to $M_\infty = 0.8$ are; $P_t = 1.524 P_\infty$, $T_t = 1.128 T_\infty$, $P_\infty = 1$ atm, $T_\infty = 500\text{K}$, $f_{\text{H}_2\text{O}} = 0.5$, and $f_{\text{air}} = 0.5$. For both flows, the wall temperature was maintained at $T_w = 1,500\text{K}$ and the pressure at the channel exit was taken to be one atmosphere.

The variation in axial velocity across the channel is shown in Fig. 13a for different x locations. It is clearly evident that the fluid velocity in the inviscid core increases along the axial length due to increase in the boundary layer. A fully-developed flow has not been achieved at the channel exit. Figure 13b shows the variation of normal component of velocity across the channel at various axial locations. The two-dimensional effects are clearly evident from the results $x = 0.015$ m which is predominantly in the entrance region. The magnitude of v velocity

decreases as x increases; it is positive in the lower half and negative in the upper half of the channel due to the symmetry of the problem. For a fully-developed flow, the v component of velocity should be zero.

The variation in temperature across the channel is shown in Fig. 14 for different x locations. The temperature decreases from the walls to the center of the channel indicating the development of the thermal boundary layer. The flow is not thermally developed at the exit of the channel.

The variations in conductive and radiative fluxes along the length of the plate are shown in Fig. 15 for different y locations. The fluxes are zero along the centerline of the plate because of physical symmetry. The conductive flux increases slowly with increasing x and becomes essentially constant at the channel exit. The radiative interaction is strong in the first ten percent of the length and then it slowly decreases and reaches about the same value as conductive flux at the exit.

The variations in q_{Cy} , q_{Ry} and q_{Ty} with y are shown in Figs. 16, 17 and 18, respectively. It is noted that the variation in conductive flux across mainly with the first 20% distance from the wall (Fig. 16). The situation, however, is not the same with respect to the radiative transfer (Fig. 17). The radiative interaction occurs in the entire width of the channel. The results presented in Fig. 18 demonstrate that the rate of total energy transfer in the y direction is highest closer to the entrance ($x = 0.015$ m) than any other x locations. This is a result of high enthalpy flow and strong radiative interaction in this region.

Figure 19 shows the variation of radiative and conductive flux across the channel. The radiative flux peaks at some distance away from the wall while conductive flux peaks at the wall. This is because at the lower wall the effect of positive heat flux is partially cancelled by the negative flux from the layers of hot gases next to the wall. At a small distance away from the wall, however, the positive flux from both the wall and gas combine to give a maximum heat flux. Farther into the gas, the flux from the wall and hot gas is attenuated by the cooler gas and is partially cancelled. At the center of the channel, the fluxes from both modes cancel each other. This effect prevails throughout the length of the channel as is clearly evident from the results of Figs. 19a and 19b and in Ref. 44.

The variation of the radiative, conductive and normal component of the total flux across the channel is shown in Fig. 20 for $x = 0.06$ m and 0.15m. The total flux includes the convective (flow), radiative and conductive fluxes. It is increasing to note that except very near the boundary, the total flux is about an order of magnitude higher than the radiative flux and much higher than the conductive flux. In other words, according to the definition used in this study, the convective (flow) energy is the predominate mode of energy transfer. This trend is result continues for all axial stations [44].

The results for $M_\infty = 0.8$, in general, show the same trend as the results for $M_\infty = 0.3$. Certain definite changes, however, are noted specific cases. For $M_\infty = 0.8$, the magnitude of velocity variations obviously are relatively higher but the velocity boundary layers are thinner [44]. The temperature variations shown in Fig. 21 for $M_\infty = 0.3$. This is because T_∞ and T_w are the same for both flows. The thermal boundary layer, however, is thicker for $M_\infty = 0.3$.

A comparison of $M_\infty = 0.8$ and 0.3 results for q_{Cy} , q_{Ry} and q_{Ty} is shown in Fig. 22 for $x = 0.12$ m. The results demonstrate that while conductive and total energy fluxes are influenced considerably by changes in the Mach number, the radiative energy transfer is insensitive to such changes. This is because radiation is influenced primarily by specified temperature and pressure conditions and these conditions are the same for both cases.

VII. Concluding Remarks

Analytical formulations and numerical procedures have been developed to investigate the radiative interaction of absorbing-emitting species in laminar fully-developed flows between parallel plates and within a circular tube. The general nongray results for the circular tube geometry have been obtained for the first time. The results demonstrate the relative ability of various participating species for radiative interactions.

Two-dimensional compressible Navier-Stokes equations have been used to investigate the influence of radiative energy transfer on the entrance region flow under subsonic flow conditions. Computational procedures have been developed to incorporate gray as well as nongray formulations for radiative flux in the general governing equations. Specific results have been obtained for different amount of water-vapor in water vapor-air mixtures. Results demonstrate that the radiative interaction increases with an increase in pressure, temperature and the amount of water vapor. This can have a significant influence on the overall energy transfer in the system. Most energy, however, is transferred by convection in the flow direction. As a result, the radiative interaction does not alter the flow field significantly. Further parametric studies are needed to make definite recommendations.

VIII. Acknowledgements

This work was supported by the NASA Langley Research Center through Grants NAG-1-363 and NAG-1-423. For fully-developed flows between parallel plates and within a circular tube, the gray gas solutions for linearized radiation were suggested originally by Professor R. D. Cess in Refs. 17 and 23.

IX. References

1. Sparrow, E. M. and Cess, R. D., Radiation Heat Transfer, Brooks/Cole, Belmont, Calif., 1966 and 1970. New Augmented Edition, Hemisphere Publishing Corp., Washington, D.C., 1978.
2. Hottel, H. C. and Sarofim, A. F., Radiative Transfer, McGraw-Hill Book Co., New York, 1967.
3. Siegel, R. and Howell, J. R., Thermal Radiation Heat Transfer, McGraw-Hill Book Co., New York, 1971; Second Edition, 1981.
4. Ozisik, M. N., Radiative Transfer and Interaction with Conduction and Convection, John Wiley & Sons, Inc., New York, 1973.

5. Edwards, D. K., Radiation Heat Transfer Notes, Hemisphere Publishing Corporation, Washington, D.C., 1981.
6. Cess, R. , "The Interaction of Thermal Radiation with Conduction and Convection Heat Transfer," Advances in Heat Transfer, Vol. 1, Academic Press, New York, 1964.
7. Sparrow, M., "Radiation Heat Transfer between Surfaces," Advances in Heat Transfer, Vol. 2, Academic Press, New York, 1965.
8. Viskanta, R., "Radiation Transfer and Interaction of Convection with Radiation Heat Transfer," Advances in Heat Transfer, Vol. 3, Academic Press, New York, 1966.
9. Tien, C. L., "Thermal Radiation Properties of Gases," Advances in Heat Transfer, Vol. 5, Academic Press, New York, 1968.
10. Cess, R. and Tiwari, S. N., "Infrared Radiative Energy Transfer in Gases," Advances in Heat Transfer, Vol. 8, Academic Press, New York, 1972.
11. Edwards, D. K., "Molecular Gas Band Radiation," Advances in Heat Transfer, Vol. 12, Academic Press, New York, 1976.
12. Tiwari, S. N., "Band Models and Correlations for Infrared Radiation," Radiative Transfer and Thermal Control (Progress in Astronautics and Aeronautics), Vol. 49, American Institute of Aeronautics and Astronautics, New York, 1976.
13. Tiwari, S. N., "Models for Infrared Atmospheric Radiation," Advances in Geophysics, Vol. 20, Academic Press, New York, 1978.
14. Viskanta, R., "Radiation Heat Transfer," Fortschrift der Verfahrenstechnik, Vol. 22A, 1984, pp. 51-81.
15. Viskanta, R. and Menguc, M. P., "Radiation Heat Transfer in Combustion Systems," Progress in Energy Combustion Sciences, Vol. 13, 1987, pp. 97-160.
16. Edwards, D. K., Glassen, L. K., Hauser, W. C. and Tuchscher, J. S., "Radiation Heat Transfer in Nonisothermal Nongray Gases," Journal of Heat Transfer, Vol. 89, Series C, No. 3, August 1967, pp. 219-229.
17. Cess, R. D. and Tiwari, S. N., "Heat Transfer to Laminar Flow of an Absorbing-Emitting Gas Between Parallel Plates," Heat and Mass Transfer-USSR, Vol. 1, May 1968, pp. 229-283.
18. Kuroksi, Y., "Heat Transfer by Simultaneous Radiation and Convection in an Absorbing and Emitting Medium in a Flow Between Parallel Plates," Fourth International Heat Transfer Conference, Vol. II, Paper R2.5, Paris-Versailles, 1970.
19. Larsen, P. A. and Lord, H. A., "Convective and Radiative Heat Transfer to Water Vapor in Uniformly Heated Tubes," Fourth International Heat Transfer Conference, Vol. III, Paper R2.6, Paris-Versailles, 1970.
20. Pearce, B. E. and Emery, A. F., "Heat Transfer by Thermal Radiation and Laminar Forced Convection to an Absorbing Fluid the Entry Region of a Pipe," Journal of Heat Transfer, Vol. 92, 1970, pp. 221-230.

21. Kurosaki, Y., "Radiation Heat Transfer in a Flow Between Flat Plates with Temperature Slip at the Walls," Fifth International Heat Transfer Conference, Vol. 1, Tokyo, 1971, pp. 98–107.
22. Echigo, R., Hasegawa, S., and Miyazaki, Y., "Composite Heat Transfer with Thermal Radiation in Nongray Medium-Part I: Interaction of Radiation with Conduction," International Journal of Heat and Mass Transfer, Vol. 14, No. 12, December 1971, pp. 2001–2015.
23. Tiwari, S. N. and Cess, R. D., "Heat Transfer to Laminar Flow of Nongray Gases Through a Circular Tube," Applied Scientific Research, Vol. 25, No. 314, December 1971, pp. 155–170.
24. Greif, R. and McEligot, D. M., "Thermally Developing Laminar Flows with Radiative Interaction Using the Total Band Absorptance Model," Applied Scientific Research, Vol. 25, December 1971, pp. 234–244.
25. Edwards, D. K. and Balakrishnan, A., "Thermal Radiation by Combustion Gases," International Journal of Heat and Mass Transfer, Vol. 16, No. 1, January 1973, pp. 25–40.
26. Edwards, D. K. and Wassel, A. J., "The Radial Radiative Heat Flux in a Cylinder," Journal of Heat Transfer, Vol. 95, Series C, No. 2, May 1973, pp. 276–277.
27. Donovan, T. E. and Greif, R., "Laminar Convection with an Absorbing and Emitting Gas," Applied Scientific Research, Vol. 31, No. 3, August 1975, pp. 110–122.
28. Martin, J. K. and Hwang, C. C., "Combined Radiant and Convective Heat Transfer in Laminar Steam Flow Between Gray Parallel Plates with Uniform Heat Flux," Journal of Quantitative Spectroscopy and Radiative Transfer, Vol. 15, December 1975, pp. 1071–1081.
29. Jeng, D. R., Lee, E. J., and DeWitt, K. J., "A Study of Two Limiting Gases in Convective and Radiative Heat Transfer with Nongray Gases," International Journal of Heat and Mass Transfer, Vol. 20, No. 7, July 1977, pp. 741–751.
30. Tiwari, S. N., "Applications of Infrared Band Model Correlations to Nongray Radiation," International Journal of Heat and Mass Transfer, Vol. 20, No. 7, July 1977, pp. 741–751.
31. Greif, R., "Laminar Convection with Radiation: Experimental and Theoretical Results," International Journal of Heat and Mass Transfer, Vol. 21, April 1978, pp. 477–480.
32. Balakrishnan, A. and Edwards, D. K., "Molecular Gas Radiation in the Thermal Entrance Region of a Duct," Journal of Heat Transfer, Vol. 101, 1979, pp. 489–495.
33. Kobiyama, M., Taniguchi, H. and Saita, T., "The Numerical Analyses of Heat Transfer Combined with Radiation and Convection," Bulletin of the Japanese Society of Mechanical Engineering, Vol. 22, No. 167, May 1979, pp. 707–714.
34. Im, K. H. and Ahluwalia, R. K., "Combined Convection and Radiation in Rectangular Ducts," International Journal of Heat and Mass Transfer, Vol. 27, No. 2, February 1984, pp. 221–231.
35. Tiwari, S. N. and Singh, D. J., "Interaction of Transient Radiation in Fully Developed Laminar Flows," AIAA Paper 87–1521, June 1987; also in Applied Scientific Research, December 1989.

36. Anderson, D. A., Tannehill, J. C. and Pletcher, R. H., Computational Fluid Mechanics and Heat Transfer, Hemisphere Publishing Corporation, 1984.
37. Patch, R. ., "Effective Absorption Coefficient for Radiant Energy Transport in Nongray Nonscattering Gases," Journal of Quantitative Spectroscopy and Radiative Transfer, Vol. 7, No. 4, July/August 1967, pp. 611-637.
38. Tiwari, S. N., "Radiative Interaction in Transient Energy Transfer in Gaseous System," Dept. of Mechanical Engineering and Mechanics, Old Dominion University, Norfolk, Virginia, Progress Report NAG-1-423, December 1985; also NASA-CR-176644 NAS 1.26:176644, December 1985.
39. Mani, M. and Tiwari, S. N., "Investigation of Chemically Reacting and Radiating Supersonic Internal Flows," NASA-CR-180540, December 1986; also, "Investigation of Supersonic Chemically Reacting and Radiating Channel Flow," NASA-CR-182726, January 1988 (also, Ph.D. Dissertation by M. Mani, Old Dominion University, Norfolk, Virginia, May 1988).
40. Tiwari, S. N. and Singh, D. J., "Transient Radiative Energy Transfer in Incompressible Laminar Flows," NASA-CR-182605, June 1987.
41. Tiwari, S. N. and Trivedi, P. A., "Infrared Radiative Interactions in Laminar Duct Flows," Dept. of Mechanical Engineering and Mechanics, Old Dominion University, Norfolk, Virginia, Progress Report NAG-1-363, December 1989.
42. MacCormack, R. W., "The Effect of Viscosity in Hypervelocity Impact Cratering," AIAA Paper 69-354, May 1969.
43. Kumar, A., "Numerical Analysis of the Scramjet Inlet Flow Field Using Two-Dimensional Navier-Stokes Equations," AIAA Paper 81-0185, January 1981.
44. Singh, D. J. and Tiwari, S. N., "Investigation of Radiative Interactions in Subsonic Entrance Region Flows," Dept. of Mechanical Engineering and Mechanics, Old Dominion University, Norfolk, Virginia, Progress Report NAG-1-423, November 1989.

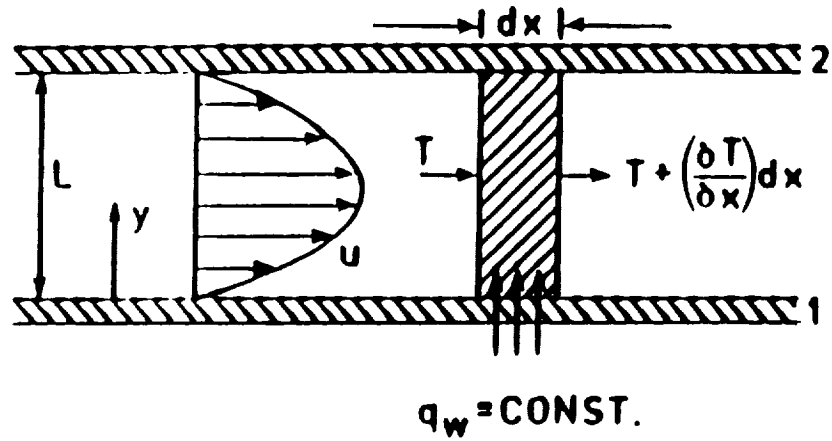


Fig. 1a Laminar flow between two parallel plates with constant wall heat flux.

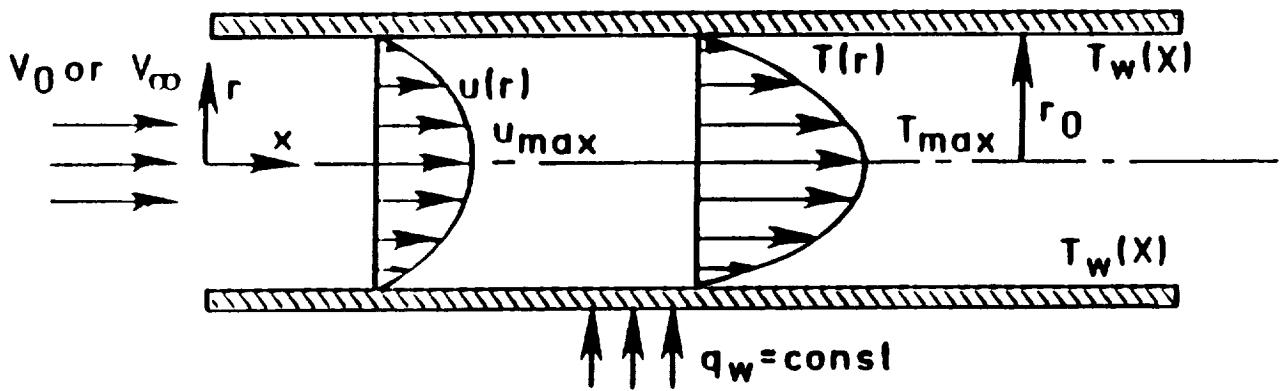


Fig. 1b Laminar flow in a circular tube with constant wall heat flux.

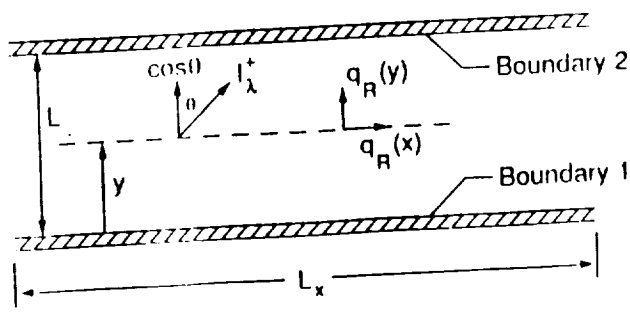


Fig. 1c Radiating gas between parallel boundaries.

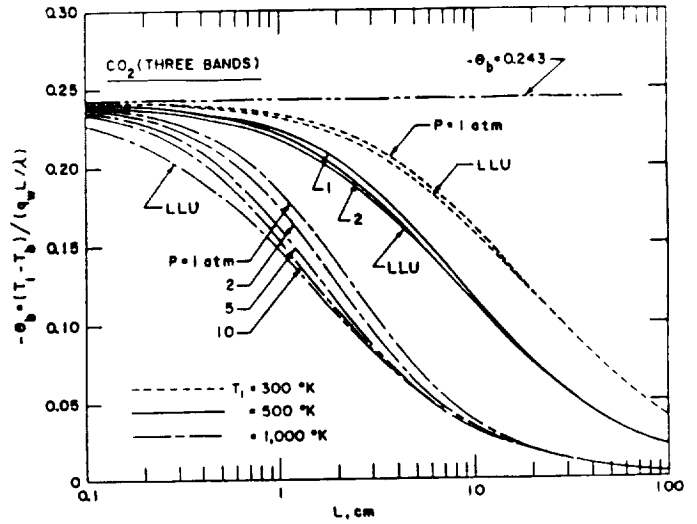


Fig. 1 Variation of bulk temperature with plate spacing for CO₂; T₁=300K, 500K and 1,000K.

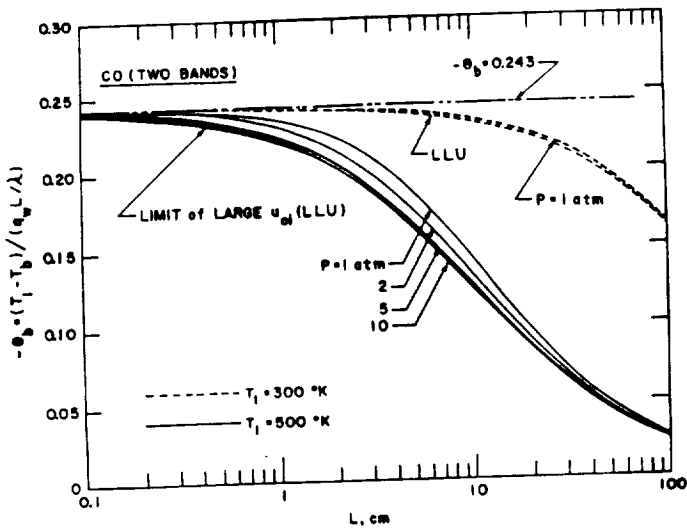


Fig. 2a Variation of bulk temperature with plate spacing for CO; T₁=300K and 500K.

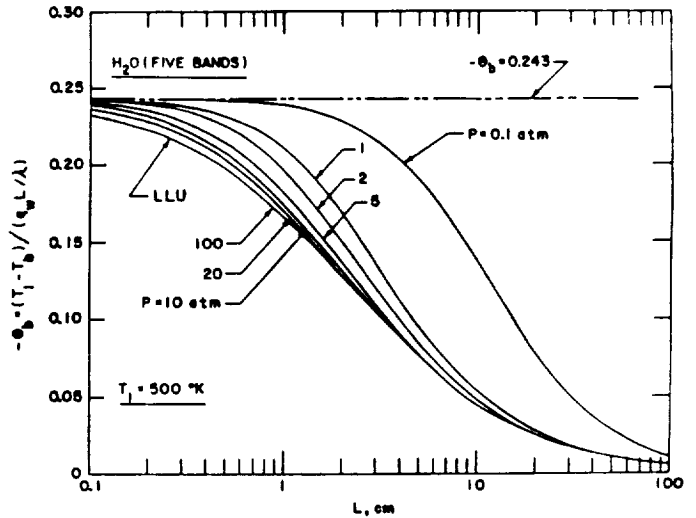


Fig. 4a Variation of bulk temperature with plate spacing for H₂O; T₁=500K.

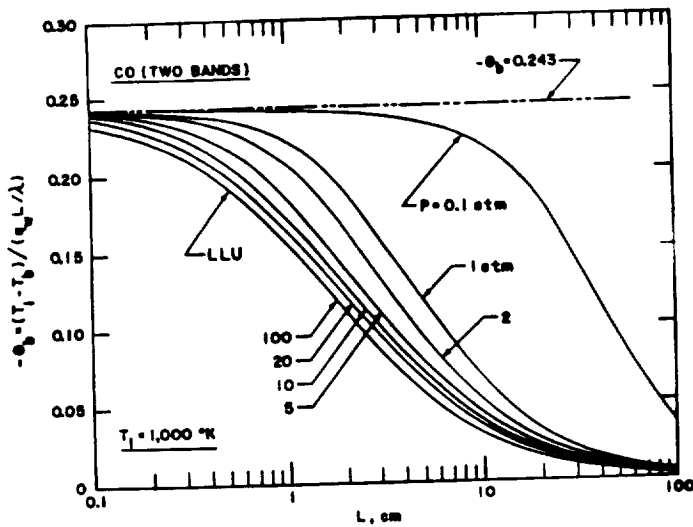


Fig. 2b Variation of bulk temperature with plate spacing for CO; T₁=1,000K.

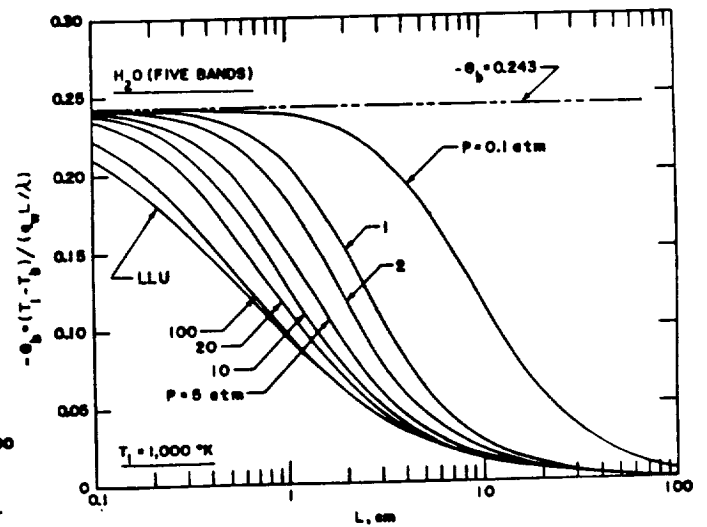


Fig. 4b Variation of bulk temperature with plate spacing for H₂O; T₁=1,000K.

~~SECRET~~ INTERNATIONAL CLONE

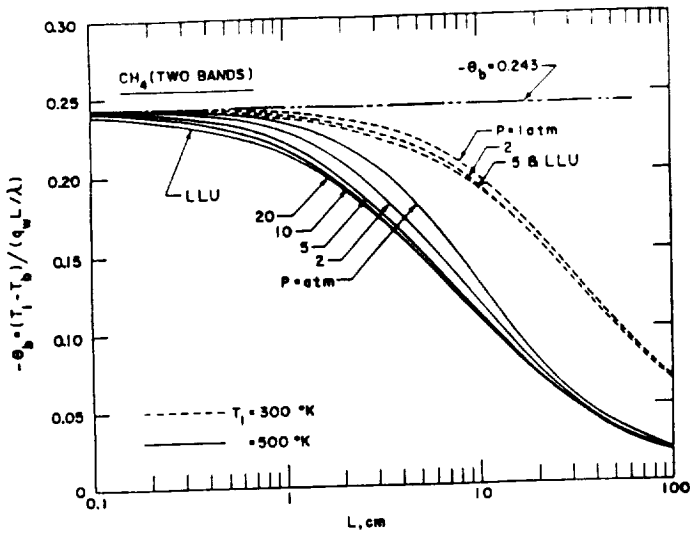


Fig. 5a Variation of bulk temperature with plate spacing for CH_4 ; $T_1=300\text{K}$ and 500K .

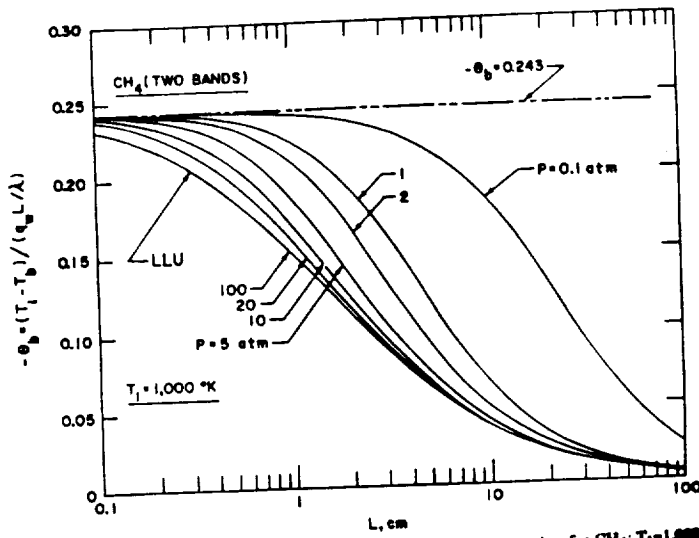


Fig. 5b Variation of bulk temperature with plate spacing for CH_4 ; $T_1=1,000\text{K}$.

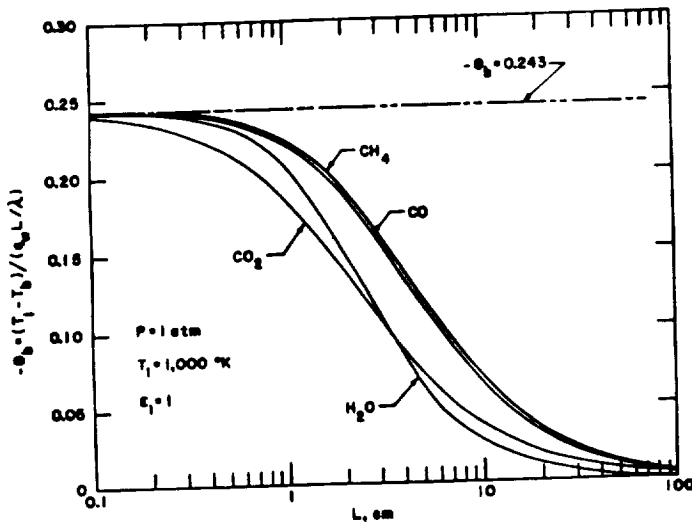


Fig. 6 Comparison of bulk temperature results for parallel plates; $T_1=1,000\text{K}$ and $P=1\text{atm}$.

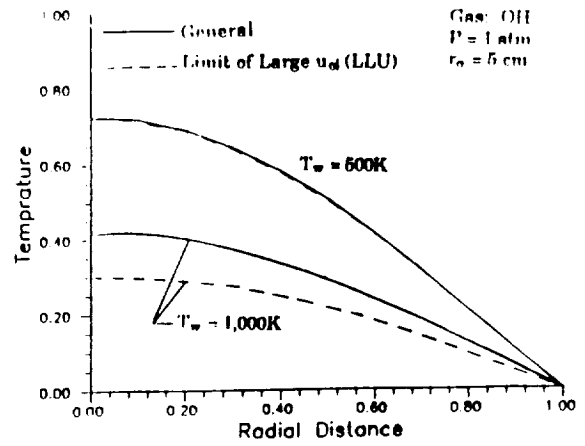


Fig. 7 Temperature variation in a tube; $P=1\text{atm}$ and $r_0=5\text{cm}$.

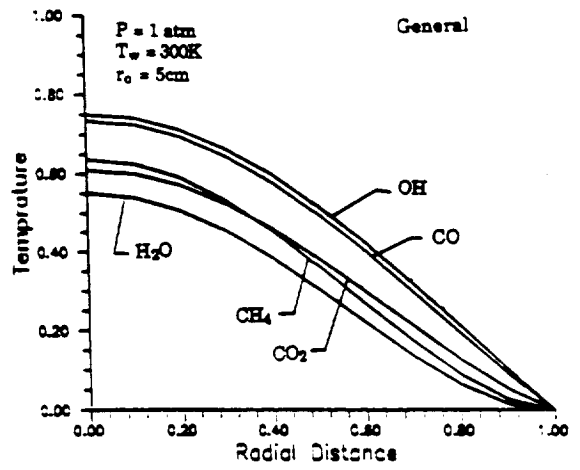


Fig. 8 Comparison of temperature variation in a tube; $P=1\text{atm}$, $T_w=300\text{K}$, and $r_0=5\text{cm}$.

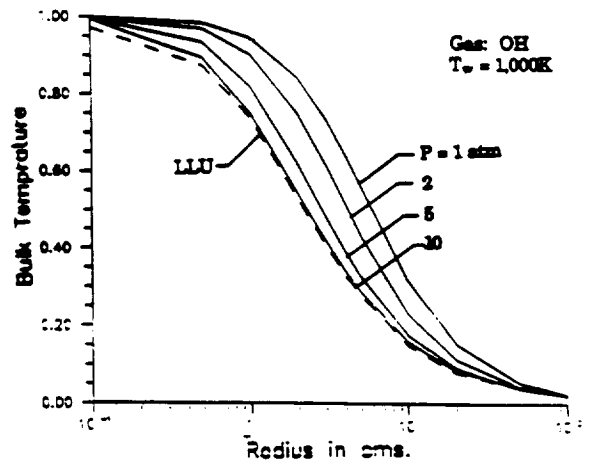


Fig. 9 Variation of bulk temperature with radius for OH ; $T_w=1,000\text{K}$.

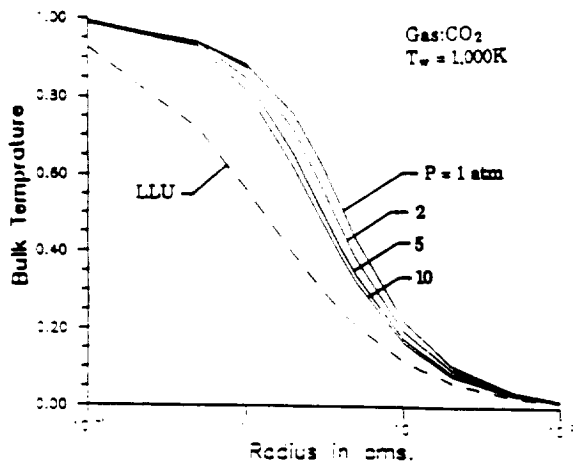


Fig. 10 Variation of bulk temperature with radius for CO_2 ; $T_w = 1,000\text{K}$.

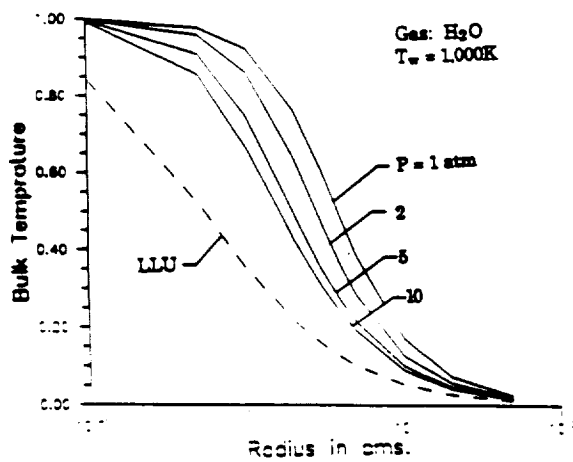


Fig. 11 Variation of bulk temperature with radius for H_2O ; $T_w = 1,000\text{K}$.

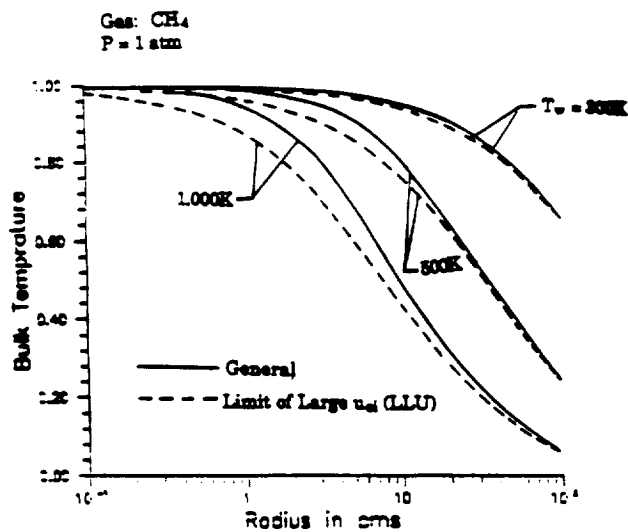


Fig. 12 Variation of bulk temperature with radius for CH_4 ; $P = 1 \text{ atm}$.

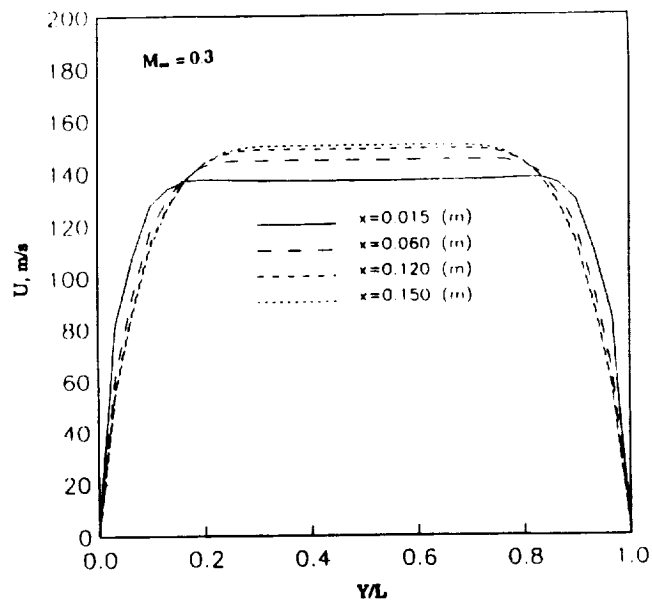


Fig. 13a Variation of axial velocity across the channel at various x stations, $M_\infty = 0.3$.

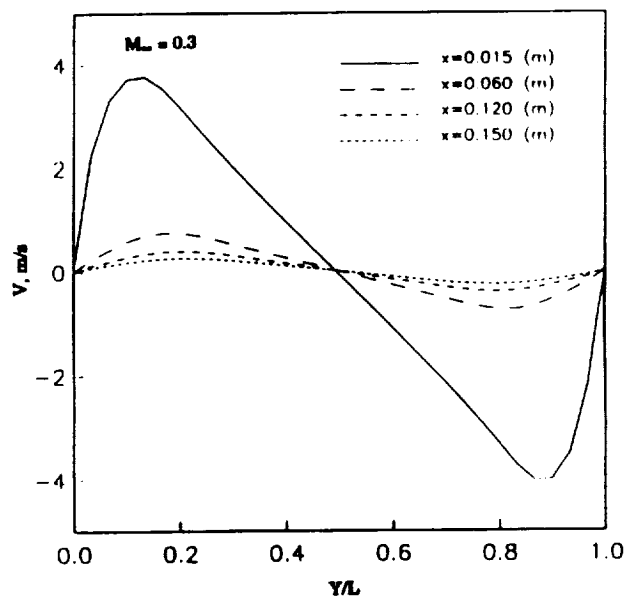


Fig. 13b Variation of normal velocity across the channel at various x stations, $M_\infty = 0.3$.

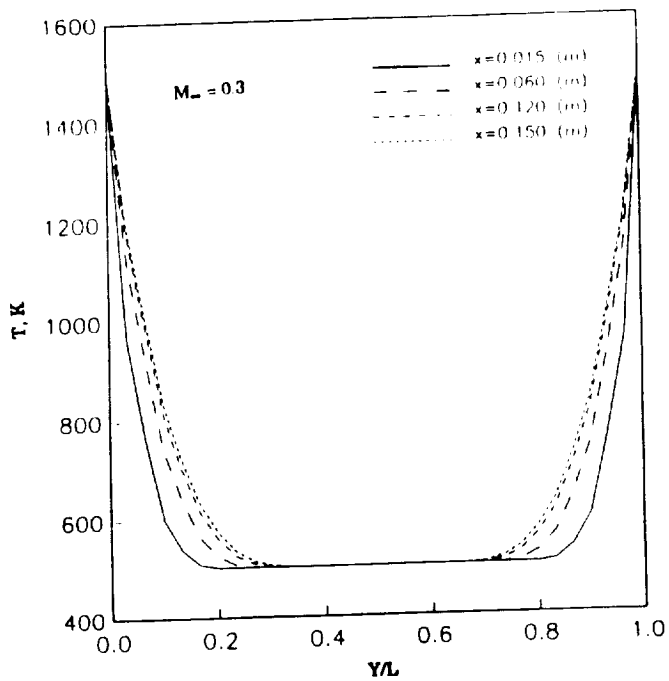


Fig. 14 Temperature variation across the channel at various x stations, $M_\infty = 0.3$.

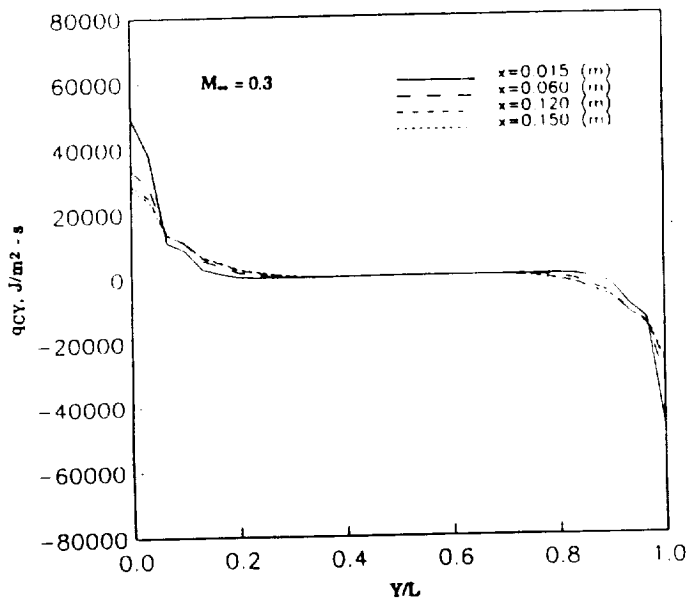


Fig. 16 Variation of q_{cy} with y for different x locations, $M_\infty = 0.3$.

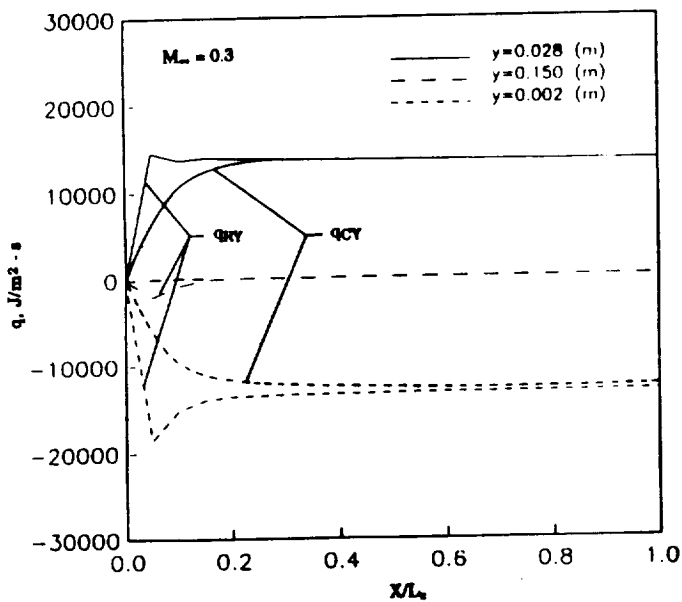


Fig. 15 Variation of q_w and q_{by} with x for different y locations, $M_\infty = 0.3$.

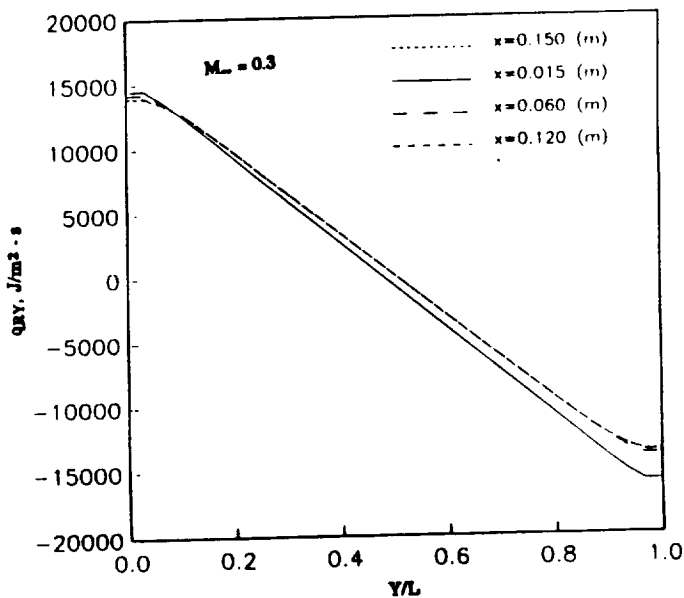


Fig. 17 Variation of q_{by} with y for different x locations, $M_\infty = 0.3$.

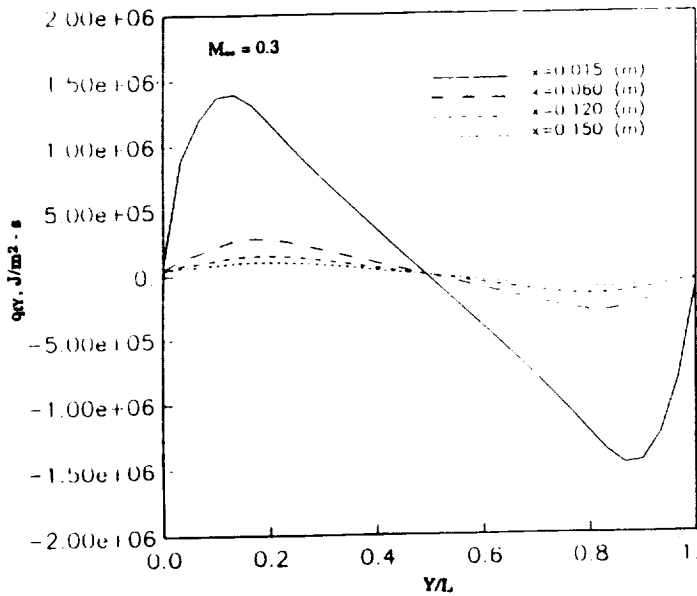


Fig. 18 Variation of q_{xy} with y for different x -locations, $M_{\infty} = 0.3$.

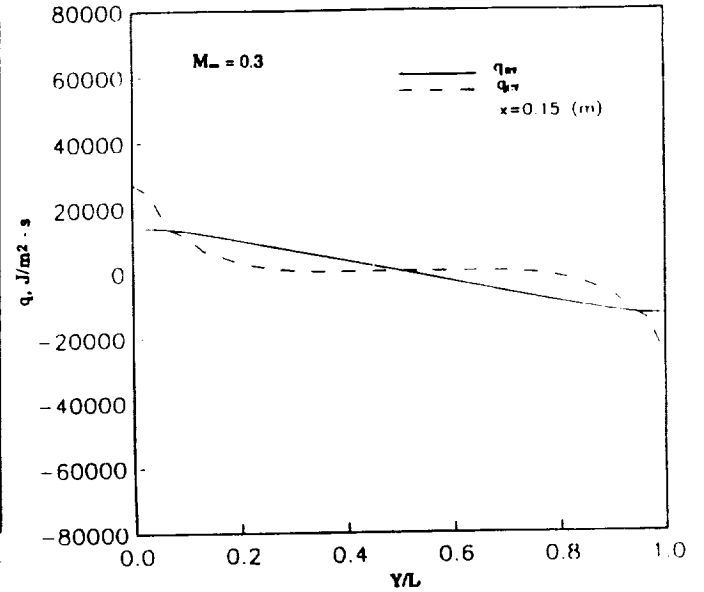


Fig. 19b Variation of q_{xy} and q_{yy} with y for $x = 0.15$ (m), $M_{\infty} = 0.3$.

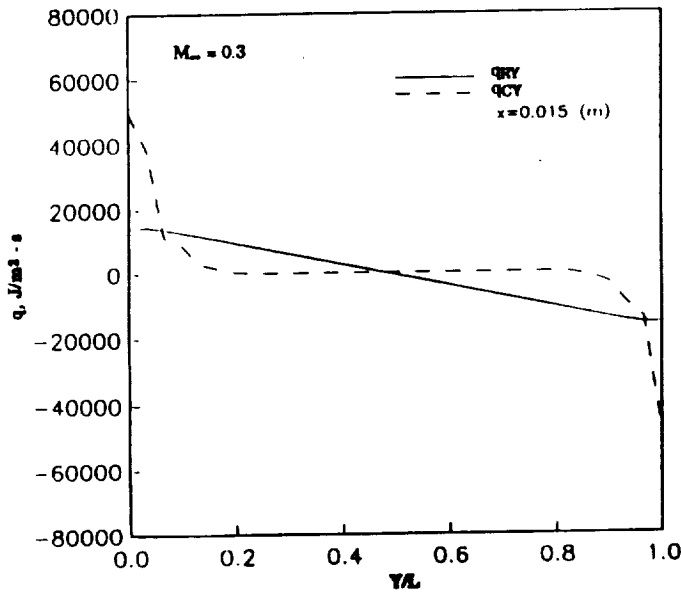


Fig. 19a Variation of q_{xy} and q_{yy} with y for $x = 0.015$ (m), $M_{\infty} = 0.3$.

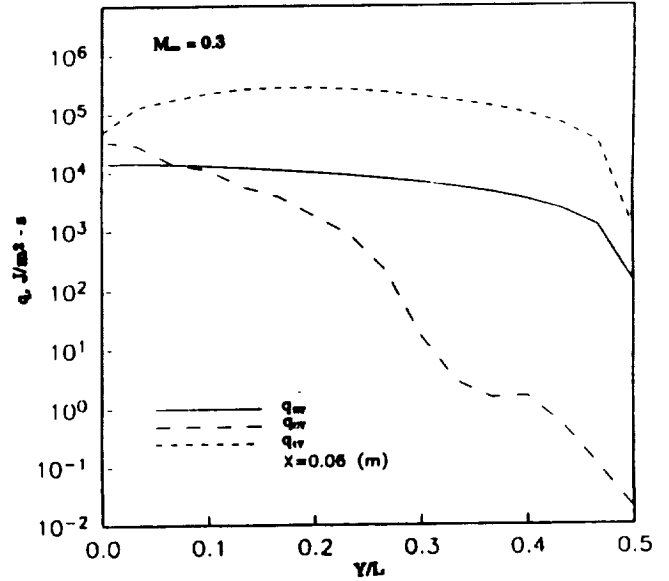


Fig. 20a Variation of q_{xy} , q_{yy} and q_{zz} with y for $x = 0.05$ (m), $M_{\infty} = 0.3$.

ORIGINAL PAGE IS
OF POOR QUALITY

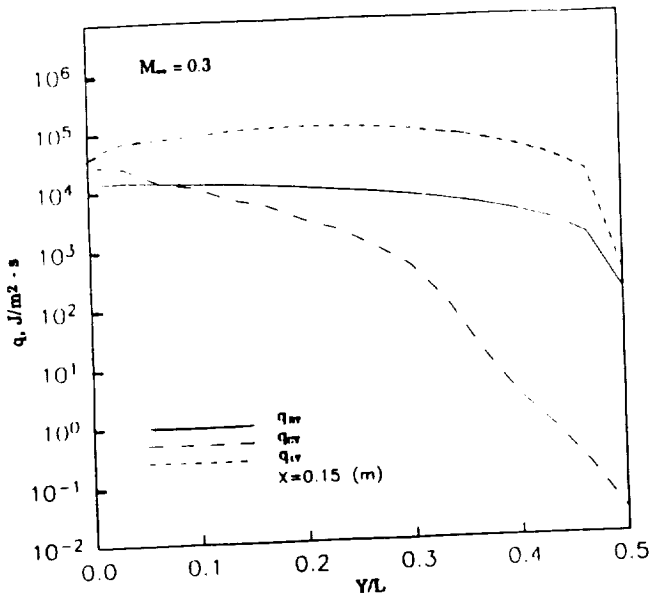


Fig. 20h Variation of q_w , q_m and q_v with y for $x = 0.15$ (m), $M_\infty = 0.3$.

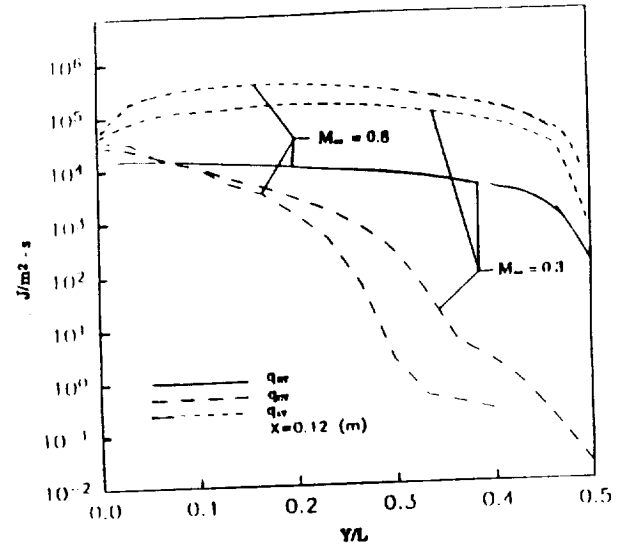


Fig. 22 Comparison of $M_\infty = 0.8$ and 0.3 results for q_w , q_m and q_v at $x = 0.12$ m.

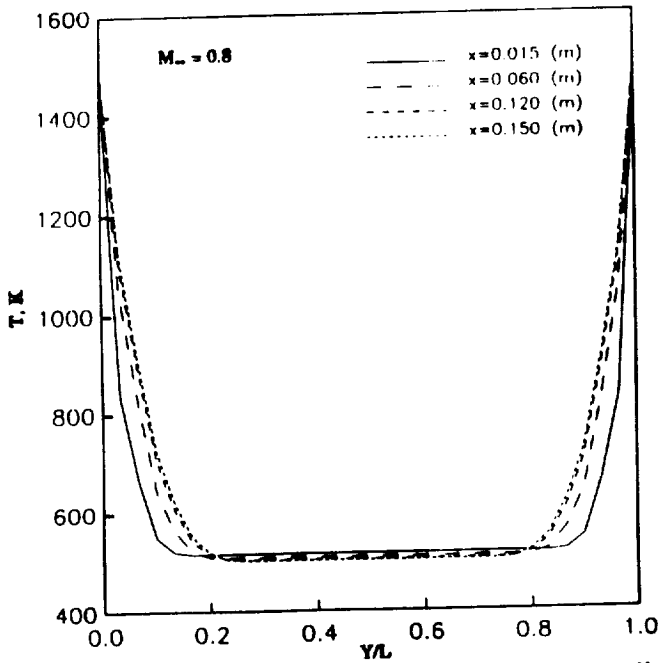


Fig. 31 Temperature variation across the channel at various x -stations, $M_\infty = 0.8$.

ORIGINAL PAGE IS
OF POOR QUALITY

APPENDIX J

*Received
1/11/90*

INVESTIGATION OF RADIATIVE INTERACTIONS IN HIGH-SPEED ENTRANCE REGION FLOWS

By

S. N. Tiwari* and D. J. Singh†

Department of Mechanical Engineering and Mechanics
Old Dominion University
Norfolk, Virginia 23529-0247

Presented at the

THIRD INTERNATIONAL CONGRESS OF FLUID MECHANICS

Cairo, Egypt

January 2-4, 1990

* Eminent Professor, Director ICAM

† Graduate Research Assistant

~~SECRET~~ INTERNATIONAL FLIGHT

INVESTIGATION OF RADIATIVE INTERACTIONS IN HIGH-SPEED ENTRANCE REGION FLOWS

S. N. Tiwari and D. J. Singh

Abstract

The influence of radiative energy transfer on the entrance region flow is investigated under supersonic flow conditions in a channel. Two-dimensional compressible Navier-Stokes equations are solved numerically in conjunction with the radiative flux equations. The channel walls are assumed to be black. Nongray as well as pseudo gray gas models are used to represent the absorption-emission characteristic of the medium. The participating species considered are different amounts of water vapor in water vapor-air mixtures. Results obtained for different flow conditions indicate that the radiative interaction can moderately influence the overall energy transfer, but the flowfield is not changed significantly.

1. INTRODUCTION

The analysis of combined modes of heat transfer involving conduction, convection and radiation has been the subject of considerable research in the last several years. The problem of combined modes of energy transfer is a very complicated phenomenon. While conduction and convection processes can be described by differential equations, radiation is described by integral equation. The integrations are with respect to frequency, solid angle, and spatial coordinates. At present, there is no analytical solution available for governing equations describing the combined modes of energy transfer, even for simple geometries. However, with the availability of fast computers, it is possible to solve these complicated equations numerically.

In many engineering problems involving high temperature gases such as reentry, hypersonic propulsion, design of combustion chambers for high pressure spacecraft engines, chemical transfer vehicles, heavy lift launch vehicles, and furnaces, the radiative interaction becomes very important. Under certain conditions, the radiation is the predominant mode of heat transfer. Basic formulations on radiative transfer in participating mediums are available in standard references [1-8]. The review articles presented in [9-15] are useful in understanding the radiative properties of participating species and the nature of nongray radiation. In most of the studies involving radiation, certain simplifying assumptions such as gray gas [16-18], fully developed flow [19-22], constant thermophysical properties [23-25] and linearized radiation [10, 20-22, 26-30] are invoked. The validity of radiative transfer analysis depends upon the accuracy with which absorption-emission characteristics of participating species are modeled. There are several models available in literature; and these are reviewed critically in [12, 13].

In general, there has been a lack of studies on radiative interaction in the entrance region of ducts. In this region, momentum and energy equations cannot be decoupled. Some simplified studies on this problem are available in [5, 31-33] and the cited references. Most of these studies are restricted to constant properties and incompressible flows. Im and Ahluwalia [34] analyzed the combined conduction, convection and radiation in rectangular ducts by solving

simultaneously the fluid dynamical and the radiation transport equations. The flow was assumed as parabolic thereby excluding the possibility of flow recirculation. Soufiani and Taine [35] studied the thermal and dynamical entrance region for a steady laminar flow between two parallel plates. The walls were considered diffuse and fluid as homogeneous absorbing, emitting and nonscattering medium. The viscous dissipation effects and axial diffusion were neglected in the energy equation. The results showed a significant difference in temperature and velocity profiles by inclusion of radiation. Mani et al. [36] studied the chemically reacting and radiating supersonic flow between parallel plates in a channel with a ten degree ramp. They showed that in the case of flow without chemical reaction, most of the energy is transferred by convection. As a result, the flow field is not affected significantly.

The objective of this study is to investigate the influence of radiative interactions on the subsonic and supersonic region flows. To accomplish this, a mixture of water vapor an air flowing laminary between parallel plates is considered. The walls are maintained at constant temperatures. The strong temperature gradient between walls and the fluid requires the use of temperature dependent fluid properties. The flow and energy conservation equations, therefore, are solved simultaneously. The effects of various parameters such as Mach number, pressure, amount of participating species, and the plate separation distance are investigated.

2. BASIC THEORETICAL FORMULATION

2.1 Flow Equations

Two-dimensional Navier-Stokes equations in fully conservative form are used to describe the flow field. These equations, in physical domain, can be written as (Fig. 1)

$$\frac{\partial U}{\partial t} + \frac{\partial F}{\partial x} + \frac{\partial G}{\partial y} = 0 \quad (2.1)$$

where vectors U , F and G are expressed as

$$\begin{aligned} U &= [\rho \quad \rho u \quad \rho H - P] \\ F &= [\rho \quad \rho u^2 + p - \tau_{xx} \quad \rho uv - \tau_{xy} \quad (E_t + p)u - u\tau_{xx} - v\tau_{xy} + q_{Cx} + q_{Rx}] \\ G &= [\rho \quad \rho uv - \tau_{xy} \quad \rho v^2 + p - \tau_{yy} \quad (E_t + p)v - u\tau_{xy} - v\tau_{yy} + q_{Cy} + q_{Ry}] \end{aligned}$$

The viscous stress terms are given by

$$\tau_{xx} = \frac{2}{3}\mu \left(2\frac{\partial u}{\partial x} - \frac{\partial v}{\partial y} \right) \quad (2.2a)$$

$$\tau_{yy} = \frac{2}{3}\mu \left(2\frac{\partial v}{\partial y} - \frac{\partial u}{\partial x} \right) \quad (2.2b)$$

$$\tau_{xy} = \mu \left(2\frac{\partial u}{\partial x} + \frac{\partial v}{\partial y} \right) = \tau_{yx} \quad (2.2c)$$

where q_{Cx} and q_{Cy} are component of conductive flux in x and y directions, respectively, and are expressed as

$$q_{Cx} = -K \frac{\partial T}{\partial x} \quad (2.3a)$$

$$q_{Cy} = -K \frac{\partial T}{\partial y} \quad (2.3b)$$

The terms q_{Rx} and q_{Ry} in the definitions of vector F and G represent the radiative flux in x and y directions, respectively. The relations for the radiative flux are developed in Sec. 3. The total energy flux in a given direction is given by the corresponding last term in the definition of F and G . The coefficient of viscosity μ is evaluated using the Sutherland's formula and the coefficient of thermal conductivity is calculated by using a constant value of the Prandtl number equal to 0.72. In order to complete the system, the equation of state is used as

$$P = \rho RT \quad (2.4)$$

The above equations can be used for subsonic as well as supersonic flows. However, the boundary conditions are numerical procedures for the two flows are quite different.

2.2 Inlet and Boundary Conditions

The treatment of the inflow boundary conditions is guided by the theory of characteristic. A locally one-dimensional flow has four characteristic equations with slopes u , $u+c$, u and $u-c$. If the flow is subsonic at the inflow, then the $u-c$ characteristic has a negative slope and it propagates information from the interior upstream to the inflow boundary. In this case, only three quantities can be specified at the inflow and the fourth quantity must be allowed to vary as the solution progresses.

In this study, the stagnation pressure, stagnation temperature and flow angle are specified at the inflow. These quantities are related to the state pressure and state temperature by the following equations

$$\frac{P_t}{P} = \left(1 + \frac{\gamma - 1}{2} M^2\right)^{\gamma/(\gamma-1)} \quad (2.5)$$

$$\frac{T_t}{T} = \left(1 + \frac{\gamma - 1}{2} M^2\right) \quad (2.6)$$

$$\frac{v}{u} = \tan(\theta_{IF}) \quad (2.7)$$

Equations (2.5)-(2.7) are a system of three equations in four unknown, P , T , u and v . To complete the system of equations, a zero order extrapolation is used for the pressure at the inflow. The outflow boundary is also calculated based on theory of characteristic. For subsonic flow at the outflow, the $u-c$ characteristic propagates information upstream from the boundary to

the interior, i.e. only one quantity can be specified at the outflow. The state pressure is specified at the outflow while u and v and T are calculated using a zeroth-order extrapolation. Along the surfaces, following boundary conditions were applied

$$u = 0, \quad v = 0, \quad \frac{\partial P}{\partial y} = 0, \quad T = T_w \quad (2.8)$$

The density is obtained from the equation of state using the computed surface pressure and prescribed surface temperature. Fourier's heat conduction law is used to calculate the conductive heat flux.

For supersonic flows, the inflow properties are assumed to be chemically frozen. The outflow conditions are calculated from adjacent nodes using a first order extrapolation. The pressure at walls are calculated by a second order one-sided differencing procedure. The free stream conditions considered for each case are indicated in discussing the results.

3. RADIATIVE TRANSFER MODELS

Radiative transport is a quite complicated phenomenon, as an element not only exchanges energy with its neighbors, but also from all other elements. This results in an integral expression with integration with respect to frequency, solid angle, and spatial coordinates. The applicability and validity of the radiative transfer in a physical problem depends on the accuracy with which the radiation is modeled. In most studies, the "tangent slab approximation" [8, 10, 36] is invoked; it treats the gas layer as one-dimensional slab in evaluation of the radiative flux (Fig. 1). In recent years, there have been few studies [36–39] which include the multidimensional effects. In this section, a brief discussion of various absorption models is given and essential equations for the radiative flux are presented.

3.1 Absorption Models

The gray gas approximation is the simplest model to calculate the radiative flux. Although unrealistic, this model has yielded accurate prediction of heat flux burning rates in moderate size fires [40]. It has also been useful for estimating the total radiative flux in furnaces [41]. In this model, the absorption coefficient is assumed to be independent of frequency. It overestimates the radiative flux because participating gas is actually transparent over large region of spectrum, and may be practically opaque in other regions. Thus, an attempt to represent the entire spectrum with a mean absorption coefficient will lead to overestimation of radiant flux in the transparent and opaque regions. The model, however, is very useful as first approximation in providing insight into the parametric trends to be expected in the system and in estimating the significance of radiation.

There are various nongray models available which relax the gray gas assumption. A few of these are line by line models, narrow band models and wide band models. These are discussed here briefly.

The line by line models [12, 13] by far are the most accurate models available. They account for each line of the absorbing species. However, these models are very expensive to

use. Since most applications require knowledge of only the properties averaged over spectral range, the narrow band models which are computationally fast and accurate are widely used. Four commonly used narrow band models are the elasser, statistical, random elasser and quasi random [12, 13]. Next in order are the wide band models which provide correlations that are valid over the entire band pass. These correlations are quite accurate for many engineering applications. The most commonly used wide-band model correlations are the Edwards exponential wide band, Tien and Lowder, and Cess and Tiwari [9–13]. The application of a model to a particular case depends on the nature of the absorbing emitting species.

3.2 Radiative Flux

For a nonscattering medium and diffuse boundaries, the expression for the radiative flux is given as [1, 42]

$$q_{R\omega}(y) = 2e_{1\omega}E_3(\kappa_\omega y) - 2e_{2\omega}E_3[\kappa_\omega(L - y)] + 2 \left\{ \int_0^y e_\omega(\xi)\kappa_\omega E_2[\kappa_\omega(y - \xi)]d\xi - \int_y^L e_\omega(\xi)\kappa_\omega E_2[\kappa_\omega(\xi - y)]d\xi \right\} \quad (3.1)$$

where

$$E_2(\eta) = \frac{3}{2} \exp\left(-\frac{3\eta}{2}\right)$$

and

$$E_3(\eta) = \frac{1}{2} \exp\left(-\frac{3\eta}{2}\right)$$

The total radiative flux is given by

$$q_R = \int_0^\infty q_{R\omega} d\omega \quad (3.2)$$

For a gray medium, κ_ω is independent of the wave number and an expression for the radiative flux is obtained from Eqs. (3.1) and (3.2) as

$$q_R = (y) = e_1 - e_2 + \frac{3}{2} \left\{ \int_0^y [e(\xi) - e_1] \exp\left[-\frac{3}{2}\kappa(y - \xi)\right] \kappa d\xi - \int_y^L [e(\xi) - e_2] \exp\left[-\frac{3}{2}\kappa(y - \xi)\right] \kappa d\xi \right\} \quad (3.3)$$

Differentiating Eq. (3.3) twice, the integrals are eliminated and there is obtained a nonhomogeneous ordinary differential equation as [1, 36]

$$\frac{1}{\kappa^2} \frac{d^2 q_R(y)}{dy^2} - \frac{9}{4} q_R(y) = \frac{3}{\kappa} \frac{de(y)}{dy} \quad (3.4)$$

This is a second order differential equation; hence it requires two boundary conditions. For nonblack diffuse surfaces, these are given as

$$\left(\frac{1}{\varepsilon_1} - \frac{1}{2}\right)[q_R(y)]_{y=0} - \frac{1}{3\kappa} \left[\frac{dq_R}{dy}\right]_{y=0} = 0 \quad (3.5a)$$

$$\left(\frac{1}{\varepsilon_1} - \frac{1}{2}\right)[q_R(y)]_{y=L} + \frac{1}{3\kappa} \left[\frac{dq_R}{dy}\right]_{y=L} = 0 \quad (3.5b)$$

In order to solve Eq. (3.4), one needs an expression for κ , which is given as

$$\kappa = \frac{P_j}{\sigma T^4(y)} \sum_{i=1}^n e_{\omega_i}(T) S_i(T) \quad (3.6)$$

Here, κ represents the Planck mean absorption coefficient and is function of temperature and species partial pressure P_j .

An expression for the divergence of radiative flux in the optically thin limit is obtained from Eq. (3.1) as [1].

$$\frac{dq_{R\omega}}{dy} = 2\kappa_{\omega}[2e_{b\omega}(y) - e_1 - e_2] \quad (3.7)$$

In the optically thick limit, Eq. (3.1) reduces to [1]

$$q_{R\omega} = -\frac{4}{3\kappa_{\omega}} \frac{de_{b\omega}}{dy} \quad (3.8)$$

Equations (3.7) and (3.8) can be used to obtain limiting solutions for the gray model.

For a nongray model consisting of n-molecular (vibration-rotation) bands, a combination of Eqs. (3.1) and (3.2) results in [1, 42]

$$\begin{aligned} q_R(\xi) = & e_1 - e_2 \\ & + \frac{3}{2} \sum_{i=1}^n A_{oi} u_{oi} \left\{ \int_0^{\xi} F_{1\omega_i}(\xi') \bar{A}'_i \left[\frac{3}{2} u_{oi} (\xi - \xi') \right] d\xi' \right. \\ & \left. - \int_{\xi}^1 F_{2\omega_i}(\xi') \bar{A}'_i \left[\frac{3}{2} u_{oi} (\xi' - \xi) \right] d\xi' \right\} \end{aligned}$$

where

$$F_{1\omega_i}(\xi) = e_{\omega_i}(\xi) - e_{1\omega_i}, F_{2\omega_i}(\xi) = e_{\omega_i}(\xi) - e_{2\omega_i}, \xi = y/L = u/u_o$$

and $\bar{A}'(u)$ denotes the derivative of $A(u)$ with respect to u . Equation (3.9) is the most convenient equation to use when employing the band model correlations in nongray radiative transfer analyses. Spectral properties and correlation quantities for various participating species are available in [9, 11].

In the optically thin limit [1, 10], $\bar{A}(u) = u$ and $\bar{A}'(u) = 1$. In this limit, the divergence of radiative flux is obtained by differencing Eq. (3.9) as

$$\frac{dq_R}{dy} = \frac{3}{2} \sum_{i=1}^n \frac{A_{oi} u_{oi}}{L} [2e_{\omega_i}(y) - e_{1\omega_i} - e_{2\omega_i}] \quad (3.10)$$

In the large path length (i.e., for $u_{oi} \gg 1$ for each band), $\bar{A}(u) = \ln(u)$ and $\bar{A}'(u) = 1/u$. Consequently, in this limit, one obtains a simple relation from Eq. (3.9) as [1, 10]

$$\frac{dq_R}{d\xi} = \sum_{i=1}^n A_{oi} \int_0^1 \frac{de_{\omega_i}}{d\xi'} \frac{d\xi'}{\xi - \xi'} \quad (3.11)$$

Equations (3.10) and (3.11) are used to obtain limiting solutions for nongray radiation.

For nongray radiative interactions, the continuous correlation proposed by Tien and Lowder [9] is employed in this study. This correlation is relatively simple and provides accurate results for pressures higher than 0.5 atmosphere.

4. METHOD OF SOLUTION

The governing equations, Eqs. (2.1) through (2.3), are transformed from the physical plane (x, y, t) to computational domain (ξ, η, t) to facilitate the treatment of general geometry. Equations (2.1) and (2.2) are expressed in the computational domain as

$$\frac{\partial \hat{U}}{\partial t} + \frac{\partial \hat{F}}{\partial \xi} + \frac{\partial \hat{G}}{\partial \eta} = 0 \quad (4.1)$$

where

$$\hat{U} = UJ$$

$$\hat{F} = Fy_\eta - Gx_\eta; \hat{G} = Gx_\xi = Fy_\xi$$

$$J = x_\xi y_\eta - y_\xi x_\eta$$

Equation (4.1) is solved by a time-asymptotic two steps, explicit MacCormack method [43]. This method is second order accurate in space. If a solution to Eq. (4.1) is known at some time $t = n\Delta t$, then the solution at next time step $t = (n+1)\Delta t$ can be calculated from

$$\hat{U}_{i,j}^{n+1} = L(\Delta t)\hat{U}_{i,j}^n$$

for each grid point (i, j) . The operate L consists of predictor and corrector steps. For this study, the code developed by Kumar [44] was modified to include the radiation model. The details of the solution procedure are available in [44, 45].

The radiative flux equations, Eq. (3.4), is discretized using the central differencing scheme as

$$\begin{aligned} \frac{2}{\Delta y_j^2(1 + \beta_j)} q_{j-1} - \left[\frac{2}{\Delta y_j(1 + \beta_j)} \left(\frac{1}{\beta_j \Delta y_j} + \frac{1}{\Delta y_j} \right) + \frac{9}{4} \kappa_j^2 \right] q_j \\ + \frac{2}{\Delta y_j^2(1 + \beta_j) \beta_j} q_{j+1} = 1.5 \kappa_j \left[\frac{e_{j+1} - e_j}{\beta_j \Delta y_j} + \frac{e_j - e_{j-1}}{\Delta y_j} \right] \end{aligned} \quad (4.2)$$

where

$$\Delta y_j = y_j - y_{j-1}$$

$$\beta_j = \frac{y_{j+1} - y_j}{y_j - y_{j-1}}$$

Equation (4.2) along with Eq. (3.5) forms a tridiagonal system of equation, which can be efficiently solved by the Thomas algorithm.

In the nongray gas formulation, the divergence of the radiative flux is evaluated using a central differencing scheme and is treated as radiative source term in the energy equation. Since the nongray formulation involves an integro-differential equation, the radiative flux term is uncoupled and treated separately [45].

5. RESULTS AND DISCUSSION

Based on the theory and computational procedure described in the previous sections, a computer code was developed to solve the two-dimensional Navier-Stokes equations for radiating supersonic laminar flows between two parallel black plates. A similar but different code was developed for radiating subsonic flows. The dimensions of the channel were taken as 3 cm x 10 cm for the supersonic flow case and 3 cm x 15 cm for the subsonic case. The radiative interaction was considered only in the normal direction. Extensive results have been obtained for pure H₂O as participating species and different mixture of H₂O and air flowing laminarly between the plates. These are available in [36, 45] for the supersonic case and in [46] for the subsonic case. Selected results for both case are presented and discussed in this section; results for supersonic flows are presented first.

For the case of supersonic flow, a comparison of the divergence of radiative flux for general (nongray), gray, and their optically thin limit models is presented in Fig. 2 for two different y-locations (y=0.2 and 1.5 cm). The inflow conditions for this case are $P_\infty = 1$ atm, $T_\infty = 1,700$ K, $M_\infty = 4.3$, $f_{H_2O} = 0.5$, $f_{O_2} = 0.1$, and $f_{N_2} = 0.4$. The gray formulation is based on the Planck mean absorption coefficient which accounts for the detailed information on different molecular bands. As such, this approach is referred to as the "pseudo-gray formulation." The range of optical thickness calculated in [45] was found to be between 0.003 and 0.4. Thus, for the physical model and inflow conditions considered, the radiative interaction is essentially in the optically thin range. No significant difference in results is observed for the two y-locations; this is a typical characteristic of the optically thin radiation [1, 10]. The solution of the gray formulation requires about ten times less computational resources in comparison to the solution

of the nongray formulation [45]. As such, for basic parametric study, all other results presented in this section were obtained by using the pseudo-gray gas formulation.

Another case considered for the supersonic flow corresponds to the inflow conditions of $P_\infty = 1$ atm, $T_\infty = 1,700$ K, $U_\infty = 2574$ m/s ($M_\infty = 3.0$), and various amounts of water vapor and air mixtures. The results for radiative flux are illustrated in Figs. 3 and 4 as a function of the nondimensional y -coordinate. For $P = 1$ atm, the results presented in Fig. 3 for different water vapor concentrations indicate that the radiative interaction increases slowly with an increase in the amount of the gas. The results for 50% H_2O are illustrated in Fig. 4 for two different pressures ($P_\infty = 1$ and 3 atm) and x -locations ($x = 5$ and 10 cm). It is noted that the increase in pressure has dramatic effects on the radiative interaction. The conduction and radiation heat transfer results are compared in Fig. 5 for $P = 3$ atm and for two different x -locations ($x = 5$ and 10 cm). The results demonstrate that the conduction heat transfer is restricted to the region near the boundaries and does not change significantly from one x -location to another. The radiative interaction, however, is seen to be important everywhere in the channel, and this can have significant influence on the entire flowfield. The results presented in Figs. 3–5 should be physically symmetric; but, due to the predictor-corrector procedure used in the McCormack's scheme, they exhibit some unsymmetrical behavior.

The results for subsonic flows were obtained for two specific Mach numbers, $M_\infty = 0.8$ and $M_\infty = 0.3$. Most results presented here are for $M_\infty = 0.8$; however, certain results for $M_\infty = 0.3$ are also presented for comparative purposes.

The free stream (inflow) conditions corresponding to $M_\infty = 0.8$ are, $P_t = 1.524 P_\infty$, $T_t = 1.128 T_\infty$, $P_\infty = 1$ atm, $T_\infty = 500$ K, $f_{H_2O} = 0.5$, and $f_{air} = 0.5$. The wall temperature was maintained at $T_w = 1,500$ K. The pressure at the channel exit was taken to be one atmosphere.

The variation in axial velocity across the channel is shown in Fig. 6a for different x locations. It is clearly evident that the fluid velocity in the inviscid core increases along the axial length due to increase in the boundary layer. A fully-developed flow has not been achieved at the channel exit. Figure 6b shows the variation of normal component of velocity across the channel at various axial locations. The two-dimensional effects are clearly evident from the results of $x = 0.015$ m which is predominantly in the entrance region. The magnitude of v velocity decreases as x increases; it is positive in the lower half and negative in the upper half of the channel due to the symmetry of the problem. For a fully-developed flow, the v component of velocity should be zero.

The variation in temperature across the channel is shown in Fig. 7 for different x locations. The temperature decrease from the walls to the center of the channel indicating the development of the thermal boundary layer. The flow is not thermally developed at the exit of the channel.

The variations in conductive and radiative fluxes along the length of the plate are shown in Fig. 8 for different y -locations. The fluxes are zero along the centerline of the plate because of physical symmetry. The conductive flux increases slowly with increasing x and becomes essentially constant at the channel exit. The radiative interaction is strong in the first ten percent of the length and then it slowly decreases and reaches about the same value as conductive flux at the exit. The variation in total energy flux (q_{ty}) with x is illustrated in Fig. 9 for different

y-locations. A comparison of results presented in Figs. 8 and 9 demonstrates that the rate of convective (flow) energy is considerably higher than the rate of conductive or radiative energy transfer.

The variations in q_{Cy} , q_{Ry} and q_{Ty} with y are shown in Figs. 10, 11 and 12, respectively. It is noted that the variation in conductive flux occurs mainly within the first 20% distance from the wall (Fig. 10). The situation, however, is not the same with respect to the radiative transfer (Fig. 11). The radiative interaction occurs in the entire width of the channel. This is similar to the results for supersonic flow presented in Fig. 5, although the extent of interaction is entirely different. The results presented in Fig. 12 demonstrate that the rate of total energy transfer in the y -direction is highest closer to the entrance ($x = 0.015$ m) than any other x location. This is a result of high enthalpy flow and strong radiative interaction in this region.

Figure 13 shows the variation of radiative and conductive flux across the channel. The radiative flux peaks at some distance away from the wall while conductive flux peaks at the wall. This is because at the lower wall the effect of positive heat flux is partially cancelled by the negative flux from the layers of hot gases next to the wall. At a small distance away from the wall, however, the positive flux from both the wall and gas combine to give a maximum heat flux. Farther into the gas, the flux from the wall and hot gas is attenuated by the cooler gas and is partially cancelled. At the center of the channel, the fluxes from both modes cancel each other. This effect prevails throughout the length of the channel as is clearly evident from the results of Figs. 13a and 13b and Ref. 46. This trend in result is somewhat similar to the trend for the supersonic flow presented in Fig. 5.

The variation of the radiative, conductive and normal component of the total flux across the channel is shown in Fig. 14 for $x = 0.06$ m. The total flux includes the convective (flow), radiative and conductive fluxes. It is interesting to note that except very near the boundary, the total flux is about an order of magnitude higher than the radiative flux and much higher than the conductive flux. In other words, according to the definition used in this study, the convective (flow) energy is the predominant mode of energy transfer. This trend in result continues for all axial stations [46].

For $M_\infty = 0.3$, the free stream conditions considered are, $P_t = 1.064 P_\infty$, $T_t = 1.018 T_\infty$, $P_\infty = 1$ atm, $T_\infty = 500$ K, $f_{H_2O} = 0.5$, and $f_{air} = 0.5$. In this case also, the wall temperature was maintained at $T_w = 1,500$ K and the channel exit pressure was one atmosphere.

The results for $M_\infty = 0.3$, in general, show the same trend as the results for $M_\infty = 0.8$. Certain definite changes, however, are noted for specific cases. For $M_\infty = 0.3$, the magnitude of velocity variations obviously are relatively lower but the velocity boundary layers are thicker [46]. The temperature variations shown in Fig. 15 for $M_\infty = 0.3$ are about the same as shown in Fig. 7 for $M_\infty = 0.8$. This is because T_∞ and T_w are the same for both flows. The thermal boundary layer, however, is thicker for $M_\infty = 0.3$.

A comparison of $M_\infty = 0.8$ and 0.3 results for q_{Cy} , q_{Ry} and q_{Ty} is shown in Fig. 16 for $x = 0.12$ m. The results demonstrate that while conductive and total energy fluxes are influenced considerably by changes in the Mach number, the radiative energy transfer is insensitive to such

changes. This is because radiation is influenced primarily by specified temperature and pressure conditions and these conditions are same for both cases.

6. CONCLUSIONS

Two-dimensional compressible Navier-Stokes equations have been used to investigate the influence of radiative energy transfer on the entrance region flow under supersonic and subsonic flow conditions. Computational procedures have been developed to incorporate gray as well as nongray formulations for radiative flux in the general governing equations. Specific results have been obtained for different amounts of water-vapor in water vapor-air mixtures. Results demonstrate that the radiative interaction increases with an increase in pressure, temperature and the amount of water vapor. This can have a significant influence on the overall energy transfer in the system. Most energy, however, is transferred by convection in the flow direction. As a result, the radiative interaction does not alter the flow field significantly. Further parametric studies are needed to make definite recommendations.

ACKNOWLEDGEMENTS

This work was supported by the NASA Langley Research Center through Grants NAG-1-423 and NAG-1-363. Some of the supersonic flow results were obtained by M. Mani.

NOMENCLATURE

A	band absorptance = $A(u, \beta)$, cm^{-1}
A_0	band width parameter, cm^{-1}
C_0	correlation parameter, $\text{atm}^{-1} - \text{cm}^{-1}$
C_p	specific heat at constant pressure $\text{kJ/kg-K} = \text{erg/gm-K}$
e_ω	Planck's function, $(\text{W-cm}^{-2})/\text{cm}^{-1}$
e_{ω_0}	Planck's function evaluated at wave number ω_0
e_1, e_2	emissive power of surfaces with temperature T_1 and T_2 , W-cm^{-2}
k	thermal conductivity, erg/cm-sec-K
P	pressure
P_i	partial pressure
P_t	stagnation pressure
Pr	Prandtl number
q_R	total radiative heat flux, $\text{J/m}^2\text{-s}$
q_c	conduction heat flux, $\text{J/m}^2\text{-s}$

$q_{R\omega}$	spectral radiation heat flux, $(w\text{-cm}^{-2})/\text{cm}^{-1}$
S	integrated intensity of a wide band, $\text{atm}^{-1}\text{-cm}^{-2}$
T	temperature, K
T_1, T_2	wall temperature, K; $T_1 = T_w$
u	nondimensional coordinate = SPy/A_o
u_o	nondimensional path length = SPL/A_o
θ	flow angle
κ_ω	spectral absorption coefficients, cm^{-1}
ξ, η	computational coordinate
ρ	density, kg/m
σ	Stefan-Boltzmann constant, $\text{erg}/(\text{sec}\text{-cm}^2\text{-K}^4)$
ω	wave number, cm^{-1}
ω_o	wave number at the band center, cm^{-1}

REFERENCES

1. Sparrow, E. M. and Cess, R. D., Radiation Heat Transfer, Brooks/Cole, Belmont, Calif., 1966 and 1970. New Augmented Edition, Hemisphere Publishing Corp., Washington, D.C., 1978.
2. Hottel, H. C. and Sarofim, A. F., Radiative Transfer, McGraw-Hill Book Co., New York, 1971; Second Edition, 1981.
3. Siegel, R. and Howell, J. R., Thermal Radiation Heat Transfer, McGraw-Hill Book Co., New York, 1971; Second Edition, 1981.
4. Ozisik, M. N., Radiative Transfer and Interaction with Conduction and Convection, John Wiley & Sons, Inc., New York, 1973.
5. Edwards, D. K., Radiation Heat Transfer Notes, Hemisphere Publishing Corporation, Washington, D.C., 1981.
6. Cess, R. D., "The Interaction of Thermal Radiation with Conduction and Convection Heat Transfer," Advances in Heat Transfer, Vol. 1, Academic Press, New York, 1964.
7. Sparrow, E. M., "Radiative Heat Transfer Between Surfaces," Advances in Heat Transfer, Vol. 2, Academic Press, New York, 1965.
8. Viskanta, R., "Radiation Transfer and Interaction of Convection with Radiation Heat Transfer," Advances in Heat Transfer, Vol. 3, Academic Press, New York, 1966.
9. Tien, C. L., "Thermal Radiation Properties of Gases," Advances in Heat Transfer, Vol. 5, Academic Press, New York, 1968.

10. Cess, R. D. and Tiwari, S. N., "Infrared Radiative Energy Transfer in Gases," Advances in Heat Transfer, Vol. 8, Academic Press, New York, 1972.
11. Edwards, D. K., "Molecular Gas Band Radiation," Advances in Heat Transfer, Vol. 12, Academic Press, New York, 1976.
12. Tiwari, S. N., "Band Models and Correlations for Infrared Radiation," Radiative Transfer and Thermal Control (Progress in Astronautics and Aeronautics), Vol. 49, American Institute of Aeronautics and Astronautics, New York, 1976.
13. Tiwari, S. N., "Models for Infrared Atmospheric Radiation," Advances in Geophysics, Vol. 20, Academic Press, New York, 1978.
14. Viskanta, R., "Radiation Heat Transfer," Fortschrift der Verfahrenstechnik, Vol. 22A, 1984, pp. 51-81.
15. Viskanta, R. and Menguc, M. P., "Radiation Heat Transfer in Combustion Systems," Progress in Energy Combustion Science, Vol. 13, 1987, pp. 97-160.
16. Lick, W., "Transient Energy Transfer by Radiation and Conduction," International Journal of Heat and Mass Transfer, Vol. 8, January 1965, pp. 119-127.
17. Hazzah, A. S. and Beck, J. V., "Unsteady Combined Conduction — Radiation Energy Transfer Using a Rigorous Differential Method," International Journal of Heat and Mass Transfer, Vol. 13, March 1970, pp. 517-522.
18. Chang, Y. P. and Smith, R. C., Jr., "Steady and Transient Heat Transfer by Radiation and Conduction in a Medium Bounded by Two Coaxial Cylindrical Surfaces," International Journal of Heat and Mass Transfer, Vol. 13, January 1970, pp. 69-80.
19. Cess, R. D. and Tiwari, S. N., "The Interaction of Thermal Conduction and Infrared Gaseous Radiation," Applied Scientific Research, Vol. 20, January 1969, pp. 25-39.
20. Martin, J. K. and Hwang, C. C., "Combined Radiant and Convective Heat Transfer in Laminar Steam Flow Between Gray Parallel Plates with Uniform Heat Flux," Journal of Quantitative Spectroscopy and Radiative Transfer, Vol. 15, December 1975, pp. 1071-1081.
21. Kobiyama, M., Taniguchi, H. and Saita, T., "The Numerical Analyses of Heat Transfer Combined with Radiation and Convection," Bulletin of the Japanese Society of Mechanical Engineering, Vol 22, No. 167, May 1979, pp. 707-714.
22. Tiwari, S. N. and Singh, D. J., "Interaction of Transient Radiation in Fully Developed Laminar Flows," AIAA Paper 87-1521, June 1987.
23. Kuroksi, Y., "Heat Transfer by Simultaneous Radiation and Convection in an Absorbing and Emitting Medium in a Flow Between Parallel Plates," Fourth International Heat Transfer Conference, Vol. II, Paper R2.5, Paris-Versailles, 1970.
24. Larsen, P. A. and Lord, H. A., "Convective and Radiative Heat Transfer to Water Vapor in Uniformly Heated Tubes," Fourth International Heat Transfer Conference, Vol. III, Paper, R2.6, Paris-Versailles, 1970.

25. Kurosaki, Y., "Radiation Heat Transfer in a Flow Between Flat Plates with Temperature Slip at the Walls," Fifth International Heat Transfer Conference, Vol. I, Tokyo, 1971, pp. 98–107.
26. Cess, R. D. and Tiwari, S. N., "Heat Transfer to Laminar Flow of an Absorbing-Emitting Gas Between Parallel Plates," Heat and Mass Transfer-USSR, Vol. 1, May 1968, pp. 229–283.
27. Tiwari, S. N. and Cess, R. D., "Heat Transfer to Laminar Flow of Nongray Gases Through a Circular Tube," Applied Scientific Research, Vol. 25, No. 34, December 1971, pp. 155–170.
28. Jeng, D. R., Lee, E. J., and DeWitt, K. J., "A Study of Two Limiting Cases in Convective and Radiative Heat Transfer with Nongray Gases," International Journal of Heat and Mass Transfer, Vol. 19, June 1976, pp. 589–596.
29. Tiwari, S. N., "Applications of Infrared Band Model Correlations to Nongray Radiation," International Journal of Heating and Mass Transfer, Vol. 20, No. 7, July 1977, pp. 741–751.
30. Greif, R., "Laminar Convection with Radiation: Experimental and Theoretical Results," International Journal of Heat and Mass Transfer, Vol. 21, April 1978, pp. 477–480.
31. Pearce, B. E. and Emery, A. F., "Heat Transfer by Thermal Radiation and Laminar Forced Convection to an Absorbing Fluid in the Entry Region of a Pipe," Journal of Heat Transfer, Vol. 92, 1970, pp. 221–230.
32. Balakrishnan, A. and Edwards, D. K., "Molecular Gas Radiation in the Thermal Entrance Region of a Duct," Journal of Heat Transfer, Vol. 101, 1979, pp. 489–495.
33. Lin, J. D. and Huang, J. M., "Numerical Analysis of Graetz Problem with Inclusion of Radiation Effect," Paper No. 6–4 (Poster Session 6), 25th National Heat Transfer Conference, Houston, TX, July 24–27, 1988.
34. Im, K. H. and Ahluwalia, R. K., "Combined Convection and Radiation in Rectangular Ducts," International Journal of Heat and Mass Transfer, Vol. 27, No. 2, February 1984, pp. 221–231.
35. Soufiani, A. and Taine, J., "Application of Statistical Narrow Band Model to Coupled Radiation and Convection at High Temperature," International Journal of Heat and Mass Transfer, Vol. 30, No. 3, March 1987, pp. 437–447.
36. Mani, M., Tiwari, S. N. and Drummond, J. P., "Numerical Solution of Chemically Reacting and Radiating Flows," AIAA Paper 87–0324, January 1987; also, "Investigation of Two-Dimensional Chemically Reacting and Radiating Supersonic Channel Flows," AIAA Paper 88–0462, January 1988.
37. Latko, R. J. and Promraning, G. C., "Two-Dimensional Radiative Transfer by Synthesis Method," Journal of Quantitative Spectroscopy and Radiative Transfer, Vol. 31, No. 4, April 1984, pp. 339–372.
38. Tsai, S. S. and Chan, S. H., "Multi-Dimensional Radiative Transfer in Nongray Gases — General Formulation and the Bulk Radiative Exchange Approximation," Journal of Heat Transfer, Vol. 100, August 1978, pp. 486–491.

39. Crosbie, A. L. and Schrenker, R. G., "Radiative Transfer in a Two-Dimensional Rectangular Medium Exposed to Diffuse Radiation," Journal of Quantitative Spectroscopy and Radiative Transfer, Vol. 31, No. 4, April 1984, pp. 339–372.
40. Modak, A. T., "Thermal Radiation from Pool Fires," *Combustion and Flames*, Vol. 29, February 1977, pp. 177–192.
41. Hottel, H. C., Heat Transmission, McAdams, W. H., (Editor), 3rd Edition, McGraw-Hill, New York, 1954.
42. Tiwari, S. N., "Radiative Interaction in Transient Energy Transfer in Gaseous System," Dept. of Mechanical Engineering and Mechanics, Old Dominion University, Norfolk, Virginia, December 1985; also NASA-CR-176644 NAS 1.26:176644, December 1985.
43. MacCormack, R. W., "The Effect of Viscosity in Hypervelocity Impact Cratering," AIAA Paper 69–354, May 1969.
44. Kumar, A., "Numerical Analysis of the Scramjet Inlet Flow Field Using Two-Dimensional Navier-Stokes Equations, AIAA Paper 81–0185, January 1981.
45. Mani, M. and Tiwari, S. N., "Investigation of Chemically Reacting and Radiating Supersonic Internal Flows," NASA-CR-180540, December 1986; also, "Investigation of Supersonic Chemically Reacting and Radiating Channel Flow," NASA-CR-182726, January 1988 (also, Ph.D. Dissertation by M. Mani, Old Dominion University, Norfolk, Virginia, May 1988).
46. Singh, D. J. and Tiwari, S. N., "Investigation of Radiative Interactions in Subsonic Entrance Region Flows," Department of Mechanical Engineering and Mechanics, Old Dominion University, Norfolk, Virginia, Progress Report NAG-1–423, November 1989.

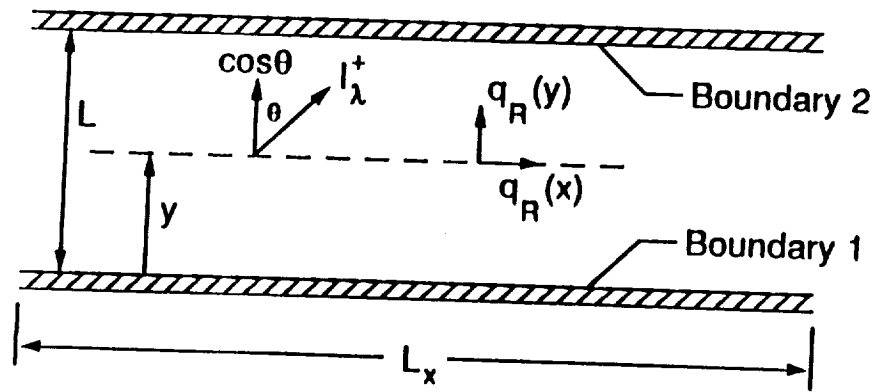


Fig. 1 Radiating gas between parallel boundaries.

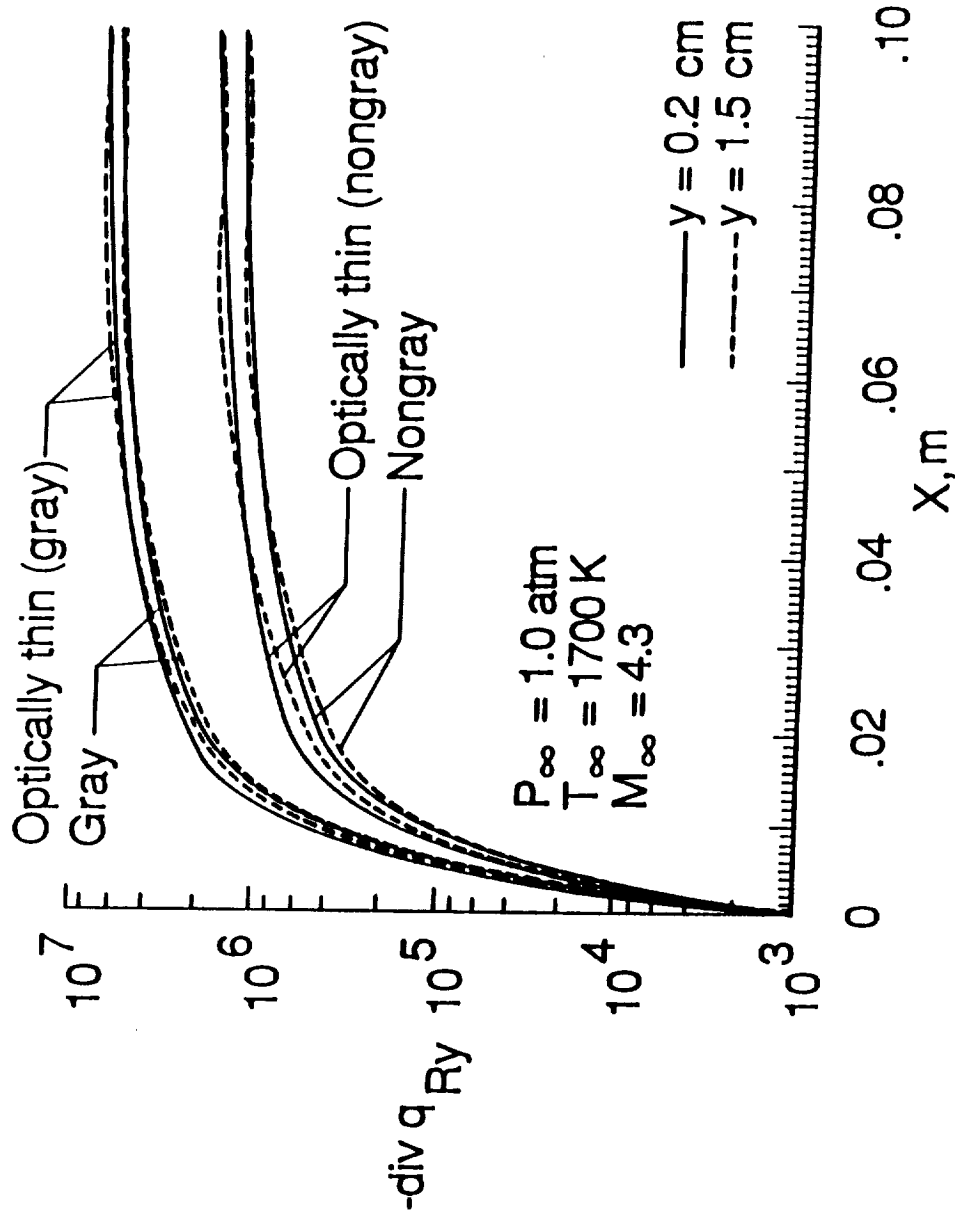


Fig. 2 Divergence of radiative flux along the channel for gray and nongray models, $M_{\infty} = 4.3$.

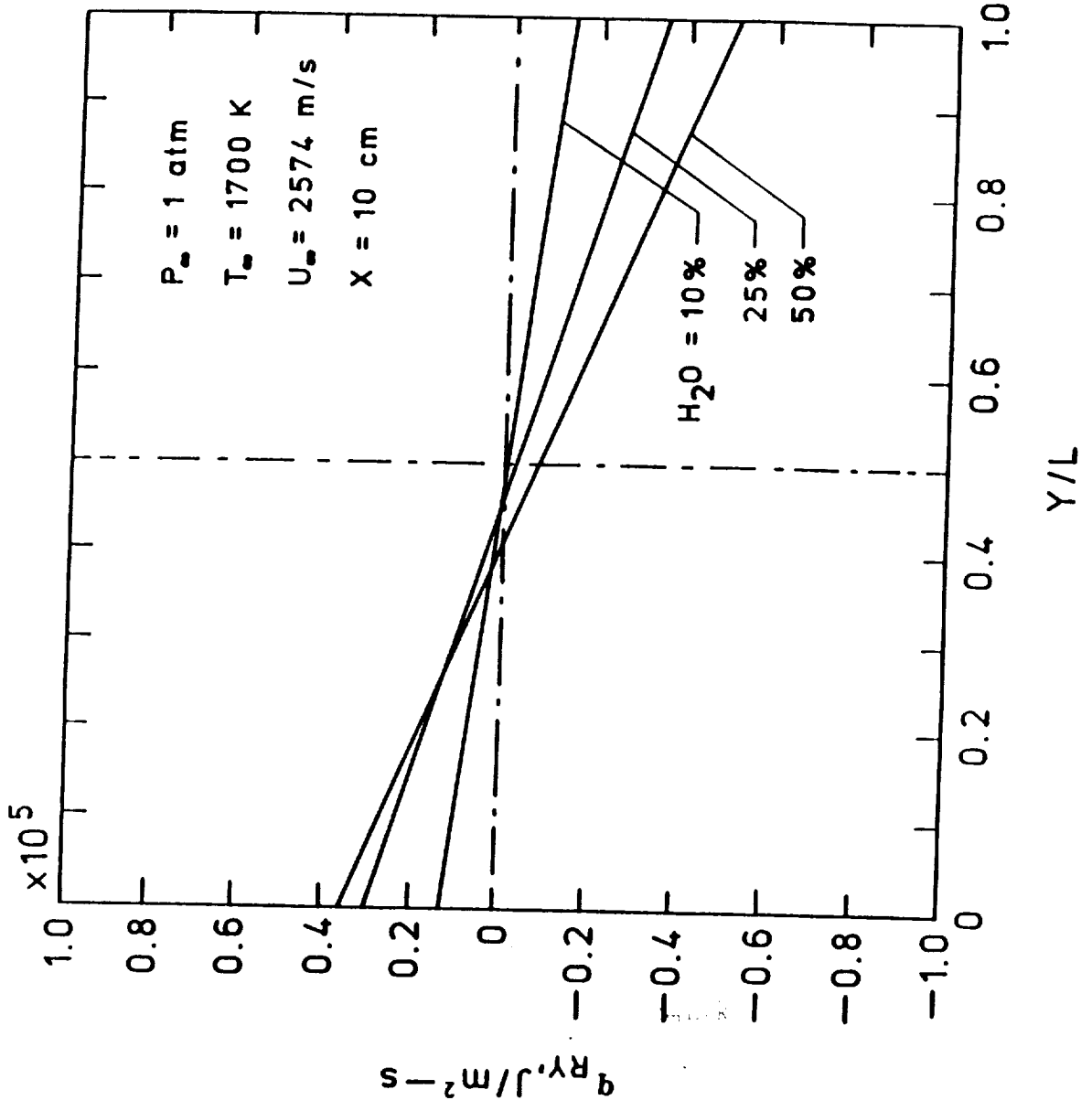


Fig. 3 Radiative flux vs. y at the channel exit, $M_{\infty} = 3.0$.

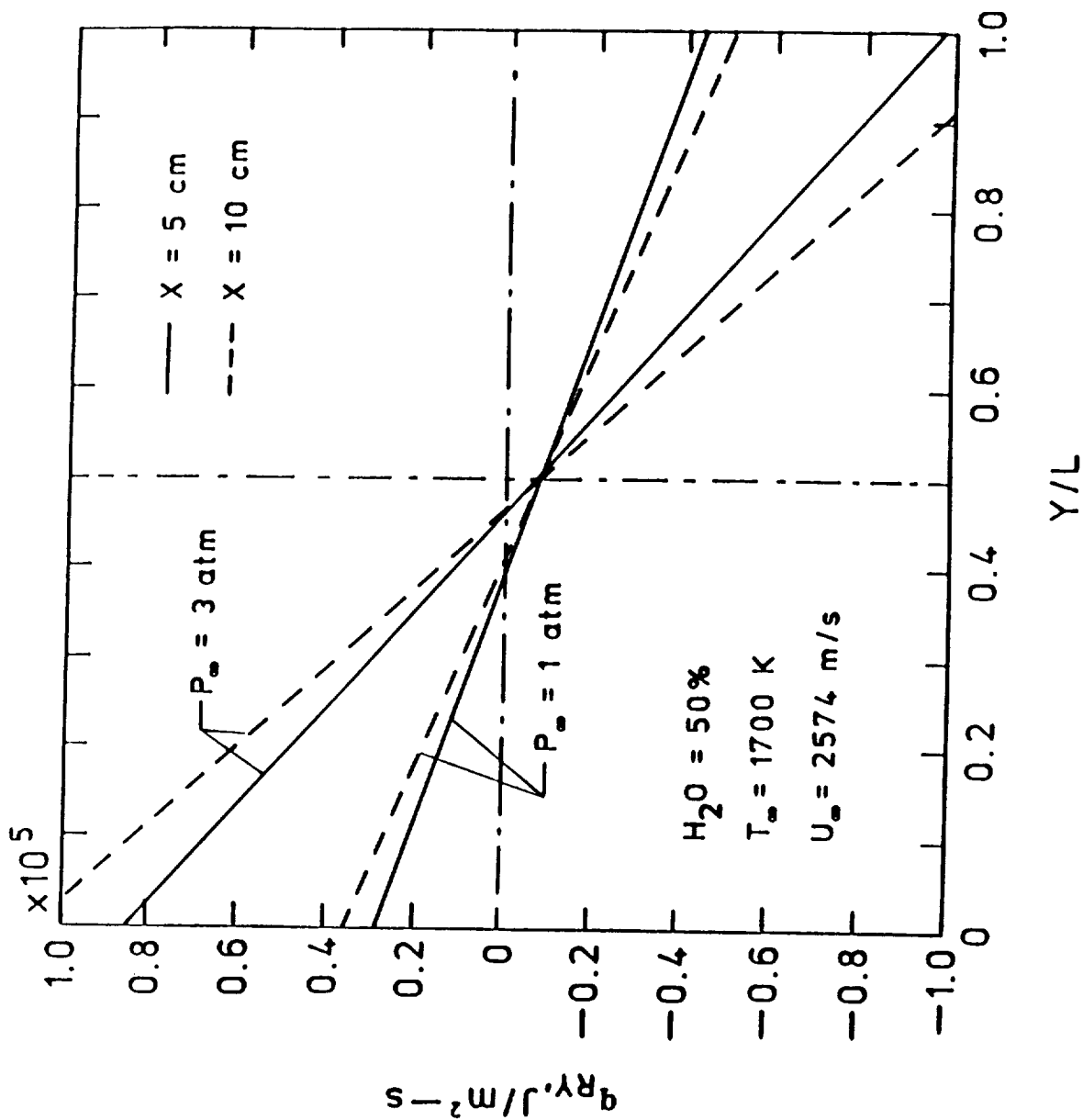


Fig. 4 Radiative flux vs. y at $x = 5$ and 10 cm, $M_\infty = 3.0$.

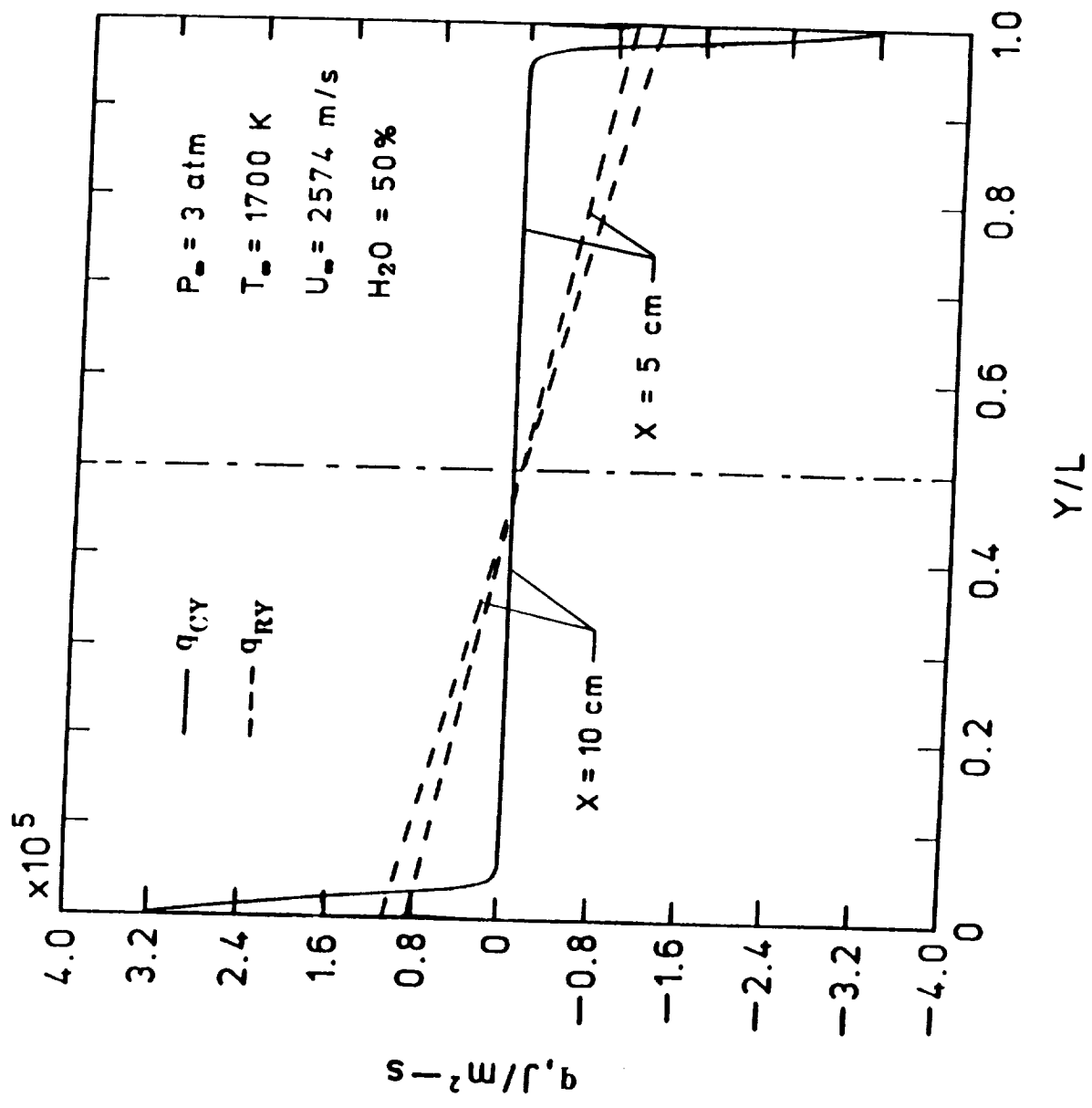


Fig. 5 Radiative and convective flux vs. y at $x = 5$ and 10 cm , $M_\infty = 3.0$.

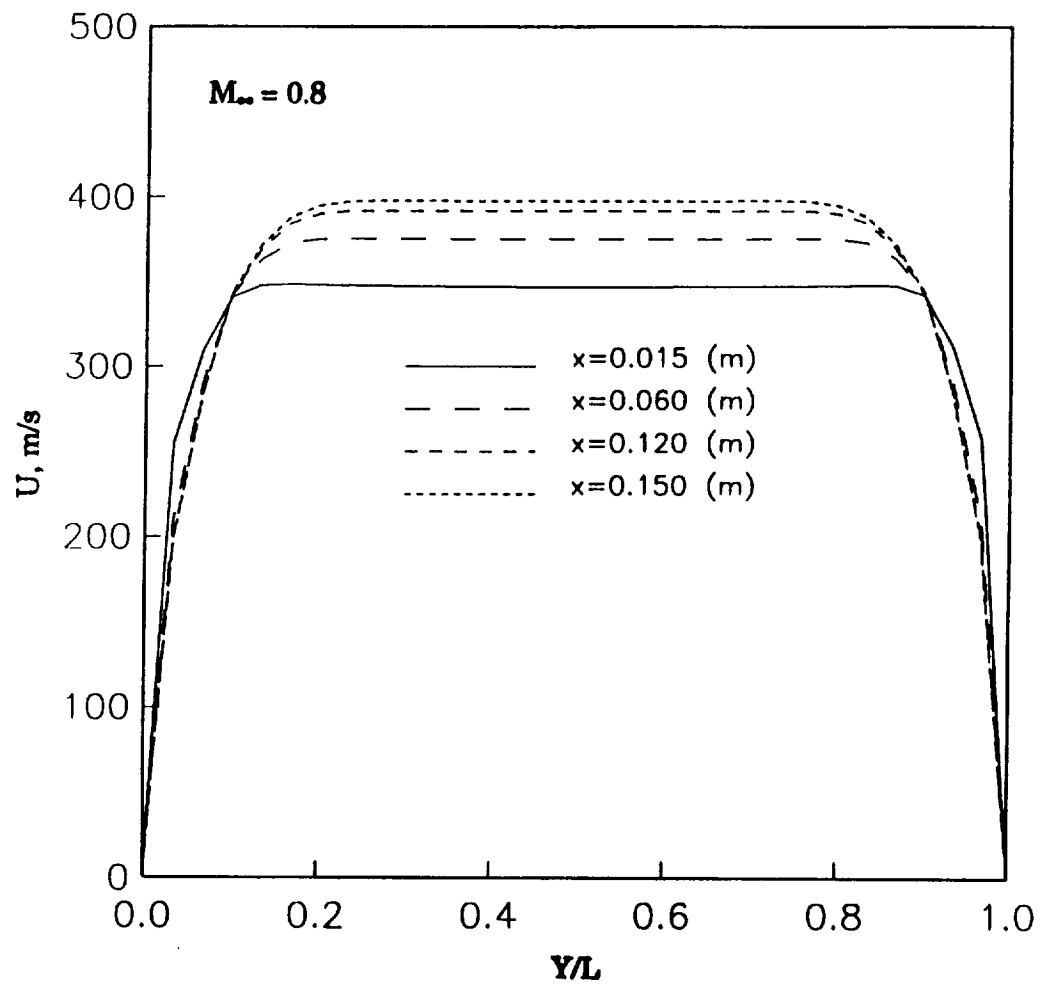


Fig. 6a Variation of axial velocity across the channel at various x stations, $M_\infty = 0.8$.

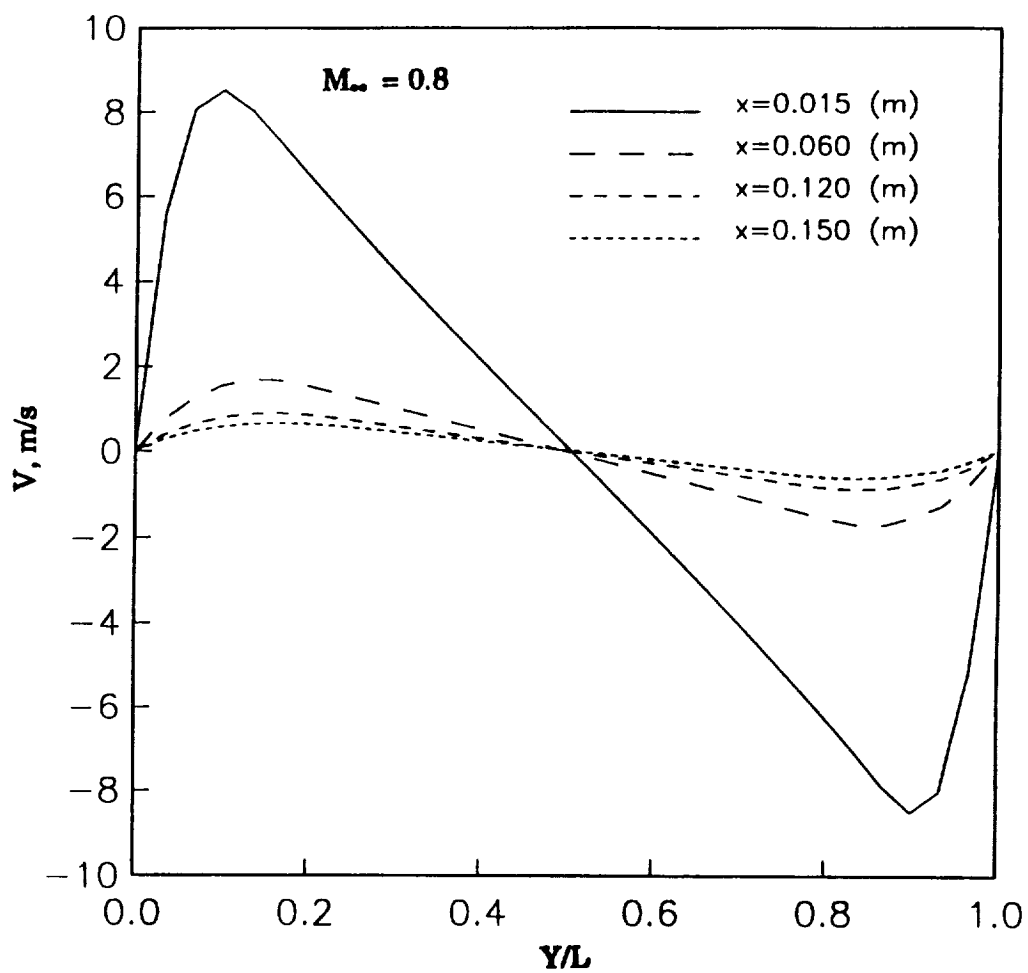


Fig. 6b Variation of normal velocity across the channel at various x stations, $M_\infty = 0.8$.

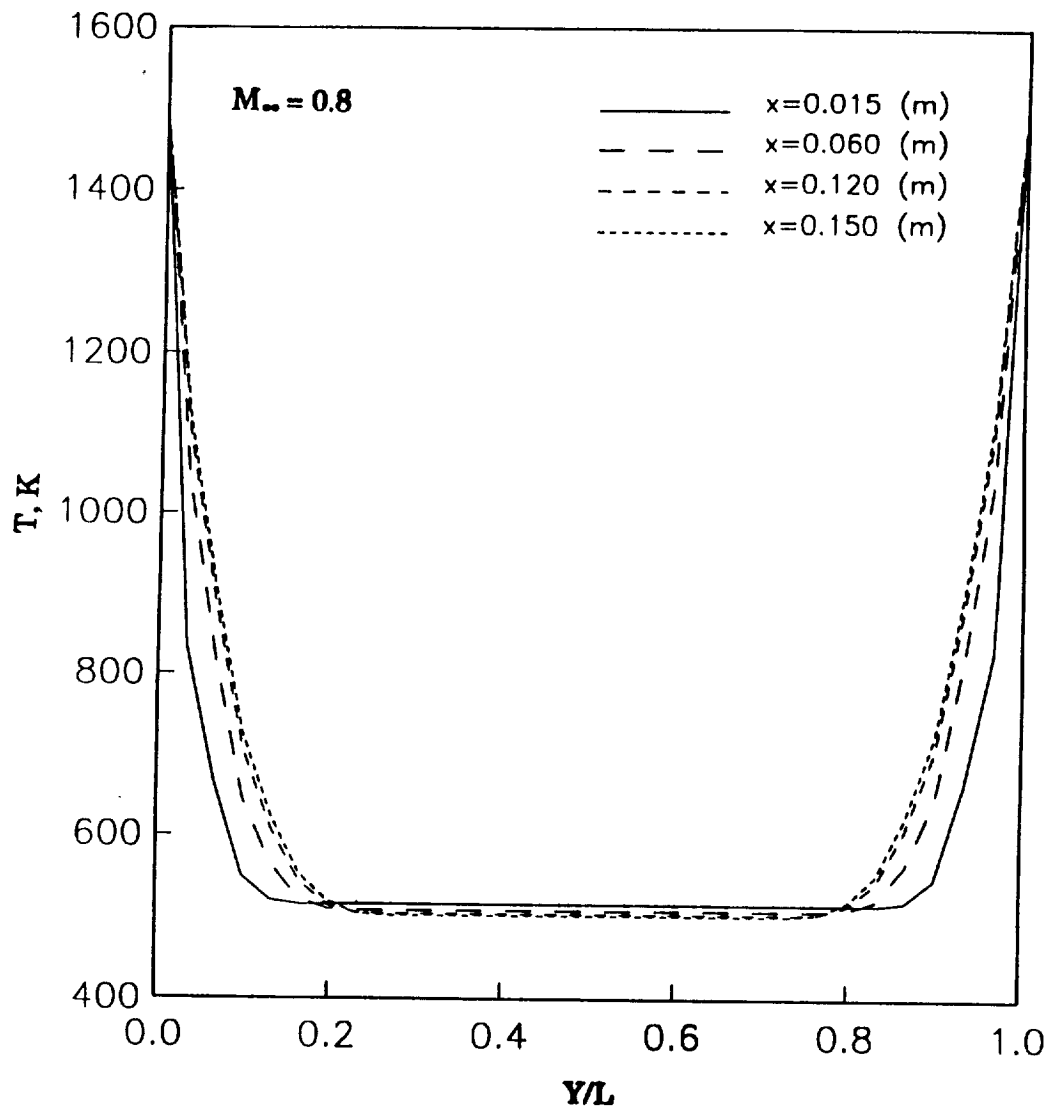


Fig. 7 Temperature variation across the channel at various x stations, $M_\infty = 0.8$.

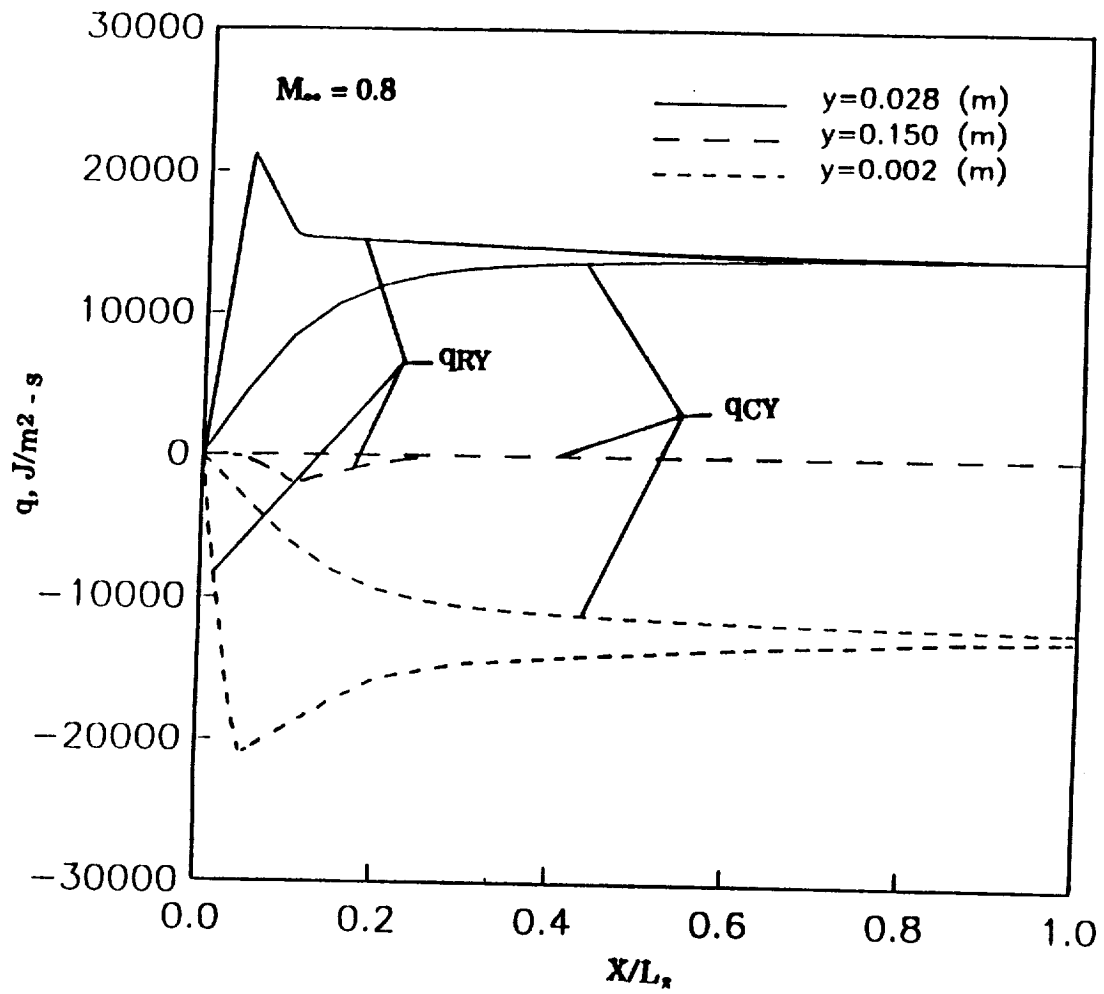


Fig. 8 Variation of q_{CY} and q_{RY} with x for different y - locations, $M_\infty = 0.8$.

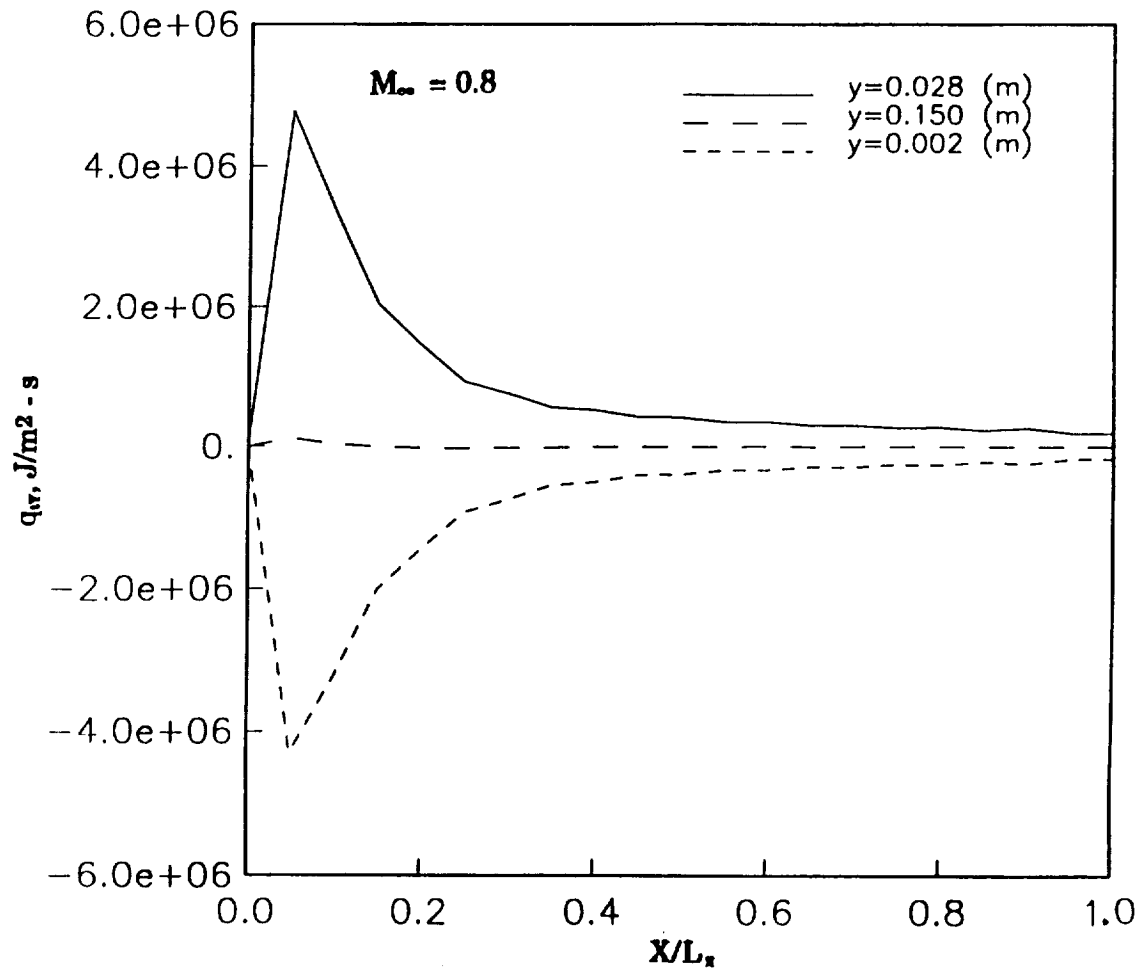


Fig. 9 Variation of q_w with x for different y locations, $M_\infty = 0.8$.

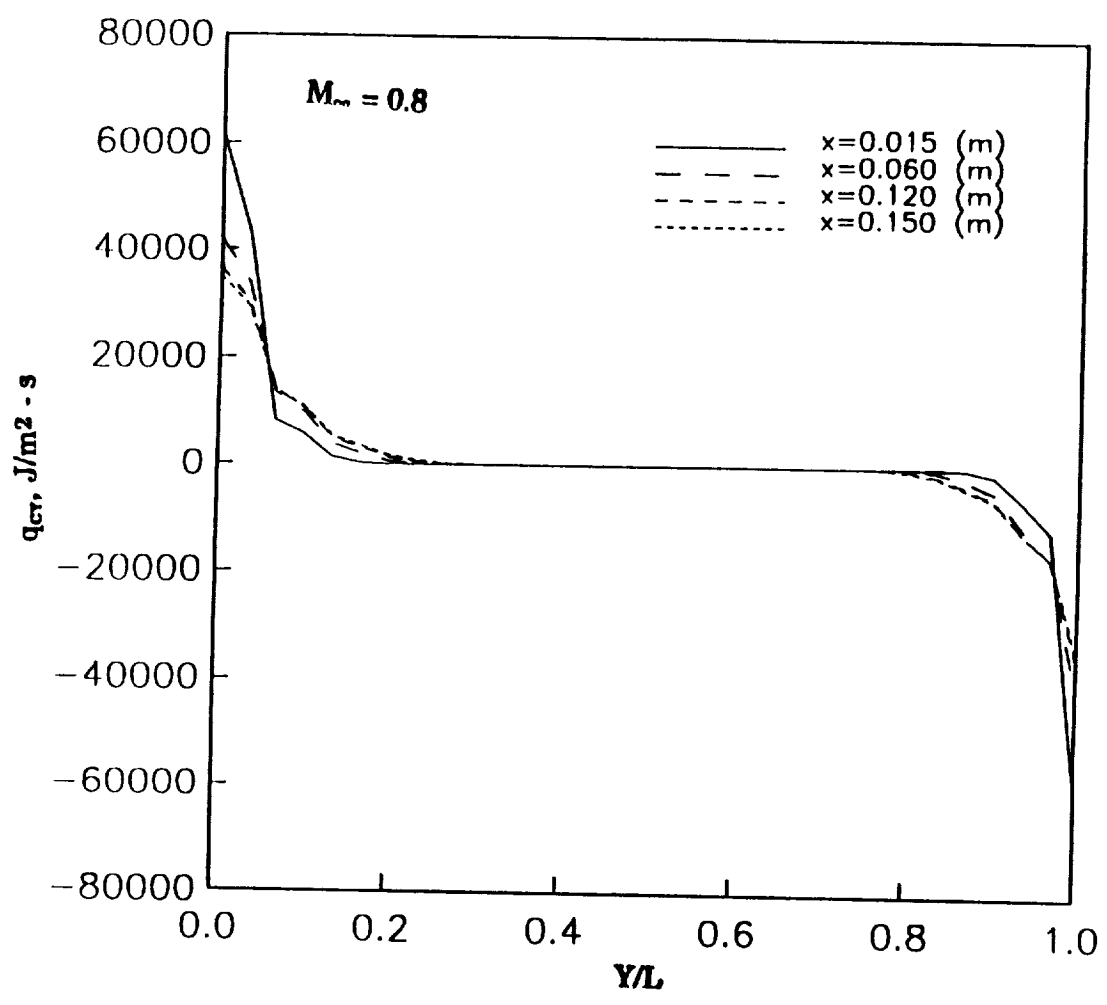


Fig. 10 Variation of q_{cv} with y for different x - locations, $M_\infty = 0.8$.

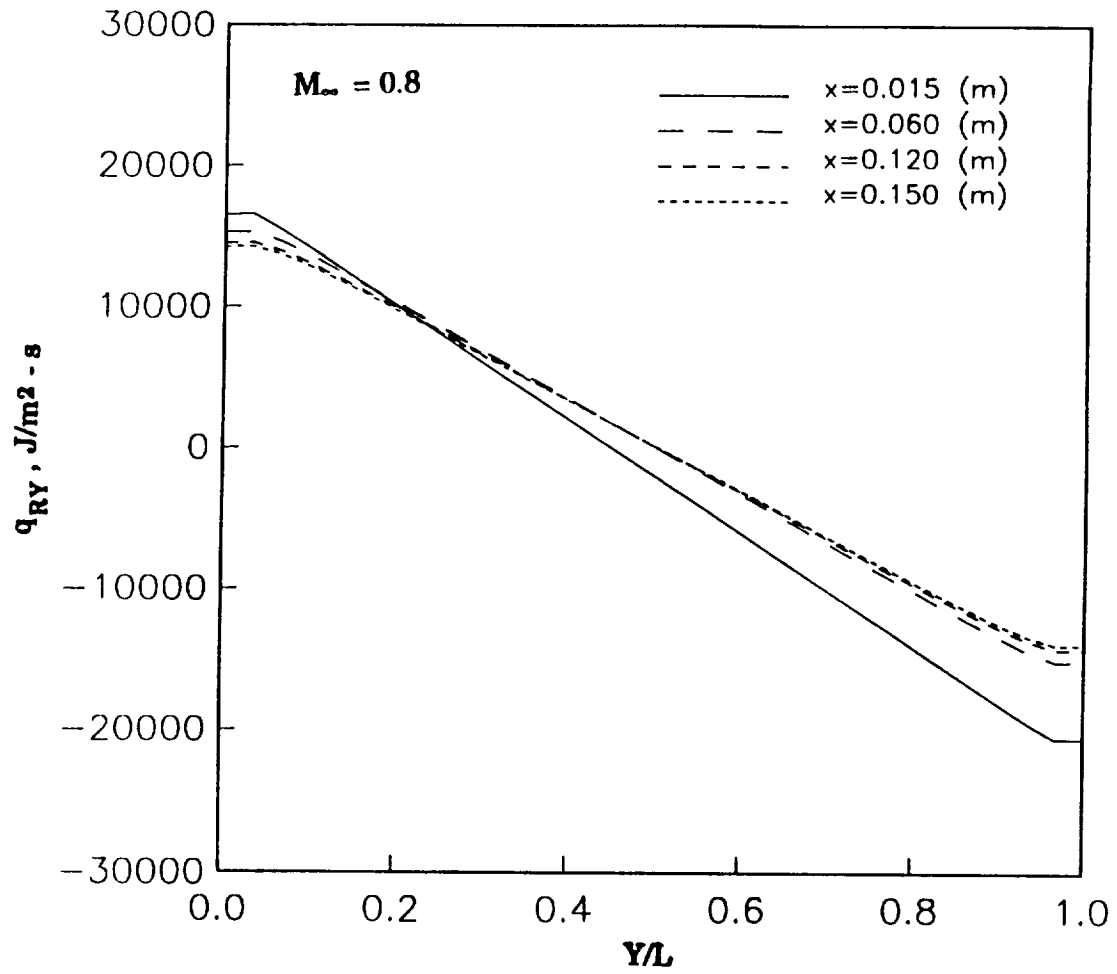


Fig. 11 Variation of q_{RY} with y for different x - locations, $M_\infty = 0.8$.

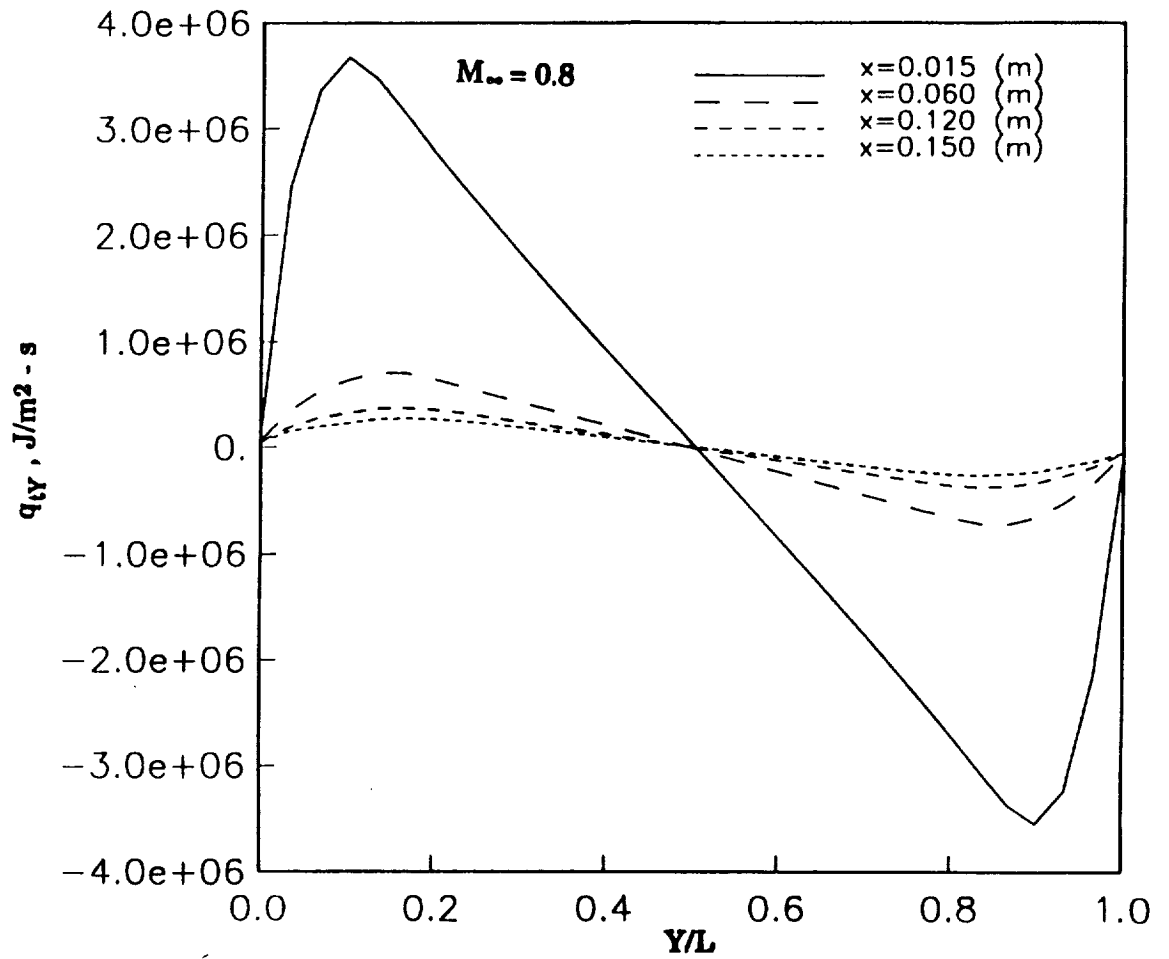


Fig. 12 Variation of q_y with y for different x - locations, $M_\infty = 0.8$.

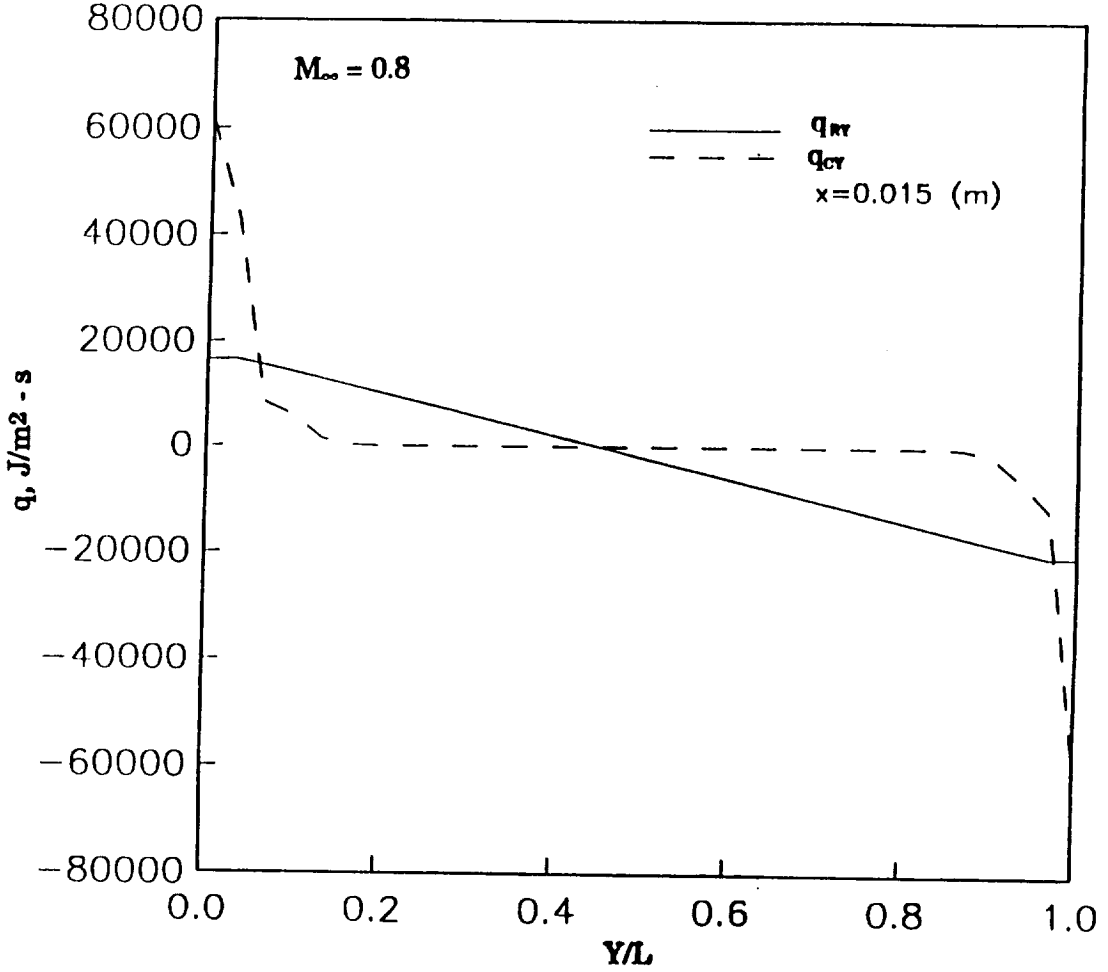


Fig. 13a Variation of q_{cy} and q_{ry} with y for $x = 0.05 \text{ (m)}$, $M_\infty = 0.8$.

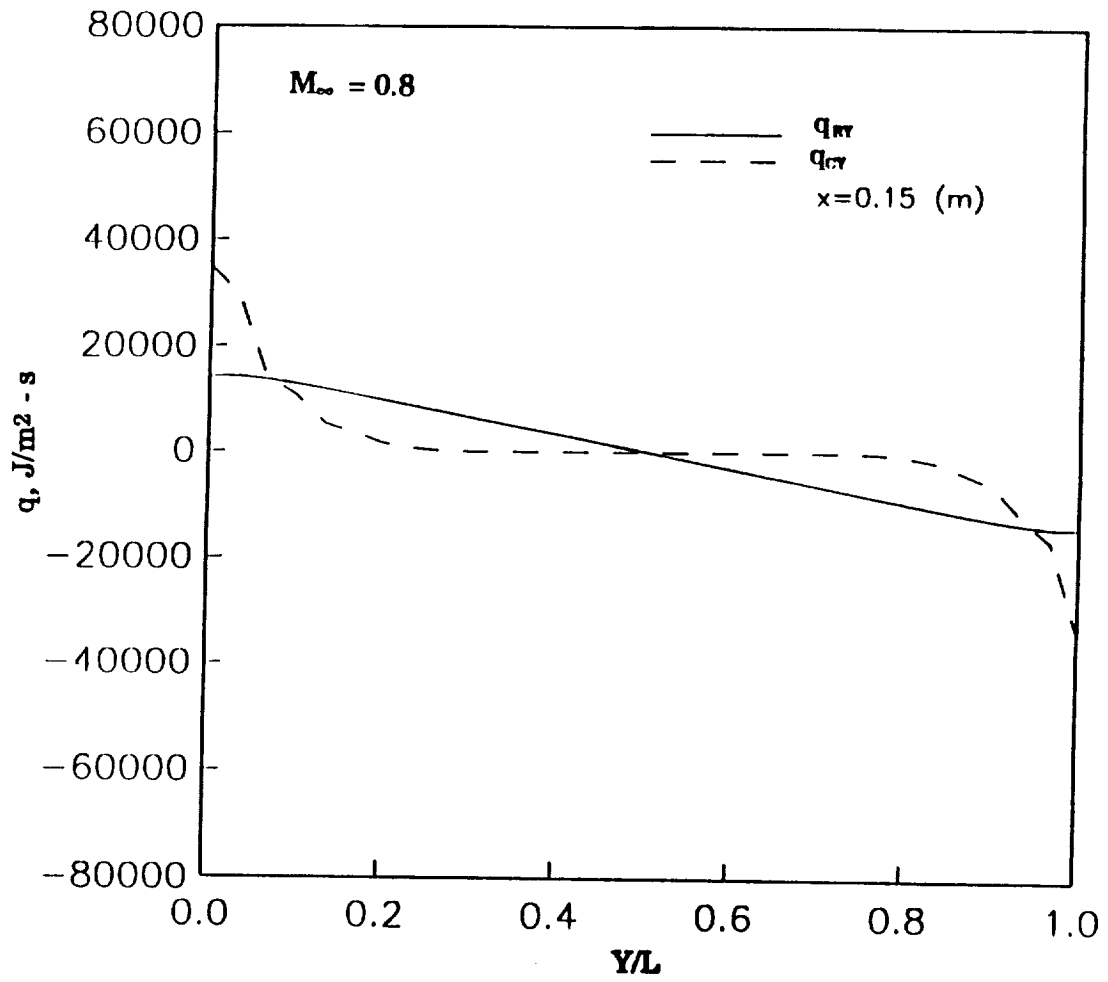


Fig. 13b Variation of q_{cy} and q_{ry} with y for $x = 0.15 \text{ (m)}$, $M_{\infty} = 0.8$.

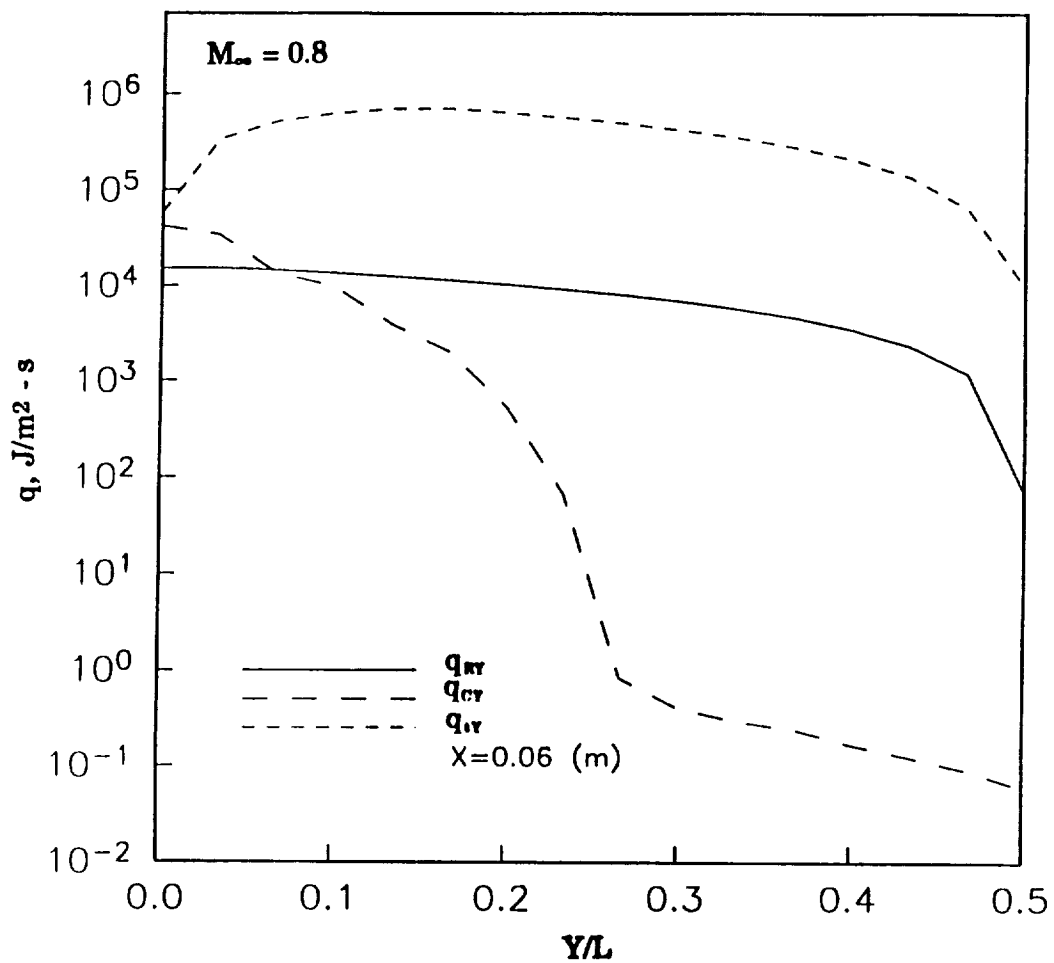


Fig. 14 Variation of q_{cy} , q_{cy} and q_{cy} with y for $x = 0.06$ (m), $M_{\infty} = 0.8$.

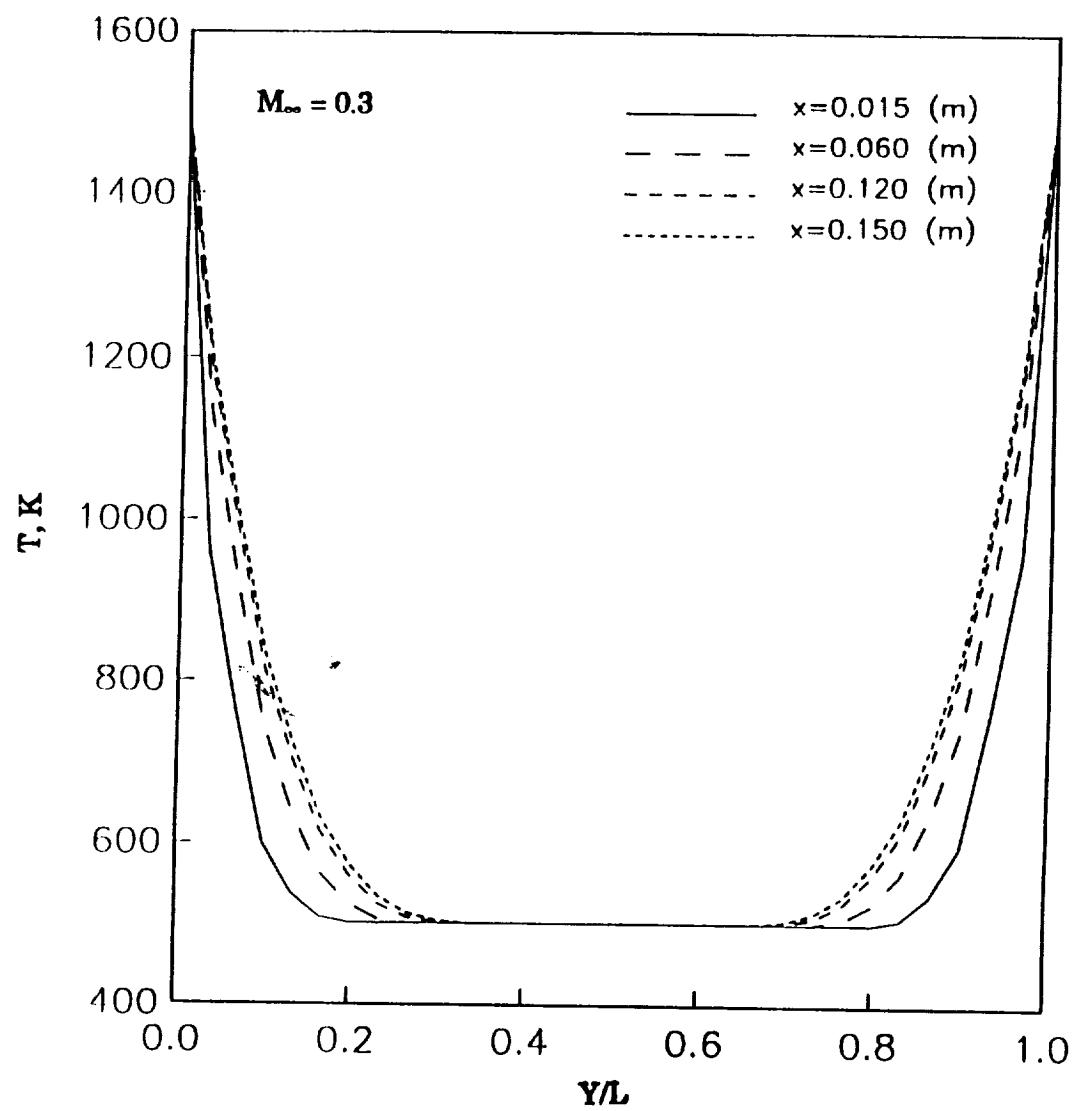


Fig. 15 Temperature variation across the channel at various x - stations, $M_\infty = 0.3$.

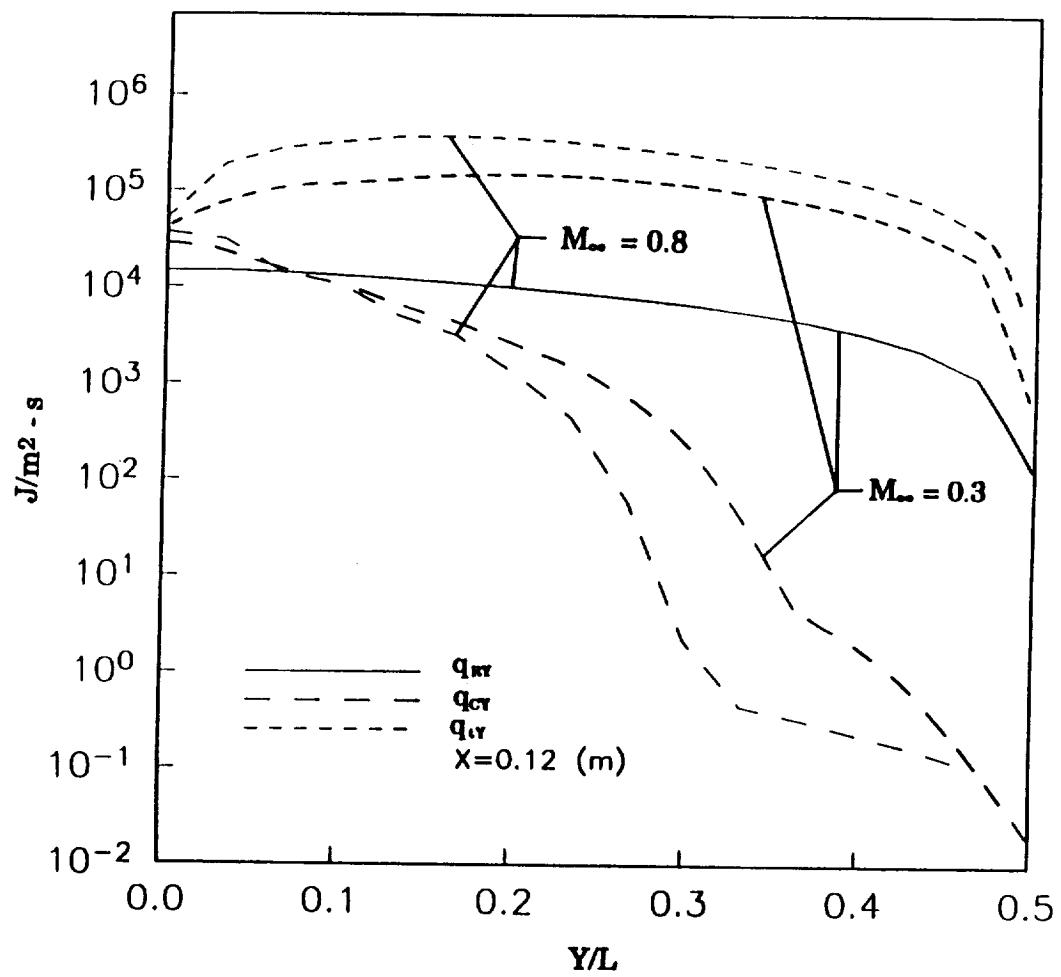


Fig. 16 Comparison of $M_\infty = 0.8$ and 0.3 results for q_{cy} , q_{ly} and q_w at $x = 0.12$ m.

